Author:
Owton, Tom

Title:
Predicting Social Vulnerability from Satellite Imagery with Deep Learning to Improve Urban Flood Risk Mapping

Predicting Social Vulnerability from Satellite Imagery with Deep Learning to Improve Urban Flood Risk Mapping

Thomas Alexander Owton

"A dissertation submitted to the University of Bristol in accordance with the requirements for award of the degree of PhD in Geography / Advanced Quantitative Methods in the Faculty of Social Sciences and Law, School of Geographical Sciences, December 2020."

Word count: 65531

Abstract

Flooding presents a challenge as a natural hazard, with around 1.1bn people threatened worldwide. Global flood models are useful in managing this risk because of their complete coverage. However, these models allocate flood risk based on national level income disaggregated by population density. Global flood risk maps as a result do not adequetly account for local variations in social vulnerability. The construction of high-resolution social vulnerability is challenging in low and middle income countries due to a lack of reliable household data. Informal settlements are particularly socially vulnerable environments to flooding due to factors related to a lack of legal tenure and poor provision of services. However, there are no comprehensive, global informal settlements maps that could be integrated with existing global flood models.

But informal settlements are an environment clearly identifiable from satellite imagery, a task which has recently been dramatically improved using deep learning in the form of Convolutional Neural Networks (CNNs). I use a CNN to map informal settlements using Slum Dwellers International (SDI) Know Your City as a proxy for social vulnerability. Both a pixel-based and area-based approach are used because the benefits of each method are recognised.

Using Cape Town as a case study, the flood risk map using the informal settlement layer derived from the CNN is contrasted to a traditional population-based flood risk map. The flood inundation layer for each is derived from the Fathom Global Flood Model Version 2. Different methods of spatially allocating flood risk using the informal settlement layer are produced to inform policymakers of the various methods of producing maps which spatially allocate risk to socially vulnerable environments. I also calculate the number of additional informal settlement dwellers demonstrated to be disproportionately at risk by the new flood risk mapping method.

Acknowledgements

I would, most of all, like to thank my supervisors, Dr. Sean Fox and Dr. Jeffrey Neal, for their help over the last 4 years with my PhD. I would like to thank Dr. Levi Wolf, Professor Richard Harris and Professor Majid Mirmehdi for their additional help as well as my housemate, Laurence Kedward, and my parents for their help proof reading chapters.

I would also like to thank Ncediswa Notywala from SDI for allowing access to their Know Your City dataset and for the University of Bristol School of Geographical Sciences Hydrology Group and Dr. Laurence Hawker for access to the Fathom Model flood inundation data.

I would also like to thank my funders at the Economic and Social Research Council (ESRC) through their Advanced Quantitative Methods (AQM) programme.

Author's Declaration

I declare that the work in this dissertation was carried out in accordance with the requirements of the University's Regulations and Code of Practice for Research Degree Programmes and that it has not been submitted for any other academic award. Except where indicated by specific reference in the text, the work is the candidate's own work. Work done in collaboration, or with the assistance of, others, indicated as such. Any views expressed in the dissertation are those of the author.

Signed …..Thomas Owton…… Date ……11/05/2020……

Table of Contents

List of Tables

List of Figures

Chapter 2

Chapter 3

Chapter 4

List of Equations

List of Abbreviations

AUC, Area Under the (ROC) Curve

CIESEN, Center for International Earth Science Information Network

CNN, Convolutional Neural Network

DEM, Digital Elevation Model

EAE, Expected Annual Exposure

FCN, Fully Convolutional Network

GAN, Generative Adversarial Network.

GDP, Gross Domestic Product

GFM, Global Flood Model

GUF, Global Urban Footprint

HRPDM, High Resolution Population Density Map

HRSL, High Resolution Settlement Layer

LSMS, Living Standards Measurement Surveys

OBIA, Object-based Image Analysis

PBIA, Pixel-based Image Analysis

ROC, Receiver Operating Characteristic

SDI, Slum/Shack Dwellers International

UNDRR, United Nations Office for Disaster Risk Reduction

1. Reconsidering Social Vulnerability: A Review of Concepts and Approaches to Flood Risk Mapping and a Proposal for a New Methodological Direction

1.1 Overview of Research Problem

Natural hazards continue to represent a threat to the life and wellbeing of people across the world. There have been an estimated 1.6 million fatalities resulting from natural hazards since 1990, an average of approximately 65,000 annually (UNDRR, 2015a). The annual financial cost of events including earthquakes, floods, tropical cyclones and tsunamis in urban areas alone is an estimated $314bn (UNDRR, 2015a). Furthermore, the extent of suffering which these events cause is increasing and this pattern is predicted to continue. Between 2008 and 2012 the Internal Displacement Monitoring Centre (IDMC, 2014) estimated that natural hazards displaced 143.9 million people in this time period, with a rising trend. Today about one seventh of the world's population reside in low quality housing with a lack of access to services (Mitlin and Satterthwaite, 2013) and with rapid population growth expected in these areas, the total population globally living in these informal settlements is expected to continue to grow (Lewis and Purcell, 2014), expected to increase by 1 billion by 2035 (WBEF, 2020)

Informal settlements are built environments usually existing in low and middle income countries and are typically characterised by a lack of formal planning and poor provision of services such as water and sewage and where the residents lack legal tenure of the land where they live (UN-Habitat, 2003). For these reasons among others, vulnerability to natural hazards is well documented as being higher in these places (Ergunay, 2011, Tas et al, 2013, Rufat et al, 2015, Colten et al, 2006, Porio, 2011, Cutter et al, 2000, 2003, Pelling, 1998, Wisner et al, 2004, Brouwer et al, 2007, Chatterjee, 2010, Adger, 1999, Adeola, 2009, Chomsri and Sherer, 2013, Parker et al, 2009). With the global total population living in informal settlements set to increase, vulnerability to natural hazards is therefore expected to rise in the future (Lewis and Purcell, 2014). Increasing risk from hydro-meteorological hazards in particular is due to anthropogenic climate change and associated anomalies in weather patterns and intensification of specific hazards events (Zhou et al, 2019) as well as drought and resource scarcity (UNDRR, 2013). It is also rare for investment decisions to take into account the level of disaster risk, although this is beginning to change (De Bono et al, 2013, Ingirige et al., 2014).

Whilst society should look to find ways of researching and reducing the risks to populations from all hazards, for a number of reasons this thesis focusses mainly but not exclusively on flooding. At present more people are exposed to flooding than any other natural hazard (Brecht et al, 2013). Floods affect more people and cause more fatalities than earthquakes, volcanic eruptions and tsunamis for example (Our World in Data, 2019). These hazards generally affect the boundaries of tectonic plates, whereas floods can occur theoretically anywhere. However, at a local scale the effects of flooding are more spatially constrained to certain areas with dependency on river locations and topography. This makes it easier to forecast the precise locations of flooding, giving greater possibility for allocating defences and alleviating human suffering, as opposed to other natural hazards whose spatial location is not as easy to predict. For example, earthquake hazards are less spatially constrained on a local spatial scale and are hence not as specific in the areas they affect. Moreover, unlike geological hazards such as volcanic eruptions, tsunamis and earthquakes, hydro-meteorological hazards such as floods are forecast to increase in intensity and frequency as a result of anthropogenic climate change (Zhou et al, 2019). Floods can be forecast more easily than geological hazards and hence adaptation and mitigation can have a greater benefit with floods than earthquakes. Additionally, the proportion of people living in circumstances which make them vulnerable to flooding is increasing, with the construction of property and settlements on floodplains continuing to be a problem. In the period 1970-2010, the total population exposed to flooding almost doubled (Jongman et al, 2012).

A vital tool in mitigating against the threat of flood risk is mapping. Traditional flood modelling has been carried out at the catchment level (Trigg et al, 2016). Such detailed local maps lack coverage however, particularly in the low and middle income countries, and where maps exist their methodologies are often inconsistent (Trigg et al, 2016).

Improvements in computing power and more efficient representations of river flow (Trigg et al, 2016) however have allowed similar flood maps to be produced globally using global flood models (GFMs). These have the advantage over localised versions because of their consistency across space and complete coverage (Trigg et al, 2016, Sampson et al, 2015). These GFMs have applications in areas such as flood defence allocation (Bernhofen et al, 2018), disaster risk management (Sampson et al, 2015) and insurance (Sampson et al, 2015, Trigg et al 2016).

Due to the difficulties of adequately representing human social vulnerability, flood risk maps derived from GFMs use a crude representation of the human component of risk. They rely on

national level income which is then spatially disaggregated by population, effectively assuming each individual within a country generates an equal amount of economic activity (Trigg et al 2016, van Vuuren et al, 2007, Jongman et al, 2012, Ward et al, 2017, Smith et al, 2019). This approach is incapable of representing social vulnerability for a number of reasons.

First, due to geographical inequalities, the assumption that economic output will be distributed perfectly according to population density is a flawed one because it presumes everyone has identical income. This method as a result obscures sub-national variation in income levels. Second, the approach is fundamentally designed to measure the consequences of flooding on economic output, rather than the vulnerability to persons. But if the objective of the mapping exercise is to mitigate the impact on human lives, the traditional approach has the adverse effect of disproportionately allocating risk to the most affluent areas. It is well established that the wealthier an area is, the less socially vulnerable the population are and vice versa. For policymakers looking to identify areas of socially vulnerable populations at risk from flooding, a fundamentally different approach to mapping is therefore needed.

A cost-efficient method of mapping social vulnerability, able to be attached to a GFM therefore has the potential to enhance the research community's ability to produce flood risk maps which sufficiently account for social vulnerability. This new method would be an alternative to the traditional method of population disaggregated income. This is the main research aim of this thesis.

The relevant international agency, the United Nations Office for Disaster Risk Reduction (UNDRR), agree with this sentiment. The third and fourth priorities of the UNDRR's (2015c) influential Sendai Framework for disaster risk reduction cover investment in socioeconomic conditions and preparedness for natural disasters. As a result, knowledge of the spatial distribution of social vulnerability is crucial if this is to be implemented effectively (UNDRR, 2015c). Consequently, as the global community seeks to enact these goals, the mapping and quantifying of social vulnerability becomes increasingly important.

A significant problem lies in a lack of data in order to produce social vulnerability maps. Amongst present studies, insufficient attention has been placed upon how such mapping can take place in data sparse environments (Kohli et al, 2012, Taubenbock and Kraff, 2014, Zeng et al, 2012). Most notably, informal settlements or slums are environments where often a census or any other formal data collection does not take place. As a result, the most vulnerable

environments are typically those that researchers have the least information on. Household surveys such as Living Standards Measurement Surveys and Demographic and Household Survey have been proposed as an alternative data source, but these are costly to carry out and lack validity after some time (Busgeeth et al, 2008). Different surveys also usually have contrasting methodologies (Preston et al, 2011). Such deficiencies also mean another problem exists. The lack of validity associated with these social vulnerability maps means that they cannot be coupled to GFMs (Birkmann, 2007, Lummen and Yabada, 2014). These traditional population-based flood risk maps are resultantly characterised by a high level of generalisation and a crude representation of social vulnerability (Lummen and Yamada, 2014), as previously mentioned. The Disaster Risk Hotspots project for example merely derives the desired output by contrasting gridded population data with GDP for six different types of hazard (Lummen and Yabada, 2014).

On the basis of these gaps in our current capabilities and the potential shown by new techniques, a clear statement of the aims of this thesis can be established. The thesis aims to demonstrate the potential of vulnerable population-based risk mapping of flood risk. I will use deep learning applied to visible light satellite imagery on more traditional in-situ data collected by residents in order to detect informal settlements to accomplish this social vulnerability mapping. This social vulnerability map will subsequently be coupled to flood inundation outputs from a GFM to produce a set of final flood risk maps. There will be a focus on making the method open and cost-efficient to make it appropriate for low- and middle-income countries. The new method of mapping will be contrasted to more traditional mapping methods to evaluate its benefits as a social vulnerability map and consequently its utility for policymakers.

1.2 Concepts and Definitions

In producing a method of social vulnerability mapping appropriate for flood risk mapping, the first step is to define the key terms which are associated with and contribute to the concept of risk. This will enable any produced method to be consistent with how the research community understands the contributors to flood risk and how they relate to one another.

Natural disasters are the result of an interface of natural processes and human agency. Intuitively, a classification of the various contributory factors can assist in reducing their negative consequences. Inevitability such inquiry generates disagreement over definitions, since they are multivariate concepts (Romero-Lankao et al, 2016) used to describe the various

contributing factors to loss of life, injury and damage to property from such events. In this section I provide present definition of the terms: disaster, hazard, exposure, social vulnerability and risk.

Disaster

The occurrences of damaging events are regularly attributed the category "disaster". Definitions of disaster typically centre on the associated human impacts. For example, Lummen and Yamada (2014:1087) define a disaster as a "serious and widespread disruption of the normal functioning of a community or a society, as a result of a physical phenomenon of natural, socio-natural or anthropogenic origin". Many definitions also place emphasis on events such as those exceeding the ability of the affected community to cope and resist (Cutter et al, 2009, Lummen and Yamada, 2014). Other important aspects of this phenomenon are the intersection of a particular hazard event and a socially vulnerable population (Wolf, 2012) as well as a disaster being defined as coming from an individual event rather than a collection or trend (Cutter et al, 2009).

The International Disaster Database or EM-DAT defines a disaster as being an event which satisfies one of four conditions: (1) ten or more people killed, (2) one hundred or more displaced or injured, (3) a call for international assistance or (4) a declaration of a state of emergency (Centre for Research on the Epidemiology of Disasters, 2017).

As opposed to the concept of risk, which is by definition probabilistic, a disaster represents an actualised version of what an entity being "high risk" might signify. Many definitions of a disaster reflect this, where Lummen and Yamada (2014:1088) additionally define a disaster as when "the threat of a natural hazard becomes a reality, and the event is met with existing risks and vulnerabilities" and when the consequences are overwhelming to people and places.

This research focusses on the interface between vulnerable populations and the hazards and as a result it is helpful in this study to emphasise a disaster as being an interaction of both these phenomena. Additionally, because the aim of this project is to map human populations it is desirable to define a disaster which makes reference to human impacts in spite of the fact they ultimately are natural events.

How the negative effects of a disaster are measured is an important aspect of how a disaster is defined. Natural hazards can damage economic development, especially in low and middle

income countries. In some low and middle income countries, natural hazards can inflict damage amounting for up to 15% of GDP (UNDRR, 2013). For example, there is empirical evidence that powerful tropical cyclones hamper long term economic growth (Hsiang and Jina, 2014). The cost of recovering from these events could have been invested in measures associated with long term economic development, such as health and education. In many countries, the average annual loss amounts to more than 10% of annual capital investment and in some countries such as Myanmar for example this figure is as high as 30% (UNDRR, 2015a). Therefore, appropriately targeted investment in disaster risk reduction has the potential to improve in the long run the living standards of people in these countries.

Consequently, because it fails to account for socioeconomic impact, using the number of fatalities can underestimate the true human cost of these natural disasters. As a result, the use of "life years" instead of the number of fatalities has gained some traction (UNDRR, 2015a). The aim of the life years concept is to factor in the lost opportunity for social and economic development and the impact on overall human welfare which goes beyond traditional metrics which simply measure the number of fatalities or injuries (UNDRR, 2015a). Noy (2015) proposes a popular version which factors in the median age of those who are killed and their life expectancy to take into account the number of years they have lost as a result of their deaths. A welfare reduction coefficient is also used to factor in injuries in a similar way. Measures of the amount of damage are converted into "life years" by accounting for the opportunity cost of the lost socioeconomically developmental policies (Noy, 2015).

As an example, in comparison to the more than 1 million killed annually by tuberculosis, the 65,000 killed by natural disasters pales in comparison. In contrast, an estimate of the life years lost from natural disasters is 42 million annually (Noy, 2015), similar to the estimate of 43 million for tuberculosis to give an example (UNDRR, 2015a). Moreover, around 80% of these are spread across low income countries (UNDRR, 2015a). The expression of disaster impact in terms of the number of fatalities leads to the impacts being underestimated and being given too little attention and financial support in the international community (UNDRR, 2015a).

Hazard

A hazard intuitively refers to potentially damaging events or phenomena, which can be natural or technological (UNDRR, 2009), which have the potential to cause loss of life or damage to property (Geiss and Taubenbock, 2013).

Much of the literature however views a more pragmatic approach as defining a hazard as a likelihood of an event such as this occurring. The definition of such an "event" is constrained to only events which exceed a given threshold (Robinson et al, 2006, Geiss and Taubenbock, 2013). Such an approach is more efficient from a perspective of seeing hazard as a component of risk.

Resultantly, from these principles I produce a definition of "hazard" in the context of flooding which is as follows: "the probability of a flood inundation event taking place as the likelihood of exceedance of a certain intensity threshold".

In looking at flooding this translates to what is referred to as a return period. Such a concept references the length of time for a flood inundation event of a given intensity to occur on average (Gumbel, 1941). For example, a "1 in 100 year" flood event implies a flood event of an intensity such that it will on average occur once in a 100 year period (Gumbel, 1941).

The hazard component in this thesis is the output from a GFM. A GFM output spatially maps these flood return periods to allow estimates of the probability of a given spatial location being flooded in a given year (Emerton et al, 2020).

There is also debate surrounding whether what is meant by a hazard refers to the triggering event or the actual mechanism leading from the phenomenon which cause human suffering (Brooks, 2003). From the perspective of my study, I am looking at mapping overall risk of harm. I place attention on the natural hazard event itself as a whole i.e. the flood as opposed to all of the elements of the event which directly cause harm to people. Examples of these components of the flood hazard for floods may include disease, drowning, building collapse and crop failure. Defining each of these as individual hazards is problematic from a perspective that in a given flood many of these are likely to occur together, making defining them separately lack validity.

Exposure

Exposure refers to people and property which are located such that they could be affected by a natural hazard. Houses situated and people living on a flood plain for example can therefore be considered "exposed" to flooding. As a result of this agreement, this research sees no problem in adopting the standard UNDRR (2009:15) definition as when "People, property, systems, or other elements present in hazard zones that are thereby subject to potential losses".

Social Vulnerability

It is only relatively recently that the research community has conceptually focussed on the social contributors to risk and disasters rather than the physical ones because many felt the former factors were being ignored, in response to the traditionally hazard centric view of risk (Geiss and Taubenbock, 2013, Schneiderbauer and Ehrlich 2004, Villagra´n De Le´on, 2006). O'Keefe et al (1976) were one of the early pioneers of identifying what is now referred to as social vulnerability, arguing that the study of the natural events in question are insufficient in explaining the effects of many events. From a policy perspective, by 1994 the UN International Decade for Natural Disaster Reduction in their 1994 and 2004 conferences both urged a shift in attention towards the underlying social causes of disasters and their intersection with natural hazards (Thomalla et al, 2006).

Definitions of social vulnerability refer to the incapacity of people to cope with hazards based on their social circumstances (Clark et al, 1998) and how these contribute to people being negatively affected and attenuate the effects of a hazard (Cutter et al, 2009). The concept can be applied to the preparation, recovery and response stages of a disaster (Geiss and Taubenbock, 2013).

Other definitions of social vulnerability have focussed on the inequality aspect, how usually those in socially vulnerable situations can be defined relative to others, with regard to specific hazard events (O'Keefe et al. 1976; Susman et al. 1983, Clark et al, 1998).

Social vulnerability may be consisdered a function of susceptibility and adaptive or coping capacity. The former refers to the "predisposition of the elements at risk" (Kienberger, 2012:2005) whereas the latter describes the resources in and attributes of the community, individuals and organisations which can reduce the adverse effects of natural hazards or to reduce these existing vulnerabilities (Lummen and Yamada, 2014, UNDRR, 2009). This is indicated in the conceptual equation 1-1:

$$Social\ Vulnerability\ =\ f(Susceptibility, Adaptive\ Capacity, Coping\ Capacity)$$

(1-1)

Kienberger (2012)

Both the susceptibility and coping capacity elements are closely tied to people's socioeconomic conditions and therefore can be considered part of what makes someone socially vulnerable. Definitions of social vulnerability have incorporated the capacity of people to cope as well as their susceptibilities (Wisner et al, 2004).

The idea of social vulnerability is predictive since it is a probabilistic assessment of future susceptibility to a given natural hazard event (Wolf, 2012) and it is a concept which describes present attributes in relation to a hypothetical, future event (Wolf, 2012). As an example of this disagreement, many have sought to define social vulnerability not as a predictive and probabilistic concept in reference to a future event but instead as simply an assessment of the damage after the event as a form of postdiction (Villagrán de León, 2006, Birkmann, 2005a). This approach however suffers from hindsight bias and it lacks validity in being useful for mitigating future hazards, even though such analysis is useful for mitigating future events.

Additionally, it has often been found that from this perspective, exposure and social vulnerability do not necessarily occur at the same time (Cutter et al, 2000). An example demonstrating this is from Chakraborty et al (2005) in Hillsborough County, Florida. Here the authors analysed the spatial distribution of exposure and social vulnerability with respect to tropical cyclones with data from the National Hurricane Center Risk Analysis Program or HURISK. Probabilities of flooding were obtained from insurance maps. A geophysical risk index was derived from these two measures. Social vulnerability derived from census tracts based on a number of socioeconomic variables were contrasted with the former. The results showed that those most exposed areas, on the coast, did not have the most socially vulnerable populations. Similar patterns exist have been found to exist in low and middle income countries (Etwire et al, 2013, Muller et al, 2020). This shows the importance of producing robust measures of social vulnerability independent of actual exposure to natural hazards.

Unlike the exposure concept which may be measured objectively, social vulnerability is a much more holistic idea and hence its definition and quantitative measurement are more difficult. For the purposes of this thesis, in order to make social vulnerability a quantitative measure it should be considered an all-encompassing definition accounting for all of the various factors which can influence social vulnerability. This way, vulnerability is described as something quantitative but at the same time its holistic, multivariate nature is accounted for. Social vulnerability can be considered hard to quantify and highly variable across space and across

individuals due to its complexity (Cutter et al, 2003, Birkmann, 2005b, King, 2001) which makes quantifying and mapping the phenomenon challenging.

It can be that social vulnerability to one hazard will be correlated with that for other hazards (Brooks, 2003). Some researchers have as a result expressed social vulnerability as a hazard variant concept (Alwang et al, 2001). Similarly, Ebert et al (2007) state that exposure of this sort is extended to the physical environment, an example being the quality of the built environment, whereas people's specific life circumstances are what social vulnerability refers to.

However, it is also common that social vulnerability is expressed with regards to a specific hazard, rather than a multitude of hazards simultaneously (Ebert et al, 2007, Clark et al, 1998, Wisner et al, 2004), especially since often social vulnerability does not manifest itself in the same way to all natural hazards at the same time (Kuhlick et al, 2011, Rufat et al, 2015, Brooks, 2003).

Such a perspective strengthens the case for examining flooding primarily in this research rather than looking at social vulnerability to all hazard types simultaneously. Many socioeconomic attributes will also influence one's social vulnerability to different hazards in different ways. Others have however placed emphasis on social vulnerability being multi-hazard place-based concepts where the social vulnerability of the community is expressed as a function of all possible hazards and their consequences (Cutter et al, 2000, Cutter et al, 2003). Hewitt (1983) for example argues that hazard specific approaches invariably direct attention towards large scale geophysical hazards instead of more regular dangers associated with a particular place. In this sense there can be a tendency for greater attention being paid to more severe and infrequent hazards, what he calls "intensive" vulnerability as opposed to more regular small scale events, what he calls "extensive" vulnerability. This is because too often risk is portrayed as something which can be measured objectively rather than a concept which includes the holistic nature of social vulnerability. Such an effect occurs as a result of the inherent social construction of risk information (UNDRR, 2015a) where an inherent desire to see vulnerability as something which can be objectively measured leads to a greater emphasis on the large scale hazards associated with intensive risk where expsoure is the dominant factor (UNDRR, 2015a).

As an example of this point Brooks (2003) mentions how reasonable forecasts of future sea level rise can be made, but social vulnerability is much harder to estimate. Such an information

imbalance means for long term states, the definition of risk may be disproportionately weighted in favour of the hazard and exposure elements of risk rather than social vulnerability (Brooks, 2003).

Along similar lines, despite the disagreements, social vulnerability is still treated as a scientific idea as if it were something wholly positivist and empirical rather than subjective (Bogardi and Birkmann 2004, Lein, 2009, Cutter, 1996; Hogan and Marandola, 2005; Adger, 2006, Romero-Lankao et al, 2016). Consequently, attempts to map and index social vulnerability naturally vary according to what definition is used, yet it is still often treated as a scientific concept (Romero-Lankao et al, 2016, Birkmann, 2005b).

As a result, attempts at examining social vulnerability empirically or quantitatively have been criticised as being ignorant of the individual subject (Wisner et al, 2004). Often social vulnerability is portrayed as something quantitative however (Cutter, 2003), when in reality a quantitative estimate of social vulnerability is based on less information than we perceive that we have. This makes any ostensibly scientific judgement in fact highly subjective. As a result, often people's and media outlets' perception of our vulnerability is based on emotion and a politicisation of how vulnerable we are. Additionally, often concepts such as social vulnerability have been critiqued as being problematic from a postmodern perspective as beng problematic when it is attempted to be defined and measured in a Western context and imported and applied to low and middle income countries (Simon, 2003).

For these reasons, Cutter (2003) argues for the creation of a discipline called "Vulnerability Science" and to find common ground between quantitative and qualitative views and additionally between scientific and social scientific viewpoints. Scientific definitions commonly seek to simplify social vulnerability into a metric that is easy to measure and quantify, whereas social science focusses on social vulnerability as a holistic phenomenon comprising more processes than any simple quantitative measure or index could ever hope to capture fully (Cutter et al, 2003, Birkmann, 2005b, King, 2001). There are disagreements in the literature regarding how this unification should be approached (Tate, 2013). In my research I intend to address this dichotomy by incorporating the holistic nature of social vulnerability through adopting a place-based approach to mapping it. A place-based approach allows an integration of social vulnerability's complexity because the place level is the context through which many of the factors which make communities socially vulnerable manifest. As a result,

my place-based approach will enable social vulnerability's complexity to be modelled but my research will still be fundamentally quantitative in nature.

All things considered, the definition of social vulnerability used in this study is as follows:

The propensity for individual and contextual socioeconomic factors to cause certain places to be at a greater likelihood of being more negatively affected by a given hazard than other places.

This research seeks to make inferences of how the mapping of risk can be improved, and therefore it is interested in studying all possible ways in which socioeconomic factors can be of influence. As a consequence, the susceptibility, adaptive capacity and coping capacity elements of vulnerability are all to be considered "pathways" in which socioeconomic circumstances can influence the resultant social vulnerability of both people and places. This is consistent with what Brooks (2003:5) calls the "independent of the hazard" definition of social vulnerability which places emphasis on any factor not directly influencing or influenced by the hazard being considered an aspect of social vulnerability.

An important question arises as to whether vulnerability exists only ever as an interaction with hazards and the exposure associated with these (Birkmann, 2005a). In other words, should people living in a hypothetical place where no natural hazards occur, but whose living conditions would normally be classed as constituting social vulnerability be considered so? From a more pragmatic perspective, the paradigm could be restated as proposing that if two people have identical living conditions, but one is at greater overall exposure to natural hazards overall, is that person more socially vulnerable than the other (Kienberger, 2012)? The research community is very much divided on this issue, with the UNDP recognising socially constructed exposure as part of social vulnerability but with the UNDRR taking the opposing view (Birkmann, 2005a). Socially constructed exposure is the phenomenon whereby socioeconomic factors such as a lack of income force certain people to reside in environmnets exposed to flooding. From the context of how this thesis aims to measure social vulnerability, I am interested in methods of empirically measuring socioeconomic circumstances and how they contribute to worsening people's chances of surviving hazards or avoiding negative consequences. This research focusses on measurement of these conditions independent of the hazard, which could exist in any geographical area regardless of the threat of natural hazards.

Such considerations lead this research to adopt a hazard independent view of social vulnerability implying one can be socially vulnerable yet face no threat from natural hazards.

In similar respects, one must establish whether human influences on the physical characteristics of hazards themselves are an aspect of social vulnerability. O'Keefe et al (1976) identify the influence on droughts in Africa of human-induced environmental change. Another example is human alterations of river catchments (Brooks, 2003). In this thesis I see no purpose in classifying something more related to the actual action of the hazard itself rather than any socioeconomic circumstances as social vulnerability.

My hazard independent view of social vulnerability is adopted in spite of the fact that one's socioeconomic situation may affect one's exposure. A person living with low socioeconomic status may only be able to afford to live in a high exposure area such as a floodplain for example. Once people live in exposed locations, the source of exposure is more directly associated with the hazard itself rather than people's socioeconomic circumstances. In this thesis I am focussing on how people's exposure and social vulnerablility interact to make them at risk rather than why they are exposed in the first place.

Additionally, the measurement of exposure arising from location can be measured empirically and as a result is of a contrasting nature to the holistic and more difficult to quantify character of social vulnerability. Social vulnerability is identified as a complex social process involving many constituent interacting factors, which is difficult to define quantitatively. As a result, I believe that one's socioeconomic circumstances which contribute to exposure should be considered a separate phenomenon than social vulnerability in order to separate the easier to measure exposure and the holistic phenomenon of social vulnerability.

Risk

Risk is the resultant and all-encompassing concept describing the potential for harmful consequences to occur, a view the research community is largely consensual with. Risk is as such a probabilistic notion and definitions reflect this (Brooks 2003). It is also predictive and imaginary of future events rather than present ones (Taubenbock et al, 2008).

UNDRR (2004, 2009) define risk as the probability of negative consequences resulting from interactions between socially vulnerable populations and hazardous circumstances. Similarly, Cutter et al (2009:2) define risk as "the likelihood of incurring harm, or the probability that

some type of injury or loss would result from the hazard event". Such an emphasis is placed in the literature on risk as an interaction between the hazard and the socially vulnerable population (Wisner et al, 2004).

Where risk is widely seen to be the combination of many such concepts, one subdivision of the concept is an internal and external dichotomy (Bohle, 2001). The internal looks at the capacity of people to anticipate, cope with and recover from these disasters and the external side describes the nature of the hazard (Taubenbock et al, 2008). These subdivisions may also be labelled as outcome risk and event risk respectively (Sarewitz et al, 2003). Geiss and Taubenbock (2013) and Pelling (1999) propose a similar dichotomy whereby risk is divided into its constituent parts. The first of these relates to the location, likelihood and intensity of the hazard event, corresponding to what I describe as hazard and exposure, the other is associated with the specific elements at risk and their susceptibility, which corresponds to what I call social vulnerability. Such descriptions may confine risk to a certain time period (Geiss and Taubenbock, 2013). However, such an approach has come under criticism since different factors can influence an individual's risk at different phases of a hazard event (Rufat et al, 2015).

This study will attempt to examine risk from such an internal/external perspective, using a probabilistic assessment of the likelihood of future harm based on the interaction of a hazard and a socially vulnerable population.

The internal/external may be similarly represented using a conceptual model known as a "risk equation" which attempts to explain risk by describing it as a product of a series of phenomena. It is however more accurate to describe a risk equation as a family of conceptual models since it has been stated in many different, albeit similar ways, as Table 1-1 demonstrates. In effect such presentations simply represent a visual demonstration of the constituent parts which contribute to risk, such as the Bohle (2001) dichotomy of internal and external risk.

Risk Equation Form	Notes	Reference
$$Risk = Hazard \times Vulnerability \quad (1\text{-}2)$$		UNDP (2004)
$$Risk = Hazard \times Vulnerability \times Elements\ at\ Risk \quad (1\text{-}3)$$	Area Specific	Ebert et al (2007)
$$Risk = Hazard \times Vulnerability \times Exposure \quad (1\text{-}4)$$		Kienberger (2012)
$$Risk = Hazard \times \left(\frac{Vulnerability}{Coping\ Capacity} - Adaptive\ Capacity\right) \quad (1\text{-}5)$$		Wisner et al (2012)

Table 1-1 Tabular Presentation of Risk Equations

Some conceptual models however do not incorporate the form of an equation but instead simply assert risk as a function of a number of factors, namely hazard, social vulnerability and exposure (Davidson and Shah, 1997, Bollin et al, 2003).

Importantly, these conceptual models claim simply to summarise the relationship between the concepts in general terms. In other words, the equation is not claiming to model the relationship between risk, hazard and social vulnerability perfectly. Multidisciplinary research is as a result needed to more fully analyse these relationships (Taubenbock et al, 2008:410).

Along such lines and as with social vulnerability, and in particular in this thesis where I am looking to define risk quantitatively, a crucial aspect of how to view risk lies in our perception of it. Cutter (2003) uses the example of the September 11th terrorist attacks, where despite all of the well-developed intelligence and national security procedures designed to prevent attacks such as this, the attack was not prevented. The example the author gives is designed to show how we view the level of risk to which we are subjected, we always have less information than we perceive (Cutter, 2003). In terms of risk, there is therefore a perception problem. As a result,

risk as a concept is dominated by our awareness of what level of risk as a society we are happy to tolerate based on political rather than scientific judgement (Cutter, 2003).

1.3 Social Vulnerability in Informal Settlements

A variety of factors contribute to social vulnerability from the individual to the national level and across a variety of places and contexts with some consensus (Cutter et al, 2003). A comprehensive review of factors is provided by Rufat et al (2015).

One place which the research community has established as playing host to a particularly socially vulnerable population is informal settlements (Ergunay, 2011, Tas et al, 2013, Rufat et al, 2015, Colten et al, 2006, Porio, 2011, Cutter et al, 2000, 2003, Pelling, 1998, Wisner et al, 2004, Brouwer et al, 2007, Chatterjee, 2010, Adger, 1999, Adeola, 2008, Chomsri and Sherer, 2013, Parker et al, 2009). They as a result warrant particular attention with the aim of this thesis being the mapping of social vulnerability. The ways in which informal settlements are particularly socially vulnerable environments are subsequently categorised, examined and presented in Table 1-2.

Location factors are important reasons why these environments are especially physically vulnerable. Usually such settlements often arise from a context of rural-urban migration and uncontrolled urban sprawl and resultant limited land availability (Porio, 2011) and dwellers sometimes have little option but to live in these environments to avoid paying rents (Tas et al, 2013). Across Africa for example in the years 1975-2000 the annual growth in urban population was 4.21% (Simon, 2008). Although I have previously argued that such "socially constructed exposure" should not constitute social vulnerability, it is important in explaining how social vulnerability and exposure commonly overlap and why such hotspots require special attention in risk mapping.

Socioeconomic Status

Informal settlement dwellers are widely considered to be of low socioeconomic status and have low income and lack of access to resources (Rufat et al, 2015). These factors are widely considered to be among the most influential in contributing to social vulnerability. A sufficient income allows the purchase of goods, services and resources which facilitate preparation and coping capacity to flooding (Chatterjee, 2010, Cutter et al, 2000, 2003, Porio, 2011, Romero-Lankao et al, 2016). A low socioeconomic status may lead to people to lack the optimal social

linkages with which to provide information on coping strategies. (Pelling, 1998). Additionally, evidence shows those with a higher income have a greater willingness to prepare for flooding (Paul and Routray, 2011). A lack of access to resources such as water, electricity, health and sewage can also manifest themselves as secondary factors making individuals socially vulnerable, such as through separation, illness and disability (Porio, 2011).

In these respects, particular attention should be paid to one personal resource. The quality of the housing in which individuals live is important in determining their social vulnerability. This is because poorly built dwellings exhibit greater fragility and are less able to survive structurally and protect the inhabitants during a given flood event (Cutter et al, 2000, 2003, Clark et al, 1998). This is particularly the case in informal settlements, which are characterised by the presence of unplanned dwellings (Kohli et al, 2012).

A higher financial value of homes is also significant because such people are more likely to make preparations because the potential losses are greater (Paul and Routray, 2011). Similarly, flood defences are likely to be prioritised for areas with more valuable property (Chatterjee, 2010, Chomsri and Sherer, 2013). Living in a dwelling with multiple floors also allows refuge from flood waters upstairs (Geiss and Taubenbock 2013, Ebert et al, 2007). This is another factor making informal settlements at particular risk of flooding because multiple floors are rare with informal settlement dwellings (Kohli et al, 2012). Overall such socioeconomic variables as income, household assets and quality of housing are significant determinants of social vulnerability.

Lack of Planning

An informal settlement naturally lacks official planning and legality in its construction, which make it vulnerable to flooding. Many developments and changes to fluvial environments can cause problems such as the unauthorised alterations to embankments, the construction of nearby roads, extraction from rivers and disposing of waste near to rivers (Ergunay, 2011, Tas et al, 2013). All of which can make flooding more likely. A lack of official planning can be influential due to a resultant poor transport infrastructure. The quality of transport influences the ease of evacuation and the ability of aid to come in after a disaster (Rufat et al, 2015, Colten et al, 2006). Such a phenomenon is an aspect of social vulnerability under the "independent of the hazard" definition of Brooks (2003:5) which I adopt. It states that any facilitator of vulnerability that is not directly related to the hazard is an aspect of social vulnerability. Often

due to informal settlements' favourable location for employment but low living cost, they are extremely attractive to rural-urban migrants, making the population growth here very high. Such a high rate of urbanisation means that certain services such as water, health and sewage cannot keep pace (Porio, 2011, Cutter et al, 2000, 2003).

Political Apathy and Indifference

Including from such a planning perspective, many factors of relevance in informal settlements are related to political indifference. With planning and apathy from governors and ignorance of local people's subjectivities (Wisner et al, 2004), people are often forced to pursue their own mitigation strategies (Tas et al, 2013, Pelling, 1998), even though they may lack the knowledge of how to do this (Tas et al, 2013). Other findings (e.g. Porio, 2011) have found that people sometimes look to the authorities to help and are as such reluctant to pursue their own mitigation. There are also political factors associated with the fact that decisions on which places to protect against flooding will inevitably benefit areas with higher value property (Chatterjee, 2010). The lack of institutional trust created by political apathy can inhibit effective disaster management and co-operation between stakeholders (Nakagawa and Shaw, 2004). This can often particularly be the case for informal settlements in large cities in low and middle income countries because these places can lack a unified governance structure covering the whole city (Simon and Leck, 2015).

Inequality

In this respect another political connection lies in how the inequality of a community dictates how resources are allocated. Places with higher income inequality tend to have a tendency to allocate resources towards the few rather than the collective (Brouwer et al, 2007). The influence of powerful actors can also increase the vulnerability of some populations, often through the control of access to information and a lack of subjectivity regarding the heterogeneity of the community (Chatterjee, 2010, Pelling, 1998). On the other hand however, the existence of an unequal society can allow sufficient capital accumulation to facilitate and make financially worthwhile flood protection and other measures. Adger (1999:255) identifies that "under certain circumstances inequality facilitates provision of services for the good of communities by those with cumulated assets". With respect to informal settlements such a mechanism may be relevant if they are in close spatial proximity to more formal areas.

Prevalence of Social Networks

The extent at which the prevalence of social networks helps to mitigate against the adverse effects of natural hazards is debated in the literature. Access to social networks can be a good source of information and aid and can assist people with mitigation strategies (Chomsri and Sherer, 2013, Adeola, 2009). However, other findings suggest that peers' recommendations do not necessarily motivate people to evacuate and they have a distorted view of flood risk as being binary rather than probabilistic (Parker et al, 2009).

Socioeconomic Status	Mechanism	Spatial Scale Effective at	Reference
Income and access to resources	Coping capacity and preparation is dependent on access to resources, income allows spending on goods and services which facilitate protection.	Household	Chatterjee (2010), Cutter et al (2000, 2003), Porio (2011), Romero-Lankao et al (2016)
	Limited access to technology can limit the level of community involvement in preparation and recovery.	Community	Pelling (1998)
	Income associated with a greater willingness to prepare for hazard events.	Household	Paul and Routray (2011)
	A lack of these resources can lead to things like disability and long term sickness which can in turn make one more vulnerable to natural hazards.	Individual	Porio (2011)
	Those of higher socioeconomic status are typically able to more quickly return to their homes.	Household	Green et al (2007)
Quality of Housing	Poorly constructed houses by definition have greater fragility, meaning they are more likely to be damaged and fail to provide protection to the inhabitants in a given flood event.	Household	Cutter et al (2000, 2003), Clark et al (1998)
	Greater willingness to prepare if people own their homes because the potential losses are greater.	Household	Paul and Routray (2011)
	Flood defences are more likely to be prioritised for more valuable property.	Municipal	Chomsri and Sherer (2013), Chatterjee (2010)
	Having more than one floor allows for refuge to be taken upstairs in a flood.	Household	Geiss and Taubenbock (2013), Ebert et al (2009), Ebert et al (2007)
Social Capital	Institutional trust in leaders, community participation and strong social networks between stakeholders help ensure effective disaster governance.	Municipal	Nakagawa and Shaw (2004)
Lack of Planning	No planning in terms of how informal settlements are built can cause floods because rivers may have been developed or bridged etc.	Community	Ergunay (2011), Tas et al (2013)

	Poor quality of transport infrastructure inhibits the ability of evacuation to occur and for help to come in.	Community	Rufat et al (2015), Colten et al (2006)
	Uncontrolled urbanisation and high population growth rate means that city planning and services such as water, sewers and other infrastructure cannot keep pace with rate of city growth.	Municipal	Porio (2011), Cutter et al (2000, 2003)
Political Apathy and Indifference	Ignorance on the local planners with respect to individuals' subjectivities, and a lack of willingness from them to help out, meaning people are forced to pursue their own mitigation strategies.	Municipal	Pelling (1998) Wisner et al (2004) Tas et al (2013),
	People may lack the knowledge to have their own mitigation strategies.	Household	Tas et al (2013)
	People often expect authorities to help them and so are reluctant to make their own preparations.	Household	(Porio, 2011)
	Institutional trust in leaders, community participation and strong social networks between stakeholders help ensure effective disaster governance. Informal settlement dwellers can lack institutional trust.	Municipal	Nakagawa and Shaw (2004)
Inequality	A tendency for resources to be allocated to the few rather than the many.	Community	Brouwer et al (2007)
	The influence of powerful actors can control access to information.	Community	Chatterjee (2010), Pelling (1998)
	Can provide sufficient capital and reason for flood protection and provision of goods by the elites.	Community	Adger (1999)
Prevalence of Social Networks	Social networks can act as a source of information and aid.	Community	Adeola (2009), Chomsri and Sherer (2013)
	On the other hand, people are not necessarily motivated by their peers' recommendations to evacuate.	Community	Parker et al (2009)

Table 1-2: Factors Contributing to Social Vulnerability in Informal Settlements

To summarize, informal settlements represent a particularly socially vulnerable environment. A lack of planning, the low socioeconomic status of dwellers, poor housing quality, a poor quality of services such as water and political apathy combine to cause this. Informal settlements being a particularly socially vulnerable environment implies that the mapping of these presents a promising pathway towards the creation of a social vulnerability layer of a flood risk map which this thesis is aiming to do.

Studies have shown that social vulnerability varies contextually and that its influences manifest themselves on different spatial scales (Rufat et al, 2015). Studies attempting to map and quantify social vulnerability have found that differences in overall social vulnerability and its constituent factors vary depending on context (Kuhlick et al, 2011, Holand and Lujala, 2013). Political economic contexts including the macroeconomic situation in a country and its political stability can also manifest themselves at the smaller scales which communities depend on for their adaptive and coping capacity (Adger, 1999). A particular example of this is how the neoliberal macroeconomic approach which can amplify economic inequalities between the settlement dwellers and others and influence how information flows and resources related to disaster mitigation are allocated (Simon, 2003).

In seeking to map social vulnerability using informal settlements as a proxy, it is necessary to view informal settlements not merely as spatial units but also as social communities. Conceptions of hazard risk frequently recognise the importance of community and place. The popular hazards-of-place model, as described by Cutter et al (2003) for example, includes the assumption of there being factors contributing to social vulnerability which manifest themselves at the community level. Both communities and social vulnerability represent a complex set of social interactions and social relationships with the surrounding environment (Chomsri and Sherer, 2013, Rufat et al, 2015, Patterson et al, 2010) and as a result many of the factors contributing to social vulnerability manifest themselves at the community level (Herrmann, 2007, Adger, 1999) often due to the institutional structures present in communities, such as social networks or infrastructure (Adger, 1999). Because the community is a fundamental determinant of social vulnerability, many studies include within their definitions of disaster the level of disruption or suffering and the exceeding of coping capacity at the community level (Adeola, 2009).

Disaster responses naturally always start at the local level (Herrmann, 2007). Many studies have highlighted the importance of rapid responses by communities before official rescue

efforts or mitigation can take place. Examples of these bottom-up community responses include direct rescue efforts, establishing community kitchens, guarding the community (Nakagawa and Shaw, 2004), aiding evacuation, tending to vulnerable people in need and identifying lost people (Patterson et al, 2010). Similarly, community-based responses to hazards can be specific to informal settlements in response to flooding, such as the use of sandbags, raised platforms, cementing footpaths, evacuation (Porio, 2011) and widening and covering drains (Chatterjee, 2010).

Specific mechanisms of social vulnerability manifesting at the community level include access to critical resources such as water, access to electricity and sanitation, income inequality, diversity of economic assets, population density (Rufat et al, 2015, Adger, 1999, Cutter et al, 2003) and the provision of services (Adger, 1999). Chomsri and Sherer (2013) additionally identify how community level attributes influence the likelihood of flood protection being provided based on the value of property in those areas. Many residents will additionally be dependent on community relations which leads to their carers' coping capacity being reduced as a result of such responsibilities. The elderly and disabled fall into this category in particular (Rufat et al, 2015, Adeola, 2009, Porio, 2011). Poverty forces many individuals in such environments to rely on a complex network of assistance in their community for their resilience to natural hazard events (Chatterjee, 2010).

The social norms, relationships and social networks existing within a community affect social vulnerability (Rufat et al 2015, Chomsri and Sherer, 2013, Nakagawa and Shaw, 2004, Adeola, 2009), particularly in the preparation for and response to a hazard event. Social networks and community organisations can be a useful source of information for individuals to cope with a disaster (Rufat et al, 2015, Perry, 2007, Chomsri and Sherer, 2013, Patterson et al, 2010), particularly if peers have past experience of such events (Porio, 2011, Cutter et al, 2003). Social networks can be a particularly important source of information if official communication breaks down after hazard events, or if infrastructure fails and radio frequencies become overused (der Heide, 2006). Such networks and access to information may help a community to prepare for and respond to a hazard collectively rather than individually (Nakagawa and Shaw, 2004). As a result, the community may have greater capacity to respond in comparison to an individualistic response (Patterson et al, 2010).

In planning for natural hazards many studies have identified the importance of municipal authorities integrating their preparation with that of local communities in disaster management.

Patterson et al (2010) suggest that informal social groups will be more efficient at preparing for and responding to natural hazards because they possess local knowledge and information inaccessible to higher authorities. Local knowledge is particularly effective in preparation for floods because it helps generate bottom-up responses independent of co-operation with any higher authorities (Patterson et al, 2010), such as the installation of sand bags and the digging of drainage ditches. Greater knowledge of people's subjectivities will exist at the local level and their local expertise in preparation and recovery rather than official levels due to the complex nature of these social relationships (Chomsri and Sherer, 2013, Perry, 2007, Adeola, 2009, Tolentino, 2007). All of these factors create the scope for the community level to play a crucial role in flood mitigation, often in partnership with municipal authorities.

Alternatively, strong social networks in these communities may have a detrimental effect on social vulnerability. Communities may monopolize resources and be exclusionary in resilience terms to outsiders' accessing resources and information (Patterson et al, 2010).

To summarise, informal settlements being a particularly socially vulnerable environment implies that the mapping of these presents a promising pathway towards the creation of a social vulnerability layer of a flood risk map which this thesis is aiming to do.

1.4 Mapping and Indexing Social Vulnerability

1.4.1 Current Methods of Social Vulnerability Mapping

As with many social phenomena, the research community has attempted to classify social vulnerability into indices and map it in order to be able to most effectively target areas through mitigation strategies. Mapping of this kind is what this thesis will aim to couple to a GFM.

The potential value of mitigation and good knowledge of disaster risk is well demonstrated, with the Sendai framework allocating $5bn of resources towards mitigation (UNDRR, 2015b). Good knowledge of the location of vulnerable populations is therefore necessary to maximise the effectiveness of this. A comparison between the effects of two cyclones in Bangladesh demonstrates the difference effective mitigation can make. Cyclone Phailin in October 2013 was of very similar intensity and location to a cyclone in October 1999 but killed only 47 people, as opposed to the 9843 people killed by the earlier event. Effective management largely lead to this improvement (GFDRR, 2013; UNEP, 2013). In a similar respect at present 82 countries have disaster loss databases and 2440 cities have programmes taking place to improve their resilience (UNDRR, 2015b). As well as helping governments in making wiser choices,

70-85% of investment is from the private sector (UNDRR, 2015a). This further suggests that good risk mapping has the potential to improve mitigation efforts since evidence is beginning to exist that private firms are accounting for natural hazard risk when making investment decisions (De Bono et al, 2013, Ingirige et al., 2014). Across a range of environments, an empirical approach has been recognised as important but efforts at mapping have largely used qualitative rather than quantitative methods (Siagian et al, 2014). A quantitative as opposed to a qualitative approach is necessary because it allows informal settlements to be mapped with consistency across environments. Techniques of indexing can also be classified as either deductive or inductive. Whilst inductive techniques rely on statistical relationships, deductive ones focus on a qualitative, theoretical understanding and a consultation of previous research and expert opinion (Yoon, 2012). The inventory method is an alternative approach which seeks to extrapolate future risk from past losses (Zeng et al, 2012). However, there are general problems with this method since it posits a reducibility of future hazards to past hazards which may not necessarily be valid, especially in informal settlements whose built environment can be very fast changing.

The most common (Fekete, 2019) method of creating a social vulnerability index independent of the level of development of the society in question is to use multi-variable, administrative level data, often from a census (Yoon, 2012, Armstrong and Larkin, 2019, Sahoo and Bhaskaran, 2018).

Some early seminal studies (Wu et al, 2002, Cutter et al, 2000) simply use the raw census data values, with the social vulnerability expressed for each variable in each district merely expressed as a ratio of the maximum in the study area. However, as a result of their crude methods these studies exhibit the purpose of demonstrating the value of GIS and mapping to disaster mitigation rather than creating indices which are usable, valid and accurate. As a result, instead the more commonly preferred option for creating indices is to perform a dimensional reduction using a principal components analysis, factor analysis or analytical hierarchical processing type procedure. This method reduces the census data into a more manageable and interpretable version in the form of a series of uncorrelated factors (Yoon, 2012, Zebardast, 2013). Hence, factor analysis of this kind "aims at finding a linear combination of variables that accounts for as much variation in the original variables as possible" (Fekete, 2009: 395). The loadings allow the relative contribution to be gauged of each factor towards the resultant social vulnerability (Clark et al, 1998). Detailed descriptions of the precise methodology are provided by Vyas and Kumaranayake (2006), Fekete (2012) and Yang et al (2015). The process

of performing the dimensional reduction begins with a consultation of the literature in question to decide which various should be included.

To create such social vulnerability indices most variables are household level aggregated to census tracts. Examples of such variables include proportion of female population (Morimoto, 2019), proportion of population in old age groups (Morimoto, 2019, Chakraborty and Mukhopadhyay, 2019), employment rate (Chakraborty and Mukhopadhyay, 2019), household tenure (Armstrong and Larkin, 2019), education levels (Armstrong and Larkin, 2019) and disabled population (Sahoo and Bhaskaran, 2018). Certain varibles are purely area level though, such as and medical facilities (Morimoto, 2019) and the availability of roads and rail networks (Sahoo and Bhaskaran, 2018).

The second stage of producing these maps involves data preparation such as checks for missing values (Fekete, 2012) and multicollinearity (Zebardast, 2013, Yang et al, 2015, Fekete, 2012). The usual next step is a z-score standardisation to make the variables directly comparable, making a multivariate analysis possible (Fekete, 2012, Yang et al, 2015, King, 2001). The factor loadings are subsequently computed, often involving varimax rotation. Next, in order to produce the final social vulnerability index the loadings must be combined. For this, often a weighting system is used to estimate the importance of each loading. However, there is no established way of doing this and often the weighting is simply derived from expert judgement, which as a method lacks a consistent, quantitative basis. Some however assume equal weighting to all factors (e.g. Cutter et al, 2003). If the intention is to use this index to produce a map at a given spatial scale, the weightings and factor loadings are applied to the raw data in each geographical unit to produce a map. Finally, a common practice among studies of this kind is to perform a sensitivity analysis usually using Monte Carlo simulations (Fekete, 2009).

A number of seminal studies have represented advancements in the research community's ability to map social vulnerability using a method along these lines. For example, a common problem identified by Clark et al (1998) is that data on natural hazards are aggregated to a resolution too coarse and they fail to take account of variation within demographics. As a result, the authors used factor analysis to group together variables from census data. This demonstrates the value of mapping how social vulnerability is spatially distributed and how the social vulnerability and exposure do not necessarily correlate. Moreover, the study using this methodology was able to highlight social vulnerability's commonly conceptually described holistic nature and that it cannot be reduced to any individual factor. A similar but more widely

used index, the Social Vulnerability Index, was developed by Cutter et al (2003) and this was among the first to receive widespread recognition and acclaim amongst the research community. This index incorporates a far more wide ranging set of indicators, which are argued to be generally agreed upon in the literature. Eighty-five variables from the US Census were dimensionally reduced to 11 factors using principal components analysis. At the county level, this managed to explain 76.4% of variance in all of the variables originally selected for the analysis. The dimensional reduction therefore at face value shows the percentage of the total variation in all the original variables which can be explained by the factors.

Attempts have also been made to incorporate other techniques into this basic system. Examples include analytical network processing to aggregate the variables into an index (Zebardast, 2013). Analytical network processing enables interdependence between the variables to be corrected for (Zebardast, 2013). With this methodology, the author repeated Cutter et al (2003) and their Social Vulnerability Index construction and achieved a strong correlation with their results. Decision tree analysis has also been applied in a similar way to measure the relative importance of different factors from the census tracts (Dwyer et al, 2004). Siagian et al (2014) use a hazards of place model (one which incorporates the interaction between physical and social vulnerability (Siagian et al, 2014)) to examine the relationships between physical and social contributors to vulnerability in districts in Indonesia. Here, factor analysis showed that 10 factors explained 72.5% of the variance. The most important factors found were socioeconomic status, infrastructure, gender, age, family structure and population growth.

Another technique commonly applied post-factor analysis is spatial modelling of these regions at the point at which they are produced. Generally, such a method used occurs when models of analysis, usually regression based, exhibit a spatial dependence or clustering. In social vulnerability studies, researchers have found evidence of spatial autocorrelation amongst these factor analysis derived administrative level social vulnerability values (Yoon, 2012, Zebardest, 2013). Spatial autocorrelation or in these cases positive spatial autocorrelation refers to a phenomenon whereby places nearer to each other have a tendency to be quantitatively more similar to each other. A not dissimilar pattern of spatial autocorrelation has been found at a township level in Taiwan (Lin and Hung, 2015). As well as applying a technical correction to any modelling, spatial analysis of this kind can be of substantive value in identifying geographical patterns in social vulnerability after factor analysis has been carried out.

The technique has also been applied to low and middle income countries such as Bangladesh (Ahsan and Warner, 2014). This study however suffers from a key drawback very similar to many studies of this sort in that it is reliant on a choice of factors gauged from expert opinion which lacks a consistent, quantitative basis (Cutter and Finch, 2008). Similarly, it can be argued that as a result, seemingly robust quantitative methods are actually highly subjective in their constitution (Nardo et al, 2005, Fekete, 2011). Additionally, subjectivity can enter the scientific method through the omitted variables, meaning any dimensional reduction type study will always represent a reductionist, oversimplification (Cutter, 2003).

1.4.2 Shortcomings of Current Methods

A number of problems exist with the aforementioned dimensional reduction based approach however. First, typically the administrative regions used in this construction are of a coarse spatial resolution and undergo too greater aggregation (Fekete, 2012, King, 2001), with the spatial resolution being limited by the size of the tracts where the data originally came from. This is in contrast to GFMs, which can have spatial resolutions less than 100m (Sampson et al, 2015, Bernhofen et al, 2018). This makes using this approach problematic as a means of being a social vulnerability layer to a GFM.

Dasymetrically disaggregating such data to grids appropriate for combining with flood inundation data has been performed to attempt to address this issue, based on remote sensing such as land cover class (Amadio et al, 2019) and population density (Amadio et al, 2019, Armstrong and Larkin, 2019). Often however, the variables used to disaggregate social vulnerability are insufficient to act as an indication bearing any resemblance to social vulnerability itself.

Although this represents an improvement over the traditional dimensional reduction method, often the variables used to perform the disaggregation are insufficient to be representative of social vulnerability at a spatial scale smaller than that from which the census data were originally derived. As a result therefore, the effective spatial resolution of these methods is no different to before the dasymmetric disaggregation was performed. The assumption that the final disaggregated data will be representative is dependent on the assumption of the original census tracts themselves being representative.

Often geospatial data on fatalities which have the potential to be good additions suffer from a similar problem, with National Climatic Data Center records on flood fatalities in the United

States only having a spatial resolution of 40km (Ashley and Ashley, 2008). In Buzi, Mozambique Kienberger (2012) maps social vulnerability at sub-administrative boundaries in what is referred to as the Conceptual Geon Approach. Like many other methods described here however, there is an over reliance on expert opinion in its construction and they as a result are subjective and not a fully quantitative method. I argue that methods which weight factor loading simply according to expert judgement or literature consultation can lack an empirical basis and therefore, validity in a quantitative setting. Methods featuring these can lack a sound evidential basis for mapping phenomena such as social vulnerability. The lack of an empirical basis of these social vulnerability maps also makes them incompatible with GFMs, which are definitionally strongly quantitative in nature.

In a similar respect, using administrative regions such as these means the technique can suffer from the modifiable areal unit problem (Fekete, 2012). The modifiable areal unit problem is where the results of a spatial analysis vary because the spatial units used in that analysis are defined arbitraily with an , with a possible example being census tracts (Fotheringham and Wong, 1991). Schmidtlein et al (2008) give an example of this. Here the authors aggregated social vulnerability in 54 different combinations of spatial patterns in Los Angeles, New Orleans and Charleston, South Carolina. The resultant loadings from the factor analysis differed depending on how the population statistics were aggregated (Schmidtlein et al, 2008).

Crucially also, up until now the social vulnerability indices of this kind have neglected the context behind each social vulnerability factor, in particular the stage of the hazard in which they are of influence (Rufat et al, 2015).

Whilst dimensional reduction approaches have the advantage of accounting for social vulnerability's multivariate nature by including so many variables (Fekete, 2019), there is too much focus on individual or household level variables. Most census data included do not include any factors representing community level characteristics. At the preparation, response and recovery stages of disasters the community level is an important determinant. This is because many mechanisms of flood mitigation at these stages is carried out through community co-operation, such as digging ditches, and the sharing of information on responses, as Section 1.3 outlined.

The use of an area-based method is necessary and aligns conceptually with the idea of social vulnerability because it is a place-based concept which the pixel level approach is incapable of representing in a quantitative way (Cutter et al, 2003, Birkmann, 2005b, King, 2001).

It has also been criticised for its reductionism and oversimplifying of the social vulnerability phenomenon. On this premise any index produced using this method is incapable of fully describing the phenomenon's holistic and multivariate nature (Romero-Lankao et al, 2016).

Furthermore, sometimes the dimensional reduction type methodology can combine together variables which may be interpreted as belonging to the same category but in fact in reality have little in common, with age and income being examples (Fekete, 2012). This lacks interpretability and validity. In this respect, there has been a tendency to simply use large datasets such as censuses because they are an easy, readily available source of data, regardless of whether they hold any true value in social vulnerability mapping (King, 2001). For example, in most censuses data describing the built environment or buildings are non-existent (King, 2001).

Second, usually studies of this sort do not attempt to cross validate these indices of social vulnerability with any actual geospatial data on losses or injuries. Only a few examples exist where this has been attempted. Yoon (2012) uses SHELDUS geospatial county level loss data to help overcome this problem and used 196 counties along the south and east coasts of the United States as an example. SHELDUS (Spatial Hazard Events and Losses Database for the United States) is a database of county level losses for 18 different natural hazard categories (Yoon, 2012). Databases such as this however are rare in low and middle income countries with which to do similar validations. A validation is attempted by Cutter et al (2003) featuring the social vulnerability of the county in question and the probability of a presidential declaration of a state of emergency. This however is an inappropriate form of validation due to the coarse spatial scale of the areas which the declaration correspond to.

Yang et al (2015) perform a validation using data from China's statistical yearbook as part of a factor analysis based study to find that Western Chinese provinces had populations who were more socially vulnerable in the East, albeit with a decreasing trendover time. Fekete (2009) validates his study of this kind using data from the Centre for Geosciences Potsdam after dimensionally reducing 41 variables and validating the most significant based on a logistic regression describing the probability of those individuals having to leave home. Such examples

are an exception however (Fekete, 2009). Instead, the research community has focussed extensively on analysing sensitivity in social vulnerability where socioeconomic data are richly available. Part of the reason that Monte Carlo based sensitivity analyses are popular among researchers is the fact that validation data representing actual losses are not widely available and thus the simulations are used to compensate (Fekete, 2009).

Another weakness of dimensional reduction type methods is their dependence on reliable data existing in the census tracts. For informal settlements often this is not the case (Kohli et al, 2012, Taubenbock and Kraff, 2014, Zeng et al, 2012). As their name suggests, environments such as these are usually not included in official socioeconomic data collection routines, such as the census (Wardrop et al, 2018), or if there are censuses they frequently undercounts informal settlement dwellers (Carr-Hill, 2013, Maluleke and van Eeden, 2013), particularly at rural-urban interfaces (Simon et al, 2004). Undercounts can happen for a variety of reasons, including deliberate omission by authorities (Maluleke and van Eeden, 2013), the suspicion of officials by informal settlement dweller populations (Carr-Hill, 2013) and implementation difficulties in identifying and documenting all dwelling due to their disorganised nature (Carr-Hill, 2013, Maluleke and van Eeden, 2013). Yet informal settlements are among the places with populations most socially vulnerable to flooding (Rufat et al, 2015) As a consequence, a "perfect storm" exists whereby informal settlements are among the most socially vulnerable environments, but yet there is a lack of data with which to study them and implement mitigation measures. Throughout this thesis, this will be referred to as the "informal settlement data problem".

Typically, researchers' best attempts to solve the informal settlement data problem involved in-situ or participatory methods. This usually involves household surveys and/or interviews with important actors such as local planners and the head of NGOs. With data being collected either for specific studies (Alizadeh et al, 2018, Imran et al, 2019, Musungu et al, 2012) or using pre-existing household surveys.

Participatory mapping of social vulnerability brings with it an important advantage over the dimensional reduction approach. This is an ability to account for the subjectivities and experiences of informal settlement residents and how these contribute to the social vulnerability of the community for (Borie et al, 2019a, Loggia and Govender, 2020). Many methods have been employed by these studies to accomplish this. Participatory methods have involved both quantitative methods such as mapping and enumeration and qualitative methods

such as structured interviews and focus groups with important stakeholders such as community leaders, the heads of NGOs and local governors (Usamah et al, 2014, Williams et al, 2019, Borie et al, 2019a, Borie et al, 2019b). In addition, as well as combing these in order to integrate the complex interactions between social vulnerability and its interaction with natural hazards (Salami et al, 2017).

Quantitative assessment can involve an assessment of specific determinants to flood risk such as open sewers (De Brito et al, 2018), drainage infrastructure (Taylor et al, 2020) and the sites of past flooding (Borie et al, 2019a). Researchers can also integrate into their mapping studies the residents' perception of their own risk and resilience in order to produce final maps which are more informed (Loggia and Govender, 2020).

Often studies of this kind involve expert opinion, in particular on choosing how variables and mapping methods should be chosen (de Broto et al, 2018, Salami et al, 2017). For de Broto et al (2018), incorporating the views of experts from a variety of field such as geography, social science, civil engineering and psychology, this brought with it the benefit of giving the participatory mappers more confidence in the method (De Brito et al, 2018).

Methods such as these can give detailed maps of amenities and resources specifically related to adaptive and coping capacity such as healthcare facilities (de Brito et al, 2018) and sanitation services and stormwater management (Williams, et al, 2019). On top of this, resources may be mapped which are indicative of an ability to do this such as savings (Williams et al, 2019) and the sources of income people depend on for their coping strategies (Usamah et al, 2014), as well as vulnerable fixed capital (Usamah et al, 2014).

The participatory approach and collaboration with the local community allows the incorporation of many of the factors which are subjective and contribute to social vulnerability's complexity (Salami et al, 2017, Williams et al, 2019, Borie et al, 2019a, Borie et al, 2019b) such as institutional trust (Usama et al, 2014, Loggia and Govender, 2020) and strengths of social networks (Usamah et al, 2014, Taylor et al, 2020).

Participatory methods have also been combined with a dimensional reduction approach, where the index is constructed from the mapped variables (de Broto et al, 2018). Also combined with remote sensing, but in a cost-inefficient way using drones (Loggia and Govender, 2020).

Participatory methods can allow surveyors to precisely and accurately define the locations and boundaries of informal settlements. However, such methods have a number of shortcomings. First, they are labour intensive, costly and quickly lose validity and become out of date in these fast-changing environments (Busgeeth et al, 2008, King, 2001). This, combined with the fact that the specifics of how social networks manifest and influence social vulnerability vary on local scales (Simon and Leck, 2015), make the benefits of these methods hard to replicate on large scales. Additionally, informal settlements are often difficult or dangerous to access (Busgeeth et al, 2008). Furthermore, such methods will often be inconsistent in their methodologies, since different researchers in different places will struggle to carry out surveys identically (Preston et al, 2011). As a result, household surveys are often only made up of a small sample size which can mean inaccurate measurements, especially as lower socioeconomic groups are more likely to be excluded from samples (Vyas and Kumaranayake, 2006). Here, I argue there exists a methodological mismatch between data rich and data poor environments, since concern over the sensitivity of a social vulnerability index in an informal settlement is negligible compared to the data deficiencies regarding small sample size and measurement error.

As Section 1.1 highlighted, the benefits of mapping flood risk using GFMs are its global coverage and consistency across space. Participatory methods which lack coverage due to being too labour intensive to collect, and have divergent methods in different environments are as a result wholly unsuited to being coupled to GFMs.

1.5 Potential Solutions to These Problems

1.5.1 Remote Sensing as a Solution to the Informal Settlement Data Problem

Many authors have recognised that a solution to the data poverty of informal settlements lies in remote sensing, since it provides a relatively easy, temporally resolute and consistent method of gathering data about cities and it represents a consistent methodology across space (Sudmanns et al, 2018, Taubenbock and Kraff, 2014, Geiss and Taubenbock, 2013), meaning that it is not subject to the modifiable areal unit problem experienced by census dimensional reduction studies and the inconsistency of participatory methods.

I argue that detecting informal settlements using remote sensing represents an improvement over the dasymmetric methods mentioned in Section 1.4.2. This is because as a remotely sensed variable, the presence of informal settlements communicates social vulnerability relative to the variables used for the disaggregatation. This is in spite of the fact that the detection of informal

settlements represents a more one-dimensional approach to dasymmetrically disaggregating census data based on many remotely sensed variables, such as land use and population density (Sudmanns et al, 2018, Taubenbock and Kraff, 2014, Geiss and Taubenbock, 2013).

Satellite imagery is also well established for analysing urban environments, with the most basic form being the classification of areas of a city according to land use also to identify buildings (Zhu et al, 2017). The high spatial resolution of remote sensing data is also advantageous to traditional social vulnerability mapping studies which are derived from census data, where the spatial resolution is dictated by the size of these census tracts, as discussed in Section 1.4.2. Remotely sensed data may therefore be more appropriately attached to GFMs.

A literature has developed around analysing how remote sensing can useful as a proxy for people's socioeconomic circumstances. By extension these could be used to produce remotely sensed maps of social vulnerability, with some having produced "ontologies" describing what proxies can be detected using remote sensing. The detection of informal settlements forms a particular part of this. Kohli et al (2012) provide an ontology of informal settlements in terms of how algorithms applied to satellite imagery can help detect informal settlements. Data on the shape, building density, location and building characteristics such as height and number of floors are examples given. Similarly, a literature review by Owen and Wong (2013) found that informal settlements have a tendency to exhibit dirt as opposed to impervious surfaced roads, greater textural contrast, less vegetation and lower road accessibility and have roofs with a spectral profile which can be used to detect that the settlements are informal.

A variety of factors, such as socioeconomic status, lack of planning and poor quality and housing have been established as making informal settlements environments which are particularly socially vulnerable to flooding. This, combined with the fact that they are easily identifiable using visible light satellite imagery in a way which is consistent across space, easy to collect and repeatable, presents the opportunity for these to be mapped and for this to constitute the desired social vulnerability layer of a flood risk map.

Many countries have in place frameworks for informal settlement improvement as a means of hazard mitigation and as a result such risk maps have great potential to reduce risks to natural hazards if measures such as these can be targeted to the most vulnerable people (UNDRR, 2015a).

Whilst the recognition of remote sensing as the solution to the informal settlement data problem has been suggested, traditional methods of detecting informal settlements using remote sensing are problematic. Often such methods involve a two-step process of feature extraction and subsequent classification (Wu et al, 2018a, Wurm et al, 2019). Such methods also often involve the pre-defined setting of "free parameters" which usually must be set based on prior experience (Kuffer et al, 2018, Persello and Stein, 2017, Mboga et al, 2017). Many of the methods, including GLCM and local binary patterns, have been described as "hand crafted" (Mboga et al, 2017, Wu et al, 2018b) which means that they are tailored for the detection of specific types of pattern in images rather than patterns in general (Nanni et al, 2017). Optimising these methods for general tasks as a result requires significant trial and error (Ajami et al, 2019, Wu et al, 2018b). As a result, the research community has struggled to fully automate methods of mapping informal settlements using these more traditional methods (Quinn et al, 2018).

The semi-automatic nature of these methods as a result makes them problematic for the ultimate objective of this thesis of developing a method of mapping informal settlements suitable to being a social vulnerability layer for a global flood risk map. If any such method of flood risk mapping is to be cost efficient more automatic methods of detecting informal settlements are a necessity.

1.5.2 Computer Vision and Neural Networks

The research field of computer vision is concerned with such a task of developing methods of image recognition to recognise patterns and objects to mimic human vision (Meer, 2004). It is this field of research which I turn to in this thesis in order to solve the problems with traditional methods of identifying informal settlements discussed in Section 1.5.1.

In the 1980s the development of neural networks showed great promise of revolutionising the field of computer vision. Many anticipating that neural networks would be the first reliable computer vision method which could perform image recognition to a skill comparable to human vision. They are referred to as neural networks because they aim to imitate how the human brain processes information in order to perform tasks (Zhang, 2016, Cross et al, 1995).

Described in more detail in Section 2.3.1, a neural network is a machine learning based algorithm where many data points called neurons connected by weights and biases are used to process information (Cross et al, 1995). Using a loss function measuring badness of fit, the network uses a dataset of images to adjust the weights and biases in order to improve its

accuracy (Nielsen, 2017). The process of the adjustment of these weights and biases to make the network able to perform image recognition is known as training.

The nature of a neural network as being able to analyse all pieces of information in relation to all others using neurons marks neural networks as unique in their ability to perform tasks requiring an analysis of complex, intricate patterns in high-dimensional data (LeCun et al, 2015). However, such excitement quickly waned as researchers attempted to enable their networks to perform more complex classification tasks by taking the logical step of increasing the number of layers to carry out more complex analysis. Researchers found that doing this to a neural network simply makes it harder to train, known as the vanishing gradient problem (Nielsen, 2017), which will be explained in more detail in Section 2.3.1. As a result, neural networks were largely abandoned in the 1990s by researchers as lacking further potential (LeCun et al, 2015).

As a result, early attempts at applying a quantitative approach to derive socioeconomic information using satellite imagery avoided these neural network type algorithms.

1.5.3 Deep Learning

Two developments however since then have enabled neural network type algorithms to once again become promising for computer vision tasks. The development of a number of techniques have allowed the training of neural networks with a greater quantity of layers, known as "deep learning" (Nielsen, 2017, Albawi and Mohammed, 2017). In particular, the development of Convolutional Neural Networks (CNNs), Deep Belief Networks and Restricted Boltzmann Machines around 2006 helped to overcome the vanishing gradient problem (LeCun et al, 2015, Liu et al, 2017, Albawi and Mohammed, 2017).

Additionally, since 2000 there has been rapid development of powerful GPUs (Graphics Processing Units), in particular by the United States graphics company NVIDIA (Zhang et al, 2017a). Best known for their application to video gaming, GPUs are also ideally suited to the fast training of neural networks and this has enabled the training of such neural networks between 10 and 20 times faster (LeCun et al, 2015).

These developments, in particular CNNs, are greatly responsible for the increasing awareness at a popular level of what is referred to as "artificial intelligence" in recent years. Technologies such as driverless cars (Liu et al, 2019, Fayjie et al, 2018, Lipson and Kurman, 2016), smart phones which unlock upon recognising the user's face (Datalya, 2017, El-Din et al, 2020) and

the automatic tagging of user's in photos on social media (Jang and Cho, 2016) are all examples of "artificial intelligence" which use CNNs.

As well as these well-known examples, in recent years the usage of CNNs to perform computer vision tasks with remotely sensed data has increased dramatically in performance of a wide variety of tasks. CNNs have for example been successfully used to detect land use, buildings (Zhu et al, 2017), crop types (Kussul et al, 2017), ships (Sharifzadeh et al, 2019), impervious surfaces (Huang et al, 2019), algal blooms (Yabin et al, 2018), vegetation coverage (Nijhawan et al, 2017) and car park occupancy (Ammour et al, 2017).

The approach taken by this thesis will as a result be to use deep learning to map informal settlements as a proxy for social vulnerability and to attach this to the output from a GFM. Since this thesis is methods focussed, I will apply this approach to a particular city in order to be able to specifically assess the applicability of such a procedure and to inform efforts to replicate it on larger scales.

Uses of Deep Learning in Flood Risk Management

In the field of flood management and mitigation research however the benefits of deep learning have largely focussed on the post-event detection of flooded areas and damage assessment (Yang and Cervone, 2018, Nogueira et al, 2018, Gebrihot et al, 2019) instead of the pre-event flood risk mapping which I am aiming to do in this thesis. The monitoring of floods is crucial to enable effective responses and for the planning and mitigation of future flooding events (Nogueira et al, 2018). As a result, deep learning-based post event flood detection using remotely sensed data has a role to play in effective flood risk mapping.

Yang and Cervone (2018) perform image classification of flooded areas in Texas in 2015 with an 84% accuracy using a deep learning ensemble method. Gebrhivot et al (2019) apply method detection methods to map three different flooding events North Carolina between 2016 and 2018. Nogueira et al (2018) demonstrate the possibility of performing such classifications using a range of different network architectures.

Although these studies are aiming to measure something fundamentally different than what I am in this thesis, the strengths of studies such as these have applicability to pre-event flood risk mapping which I am aiming to do in this thesis. These strengths are the large amount of information which remote sensing consistently provides both spatially and temporally (Yang and Cervone, 2018) the availability of remotely sensed data (Bischke et al, 2017) and deep

learning's ability to perform high level hierarchical abstraction of remotely sensed images (Yang and Cervone, 2018, Gebrhivot et al, 2019, Nogueira et al, 2018, Mboga et al, 2017, Persello and Stein, 2017).

Informal settlements may be mapped using remotely sensed data due to their unique visual characteristics, as discussed in Section 1.5.1. Many of the benefits of deep learning for post-event flood detection are applicable to such mapping, such as its spatial and temporal consistency. There is at present a dearth of studies however using deep learning in the field of mapping flood risk prior to the event, which this thesis will attempt to do.

Another key flaw in many social vulnerability mapping studies is they neglect to include physical hazard layers to their maps based on an actual physical flood model. Instead, many studies use remotely sensed or other raster data of physical factors contributing to flooding, such as distance from a river, slope and amount of precipitation. From these, they construct a flood hazard index using a similar method to their social vulnerability layer (Sahoo and Bhaskaran, 2018, Danumah et al, 2019, Hategekimana et al, 2018) and one study relies on informal dwellers eyewitness accounts to produce their hazard layer (Taylor et al, 2020).

This thesis in Chapter 4 will replace a flood hazard layer of this kind with a more representational physics based GFM. Not only does this have a stronger scientific foundation than one based on statistical weighting, but it is able to produce more interpretable outputs instead of a heuristic index only able to measure the flood risk in relative as opposed to absolute terms.

1.6 Background of Flooding in Cape Town

An urban environment represents the ideal place to develop and test a new risk mapping method. This is due to the high population densities in these environments and consequently large concentrations of people exposed to flooding (Hallegatte et al, 2013) and the need for flood risk mapping is as a result highest in these environments (Fewtrell et al, 2008). In particular, the presence of informal settlements is common in large cities in low and middle income countries due to large rates of rural-urban migration (Musungu et al, 2012). Large cities are additionally set to have their level of exposure to flooding increase by 2050 due to this population growth (Hallegatte et al, 2013). Methods of detecting informal settlements using deep learning are also most common well developed in cities (e.g. Helber et al, 2018, Gadiraju et al, 2018, Gram-Hansen et al, 2019). The nature of flooding in Cape Town was a large part

of the reason the city was chosen as a case study in this thesis.. In Cape Town, flooding is a frequent problem, particularly in its informal settlements (Ziervogel et al, 2016, Goncalo et al, 2007, Holloway et al, 2008) due to its winter storms, frequently heavy rains, steep mountain slopes and large amounts of low lying land (Ziervogel et al, 2016, Goncalo et al, 2007, Desportes et al, 2016). According to OpenUp (2017), there are 437 informal settlements in the Cape Town area, many of which flood every winter (Divdal, 2011). The city is for example referred to as the "Cape of Storms" (Holloway et al, 2008: 115) and the effects of climate change are likely to make such storms more severe in the future (Holloway et al, 2008).

Informal settlements are widespread in Cape Town due to high levels of rural-urban migration (Musungu et al, 2012), which has been a particular problem in South Africa (Armitage et al, 2010). The municipal authorities struggle to keep pace with the rate of rural-urban migration in their provision of services and infrastructure (Holloway et al, 2008, Ziervogel et al, 2016). Most informal settlements in Cape Town are only provided with communal sandpipes and a limited number of toilets which are often unreliable (Armitage et al, 2010). The Cape Flats in particular is home to a large number of the city's informal settlements (Drivdal, 2011) and 88,000 informal settlement households (Despotes et al, 2016).

Many informal settlements are located in marginal areas which are exposed to flooding on sandy waterlogged soils (Musungu et al, 2012, Ziervogel et al, 2016, Holloway et al, 2008) where the water table is high (Dridval, 2011). Here drainage is poor due to clogged drain ditches and dwellings in informal settlements are made of poor materials (Holloway et al, 2008, Drivdal, 2011, Ziervogel et al, 2016). A survey by Musungu et al (2012) found 83% of people in three informal settlements had experienced flooding. There are many prominent case studies of flooding disasters in Cape Town's informal settlements. In 2007 for example, 38,000 people were impacted by flooding, mostly in informal settlements (Goncalo et al, 2007).

A key reason for social vulnerability being high in informal settlements is due to political apathy from municipal authorities, which can exist in the form of the ignorance on the part of municipal authorities regarding the lived experiences and subjectivities of local individuals (Pelling, 1998, Wisner et al, 2004, Tas et al, 2013). As a result, people are forced to pursue their own mitigation strategies with limited knowledge about how to do this most effectively. (Tas et al, 2013).

There is evidence that these factors are especially prominent in South Africa and in Cape Town in particular due to political reasons. Many informal settlements originated as a result of racial

segregation form the apartheid regime before 1994 (Goncaolo et al, 2007). Since 1994 the mistrust between residents has remained, with a sense that the municipal authorities have not done enough to improve their living conditions (Drivdal, 2011). Often residents are not consulted about improvements (Desportes et al, 2016) and authorities regularly blame residents for their plight, such as accusing the laziness of residents for there being poor drainage (Desportes et al, 2016). This means attempts to provide services by the municipal authorities are frequently ineffective (Armitage et al, 2010, Ziervogel et al, 2016, Musungu et al, 2012). A case study of this is described by Armitage et al (2010), who examined attempts by authorities to install improved sewerage in the Kosovo informal settlement in Cape Town. This upgrade programme failed due to allegations of sabotage by the authorities. Additionally, it also had inadequate capacity and the authorities failed to sufficiently communicate how the system worked.

The holistic nature of social vulnerability and its many interlinked factors operating on many spatial scales requires a collaborative approach to solving the problems associated with the informal settlements between both dwellers and municipal authorities (Ziervogel et al, 2016). This is widely recognised as important for effective flood risk management in informal settlements. Due to the political apathy and mistrust mentioned previously, this is particularly difficult in Cape Town. Additionally, the agencies in charge of flood mitigation in Cape Town however are fragmented in their approach and are often unsure of their responsibilities (Desportes et al, 2016) and their mentalities contrast (Ziervogel et al, 2016). As a result, interventions by authorities are ineffective (Ziervogel et al, 2016).

From a perspective of validating an informal settlement map produced from the FCN, the city has well mapped informal settlements with which to perform such a validation. An example is a dataset mapped by non-profit civic technology lab organisation OpenUp. Such a dataset provides the possibility of evaluating the number of sizes of predicted informal settlements.

In this thesis the city of Cape Town is as a result selected as a test case to develop and test a method of mapping social vulnerability by detecting informal settlements, to be subsequently coupled to a GFM.

1.7 Informal Settlement Data

Section 1.4.2 highlighted the benefits of participatory methods, but the problem with these is they are extremely labour intensive to collect. It as a result makes sense to use a participatory

dataset to train the FCN because it is unconstrained by access to labour or resources. The benefits of participatory data are still incorporated however because the accurate defining of the boundaries of informal settlements helps in optimally training the FCN.

This study as a result uses an example of such a participatory dataset, Know Your City, which comes with spatial coordinates which precisely define the edges of each individual informal settlements.

Know Your City is a unique community-based dataset derived from Slum/Shack Dwellers International (SDI, 2019)[1]. SDI is a network of community organisations – mainly informal settlement federations in cities across the developing world who partner with municipal authorities with the aim of improving living conditions in these settlements. Founded in 1996 (SDI, 2017) through a process of exchange between communities in Africa and Asia (d'Cruz et al, 2009), SDI is a collection of associations between local authorities and informal settlement dweller federations in more than 100 cities across the Global South (Byrne et al, 2018), and it consists of over one million informal settlement dwellers (SDI, 2017). Know Your City is a programme launched in 2014 (Dobson, 2017) within SDI which aims to perform settlement profiling, mapping and enumeration (SDI, 2018). The mapping has the aim of encouraging informal settlement upgrade policies by recognising people's needs and managing these environments in the anticipation of future population growth (Tomlinson, 2017, SDI, 2018, Byrne et al, 2018, d'Cruz et al, 2009). Often the aim of the mapping is to secure the residents' tenure (d'Cruz et al, 2009) and remove the threat of eviction (Dobson, 2017).

Specific data collection for individual informal settlements is initiated by an expression of interest by the local communities to the authorities to form a relevant informal settlement dweller federation. Regularly this initiation begins with local savings groups (d'Cruz et al, 2009). SDI next carry out a readiness assessment and the data collection teams are comprised from both the community and the municipal authorities with appropriate training, with data verified by third parties (Byrne et al, 2018). Mappers are trained to use GPS units to define accurate informal settlement boundaries (Dobson, 2017, Tomlinson, 2017). The mappers are additionally trained to use walking papers (which are papers designed to allow mappers to visually represent settlements diagrammatically on paper, Makau et al, 2012). Robust results are ensured through both the municipal authorities and informal settlement federations signing

[1] I was informed by email correspondence that SDI had a policy of not sharing large datasets with external parties. However, on 5th March 2019 I was given permission from SDI to reference any data on knowyourcity.info.

off the final maps (Makau et al, 2012). One can therefore have a high degree of confidence in the boundaries of informal settlements being defined accurately. The drawing of outlines is typically followed by shack counting and enumeration to gauge the socioeconomic conditions within the settlement. The federative nature of SDI allows informal settlement groups to learn from previous mapping and enumeration efforts by different informal settlement groups (Makau et al, 2012).

Part of the justification for Cape Town as the case study this thesis will use is not just because of its propensity for flooding in its informal settlements but because good data in the Know Your City dataset exists. In Cape Town there are 75 informal settlements in the Know Your City dataset. As a result of good data on informal settlements existing in Cape Town, no field work was carried out and the study exclusively used secondary data without any local research partnership involvement.

In particular in Cape Town, South Africa, the SDI federation are working to use the mapping to improve urban resilience to natural hazards through informal settlement upgrading and to enable researchers to assess the risks in their locations (Byrne et al, 2018, Adelekan et al 2015, Pelling, 2018, Dobson, 2017). In seeking to use these data to map social vulnerability, a conceptual alignment is therefore created from what the data were originally intended to demonstrate and what this research attempts to map.

Additionally, each informal settlement contains socioeconomic data describing attributes relevant to informal settlement improvement programmes and various other amenities, such as population density, access to electricity and clean water and quality of infrastructure. Consequently, SDI data have the potential in the future to be able to train CNNs to recognise more vulnerable from less vulnerable informal settlements, something at present not utilised by similar studies. SDI has however up until now not been used by the research community performing such mapping tasks. Data from SDI therefore represent an excellent opportunity for the research community to make progress in this area.

The community level is a storng determinant of social vulnerability. As a result, in mapping informal settlements as a proxy for social vulnerability, an additional key benefit of the SDI dataset is its concurrence with communities themselves because the mapping and enumeration is community-based (Ley, 2019, Makau et al, 2012, Satterthwaite, 2020). The final polygons represent mappers self-defining their own communities, without social and spatial structure being determined from above (Dobson, 2017). Since it is mapped by the local people it gives

unique insight as to what the community is (Mitlin, 2008, Adeleken et al, 2015), with particular relevance to the experiences of those doing the mapping and defining their community accordingly (Dobson, 2017).

In conjunction with this particular advantage of Know Your City data, the mapping performed by the communities creates an "observer effect". Here, the settlement mapping and enumeration of communities by itself strengthens those communities and creates stronger social networks. This implies improved future participation, both in the mind set and capacities of the community (d'Cruz et al, 2009, Makau et al, 2012) as well as enabling the community to greater understand their own internal social structures (Makau et al, 2012). As a result, the existence of a mapped SDI neighbourhood by itself indicates a cohesive community which is conceptually relevant to the social vulnerability being studied.

The combined benefits of community based and local authority mapping is summarised and defined by Mitlin (2008) as co-production, whereby the mapping combines the central planning and resources from the authorities with local knowledge to best represent the processes existing in those communities (Satterthwaite, 2020). Such a setup regularly creates a positive response from the local people to map their settlements when the authorities are enthusiastic (Mitlin, 2008). Often, local people are suspicious of purely top down mapping approaches taking place due to fears that its purpose is to evict them (Mitlin, 2008, Satterthwaite, 2020, Makau et al, 2012). The Know Your City methodology removes any suspicion on behalf of the informal settlement dwellers regarding the motivation for the mapping taking place because it is such a joint venture.

Despite the benefits of utilising community-based mapping, the approach risks settlements being poorly drawn due to potential vested interests in the data collection process. Frequently the purpose of the mapping and enumeration is the enabling of informal settlement upgrading (Byrne et al, 2018, Adelekan et al 2015, Pelling, 2018, Dobson, 2017). As a result, the community carrying out the mapping are likely to perform mapping to maximise benefit to them rather than what best spatially reflects their community (Makau et al, 2012). The consequences for informal settlement mapping however are likely to be limited to the enumeration rather than spatial aspect of the data collection as the enumeration is what best represents the specific conditions inside the settlement.

1.8 Literature Review Summary

The main identified gaps in this literature which this thesis will address will now be summarised. GFMs have a human component which is designed to measure propensity for financial loss from flooding rather than fatality and human suffering. Methods of developing social vulnerability maps on large spatial scales have usually used a dimensional reduction type methodology. And for a number of reasons these are unsuited to acting as the social vulnerability layer for a GFM. First, they use spatial units from official datasets such as censuses which are not congruent to that of GFMs which produce gridded outputs. Second, they are dependent on official datasets which may undercount or exclude informal settlements, which are considered the most socially vulnerable environments. Third, these methods include a component of expert judgement which represents a methodological mismatch with the GFMs themselves, which are strongly quantitative in nature. Whilst these problems with social vulnerability mapping some have attempted to solve using participatory methods, these are impossible to replicate on large spatial scales in a cost effective way using a methodology which is consistent across space.

1.9 Thesis Chapter Organisation

The main gaps in the literature and current problems with social vulnerability to flood risk mapping have now been identified and the next step in this thesis is to outline the steps to be taken in filling these. The final aim of the thesis is to develop a method of mapping social vulnerability to flooding by detecting informal settlements from remotely sensed data using deep learning. This method will be developed across three research chapters with a concluding chapter summarising the contributions made with suggestions for further research given. The remainder of Chapter 1 overviews each of these research chapters.

The thesis will use a combination of a monograph type structure and a by article structure. It contains a detailed introductory chapter (Chapter 1) which lays the theoretical foundation of the work and justifies the choice of methods but at the same time three empirical chapters where each has an additional description of the methodology and each research chapter builds upon the previous.

This is used in this thesis because the concept of social vulnerability and the factors which contribute to it need to be explored in depth in order to lay a theoretical foundation for it to be empirically measured. In addition, two central dependencies of the empirical work are that

informal settlements are both detectable in satellite imagery and are a proxy for areas with socially vulnerable populations. A large amount of theoretical work is needed to justify these two assumptions.

However, it makes sense to use a paper based structure thereafter because each individual chapter builds on each the previous, yet each uses a specific methodology and makes standalone contributions by itself as well as to the thesis as a whole.

Chapter 2 aims to develop a method of detecting informal settlements in Cape Town using deep learning. This chapter aims to fill gaps in the literature on the detection of informal settlements as well as contribute to the ultimate aim of the thesis of producing a method of flood risk mapping. The U-Net CNN is used due to its ability to make accurate predictions with small sample sizes and imagery from Google Maps is used because it is freely available and so is suited to a cost-efficient method of risk mapping. The method is fine-tuned and is then scaled up beyond the original set of images to the whole of Cape Town so that it can be used to create a flood risk map later in Chapter 4, in line with the objectives of the thesis as a whole. This research uses a pixel-based approach. This means the pixel is used as the basic unit of analysis in its production of outputs and the measurement of its accuracy. Once the method has been fine-tuned 1100 pixelated outputs in total are produced for analysis in further chapters.

Chapter 3 in this thesis will build upon the outputs of Chapter 2 to expand upon the methodology by building upon the pixel-based approach used. Social vulnerability is a complex, holistic entity where the community level is a determinant. It is therefore which is hard to quantify at a pixel-level (Cutter et al, 2003, Birkmann, 2005b, King, 2001) in the way that Chapter 2 used for informal settlements. As a solution, Chapter 3 takes the 1100 fine-tuned test set outputs from Chapter 2 and converts them from pixel-based outputs to area-based outputs. A combination of the Canny edge detection algorithm and contouring are used to produce these areas. Although the main evaluation metrics used are the Jaccard Index and the F1-score, in line with the conceptual benefits of area-based compared to pixel-based methods, area-based evaluation metrics are used. These are the relative position and the area-perimeter ratio. The method is fine tuned in a similar way to Chapter 2.

Chapter 4 integrates the detection of informal settlements in Chapters 2 and 3 with physical flood modelling in Cape Town to produce a complete methodology of mapping flood risk. Section 1.1 described how the human component of global flood risk maps is designed to

measure economic loss of floods through population disaggregated income. This traditional method is compared and contrasted with the new methods developed in this thesis to assess the new methods' potential for mainstream adoption. This comparison uses a physical hazard layer in the form of the output form the Fathom Global Flood Model Version 2. The High Resolution Settlement Layer (HRSL) created by a partnership between Columbia University and Facebook Connectivity Lab is used as the gridded population dataset with which to perform the comparison. Using the different methods a number of separate flood risk maps are produced. A series of maps are also produced which directly compare how the different approaches spatially allocate risk differently to inform future efforts to produce vulnerability-based maps. A successful demonstration of the value of this approach would lend credence to new attempts at accurately mapping the spatial distribution of socially vulnerable populations.

Chapter 5 concludes the thesis and overviews the research contributions made by each of the chapters and makes recommendations for future research. It gives suggestions of how future research can use the new techniques to both improve the accuracy and results of the existing method and how the scope of the research can be expanded to produce larger scale flood risk maps with more social vulnerability variables.

2. Developing and Optimizing a Deep Fully Convolutional Network to Map Informal Settlements Using Freely Available Satellite Imagery in Cape Town

2.1 Introduction

Informal settlements are built environments usually existing in low and middle income countries and are typically characterised by a lack of planning and poor provision of services such as sewage and water and where the residents lack legal tenure of the land where they live.

The global population living in informal settlements is forecast to increase in future years (UNDRR, 2015b). This makes the effective management of such sites ever increasingly important and as a result the production of accurate methods of mapping and monitoring these sites is needed. The Sendai Framework for Disaster Risk Reduction contains goals which are dependent on such mapping and monitoring (UNDRR, 2015c). Specifically, Sendai Framework goals three and four target investment in socioeconomic conditions and preparedness for natural hazard events (UNDRR, 2015c).

Climate change mitigation also requires good informal settlement mapping techniques. Due to their lack of good service provision, informal settlement dwellers are usually efficient at waste management and resource usage (Bai et al, 2018). Enabling local support in these communities rather than causing disruption will therefore assist with climate change mitigation. Informal settlement mapping will assist local authorities to support these communities in their sustainable living (Bai et al, 2018), which can form part of the investment in socioeconomic conditions which goal 3 of the Sendai Framework calls for.

By their nature however, informal settlements usually do not have censuses which take place or if they do, their population is undercounted (Wardrop et al, 2018, Carr-Hill, 2013, Maluleke and van Eeden, 2013). Informal settlements as a result suffer from a lack of data in order to produce these maps. There has been a lack of attention in the research community towards mapping in these environments (Kohli et al. 2012, Taubenbock and Kraff, 2014, Zeng et al. 2012). This “informal settlement data problem” means that the most vulnerable environments are also those where the lowest ability exists to map and manage risk and create urban resilience.

UN estimates of total human informal settlement dwellers by UN-Habitat (Human Settlements Programme) are often underestimated. This is typically because in urban environments the

methods applied on a national scale can lack applicability on more localised urban scales (Mitlin and Satterthwaite, 2013). The experiences of individuals are often unaccounted for in UN-Habitat estimates through the fact that often low-income groups and development assistance agencies lack dialogue (Mitlin and Satterthwaite, 2013). Definitions of poverty as a result have a tendency to use a definition of poverty from developed countries applied to low and middle income countries and the informal settlement dwellers are often not consulted on their definitions of poverty (Mitlin and Satterthwaite, 2013). This applies particularly to those in informal settlements and their unique circumstances and UN estimates are often dependent on official statistics which are often absent in these environments (Mitlin and Satterthwaite, 2013).

Quantitative approaches have mostly involved in-situ surveys, defined in Section 1.4.2 as on the ground household surveys and interviews carried out usually by NGOs (non-governmental organisations), volunteers and community groups (e.g. Rahman et al. 2015, Kusumastuti et al. 2014). But there are many drawbacks to these schemes. They are very costly, labour intensive and quickly lose validity because informal settlements are such fast changing environments (Busgeeth et al. 2008, King, 2001). Informal settlements can be difficult and sometimes dangerous to access (Busgeeth et al. 2008) and surveys can lack consistency in methodology, since different researchers are unlikely to exactly replicate their methodologies in different places (Preston et al. 2011).

It has been widely suggested that the solution to this "informal settlement data problem" lies in the use of remote sensing because it is easy to consistently collect imagery across time and space with good spatial resolution (Taubenbock and Kraff, 2014, Geiss and Taubenbock, 2013). This is in addition to the fact that the nature of informal settlements makes them distinctive in visible light satellite imagery.

Traditional methods of quantitatively analysing remotely sensed data include support vector machines (Saindane et al, 2019, Persello and Stein, 2017, Leonita et al, 2018, Mboga et al, 2017), grey level co-occurrence matrices (Ajami et al, 2019, Kuffer et al, 2016, Mossoux et al, 2018, Leonita et al, 2018, Mboga et al, 2017), texture statistics (Persello and Stein, 2017, K-nearest neighbours (Gadiraju et al, 2018, Vatsavai, 2013), random forests (Mostarkssoux et al, 2018, Helber et al, 2018, Gram-Hansen et al, 2019, Leonita et al, 2018), morphological profiles (Persello and Stein, 2017, Leonita et al, 2018, Gadiraju et al, 2018), wavelet transforms Persello and Stein, 2017) and local binary patterns (Ajami et al, 2019, Persello and Stein, 2017, Mboga

et al, 2017). As Section 1.5.1 outlined, these have a strong manual component to their methodologies and can only be considered semi-automatic methods as a result (Wu et al 2018a, Wurm et al 2019, Kuffer et al 2018, Persello and Stein, 2017, Mboga et al, 2017, Ajami et al, 2019). Consequently, due to the shortcomings of many of these traditional classification methods, many studies have adopted neural networks and convolutional neural networks (CNNs) as alternatives. The nature of a neural network type algorithm, being able to analyse all pieces of information in relation to all others, makes neural networks unique in their ability to analyse complex, intricate patterns in high-dimensional data (LeCun et al. 2015, Openshaw, 1992, Zhang, 2016), something which other quantitative methods, are unsuited to. Deep learning can also automatically learn any features without the need for specific user input (Wurm et al, 2019, Stark et al, 2019, Persello and Stein, 2017) in contrast to traditional methods which are often hand crafted to identify specific types of pattern rather than patterns in general (Mboga et al, 2017, Wu et al, 2018b) or involve a two stage processof feature extraction and classification (Wu et al, 2018a, Wurm et al, 2019).

Considering these circumstances and the potential of CNNs, there is scope for a study which seeks to address the "informal settlement data problem" in order to meet the aims of the Sendai Framework for the mitigation of hazard risk. This research chapter will as a result develop a method for detecting informal settlements from remotely sensed imagery, using a CNN. Such a study would have as a result standalone benefits in terms of informal settlement mapping as well as contributing to a method of flood risk mapping in Chapter 4.

There is the potential for the SDI dataset to improve upon existing studies through its containment of attribute variables associated with social vulnerability for each informal settlement. A demonstration of the ability of deep learning to detect informal settlements using SDI data gives the opportunity for future research to distinguish more vulnerable informal settlements from less vulnerable ones from satellite imagery. Such an advancement would allow more detailed vulnerability-based flood risk maps to be produced in the future.

2.2 Literature Review

Many researchers have recognised the potential of deep learning to solve the informal settlement data problem by using CNNs to recognise informal settlements using satellite imagery and other remotely sensed data (Saindane et al. 2019, Engstrom, 2018). They can also automatically account for spatial patterns amongst pixels in comparison with traditional methods (Gadiraju et al. 2018, Engstrom, 2018).

Most studies have indicated the success of using CNNs for this purpose. Gadiraju et al (2018) carried out a comparison between a CNN and other traditional methods such as K-nearest neighbours and random forests in their ability to detect informal settlements. The CNN was found to outperform the K-nearest neighbours by 12% and the random forests by 3%. Other evidence so far points to the adoption of CNNs by researchers as representing improvements in the recognition of informal settlements (Mboga et al. 2017, Gadiraju et al. 2018, Mboga et al. 2017, Wang et al. 2019, Mboga et al. 2019).

Three main types of computer vision tasks may be performed by CNNs (Sharma, 2019, Qualcomm, 2020). The most basic is image classification, where the network assigns an individual prediction to an entire image. The second is object detection, where the positions of specific object types are identified within images. The third is segmentation, where the network assigns predictions on a pixel-wise basis across a whole image (Sharma, 2019, Qualcomm, 2020). Studies seeking to detect informal settlements have used all three sorts.

Although some studies perform image classification, where an entire image is classified as either an informal or formal settlement (Ajami et al. 2019, Ibrahim et al. 2018), most studies perform segmentation (Persello and Stein, 2017, Gram-Hansen et al. 2019, Mboga et al. 2017, Li et al, 2017, Leonita et al. 2018). For each image the network is shown, it is also shown a ground-truth mask which gives the true value of each pixel. Thus the network trains itself to recognise the desired categories based on the information in the image, producing an output consisting of predictions with dimensions corresponding to the image and ground truth mask. It is a methodology commonly performed in studies which map informal settlements using deep learning (Persello and Stein, 2017, Gram-Hansen et al. 2019, Mboga et al. 2017, Li et al. 2017, Leonita et al. 2018). This represents an improvement over the more basic methods of image classification since it is able to represent each pixel rather than each image as a whole and so much more information about each image can be summarised. As a result, this study will continue to use segmentation instead of image classification. But there are a number of issues and gaps in the present literature which demonstrate the need for additional research in this area.

Very often studies of this sort are specific to one city or country (Gram-Hansen et al. 2019). Naturally research has centred on particular cities where extensive mapping of informal settlements has taken place. Examples are Dar es Salaam (Persello and Stein, 2017, Mboga et al. 2017) Mumbai (Block et al. 2017, Maiya and Babu, 2018) and Shenzhen (Li et al, 2017). In

the case of Dar es Salaam, studies often select this city because the proportion of residents who live in informal settlements is high at 70-80% (Persello and Stein, 2017, Mboga et al. 2017).

Although deep learning studies will test the skill of their network using data which the network had previously not seen, called a "test" set, the test set would be selected from the same sample as the data from which the network is trained. In other words, the network is only tested with in-sample variation. Consequently, there is no reason why a network trained to identify informal settlements in one city would necessarily be skilful in making a similar identification outside of the original sample of images, in another city for example. This is known as the problem of generalizability. Studies which try to generalize typically give disappointing results (Gram-Hansen et al. 2019, Block et al. 2017, Helber et al. 2018, Ibrahim et al. 2019, Engstrom et al. 2016).

The imagery normally utilised is not freely available and instead comes from commercial suppliers. Examples of imagery sources include the private firm DigitalGlobe (Quinn et al. 2018, Gadiraju et al. 2018, Persello and Stein, 2017, Block et al. 2017, Helber et al. 2018, Li et al, 2017, Mboga et al. 2017, Persello and Stein, 2017) and Pleiades-1A (Verma et al. 2019, Ajama et al. 2019). But being commercially obtained, such imagery is not suitable for creating public domain, cost efficient informal settlement maps. The use of more freely available urban scene imagery for this purpose is rare with few exceptions (Maiya and Babu, 2018, Jean et al. 2016, Wang et al, 2019) who use Google Maps API. Therefore, more research is needed to establish the efficacy of using more freely available satellite imagery for the purpose of producing informal settlement maps, with the terms of use of these discussed more detail in Section 2.3.4.

The production of effective maps requires an ability to distinguish between different informal settlements as well as between the informal and formal binary. However, to the knowledge of the author, no present papers attempt to incorporate variability within informal settlements. Jean et al (2016) attempt to use a CNN to predict levels of poverty using a remote sensing method but with poor input data derived from household surveys such as Demographic Household Surveys (DHS) which include coordinate modification in the spatial data to protect the privacy of the participants. The data in the Jean et al (2016) study are as a result poorly geolocated. Ajama et al (2019) additionally attempt to use census data in Mumbai to map deprivation but only using a CNN for image classification on a level of entire images instead

of pixel-wise segmentation. The applicability of this method for mapping on a high resolution, pixel by pixel basis is as a result limited.

A conceptual understanding of a neural network in relation to an informal settlement is something which these studies consistently fail to incorporate into their methods. A neural network is a "black box" method which is simply designed to detect patterns based on the assumption of there being underlying structure without knowing what that structure is (Openshaw, 1992, Cross et al, 1995). Although a neural network possesses the ability to map non-linear patterns due to consisting of an exceptionally high number of parameters (Li and Yeh, 2002), there is no underlying theoretical foundation to the approach and the reasons for decisions taken by the networks are often uninterpretable (Openshaw, 1992). This is especially the case with an informal settlement, which is not a homogenous entity but instead amounts to a variety of amenities such as roads, roofs and trees distributed in a spatial area. An informal settlement is hence an environment which quantitative methods alone may struggle to fully describe (Quinn et al, 2018, Verma et al, 2019, Kohli et al, 2012, Owen and Wong, 2013). This may be particularly the caseat the pixel level, which may be insufficient at capturing enough spatial detail to recognise these different amenities due to a spatial mismatch (Verma et al, 2019). As a result, any developed rule set may perform differently for different parts of a specific informal settlement (Verma et al, 2019). Additionally, when objects are covered by few pixels the network may struggle to categorise them as informal settlements (Quinn et al, 2018).

Present uses of deep learning to map informal settlements frequently fail to account for this and hence their methods not only lack a conceptual grounding but fail to integrate such assumptions in their methodology. Existing studies instead focussing purely on the technical benefits of deep learning, rather than the conceptual considerations with applying the method to informal settlements.

In light of these research gaps, this chapter aims to use freely available Google Maps imagery will be used to detect informal settlements to enable a cost-efficient method of vulnerability mapping. The SDI dataset presents the opportunity for further studies to develop methods of detecting differentials in socioeconomic conditions within the informal settlement category. In Cape Town there are just 75 informal settlements in the SDI dataset. This allows however for the development of a methodology with sample sizes smaller than those typically employed by similar studies. The sample sizes used in similar research include 1836 (Verma et al. 2019),

513 (Maiya and Babu, 2018), 3000 (Quinn et al. 2018, Mboga et al. 2019) and 1080 (Mboga et al. 2017). An ability to perform such mapping using more sample sizes will open up the possibility for more cities to have their informal settlements mapped if data on only small numbers of informal settlements exists in that city.

The lack of studies which extrapolate from the training set to entire cities also presents an opportunity for this research chapter to develop upon existing studies, and which it will aim to do. Such a scaled-up map will be utilized in Chapter 4 as the social vulnerability of a flood risk map, which is the aim of the thesis as a whole.

The lack of conceptual consideration of neural network type algorithms and the implications of what this means for informal settlement detection gives the opportunity for a study. This study will as a result seek to investigate ways of combining the technical benefits of deep learning with post-processing which accounts for the nature of neural network type algorithms as "black box" methods. The result of this being a final methodology which is conceptually grounded. Post-processing methods have been used in comparable studies which involve the smoothing of the edges of areas (Stark, 2018, Mboga et al, 2019), and the removal of noise (Leonita et al, 2018). The methods employed however do not aim to correct for the black box nature of their methods with specific reference to the nature of informal settlements. The lack of this consideration in these other studies however gives the opportunity for progress to be made in this area.

2.3 Methodology

2.3.1 Introduction to Neural Networks and Convolutional Neural Networks

A neural network is a machine learning algorithm where many nodes called neurons are distributed in multiple layers in order to allow information to be processed. A generic neural network for image recognition is depicted in Figure 2-1. The red circles in the first, or input, layer represent the values of pixels in an image, and the two pixels represent output probabilities, one of which represents the true category of the input image.

In Figure 2-1, the neurons are represented by circles which each have a value called an activation. Figure 2-1 is described mathematically in Equation 2-1. Both Figure 2-1 and Equation 2-1 illustrate how the activation of a particular neuron, a_j^L for example, is calculated, based on the values of the activation in the previous layer, $L-1$ and the weights, w_{jk} which connect them to the previous layer, as well as an additional term called a bias, b_j^L.

Finally, there is an activation function σ, which defines the relationship between the activation a_j^L and the activations of the neurons a_k^{L-1} so the resultant value of a_j^L is conducive to the efficient training of the network. The subject of activation function is elaborated upon in Section 2.3.2.

The objective of a neural network is to adjust the values of the weights and biases such that an image belonging to a particular category would produce the desired outcome in the two blue output probabilities as the values of the activations are calculated throughout the network, beginning with the input neurons (Zhang, 2016). The difference between the true classes and predicted probabilities across the sample is known as the loss function and the way in which the network trains is called gradient descent. This process is called gradient descent because it treats this loss function as a function of these weights and biases and adjusts the values of these along the negative gradient of this loss function (Nielsen, 2017).

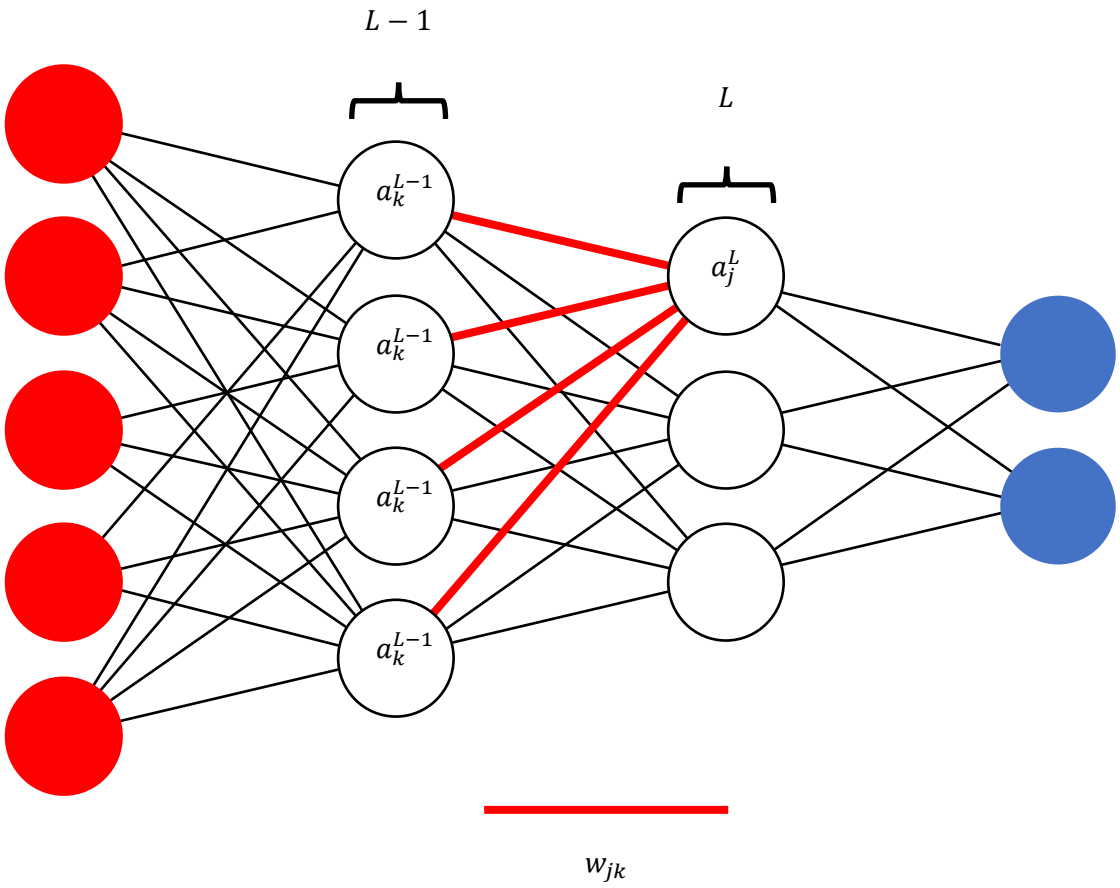

Figure 2-1 Generic Neural Network Diagram: Visualisation of a generic neural network, circles represent neurons, which have a value called an activation through which the network processes information. The red neurons represent the values of pixels and the blue pixels represent output probabilities with which to classify the input image. Equation 2-1 represents a mathematical summary of how a particular neuron's activation is calculated, where a particular neuron's activation a_j^L, is calculated from the activation of the neurons in the previous layer a_k^{L-1} and the weights which connect these, the weights, w_{jk}, represented by red lines.

$$a_j^L = \sigma\left(\sum_k w_{jk}\, a_k^{L-1} + b_j^L\right)$$

(2-1)

(Nielsen, 2017, Zhang, 2016)

j = A particular neuron in layer L to be calculated.

k = The range of neurons in layer $L - 1$.

σ = The activation function applied.

a_j^L = The activation of j neuron in layer L.

w_{jk} = the value of the weight connecting the neurons j and k.

a_k^{L-1} = The activation of each of k neurons in layer $L - 1$.

b_j^L = The bias associated with neuron j in layer L.

Once the weights and biases across the network have been adjusted, a successful neural network should be able to correctly classify an image it has not previously been trained on. Usually this is evaluated in machine learning by splitting the dataset into two groups at random, the training set and test set. The training set is shown to the network in order to "train" the network by the adjusting the weights and biases accordingly to correctly classify the training images. The test set is then used to evaluate the skill of the network by working out a classification accuracy on images the network has not previously seen, by comparing the predictions against known outcomes (Cross et al, 1995). Henceforth, the values representing these weights and biases are known as parameters.

Researchers have found that attempts to increase the complexity of a neural network by increasing the number of layers makes it harder to train; the gradient (the amount of information processed in each layer) of each layer is unstable and has a tendency to be concentrated on one or two layers regardless of the depth of the network, which is known as the vanishing gradient problem (Nielsen, 2017). The phrase "deep learning" usually describes methods developed to allow a greater number of layers, in particular with respect to CNNs.

In addition to the fully connected layers depicted in Figure 2-1, in comparison to a normal neural network, a CNN uses two additional types of layer to improve the network's ability to recognise patterns. The first is a convolutional layer, whereby instead of the neurons in the layer being fully connected as in Figure 2-1, only a small sliding section representing part of the image at once is trained, called a local receptive field (LeCun et al, 2015, Nielsen, 2017,

Liu et al, 2017). Each local receptive field is connected to one neuron in the next layer (Nielsen, 2017, Albawi and Mohammed, 2017). These improve training in two ways. First, a greater number of layers for a given number of weights can be trained, which makes deep networks easier to train (LeCun et al. 2015, Liu et al. 2017). Second, the use of these local receptive fields allows the network to more strongly account for local patterns and textures in the image (Gadiraju et al. 2018, Engstrom, 2018).

The second aspect of a convolutional layer is called a feature map. These always follow a local receptive field and allow information describing patterns in the image to be summarised in the following layer. A local receptive field connects to a feature map via a series of weights and an individual bias. The locally receptive field connects to an individual neuron in the next layer, but the locally receptive field is slid across the image to allow the activation values for each neuron in the feature map to be calculated using the set of weights and a common bias. These shared weights and biases are called a filter (Nielsen, 2017, Albawi and Mohammed, 2017).

The use of the filter means that skill the network gains in recognising a pattern in one part of an input image can be used to recognise the pattern in any area of the image, known as location invariance (Guo et al, 2017, Nielsen, 2017, Albawi and Mohammed, 2017). A CNN will typically contain many of these filter-feature map combinations to allow it to detect many different patterns in order to perform computer vision tasks. This process is described mathematically in Equation 2-2:

$$a_{x,y} = \sigma\left(b + \sum_{l=0}\sum_{m=0} w_{l,m} a_{x+l,y+m}\right) \tag{2-2}$$

(Nielsen, 2017, Wu, 2017, Albawi and Mohammed, 2017)

Where:

$a_{x,y}$ = The activation of a neuron in the feature map at position x, y.

σ = The activation function applied.

b = The shared bias of the local receptive field.

x = Horizontal dimension of the input image.

y = Vertical dimension of the input image.

l = Horizontal dimension of the local receptive field.

m = Vertical dimension of the local receptive field.

$w_{l,m}$ = The value of the weight in position l, m in the local receptive field.

$a_{x+l,y+m}$ = The activation of the input pixel being examined by the local receptive field.

Most studies mapping informal settlements using neural networks use these CNNs. In contrast to traditional methods, a CNN has the ability to learn spatial features automatically through its use of the local groups of pixels in the form of these local receptive fields (Persello and Stein, 2017), in particular hierarchical features (Mboga et al. 2017). CNNs therefore have greater potential for large scale informal settlement mapping which the research problem outlined demands (e.g. Leonita et al. 2018).

The second type of layer a CNN uses is called a pooling layer. The pooling layers have the function of reducing the dimension of or downsampling the feature map in order to be received by the next layer. They allow patterns at different spatial scales to be detected at different layers of the network. They also allow the network to have more layers and at the same time be less computationally extensive because some layers have fewer neurons than if they were not downsampled.

The most common criterion of how this is done is max pooling, where the maximum value in a window of given dimensions across the each feature map is transferred to the next convolutional layer in order to downsample it, as described in Equation 2-3. Other methods of pooling exist, such as average pooling. Max pooling however results in a greater range of values in the subsequent feature maps by preserving the more extreme values. This allows the downsampled feature maps to preserve more information (Boureau et al, 2010) and as a result max pooling been shown to help networks train (Scherer et al, 2010) and is therefore the most commonly used.

$$a_j = \max_{N \times N}(a_k, u(n, n))$$

(2-3)

(Scherer et al, 2010)

Where:

a_j = The activation value of neuron j in a feature map to be pooled.

a_k = The activation of neuron k in the pooled layer.

n = The dimensions of pooling, usually 2 (Albawi and Mohammed, 2017).

$u(n, n)$ = A window function from which the extracting the maximum value

$N \times N$ = The dimensions of the feature map to be pooled.

Although also commonly used in more traditional neural networks, CNNs often have as their final layer what is called a softmax layer. This layer converts the activation values of the penultimate layer into interpretable probabilities, ensuring all outputs sum to 1.

$$a^L_{j,softmax} = \frac{e^{a^L_j}}{\sum_k e^{a^L_k}} \tag{2-4}$$

(Nielsen, 2017, Boureau et al, 2010)

Where:

L = The output layer

j = A given neuron in layer L whose softmax value is to be calculated.

k = The range of neurons in layer L.

a^L_j = The activation of a neuron j prior to the application of the softmax function, calculated in the same way as the output of Equation 2-1.

$a^L_{j,softmax}$ = The value of a given neuron in the final softmax layer.

e = exponential constant (~2.718).

Performing Segmentation with CNNs

The basic method described can be done to perform three main types of computer vision tasks as laid out in Section 2.2, of image classification, object detection and segmentation (Sharma, 2019, Qualcomm, 2020). For reasons of spatial resolution in this research chapter I opt to do segmentation to map informal settlements in this research chapter.

Performing pixel-wise segmentation with a CNN requires an addition aspect on top of the two types of layers described. It uses what will henceforth be referred to as an encoder-decoder architecture. This architecture is similar to that laid out by an image classification based CNN, but uses operations to take the pooled layers and upsample them back eventually to the dimensions of the original image so that the output of the network is on a pixel-by-pixel basis.

In the second half of the network, or the "decoder" section pooling layers are replaced by transposed convolutional layers. These are similar to convolutional layers but aim to do the opposite of pooling layer, to upsample it and recover or "decode" from the downsampled feature maps in order to recover information representational of dimensions eventually equivalent to the original input image in order to make pixel-wise predictions (Dumoulin and Visin, 2018, Gao et al, 2019).

For a transpose convolutional layer to do this, it performs a transpose operation to a normal convolutional layer in order to perform the reverse to normal convolutional layer to produce an output larger than the input, as shown in Equation 2-5.

$$a_{x,y} = \sigma\left(b + \sum_{l=0}\sum_{m=0}\left[w_{l,m}\right]^T a_{x+l,y+m}\right)$$

(2-5)

(Nielsen, 2017, Wu, 2017, Albawi and Mohammed, 2017, Dumoulin and Visin, 2018, Gao et al 2019)

$a_{x,y}$ = The activation of a neuron in the feature map at position x, y.

σ = The activation function applied.

b = The shared bias of the local receptive field.

x = Horizontal dimension of the input image.

y = Vertical dimension of the input image.

l = Horizontal dimension of the local receptive field.

m = Vertical dimension of the local receptive field.

$\left[w_{l,m}\right]^T$ = The transposed value of the weight in position l, m in the local receptive field.

$a_{x+l,y+m}$ = The activation of the input pixel being examined by the local receptive field.

Another important aspect of the makeup of a CNN is the hyperparameters, which are important determinants in how a network trains. Bengio (2012) describes a hyperparameter as a variable set prior to the actual commencement of training, which is not directly selected by the learning algorithm.

For a CNN, or a regular neural network, a key hyperaparameter is whether to use stochastic gradient descent, batch gradient descent or mini-batch gradient descent. With stochastic gradient descent, the parameters are updated after the network has seen each individual image. An alternative to stochastic gradient descent is batch gradient descent. When training using batch gradient descent, the entirety of the training set is shown to the network before the parameters are updated to conform the training images to the values of the true values. Each of these two choices have relative advantages and disadvantages for training purposes. A compromise between batch gradient descent and stochastic gradient descent is mini-batch gradient descent. Here the network's parameters are updated after the network has seen a specified quantity of images as opposed to 1 image or the whole training set.

Another important hyperparameter for all kinds of neural networks, including CNNs, is the learning rate. The learning rate refers to the rate at which the parameters values are adjusted during each training update when the network has seen the entire batch. There are relative benefits to a high and a low learning rate, as I will elaborate upon in Section 2.4.4.

2.3.2 Description of Network Implementation

Network Architecture

A methodological development of the standard segmentation CNN lies in the use of a Fully Convolutional Network (FCN). An FCN is a type of CNN which avoids the use of fully connected layers to improve computational efficiency (Persello and Stein, 2017). In this research chapter the U-Net FCN is used in order to capitalise on this advancement. CNNs, including FCNs use an encoder-decoder architecture, as illustrated in Figure 2-2.

Originally developed by Ronneberger et al. (2015), U-Net additionally employs a skip architecture, whereby there are layers connected which "skip" other layers, instead of each layer being connected to the next sequentially. This skip layers are illustrated in the network architecture in Figure 2-2. Such a network has been carried out for similar purposes for informal

settlement mapping (Wang et al. 2019) and it is especially applicable for this study since it is particularly effective with small training set sizes (Ronneberger et al, 2015).

This is a result of the skip layers and their ability to give the output a superior resolution and better defined edges than a more traditional segmentation CNN. The skip layers allow the final prediction to have better defined edges (Wu et al, 2018a) because they allow higher resolution features derived from earlier convolutional layers to be combined with less resolute, upsampled features later in the network (Ronneberger et al, 2015). This feature derives from its individual purpose of medical imaging (Ronneberger et al, 2015). This suitability for small sample sizes makes U-Net especially useful when working with the SDI dataset because in Cape Town, it only contains 75 informal settlements.

A patch size of 256 x 256 pixels is used for each image, where the patch size refers to the size of images shown to the network after all pre-processing. Figure 2-2 visually describes the network structure. In the encoder block, there are 10 convolutional layers each with a filter size of 3x3, with 5 accompanying max pooling layers, with differing numbers of filters. There are then a further two convolutional layers with 1024 each in the centre of the network.

The decoder block then contains 5 convolutional layers with numbers of filters and filter size matching those in the encoder block. There are accompanying convolutional transpose layers. Finally, a softmax layer is used to convert the outputs into interpretable probabilities. In total, the network contains over 31 million trainable parameters.

There are 5 skip connections between the encoder block and decoder block. Here the layer in the decoder section accepts input not just from the previous layer but also from a layer from further back and concatenates them into a single layer in the network as shown in Figure 2-2.

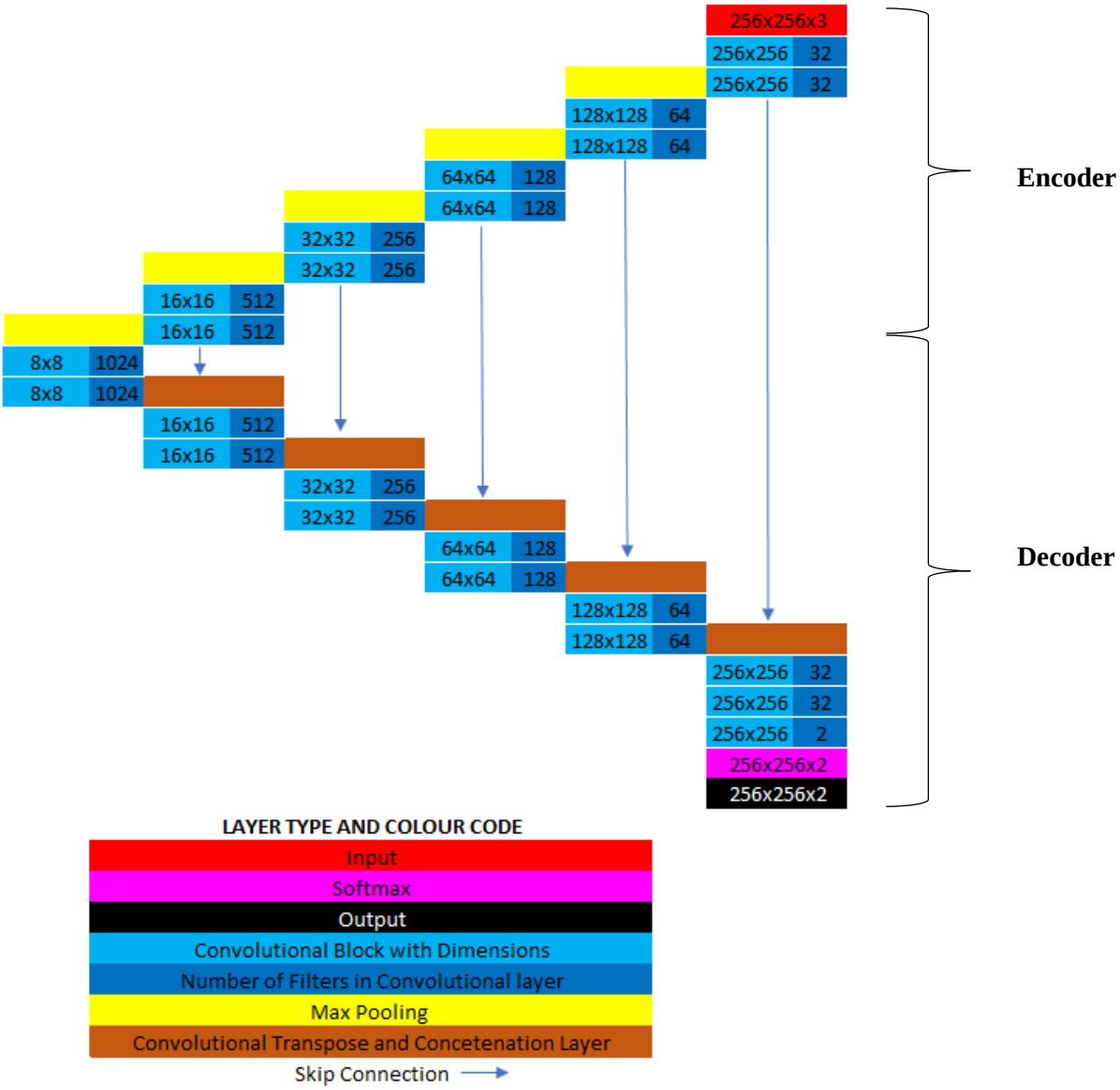

Figure 2-2: **Diagram of the U-Net.**

I use Google Colabatory (Colab), (Google, 2019). The use of Google Colab is consistent with the motivations of the research alongside the imagery because Google Colab is a freely available server. This negates any need for ownership of expensive computing hardware. The network is implemented using the Python Tensorflow library implemented using Keras. As a cloud server, Google Colab has a number of different GPUs used as hardware accelerators (Google, 2020). These include NVIDIA T4s, P4s, and P100s. When enabling GPU support the user has no control over which GPU is allocated because this depends on resource availability (Google, 2020).

Deep learning is normally understood to require large quantities of training data to be successful in computer vision tasks (LeCunn et al. 2015). When these are unavailable, dataset augmentation is a method commonly used in deep learning to compensate. It refers to methods of artificially expanding the training set, the conceptual foundation being the assumption that an image in the training set with small adjustments made is likely to still correspond to a theoretical image of a similar kind, allowing the distribution of the sample data to more closely correspond to the true distribution of images (Zhu et al, 2018). Dataset augmentation therefore amounts to an expansion of the range of patterns and textures which the network can recognise as belonging to the desired category. This study uses dataset augmentation through the flipping of each image vertically and horizontally, as this is commonly performed by similar studies (Maiya and Babu, 2018, Quinn et al. 2018).

Activation Function

The activation function is the mathematical formulation used to compute the value of one activation based on the values represented in the activations it is connected to in the previous layer. With the exception of the final convolutional layer where sigmoid activation is used, the network uses the now standard ReLU (Rectified Linear Unit) activation function as this helps to mitigate the vanishing gradient problem and is more computationally efficiency and is it as a result the standard activation function for these tasks (Nielsen, 2017, LeCun et al, 2015, Albawi and Mohammed, 2017). The ReLU function σ is defined as:

$$\sigma = \max(0, x)$$

(2-6)

(Agarap, 2018, Albawi and Mohammed, 2017, Guo et al, 2017)

Where:

x = The value of the input neuron, calculated by:

$$x = \sum_k w_{jk}\, a_k^{L-1} + b_j^L$$

(2-7)

(Nielsen, 2017, Zhang, 2016)

Where:

j = A particular neuron in layer L to be calculated.

k = The range of neurons in layer $L - 1$.

w_{jk} = the value of the weight connecting the neurons j and k.

a_k^{L-1} = The activation of each of k neurons in layer $L - 1$.

b_j^L = The bias associated with neuron j in layer L.

Loss function

The loss function is a measure of badness of fit. The network uses a dataset of labelled training examples to adjust the parameter values to minimize the loss function and improve the network's accuracy in classifying the images (Nielsen, 2017).

In any neural network, the loss function describes the relationship between the values of the network's parameters and the network's goodness of fit. The loss function is as a result what the network uses to train itself.

This research uses binary cross entropy loss, since this computationally emphasises the likelihood of a certain pixel belonging to a particular class using the maximum likelihood principle, which is ideal for a binary classification task as opposed to other loss functions such as mean squared error and mean absolute error which are more suited to regression tasks. The binary cross entropy for the network is described as:

$$E = -\frac{1}{N}\sum_{i=1}^{N} y_i * \log\left(p(y_i)\right) \tag{2-8}$$

(Ibrahim et al. 2018, Mboga et al. 2017)

Where:

E = Cross entropy loss.

N = Number of pixels in the total sample.

y_i = the class of pixel i (either 0 or 1).

$p(y_i)$ = the predicted probability of a pixel belonging to class y_i.

Another reason for utilising binary cross entropy as a loss function lies in the relative balance of the two classes, with there being only a small imbalance in favour of the "formal" class as opposed to the "informal" class of approximately 2:1. Alternative loss functions to binary cross entropy such as dice loss based functions are preferable when classes are more strongly imbalanced. These incorporate into the calculation of the loss the skill at detecting each class when weighted for the size of each class. This however is generally more used when there is a strong class imbalance, as opposed to only a small class disparity which exists here.

The loss function is a measure of badness of fit of the network's performance. The concept of this is visualised in Figure 2-3, where in training, the aim is to set the value of the parameters such that the loss function is at the red point, and the loss function is minimized. The loss function exists as a function of the parameter values, existing in high-dimensional space because of the huge number of trainable parameters which there are in the network. It is as a result not possible to mathematically find the optimal solution to this function at the global minimum, shown in red in Figure 2-3. The network as a result must train by working out the gradient of the loss function at any given point and adjust the parameter values such that the loss function is reduced. This is referred to as "gradient descent" (Nielsen, 2017). However, this concept of gradient descent raises a problem for the training of a network as is illustrated in Figure 2-3. The loss function, due to its complexity, is not a simple function with a single, minimum which the aim is to reach. The function instead contains many sub-optimal, local minima which when the network is being trained the aim is to avoid. But when the network is being trained using gradient descent, it risks getting "stuck" in one of these sub-optimal points as shown in blue in Figure 2-3. The avoidance of these points when training has implications for how to train a network, particularly the value at which the learning rate is set, which will be elaborated upon in Section 2.4.4.

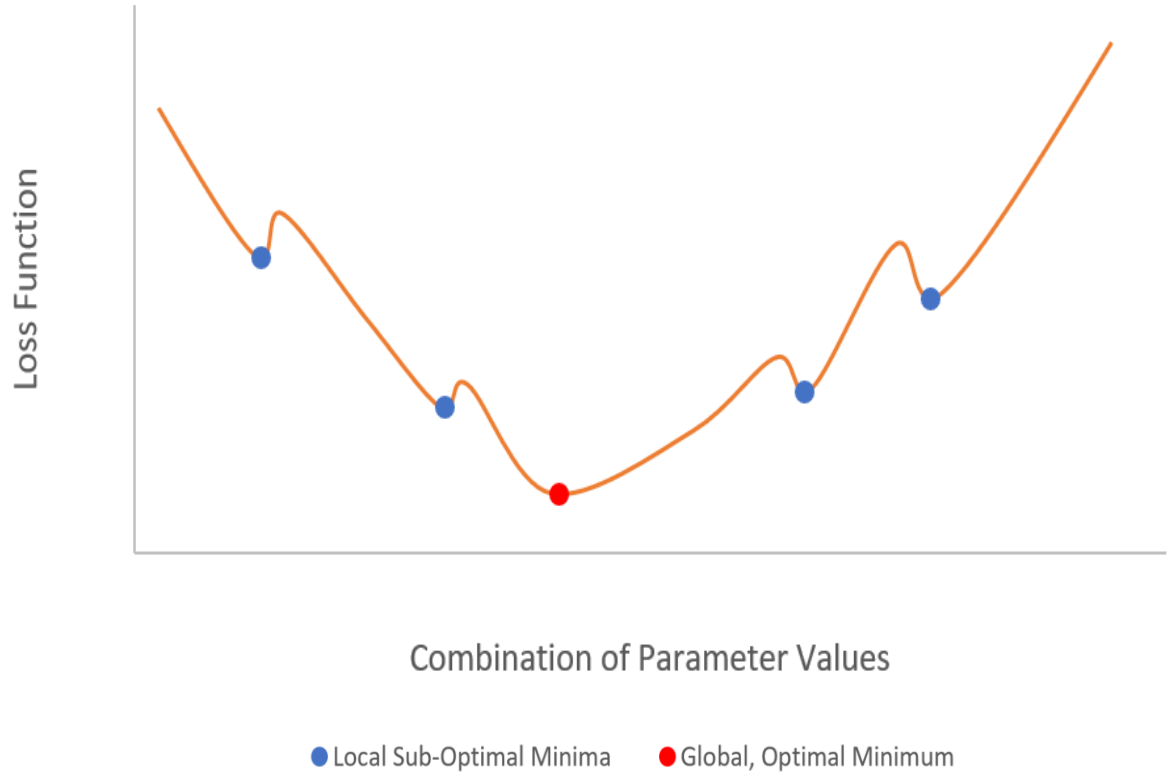

Figure 2-3 Conceptual Diagram of Loss Function: A hypothetical loss function, where the object of a neural network is to set the parameter values in order to minimize the loss function. The x-axis in reality exists in a number of dimensions equal to the number of parameters itself. In reality a loss function will have a global minimum, which is the desired outcome for the parameter values, as well as many sub-optimal minima which it is desired the network avoid getting "stuck" in.

Optimizer

The research uses the Adam optimizer as this is currently the most common to be used in deep learning (Li et al. 2019) and it brings many benefits. Adam stands for Adaptive Moment Estimation (Walia, 2017, Kingma and Ba, 2014). It applies a number of innovations in comparison to more traditional optimizers. It uses an adaptive learning rate, which involves the adaptation of the network's learning rate on a per parameter basis. This means that the network can adopt different learning rates for different parameters. It similarly uses momentum updates. Momentum in a CNN adjusts the size of the updates to a parameters on the basis on the size of the update in the previous iteration which helps prevent the network overshooting a sub-optimal minimum in the loss function (Li et al. 2019). This frequently helps a CNN to converge to a minimum in the loss function (Li et al. 2019).

The momentum of the network in Adam is also adapted on a per parameter basis in a similar fashion to the learning rate. These two elements help the network transcend saddle points where the loss function gradient is starkly different for different parameters in the network (Li et al. 2019). Adam has also been found to have faster convergence than other similar optimizers (Kingma and Ba, 2015).

Post-Processing

This study also takes steps going beyond that which previous studies mapping informal settlements have employed. The wholesale integration of conceptually grounded post-processing into the methodology is developed. An informal settlement has spatial heterogeneity in its appearance and a CNN lacks any theoretical foundation in its detection of informal settlements, as discussed in Section 2.2, meaning a CNN is therefore likely to recognise certain visual elements and not others within the informal settlement, possibly roads or trees from within the settlement which may be misclassified (Openshaw, 1992). Therefore, a gaussian blur filter is employed to introduce a spatial post-processing component to integrate any such "missing" amenities to turn the predictions from point based to area-based estimates. Second, the discriminant threshold through which a pixel is classified as informal is changed. The discriminant threshold is the dividing line between the two categories from the perspective of the raw predicted outcomes from the network's softmax layer. The theory behind changing this threshold is the assumption that a network may possess some skill in detecting amenities within the informal settlements, but insufficiently so to make the correct classification.

Experiments Run and Analysis Performed

The study first performs an exploratory experiment using a stochastic learning approach to examine the network's training and test accuracies and visualise outputs to identify potential performance improvements.

In my second experiment, I use a mini-batch gradient descent as opposed to stochastic learning. Here the network's parameters are updated after the network has seen a specified quantity of images as opposed to 1 image at a time. Such an approach is more computationally efficient but some have identified weaknesses in its ability to make good test predictions when training in this way (Keskar et al. 2016).

The second step performs a comparison of different mini-batch sizes as part of a fine-tuning process by training 100 separate networks for each of the mini-batch sizes 1, 8 and 16. Third,

the network's hyperparameters are fine-tuned once optimal mini-batch size has been established, using an additional 400 separate experiments.

Finally, once the network's learning rate and decay rate have been fine-tuned, the post-processing techniques of adjusting the gaussian blur filter size and changing the network's discriminant threshold are optimized to produce a wholesale fine-tuned methodology. The research concludes with a scaled-up map of informal settlement predictions for the whole Cape Town area utilising the same fine-tuned combination of post-processing techniques and network hyperparameters.

2.3.3 Informal Settlement Data

The study uses data from Slum Dwellers International (SDI, 2019, 2020), henceforth SDI, which is a community-based organisation aiming to carry out the mapping of informal settlements using participatory methods involving local community geolocating the precise boundaries of informal settlements.

Section 1.7 described in detail the nature of SDI as an organisation, its aims and how its data are collected. The section identified the key benefits of the SDI dataset. First, it is a participatory, in-situ dataset consequently resulting in the boundaries of informal settlements being accurately defined. Second, the dataset contains many socioeconomic variables which are connected with social vulnerability, such as the availability of electricity, quality of roads and the number of toilets per inhabitant.

However, the fact that the SDI data is participatory leads to concerns about its level of coverage, these limitations were also discussed in Section 1.7. The mapping of informal settlements in SDI is initiated by the informal settlement dweller associations rather than a more top-down approach triggered by the municipal authority. This means that there are likely to be informal settlements in Cape Town which the SDI dataset does not include. It may therefore be assumed that the SDI dataset, based on its nature as participatory by local people, instead of constituting an official data collection, will miss some informal settlements and underrepresent the number of informal settlements in Cape Town (Byrne et al, 2018).

In Cape Town, more comprehensive informal settlement datasets exist. The non-profit civic technology lab organisation OpenUp has produced a map of the predicted informal settlements in Cape Town (OpenUp, 2017). Whilst such a map is likely to be more comprehensive, the benefit which the SDI dataset has it that it similarly exists in more than 100 other cities around

the world. This as a result provides the opportunity for the final method to be replicated in other cities in a more consistent way and eventually for the method to be replicated on a more global scale.

2.3.4 Imagery

The research uses imagery from Google Maps API (Google Cloud, 2019). This API enables the downloading of patches of the satellite imagery found on Google Maps. In their raw form these images are not geospatial objects. As a result, these were georeferenced using QGIS. This was done by calibrating four points in each image where the coordinates of the true points were derived from LatLong.net (2020) and visually mapped onto the images for them to be subsequently georeferenced.

This highly manual pre-processing makes the production of these georeferenced images very labour intensive and subject to human error. Moreover, there is no direct control over the resolution of the imagery, there is only the possibility of controlling an ill-defined zoom level as can be seen on Google Maps. The true spatial resolution could therefore only be estimated manually, but the post-georeferencing resolution is 0.85m. This research selected for a zoom level of 17, which approximately corresponds to a 1m resolution.

The use of imagery from Planet Labs was also considered but was rejected in favour of Google Maps. The most resolute satellite of Planet Labs, SkySat, provides 0.7m resolution imagery this but is not accessible to researchers and the next best option, PlanetScope imagery were found to not produce good results due to its more coarse spatial resolution of 3m.

With the overarching intention of this research to create an open, cost-efficient available system for identifying informal settlements, the restrictions on the secondary use of any relevant data are important to consider. The Google Maps API imagery is publicly accessible and users can easily apply for an API Key to download imagery. However, the Google Maps imagery cannot be described as “open” since there are restrictions on its use. Most prominently, it is impossible to download images more than 640x640 pixels and the Google Maps API terms and conditions do not permit multiple images to be quilted together into one large image of a whole city. The maximum quantity of images able to be downloaded using an API key is 100,000 per month, this is sufficient for the scope of this thesis which only seeks to demonstrate the applicability of methods in a single city.

This research focusses on Cape Town, which has a total of 75 informal settlements in the SDI dataset. For each settlement the SDI data comes with coordinates which make up its outline. The midpoint of these is taken from which the request is made to Google Maps API to download an image patch for each settlement. These coordinate vector shapefiles are then converted to a raster format and reprojected using the R raster (Hijmans, 2020) and rgdal package (Bivand, 2020) to the same projection as the manually georeferenced image from QGIS.

As Section 2.3.3 mentioned, it may be assumed that the SDI dataset, based on its nature as participatory by local people, instead of constituting any official data collection, will miss some informal settlements. This is especially as the SDI data is gathered on the basis of self-selection for mapping and enumeration by the local informal settlement communities rather than being ordered by a central authority (Byrne et al, 2018). It may therefore be assumed that the SDI data underrepresents the number of informal settlements in Cape Town (Byrne et al, 2018). Incorrectly classified informal settlements missing from the SDI dataset have the potential to confuse the FCN. For this research chapter I therefore examine each of the downloaded images for any informal settlements which may not be in the SDI dataset and hence may confuse the network. Any areas which appear similar in texture to the already identified informal settlement in that image is outlined visually and classified as informal settlement. 30 additional informal settlements within the set of 75 images are identified using this method.

The implications for the addition of these extra informal settlements to the research needs to be examined. The benefit of a bottom-up community defined dataset comes inexorably with the problem of missing settlements where the community may choose to not participate. Some of the benefit of this dataset with its community defined borders are lost because some of the settlements would not have been drawn in this way. On the other hand, having areas wrongly classified due to not being in the SDI dataset would confuse the network. This is a larger concern than a slight undermining of the benefits of benefits of it being a community by manual drawing some informal settlements. As a result, despite part of the benefit of using a community based dataset being lost, the addition of these manual informal settlements is justified.

Of the 75 original images 9 were removed as a result of overlapping with other images based upon visual examination because excessively overlapping images are not able to constitute a true test set. Of the final 66, a cross validation procedure is performed for all training, whereby

the images are split at random into 44 which are used to train the network and a test set of 22 which it has not been trained on, which is used to evaluate network's performance.

For each time the network is trained, the training and test set combination of images in each set is different so that finding the best network configuration is common across the dataset rather than becoming specific to only 1 particular subset of training and test images. Performing this cross validation is necessary due to the use of a small dataset. Two individual test sets are likely to be strongly different in characteristics than another; as a result, performing a number of cross validations helps to make any results and conclusions robust. Once the training-test split has taken place, the final training set size is 44 images, which is sub-optimal for a deep learning algorithm. But, since the availability of such data is lacking, it is important to be able to use this to map informal settlements using a small dataset. Other papers which have attempted to map informal settlements using CNNs have typically used a quantity of images much greater than 66.

Similar studies utilise either a binary "informal" and "formal" (Ibrahim et al. 2019, Maiya and Babu, 2018, Mboga et al. 2017) or four classes ("informal", "urban", "rural", and "water", Verma et al. 2019, Wurm et al. 2019, Mboga et al. 2017). For reasons of parsimony this research opts for the former, a binary appraoch to allow the network to concentrate its skill in recognising the particular category of interest.

2.4 Results

2.4.1 Stochastic Learning Approach

This exploratory experiment uses stochastic learning, where the values of the parameters are updated after the network has seen each individual image, meaning the network effectively has a mini-batch size of 1. This has the advantage of being more able to recognise complex patterns due to the parameter updates being more frequent and more able to intricately map features in the training images. With stochastic learning however there is additionally a risk that the network learns noise rather than signal. Starting with performing initial analysis with stochastic learning is intuitive because it allows more rapid convergence and can help the network to be more adept at identifying more specific patterns. This is especially given the small training set size in this study means the greater computational efficiency of larger mini-batch sizes is unnecessary for this example.

With a CNN, an epoch refers to a stage of training whereby the whole of the set of training images are sequentially shown to the network. The number of epochs used in training can vary to between less than 10 to many thousands. 20 epochs and a learning rate of 0.0001 are chosen as initial hyperparameters because these are either the same as studies aimed at using CNNs to recognise informal settlements (Wurm et al. 2019) or slightly lower (Persello and Stein, 2017, Maiya and Babu, 2018). However, these other learning rates are normally used when the training set is much larger. As a result, a small learning rate to compensate for the smaller training set size is intuitive because of the lack of computing power constraint.

For this stochastic learning appraoch, overall accuracy is sufficient as an evaluation metric because it is commonly used for studies of this kind (Verma et al, 2019, Mboga et al, 2019, Mboga et al, 2017) and is able to demonstrate the network's broad skill in recognising both categories. Overall accuracy expresses as a percentage the total number of correctly classified pixels divided by the total number of pixels.

The overall accuracy from the stochastic learning approach is at 75.72%, which demonstrates some skill in detecting informal settlements. But an examination however of how the training and test accuracies and losses compare as the network trains is revealing. The losses for the training and test set are calculated from the loss function and are as a result badness of fit measures, with lower values consequently indicating more skilful network performances. Figure 2-4 graphs the training and test accuracies as the network trains across the 20 epochs. The training loss follows an expected pattern: it reduces as the network trains and it is slightly lower than the test loss. This matches expectations, since the network should be more skilful at recognising images it is trained on than those it has not seen in the test set.

a.

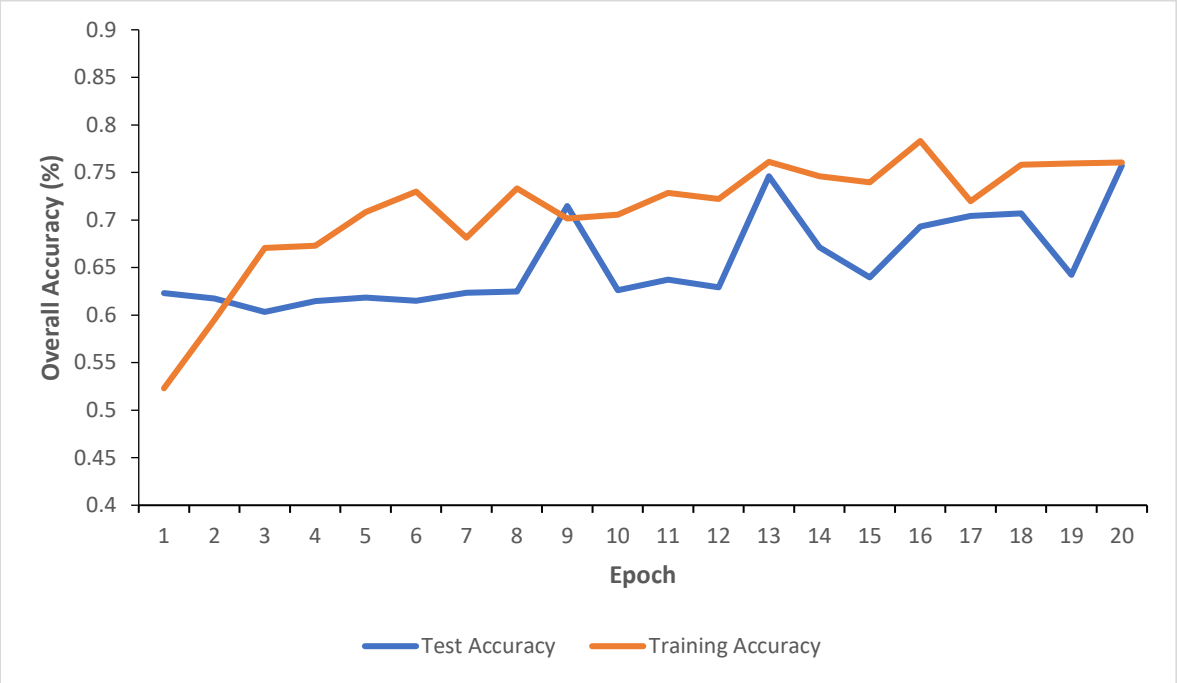

b.

Figure 2-4 Graphs of Training and Test Accuracy and Loss from the Stochastic Learning Approach.: Training and test (a.) accuracy and (b.) loss from the stochastic learning appraoch.

Both the training and test losses however are inconsistent and vary dramatically as the network trains according to Figure 2-4. This could indicate that the network is regularly overshooting minima in the loss function and is therefore unable to converge.

A further helpful insight into the stochastic learning approach's performance comes in examining the predictions made by the network in comparison with the equivalent ground-truth masks from the test set. Figure 2-5 shows these predictions rounded from their raw prediction value to a binary classification, yellow pixels meaning "informal" and purple being "formal".

a.

b.

c.

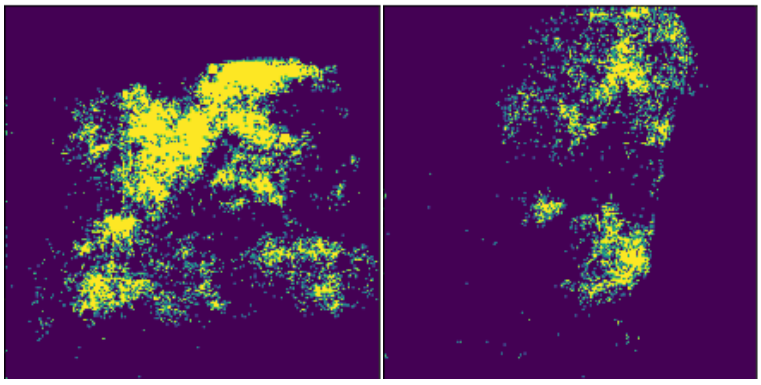

Figure 2-5 Images, Outputs and Masks from the Stochastic Learning Approach: (a.) Examples of images in the stochastic learning appraoch test set. (b.) Equivalent ground truth masks. (c.) Equivalent predictions from the network for these.

According to Figure 2-5, the network is skilled at detecting the broad areas of the informal settlements, but with a noisy pattern of detections called salt and pepper noise. Salt and pepper noise is defined as the presence of wrongly classified pixels within the broad area of another

(Castillo-Gonzalez et al, 2009). There are likely to be good place-based geographical reasons why this is the case. A network is likely to be limited to recognising certain visual elements of the informal settlement, such as the structure of the roofs for example. The network may therefore be fundamentally ignorant of certain others aspect of the informal settlements, particularly those which may be indistinguishable from similar features not unique to informal settlements. This may be creating the salt and pepper noise.

Based therefore on both empirical and conceptual reasons it is logical to apply post-processing methods to these obtained results. This takes two forms. First, the discriminant threshold through which a pixel is classified as informal is changed. This may be helpful because it could be the case that the pixels which are false negatives within the salt and pepper noise are those which the network is "not quite" placing in the correct category, and therefore their apparent misclassification is not indicative of an inherent lack of skill on behalf of the network but that the network's discriminant threshold needs to be changed. This may be arising from the informal settlement class being underrepresented in the overall dataset by around 2:1.

The other form which this post-processing takes arises from the concept that the informal settlement consists of many different entities, some the network may be less skilful at identifying than others. As a result, blurring the predictions may help the network to identify these missed features within the noisy predictions.

A further analysis of the stochastic learning approach therefore involves applying a gaussian filter to the output prediction. The gaussian blur operates with a sliding window, with the value of each pixel being transformed to a weighted average of the pixels surrounding it. The width of weights of the filter surrounding each pixel $G(x, y)$ is determined by:

$$G(x, y) = \frac{1}{2\pi\sigma^2} e^{-\frac{x^2+y^2}{2\sigma^2}}$$

(2-9)

(Young and van Vliet, 1995, Yaseen, et al, 2013)

Where:

$\sigma =$ The specified filter size in standard deviations.

$x, y =$ The distance from the blur centre point in pixels.

A variety of 9 different widths, ranging from 0 (no blur) to 17 are applied, with these figures representing the standard deviations of the gaussian blur. Subsequently to blurring, the

threshold between the two categories is varied by values between 1 and 0 to observe how the overall accuracy changes across the entirety of the possible discriminant thresholds, at intervals of 0.05. This results in 189 different combinations of blur and threshold change to analyse, which allows for a detailed examination of the effects of post-processing. Figure 2-6 visualises the difference in the kernel where $\sigma = 3$ (a.) as opposed to $\sigma = 17$ (b.) in the weights used to create the average for each pixel in the blurred predictions.

a.

0.37	0.49	0.58	0.61	0.58	0.49	0.37
0.49	0.64	0.76	0.80	0.76	0.64	0.49
0.58	0.76	0.90	0.95	0.90	0.76	0.58
0.61	0.80	0.95	1.00	0.95	0.80	0.61
0.58	0.76	0.90	0.95	0.90	0.76	0.58
0.49	0.64	0.76	0.80	0.76	0.64	0.49
0.37	0.49	0.58	0.61	0.58	0.49	0.37

b.

0.97	0.98	0.98	0.98	0.98	0.98	0.97
0.98	0.99	0.99	0.99	0.99	0.99	0.98
0.98	0.99	1.00	1.00	1.00	0.99	0.98
0.98	0.99	1.00	1.00	1.00	0.99	0.98
0.98	0.99	1.00	1.00	1.00	0.99	0.98
0.98	0.99	0.99	0.99	0.99	0.99	0.98
0.97	0.98	0.98	0.98	0.98	0.98	0.97

Figure 2-6 Visualisation of Gaussian Filter: Visual comparison of image weights used to calculate blurred predictions blur standard deviation of (a.) 3 as opposed to (b.) 17.

Figure 2-7 uses a heat map to represent these combinations of post-processing. Created using the python seaborn package, it demonstrates how the overall accuracy changes as the post-processing is applied. The accuracy before post-processing is 75.72%, but the optimal threshold change is around 0.1, with an optimal blur filter size between 3 and 9 standard deviations, which results in an increase in the overall accuracy by 2.8% to 78.5%. The apparent success of these procedures demonstrates that the overall accuracy metric by itself cannot fully describe how skilful the network is at identifying informal settlement pixels. Subsequently other evaluation metrics must be sought.

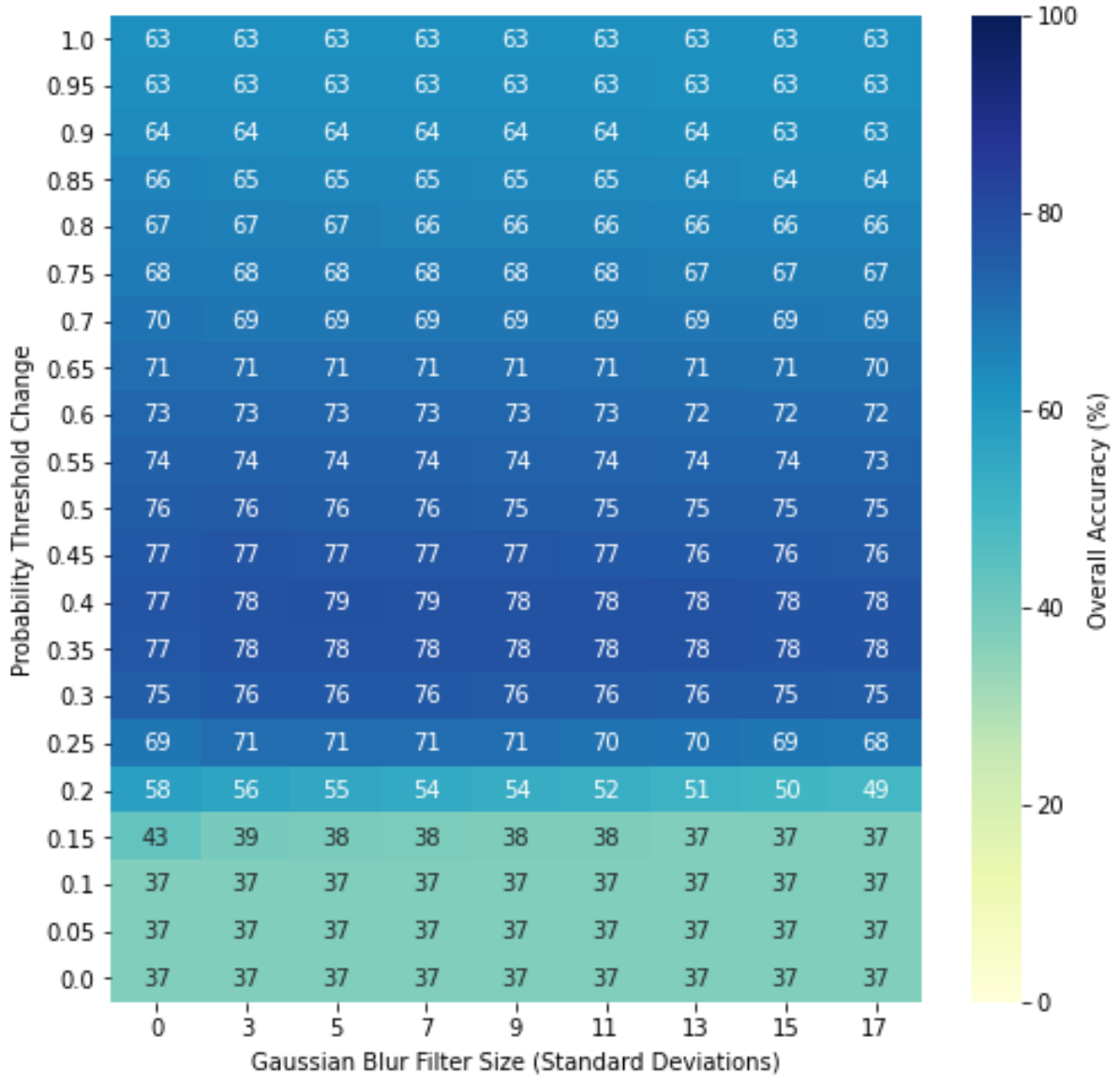

Figure 2-7 Heatmap of the Effects of Post-Processing: Heatmap summarising the overall accuracy from the stochastic learning approach with various combinations of post-processing applied. A value of 100% is optimal.

2.4.2 Evaluation Metrics

Because the stochastic learning approach showed the deficiency of overall accuracy, this research proceeds from these using the Receiver Operating Characteristic (ROC) curve as an evaluation metric. It displays results which are independent of the discriminant threshold and is therefore a suitable metric based on the findings of the stochastic learning approach (Cross et al, 1995), removing the need for any a priori threshold to be defined (Schumann et al. 2014). It allows an examination of the trade-off between the number of false predictions of informal settlements for a given number of true predictions at a pixel level. The area under the ROC

curve (AUC) is an interpretable summary statistic of an ROC curve and higher values are indicative of a network able to identify a large quantity of correctly classified pixels for a comparatively small trade off of falsely classified pixels in the same category.

$$AUC = \int_0^1 t\, df \tag{2-10}$$

Where:

AUC = Area Under the Receiver Operating Characteristic Curve (ROC).

t = True Positive Rate.

f = False Positive Rate.

The Brier score is similarly used because it maps the overall performance of the probabilistic predictions by measuring how close the predicted probabilities are from the true categories, instead of measuring the number of true or false predictions (Rufibach, 2010).

As with the ROC curve it is also not dependent on any specific a priori threshold being defined. The ROC and Brier Scores are presented in Equations 2-10 and 2-11.

$$B(p,x) = n^{-1} \sum_{i=1}^{n} (x_i - p_i)^2 \tag{2-11}$$

(Rufibach, 2010)

Where:

$B(p,x)$ = Brier Score.

p = Pixel-wise predicted probability.

x = True pixel value (0 or 1)

n = Number of Pixels.

In terms of examining the size of the blur filter which is optimal, it is evident from Figure 2-7 that changes in the blur filter size have a comparatively small effect on the overall accuracy relative to changes in the discriminant threshold. It is therefore preferable to first focus on the

optimization of the network independent of discriminant threshold prior to then finding the optimal size of the blur filter.

2.4.3 Mini-Batch Gradient Descent Approach

The use of stochastic learning may be causing the dramatic instability seen in the both the training and test loss in Figure 2-4 in the experimental stochastic learning approach. The high variance may be created from updating the parameters after each training image and making the network overshoot the global minimum in the loss function as a result (Walia, 2017). An alternative to stochastic learning lies in batch gradient descent. Here the parameter values are updated after the network sees the entire set of training images. This is more computationally efficient but can hinder the ability of the network to recognise patterns because the updates may become less precise and unable to escape sub-optimal minima in the loss function, particularly those characterised by a sharper gradient nearby gradient (Keskar et al. 2016). (Keskar et al. 2016).

Training using mini-batch gradient descent is a compromise between stochastic learning and batch gradient descent, whereby the parameter values are updated after the network has seen a pre-set number of images, known as the mini-batch size as a balance between the varying benefits.

The order of the images is shuffled so in each epoch the order of the images is different and the network sees a different combination of images in each batch (Bengio, 2012). A common approach to mini-batch size is to use a power of 2 for computational reasons, since powers of two is the method through which the GPU most efficiently processes values.

As a result, in adopting an appropriate mini-batch size, both 8 and 16 are preferable, to see if either of these represent an improvement in comparison to stochastic learning with a mini-batch size of 1. Normal mini-batch sizes in deep learning research would be a lot larger than these but these also use much larger training set sizes so they require this to make their training computationally feasible. For each of these mini-batch sizes the network is trained independently 100 times to make any conclusions robust.

The Keras fit_generator function is used which requires the user to set a value for the number of iterations per epoch. An iteration refers to the number of times in an epoch that a batch is fed through the network each epoch. This research follows standard practice in having the number of iterations per epoch roughly equal to the total training set size divided by the mini-

batch size. This corresponds to 44 iterations for the mini-batch size of 1, 6 iterations for the mini-batch size of 8 and 3 iterations for the mini-batch size of 16.

At this stage a new technique called early stopping is also introduced. Early stopping is a method designed to prevent neural networks from overfitting. Overfitting is a common obstacle when performing deep learning. It occurs when the network begins to learn patterns which are specific to the training set and not to the test set, meaning that it learns noise rather than signal (Cross et al, 1995, Nielsen, 2017).

Early stopping automatically stops the training early if there is a period of a specified number of epochs where there is no improvement in either the test loss or test accuracy. Because the exploratory stochastic learning appraoch established the deficiency of overall accuracy as a metric, the stopping criterion for early stopping is chosen as the test loss rather than the test accuracy. A patience of 10 is used, meaning the network will cease training if over a period of 10 epochs there is no improvement in the test loss.

Early stopping is introduced at this stage because it as where the process of tuning the network's hyperparameters begins, in the form of the mini-bath size. In this research which is seeking to optimize an FCN to recognise informal settlements, the use of early stopping enables a more targeted and bespoke hyperparameter tuning. It allows training with a high number of epochs without risk of overfitting, so a comparison between the different number of epochs as part of the optimisation is unnecessary (Bengio, 2012) and therefore it reduces the dimensionality of the hyperparameter space (Hinz et al. 2018). It is also easier to implement and more intuitive than more complex methods such as L2 regularization (Prechelt, 1998).

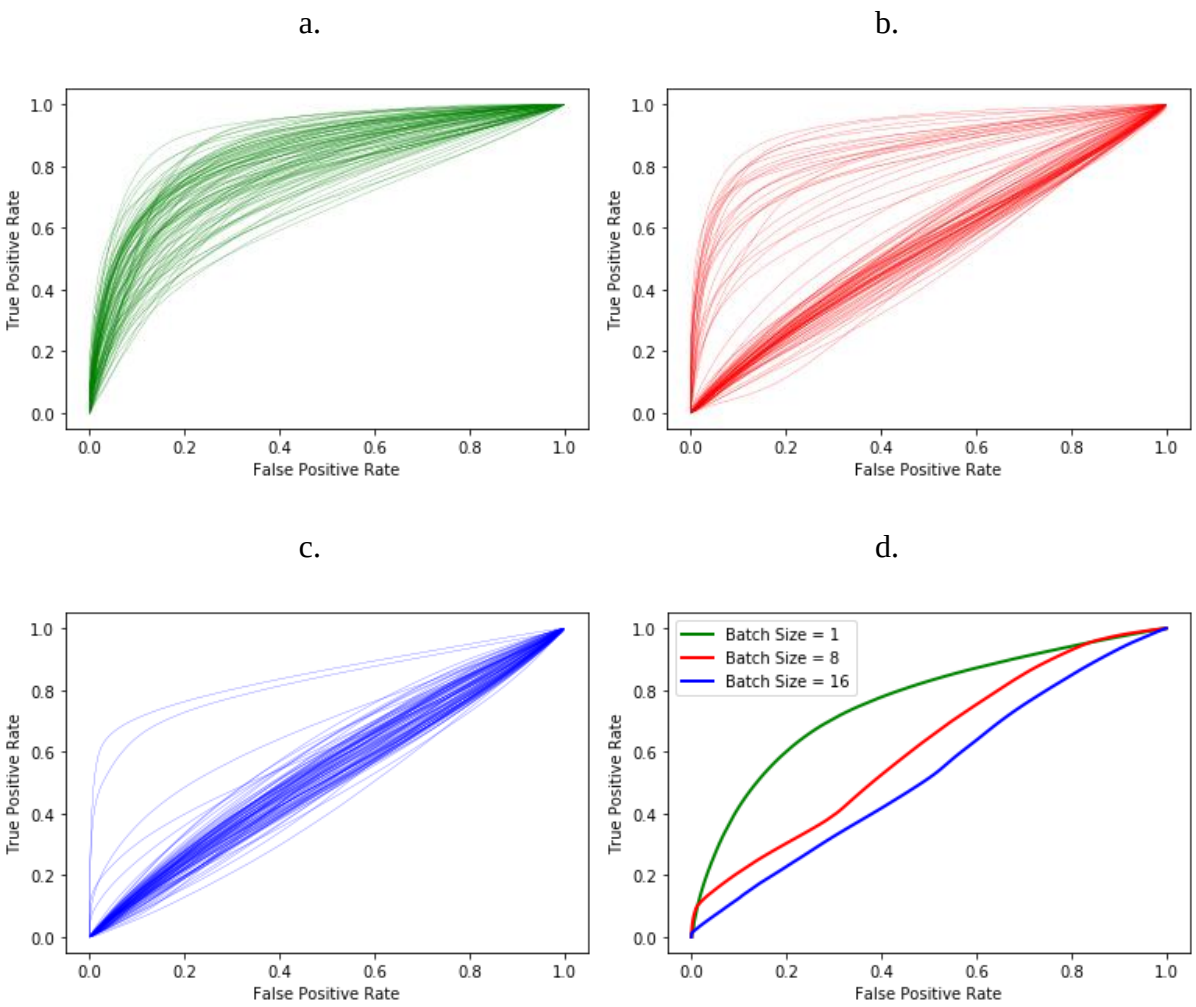

Figure 2-8 ROC curves of different Mini-bath sizes: Comparison of ROC curves for 100 experiments mini-batch size gradient Descent Approach for each of mini-batch sizes of 1 (a.), 8 (b.) and 16 (c.) as well as these aggregated for a direct comparison (d.).

It appears from Figure 2-8 that smaller mini-batch sizes are preferable and the benefit of a small mini-batch size outweighs the benefits of a large mini-batch size, with an average AUC of 0.793 as opposed to 0.607 and 0.536 for mini-batch sizes and 8 and 16 respectively. Subsequent networks consequently continue to use this mini-batch size. Figure 2-8 demonstrates that the mini-batch sizes of 8 and 16 are capable of producing results with high AUC values. These are not consistently replicated in the way that the curve with a mini-batch size of 1 does. A mini-batch size of 1 therefore seems like the most robust setting for the network.

2.4.4 Optimizing the Learning Rate and Decay Rate

Whilst it is now well established that the stochastic learning approach with a mini-batch size of 1 is best, it is next crucial to fine tune the initial learning rate and learning rate decay hyperparameters.

In optimizing the hyperparameters of the network trade-offs must be made between the number of hyperparameters tuned and the amount of training. The optimization henceforth is limited to the learning rate and decay rate. These are focussed upon as opposed to other hyperparameters because they represent a unique characteristic regarding how the network trains unlike others which are less central to the training process or add additional complexity. For example, many other hyperparameters are specific to preventing overfitting such as dropout and L2 regularization, which steps have already been taken to mitigate using early stopping. Additionally, much focus in this chapter is on the fine-tuning of the post-processing in addition to the hyperparameters and so some hyperparameters are retained at their pre-recommended settings.

The need to optimise the learning rate arises from the competing virtues and drawbacks of having a high and low learning rate. The benefit of a high learning rate is that it avoids the network getting "stuck" at a local minima before the network arrives at a global minimum (Cross et al, 1995). Equally, it may overshoot the desired global minimum in the loss function (Gandhi, 2018, Li et al. 2019). However, a low learning rate is likely to take an excessive amount of time to converge and risks being stuck in a sub-optimal local minimum before the global is reached (Walia, 2017).

A common method therefore of combining these two is to anneal the learning rate as the network trains. Both the initial learning rate and the rate of decay of the learning rate are among the most important hyperparameters to optimize (Li et al. 2019). Although the Adam optimizer is an adaptive learning rate method where individual parameters' learning rates are automatically tuned as the network trains (Kingma and Ba, 2015), the adaptive learning rates for different parameters are calculated from the initial learning rate as a starting point (Kingma and Ba, 2015).

Hyperparameter optimization usually works using trial and error, experimenting with various combinations of values. This research prefers to use random search, where a range is defined and the values of the hyperparameters are randomly selected from within this range, as opposed

to grid search where the values are pre-selected at certain points. Random search is preferable because the values are unconstrained by any prior selection criterion (Li et al. 2019). A comparison with grid search finds it to be a more efficient method of optimising hyperparameters (Hinz et al. 2018). The random search of the learning rate and decay rate is carried out on a log scale because this allows for a much greater range of values to be analysed because often substantive differences in learning rate and decay rate occur with order of magnitude changes (Bengio, 2012, Li et al. 2019).

2.4.5 Fine Tuning the Learning Rate Decay Schedule and Post-Processing

There are a number of strategies of how the decay in learning rate should take place, such as decaying the rate in steps or exponentially (Bengio, 2012). A single parameter to describe the rate of decay is to be used in order to make results more interpretable and easier to do in a random search context. Whilst this solution is less interpretable than a routine linear decay of a fixed amount per iteration, such an approach would be inappropriate for such a hyperparameter optimisation exercise because it may result in the learning rate reaching zero by the end.

The learning rate decay is described as follows:

$$LR_t = LR_0 \left(\frac{1}{1 + dt} \right) \tag{2-12}$$

Where:

LR_t = Learning rate at iteration t.

LR_0 = Initial learning rate.

t = Iteration at which the network is training.

d = Decay rate.

The network could either be most optimally trained with high initial learning rates and rapid decay or low initial learning rates and slow decay, or some combination of these. The initial learning rate is selected randomly on a logarithmic scale between 0.00001 and 0.001, and the decay rate is selected from between 0.00001 and 0.01. Here rate of decay is tuned to represent a strong spread of proportions of decay of the initial learning rate, from a minimum rate of decay, where after 100 epochs the learning rate is as high as 96% of the initial, to as low as 2%.

400 training experiments are performed for this hyperparameter random search, where the initial learning rate and decay rate are randomly selected and the previously established desirable settings of a mini-batch size of 1 where 44 iterations are used and same system of cross validation and early stopping as before are employed.

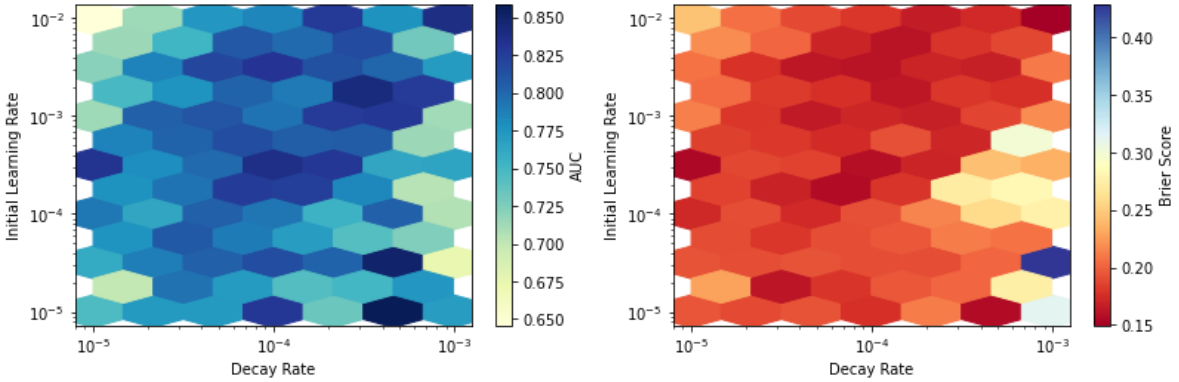

Figure 2-9. Hexbin Plots Optimising Learning Rate and Decay Rate. Hexbin heat maps of learning rates and decay rates for (a.) AUC and (b.) Brier score. Higher AUC scores and lower Brier scores are superior.

The results are shown in the hexbins in Figure 2-9. An optimal point appears to exist for medium values of initial learning rate and high values of rate of decay, with an AUC of 0.83 and Brier Score of 0.16 for these. This initial learning rate is slightly above the median value of 0.0001 and the decay is also above the median from the initial range of random values. A learning rate of 0.00016 and decay rate of 0.0013 are parsimonious representations of this optimum. Such values are intuitive because a medium to high learning rate may be allowing the network to relatively quickly converge the parameter values towards the approximate region of the global minimum of the loss function, but yet the low learning rate later in the training created by the high decay may be allowing the network to settle at this point.

Subsequent experiments aimed at optimizing the ideal threshold and size of gaussian blur filter use these values for the respective hyperparameters. The research performs another 50 similar cross validations and aggregates the results into a single optimized ROC curve, with a final mean AUC from these of 0.834 and Brier score of 0.155. Figure 2-10 presents the collective ROC curves and aggregated version.

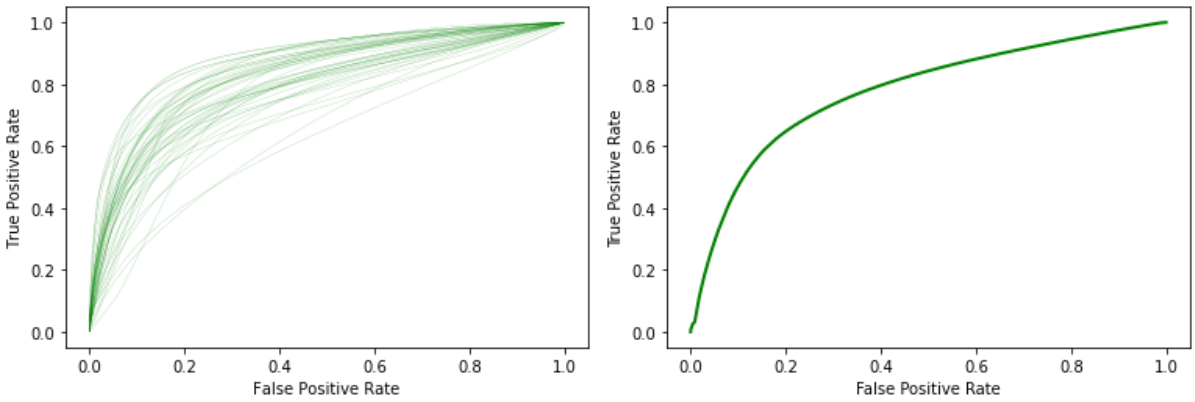

Figure 2-10 Optimised Hyperparameter ROC Curves: ROC curves from (a.) the 50 experiments using the optimized hyperparameters and (b.) the aggregated ROC curve.

The optimal threshold can be derived from these ROC curves. The optimal threshold is the point where an increase in true positive pixels is outnumbered by the number of falsely classified positive pixels which are identified. In other words, this is the point where marginal the increase in false positives becomes greater than the marginal increase in true positives. On the ROC curve this can be identified as the point where the gradient of the ROC curve reaches 1. For the aggregated ROC curve this optimum threshold is 0.28, equating to a change in threshold of 0.22 relative to the standard of 0.5. Such an estimate is intuitive given the results of the exploratory stochastic learning approach suggested an ideal threshold was similar at about 0.4.

In finding the optimum gaussian blur filter size, I return to the use of overall accuracy as a metric. After the exploratory stochastic learning approach overall accuracy was established to be a poor measure. Because however the ROC curve has allowed the optimal threshold to be found, it is then more applicable to use the overall accuracy. A gaussian blur filter of different sizes is applied to all 50 of these optimised simulations and it is assessed how the overall accuracy changes. Figure 2-11 shows how the optimum blur filter size is 3 standard deviations. This represents an improvement as opposed to having no blur of around 0.7% at the optimal threshold of 0.28. From these 50 experiments the overall accuracy before any post-processing is 74.55%. With the relevant discriminant threshold change without blurring this rises only marginally to 74.61%.

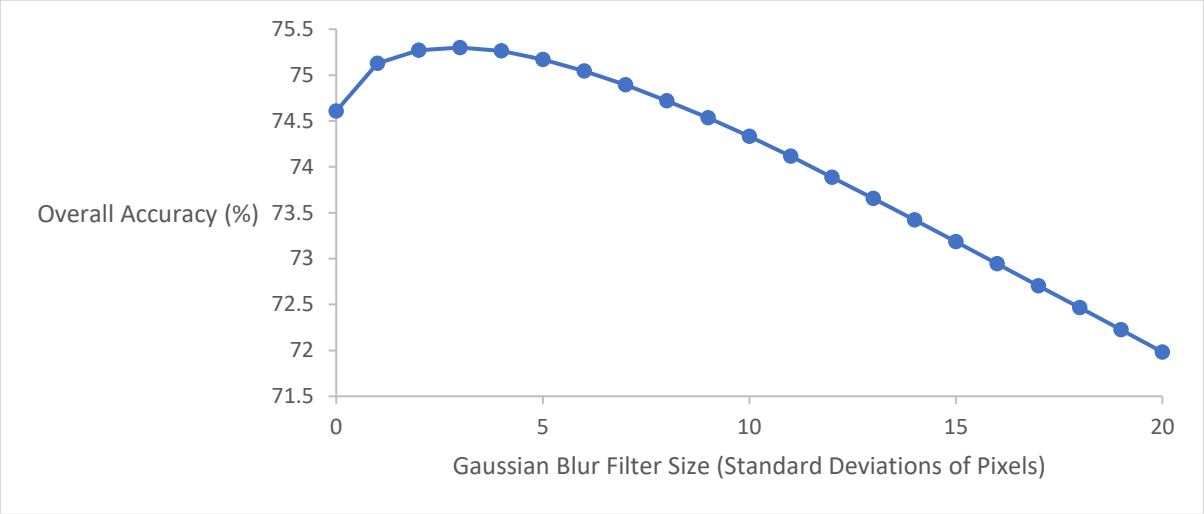

Figure 2-11 Blur Size vs. Overall Accuracy Graph: Analysis of the changes in overall accuracy by employing a gaussian blur filter at the threshold designated by prior analysis, across the 50 experiments.

2.4.6 Mapping All of Cape Town Using FCN Predictions

A skilful neural network able to identify informal settlements across Cape Town has the potential to be scaled up to the whole of the city. Studies mapping informal settlements currently do not scale up in this way, with the aim of supporting informal settlement improvement programmes (Byrne et al, 2018) and mapping natural hazard risk (Bai et al, 2018). Such a map will be utilized in Chapter 4 by coupling it to a physical flood map to produce a social vulnerability integrated flood risk map.

Global Urban Footprint (GUF) data (Global Urban Footprint, 2016) is used to act as a reference map to identify urban areas in Cape Town where potential informal settlements may exist. GUF is a gridded spatial dataset classifying areas as either urban or rural. This dataset is derived from a satellite-based Digital Elevation Model (DEM) and Synthetic Aperture Radar from TanDEM-X and TerraSAR-X respectively and is produced by the German Aerospace Center (Esch et al, 2013). The urban areas are extracted from this data to derive texture information and night time lights and surface spectral profile (Esch et al, 2013). The GUF dataset is blurred using a gaussian filter with a standard deviation of 7 in order to remove any noise and produce a more filled and consistent mask. However, the original data for the GUF dataset was collected in 2011-12 (DLR-DFD, 2016). Therefore, the dynamic nature of informal settlement environments means that informal settlements may have developed after the publication of the GUF dataset, which may not therefore be identified.

To validate the use of GUF for this purpose, the ground truth informal settlements contained within the SDI dataset can be compared with GUF to assess the percentage of informal settlements in Cape Town which are included within the GUF urban category. At an informal settlement level, GUF is capable of identifying all 75 informal settlements in the SDI dataset and the 30 additional visually identified informal settlements. On a pixel level 96.9% of informal settlement pixels are classified as belonging to the urban class. GUF data can therefore be declared to represent reliable coverage of informal settlements. Figure 2-12 demonstrates how each SDI informal settlement lies within the areas identified as urban by the GUF dataset.

The study area for this mapping ranges from a latitude of 34.01°S, to 33.80°S, and a longitude of 18.40°E to 18.70°E. Within this window the areas designated as urban by the Global Urban Footprint dataset. This corresponds to a total area of 492km^2.

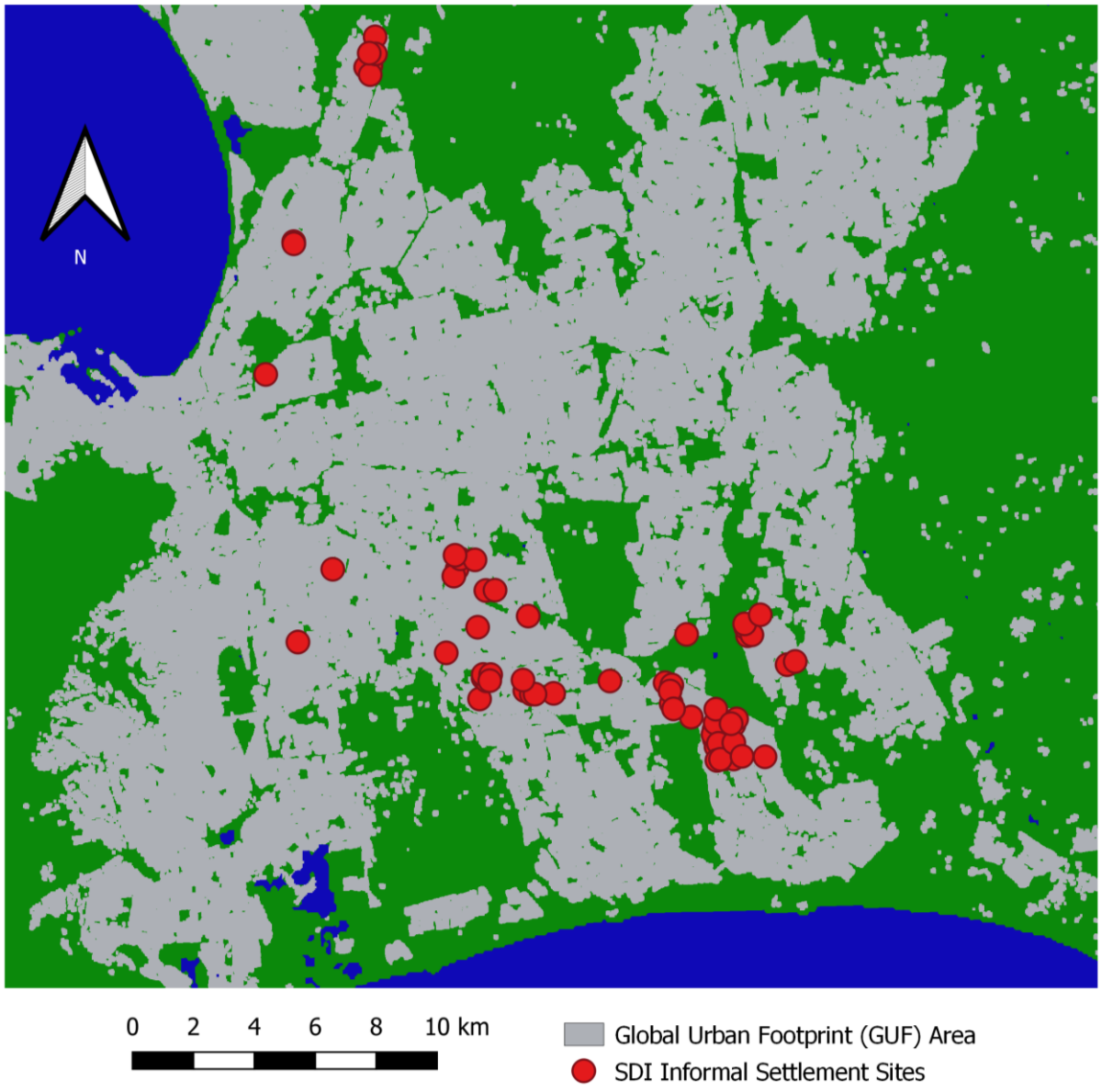

Figure 2-12: Location of SDI informal settlements within Cape Town blurred GUF mask.

The GUF mask is used to derive 9855 centre points to download images at an identical zoom level from which the network was originally fine-tuned, with the distances between these defined according to the widths of the downloaded Google Maps API images.

Using the fine-tuned learning rate and decay rate in addition to post-processing parameters, a committee of ten networks are independently trained, and predictions made for each of the ten networks aggregated for each of the 9855 images. A committee is used to avoid the network's skill and predictions being dependent on any particular training-test split. This makes the predictions more robust.

Post-processing probabilities are used in place of predictions based on the assumption that the dividing line between informal and formal environments may not be a strict dichotomy but instead a continuum, with many ontological features (Owen and Wong, 2013, Kohli et al, 2012) of informal settlements such as dwelling size and roof material being indicative of areas of socioeconomic disadvantage but nonetheless may not be recognised as an informal settlement in the strict sense.

Some pixels are classified and considered to have values above 1 due to the post-processing applied. These values are capped at 1 to make the outcomes interpretable and sensical. The 9855 output predictions are quilted into a mosaic to form a single map of predictions of probabilities of informal settlements.

The original terms and conditions of the Google Maps imagery forbid the combining of multiple images into a single large image. What is done however with quilting to scale up the method to the whole of Cape Town does not violate these terms and conditions. This is because what is done is to quilt the predicted probabilities derived from the images, not the images themselves.

The predictions are aggregated to a resolution of approximately 25 meters as a size this small will likely capture all informal settlements but makes the final output more manageable and less invasive from a privacy point of view to residents because it avoids the final map including classifications of individual households. The informal settlement predicted probabilities are presented in Figure 2-13.

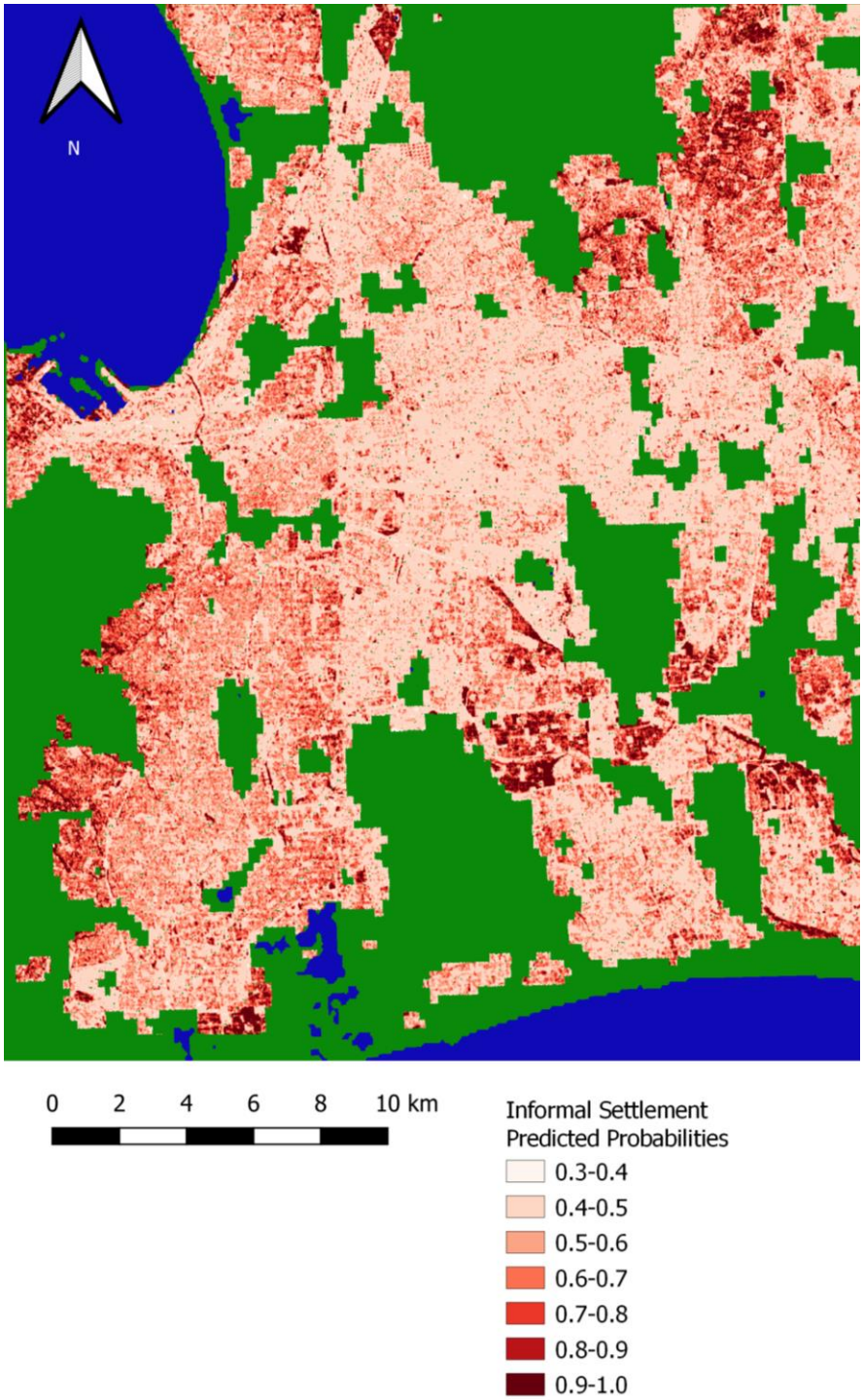

Figure 2-13 Scaled-up Map of Informal Settlement Predicted Probabilities: Outputs for the committee of 10 networks with fine-tuned post-processing applied to across Cape Town aggregated to a ~25m spatial resolution. Predictions above 1 are recoded to 1 to maintain the interpretability of predictions.

Examining the informal settlement predicted probabilities map does however reveal a weakness in this scaled-up predictions map. To the west of a latitude of approximately 18.52°E, about one third of the distance across the there is a visible change in the pixel prediction along this latitude. This is due to a difference in type of imagery or time at which the imagery was taken. To the west of 18.52°E the average pixel prediction is 0.568, to the east this value is 0.532. This is responsible for much of the differences between the SDI ground truth informal settlements shown in Figure 2-12 and the informal settlement predicted probabilities shown in Figure 2-13. To the west of 18.52°E there are very few informal settlements in the SDI dataset but high predicted probabilities.

It may be that drawbacks such as this come naturally with the use of freely available satellite imagery. If the parameters of futures studies remain to use such freely available satellite imagery, a method of ensuring that the problem seen at the 18.52°E latitude is avoidied in future studies is needed. Ambitions to attach layers such as this to GFMs using this method will inevitably encounter this problem if informal settlements are to be detected across the large spatial scales needed to allow attachment to the GFM. To solve this, the method should ensure that the sample of images used to train and test the network is from a diverse variety of locations such that the network gains similar skill in detecting informal settlements across a range of different types of visible light satellite imagery. This will make the network skilful at recognising informal settlements for many different imagery types and thus avoiding this problem.

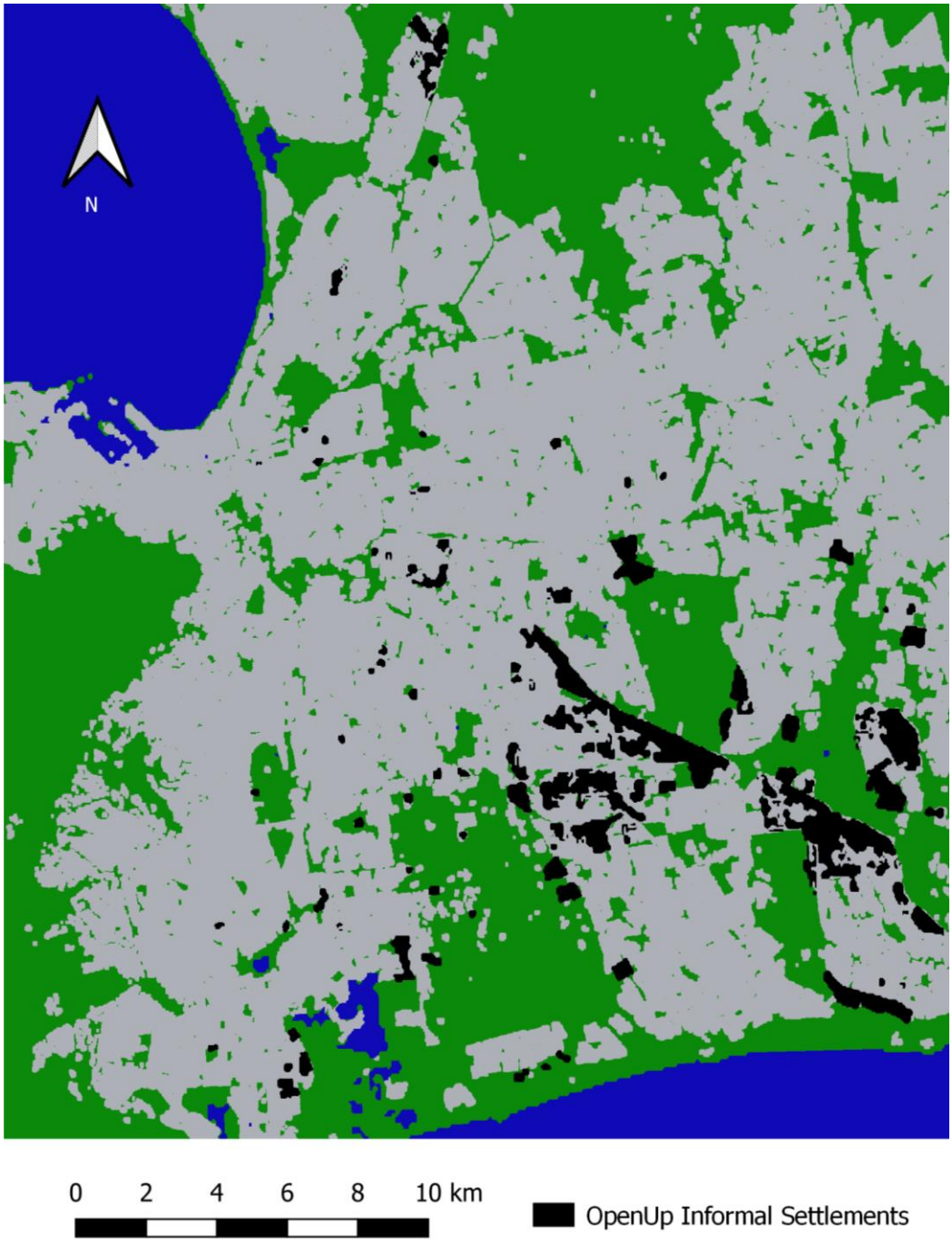

Figure 2-14: **Map of the location of informal settlements in Cape Town according to the OpenUp organisation.**

2.4.7 Evaluating Scaled Up Map

The OpenUp informal settlement map of Cape Town provides the opportunity to evaluate the scaled-up map of informal settlement predicted probabilities against a different data source, these are presented in Figure 2-14.

This evaluation takes the form of comparing the informal settlement pixelated probabilities in the areas which are informal settlements in the OpenUp map with those not deemed so. The average pixelated probability in the ground truth OpenUp informal settlements is 0.69, whereas in the areas outside informal settlements this value is 0.54. The informal settlement predicted probability map is consequently clearly skilful in identifying the areas the OpenUp map considers to be informal settlements.

With post-processing included, the 0.69 prediction of the OpenUp informal settlements seems to represent a vindication of the skill of the network. Especially given that there is a discernible difference between the predictions for the ground truth informal settlements and formal areas, at 0.15. However, the high prediction of 0.54 for the formal areas of the city is discouraging. The network appears to lack the ability to assign low predictions to areas of the city which are not informal according to the OpenUp map. The two maps are compared in Figure 2-15.

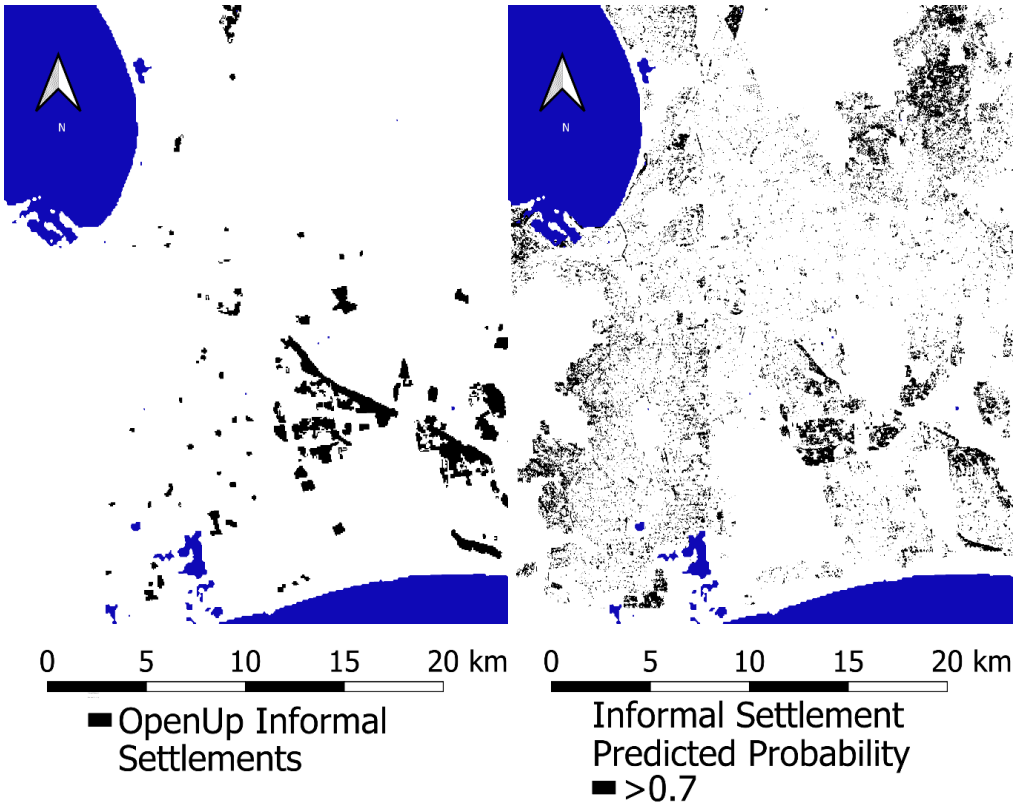

Figure 2-15: OpenUp informal settlement map and Informal Settlement Predicted Probabilities above 0.7 after post-processing.

An examination of the informal settlement predicted probabilities is revealing with regard to why the network appears to struggle in this way. A plot of the percentiles of the predictions

from the FCN in Figure 2-16 demonstrates that the network struggles to give low predictions to the most unlikely areas as being informal settlements. There is a "floor" of around 0.200 below which the network struggles to make predictions. As shown in Figure 2-16, even the 1st percentile of informal settlement prediction gives a value of 0.182, suggesting the network struggles to interpret areas very unlikely to be informal settlements accordingly. This as a result leads to an overprediction in more formal parts of the city.

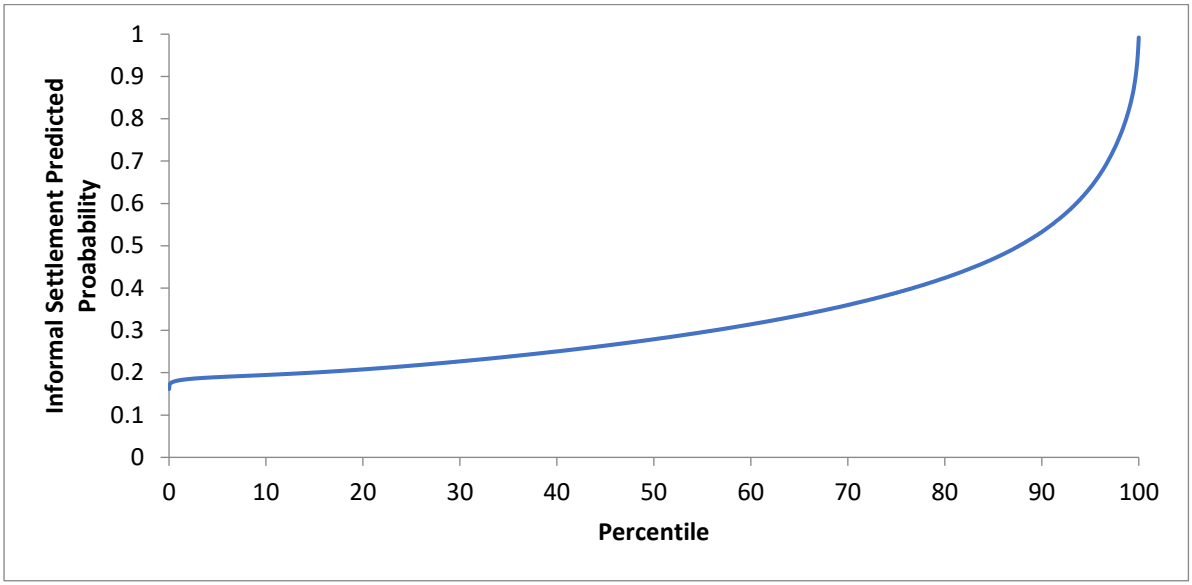

Figure 2-16: Graphic presentation of informal settlement predicted probability percentiles from across the pixels prior to post-processing being applied.

2.5 Discussion, Conclusions and Limitations

This research has demonstrated the ability to use freely available data sources and computation to map informal settlements in Cape Town, South Africa using a relatively small dataset and the network's hyperparameters and post-processing are fine-tuned to optimize performance. The research also presents a first of its kind cost-efficient informal settlement map of Cape Town derived from the final trained and optimized network. A map of this kind will enable the efficient monitoring of informal settlements and the allocation of resources aimed directly at upgrading and improving the living conditions in these environments.

The potential for improvement through changing the threshold seems limited, but some improvement can be gained through the use of gaussian blur post-processing has shown a greater applicability. In comparison to the original exploratory stochastic learning approach, which saw a substantial improvement in overall accuracy through post-processing, for final 50 fully-optimized experiments this was less pronounced. The tuning of the hyperparameters and

possibly training of the network for longer may be mitigating some of the need for post-processing. The final results however suggest that blurring could be a useful conceptually grounded form of post-processing to help map informal settlements, despite in the final analysis only a limited improvement in overall accuracy, although the fine-tuned results suggested a marked discriminant threshold change is necessary to achieve optimal results after hyperparameter fine-tuning.

Drawbacks to the results are however present with there still being a high variability in the final set of ROC curves obtained from Figure 2-10, even when using the optimized hyperparameters. This is likely to be for the large part due to variation in the nature of the training and test sets, especially given that the sample size is small.

In keeping with the objectives of the thesis, the chapter scaled up the predictions to the whole of Cape Town and was evaluated by comparing the informal settlement predicted probability values inside and outside where informal settlements are according to the OpenUp organisation, and promising results were here shown.

Future research should seek to develop further techniques to make the method generalizable. The fine-tuning of the network's hyperparameters in this study will aid this, as well as insights gained by upscaling the prediction to the whole of Cape Town, as there is scope for further evaluation of the performance of a CNN across a range of environments since there is a large test set with which to test the network's performance.

With the precise method utilising a very small dataset, the deployment of further methods of dataset augmentation will represent an important next step in developing the method. Section 2.2 highlighted how studies of this kind have particular difficulty in generalizing or having the ability to recognise informal settlements across a range of environments, not just in particular cities.

The map of Cape Town's informal settlements made in this chapter may be attached to a physical flood model. This will be useful to test the theoretical usefulness of maps of this kind. To be produced on spatial scales large enough to be of practical use however, the network used will have to be able to generalise to recognise informal settlements across a wide range of environments, not just individual cities, if it is to be able to be used to produce large scale flood risk maps.

Dataset augmentation is recognised as being helpful in making networks generalisable because its ability to expand the range of overall patterns which the network is able to recognise as belonging to a given category (Bowles et al, 2018). However, most methods of dataset augmentation, such as the image rotation performed in this chapter, are limited in their ability to make the sample distribution match the true distribution because the augmented images are constrained by pre-determined rules and functions (Bowles et al, 2018, Frid-Ader et al, 2018, Zhu et al, 2018).

As a result, an example of further study could be the use of Generative Adversarial Networks (GANs). A GAN is a novel type of neural network able to generate artificial but realistic images similar to those in the training set (Morizet, 2020). First proposed by Goodfellow et al (2014), a GAN consists of two networks coupled together, one referred to as the generator, the other a discriminator. The generator network begins by producing random noise with the discriminator determining whether the generated noise belongs to the sample of true images (Morizet, 2020). The training process leads to the generator eventually being able to turn random noise into images which appear similar to or even indistinguishable from true images in the training set. At a popular level GANs are to a great extent behind well-known artificial intelligence technologies such as deepfakes (Sample, 2020) and social media bots generating fake news (Adams, 2017).

These attributes allow GANs to be used as a powerful form of dataset augmentation because the augmented images can be produced without the constraints and thus are more able to match the images in the true distribution (Bowles et al, 2018, Frid-Adar et al, 2018, Zhu et al, 2018).

They have shown improvements in performance for various computer vision tasks, including medical imaging (Bowles et al, 2018, Frid-Adar et al, 2018), facial recognition (Di et al, 2018), facial expression recognition (Zhu et al, 2018) and remote sensing tasks (Zheng et al, 2019, Howe et al, 2019). But currently GANs have not been employed as a dataset augmentation for the detection of informal settlements from remotely sensed imagery. A study therefore attempting to make a CNN recognise informal settlements generalizable using GANs as a dataset augmentation method has the potential to help informal settlements be mapped on larger spatial scales suitable for global flood risk maps.

In replicating the methods demonstrated here for other cities, studies may seek to use similar SDI datasets, Nairobi is an example of such a city where extensive SDI data exists, as this study

has demonstrated the efficacy of using community based maps as ground truths and so future studies detecting informal settlements may seek to continue along this line of research.

An additional future research gap may be to assess whether the post-processing techniques developed here could be used in generalizability studies and how the size of the optimal gaussian blur filter changes for different cities or when validating on different cities. How this relates to the geographical theories discussed here could also be explored.

Furthermore, more advanced methods involving second order optimizers could be employed. Whilst most training uses first order optimizers, where only the first order derivative or the gradient of the loss function is calculated, a second order method calculates the second order derivative, or the rate of change of the gradient of the loss function (Li et al. 2019). This is normally highly computationally intensive, but where the training set size is relatively small in comparison to other deep learning projects, such an approach seems plausible for studies similar to this.

A problem of a lack training has led to the network failing to assign low predicted probabilities to the areas least likely to be informal settlements, as shown in Figure 2-16. This may be due to a lack of training. More training would possibly help this, perhaps by changing the tolerance of early stopping or removing the early stopping entirely and using an alternative method to prevent overfitting, such as L2 regularization. L2 regularization works by applying an extra term to the loss function corresponding to the sum of square of weights in the network in order to prioritise the training of smaller weights rather than larger ones (Nielsen, 2017). This makes the network less sensitive to small changes in input and consequently encourages it to learn signal rather than noise (Nielsen, 2017). The method may as a result allow more training to take place and overfitting to be avoided simultaneously. It should as a result avoid the “floor” seen in Figure 2-16.

3. Area-based Informal Settlement Mapping Using Deep Learning Outputs

3.1 Introduction

Chapter 2 used a Fully Convolutional Network (FCN) to produce outputs which were pixel-based and the results were evaluated using pixel-based metrics in the form of the overall accuracy, Brier Score and Area Under the ROC curve (AUC). The use of a pixel-based approach has the benefit of using a resolute and consistent spatial unit of analysis. However, when seeking to map informal settlements a pixel-based approach has limitations, most notably the lack of real-world correspondence conceptually between these pixels and the phenomenon being studied (Hussain et al, 2013, Verma et al, 2019). There are as a result conceptual benefits of mapping using an area-based rather than a pixel-based approach. The use of blurring as a form of post-processing addressed this issue to an extent by addressing the fact that an informal settlement is a heterogenous spatial unit consisting of a variety of amenities rather than being uniform, as Section 2.3.2 discussed. But the method ultimately in that chapter was still pixel-based in both the outputs which were produced and how these were evaluated.

In Chapter 1 I defined social vulnerability, which is generally more intense in informal settlements, as "the propensity for individual and contextual socioeconomic factors to cause certain places to be at a greater likelihood of being more negatively affected by a given hazard than other places". This definition highlights the importance of spatial context and the concept of place. Vulnerable households do not exist as isolated pixels, but rather members of spatially bounded communities which are salient when it comes to hazard planning and response (Hussain et al, 2013, Verma et al, 2019). Identifying the boundaries of vulnerable communities through an area-based method therefore represents an improvement on pixel-based approaches. The method proposed here as a result has the potential to combine the technical benefits of deep learning with the conceptual benefits of producing area-based rather than pixel-based outputs.

In keeping with the conceptual advantage of producing area-based rather than pixel-based outputs, many researchers advocate the use of metrics which are reflective of this and incorporate these benefits (Awrangjeb and Fraser, 2014, Cai et al, 2018, Bonnet et al, 2015, Hussain et al, 2013, Hernando et al, 2012, Clinton et al, 2010). Such measures are designed to

evaluate the ability of a method to map features reflecting the character of an area, such as its position and shape.

In mapping informal settlements however, most studies only produce outputs which are evaluated using pixel-based accuracy measures. There is a lack of studies seeking to evaluate the outputs of CNNs detecting informal settlements using area-based accuracy measures. The pixel-based outputs developed in Chapter 2 present an ideal opportunity to construct and fine tune a method of converting pixel-based outputs to area-based ones, in order to create a social vulnerability map to be coupled to a physical flood map in Chapter 4.

In light of this summary, this research chapter has the following aims. To convert the outputs of the refined FCN in Chapter 2 from pixel-based to area-based outputs, to be attached to a physical flood risk map in Chapter 4. It also aims to assess these areas using area-based evaluation metrics in order to evaluate the ability of the method to detect informal settlements.Finally, this research chapter will scale the fine-tuned method up to the whole of Cape Town, as in Chapter 2, and evaluate this against the OpenUp map.

3.2 Literature Review

3.2.1 Conceptual Benefits of Area-Based Analysis Compared to Pixel-Based Analysis

Although pixel-based image analysis (PBIA) is widely used to detect informal settlements, critics argue that such an approach lacks any real-world correspondence (Hussain et al, 2013, Verma et al, 2019). Area-based methods, otherwise known as object-based image analysis (OBIA) involve the segmentation of an image into homogenous objects followed by the analysis and classification of these objects" (Whiteside et al, 2011: 885). Area-based methods are often more conceptually applicable since individual pixels represent arbitrary units bearing no resemblance to the entity being investigated (Whiteside et al, 2011).

The term "segmentation" means something different in the deep learning and digital image processing research communities. In deep learning "segmentation" refers to the pixel-wise classification across a whole image (Sharma, 2019, Qualcomm, 2020). In the digital image processing community however, it means the subdivision of already classified pixels of an image into areas or objects (Hussain et al, 2013, Savant, 2014, Kaur and Kaur, 2014, Freixenet et al, 2002). In this thesis I use the term "segmentation" always in the context of the deep learning definition. The phrase "image partition" is used in place of the digital image processing use of the term "segmentation" in order to maintain consistent use of language.

Through image partition, area-based methods are able to express more information such as shape and spatial relationships (Hussain et al, 2013). It is distinguished from PBIA through the use of a two-stage process. First, the image is partitioned from the pixelated raw image into specific objects. Second, further classification can be performed on the resultant segments into spatially adjacent and spectrally similar components (Hussain et al, 2013, Hernando et al, 2012, Blaschke, 2010) whereas PBIA performs analysis in ignorance of such objects. Scene based classification represents a similar divergence from PBIA (Leonita et al, 2018) but where the basic unit of analysis is not objects or pixels but the entirety of an image scene (Li et al, 2017).

Recognition of the shortcomings of PBIA was widespread amongst the research community as early as the 1970s but at that time the quality of available imagery did not allow area-based application to become widespread (Hussain et al, 2013). Equally, the use of increasingly higher resolution imagery renders pixel-based techniques ineffective because the pixels are too small to show anything of interest (Sun and Meng, 2019, Kuffer et al, 2018, Mboga et al, 2019, Wurm et al, 2019, Shahzad et al, 2017, Vatsavai, 2013). A detailed comparison by Castillo-Gonzalez et al (2009) comparing a number of classification methods including using minimum distance, parallelepiped, Mahalanobis classifier, maximum likelihood and spectral angle mapper at both the pixel and area level methods found the superiority of the methods when applied at the area level. Significantly better results using area-based methods as opposed to PBIA were also produced by Whiteside et al (2011) in detecting savanna in Australia using Fractal Net image partition classified using nearest neighbours. Both Castillo-Gonzalez et al (2009) and Whiteside et al (2011) note the particular benefit of area-based methods in classifying land-cover classes with high intra-class variance such as orchards, bare soil, savanna and vineyards. Intra-class variance here means a class with a wide range in pixel values within a particular class. Furthermore, both were able to obtain outputs with less salt and pepper noise outputs using area-based methods. Along similar lines, Quinn et al (2018) find benefits of using an area-based approach in detecting informal settlements using deep learning. This was due to the wide range of features and amenities found in visible light satellite images and in particular in informal settlements.

Whereas Chapter 2 demonstrated the success of a pixel-based deep learning approach to the detection of informal settlements, the application of this method to social vulnerability for the purpose of flood risk mapping requires an area-based method. As stated in Chapter 1, the main characteristics of informal settlements that are recognisable in satellite imagery are the density of buildings and spectral profile of roofs (Kohli et al, 2012, Owen and Wong, 2013). These

visual attributes are not related to location and spatial scale to the same extent as the factors which cause social vulnerability; the factors which influence social vulnerability are dependent on the spatial scale through which they operate (Rufat et al, 2015, Adger, 1999, Fekete, 2011) and to community level factors such as the existence of social networks (Porio, 2011, Cutter et al, 2000, 2003, Adeola, 2009, Chomsri and Sherer, 2013). Therefore, an area-based approach is more suitable to converting maps of informal settlements into maps of social vulnerability.

As well as the generic advantages of area-based methods discussed, some benefits of area-based methods have been recognised with specific reference to detecting informal settlements. This is due to the task of detecting informal settlements requiring an ability to recognise complex patterns between pixels (Vatsavai, 2013, Gadiraju et al, 2018) and the features reminiscent of informal settlements cannot be accurately represented by individual pixels (Vatsavai, 2013). Pixel-based deep learning operates on a mere assumption of underlying patterns without any knowledge of what those patterns are (Openshaw, 1992). As a result, the training of a pixel-based CNN may bear no conceptual relationship to the phenomenon of social vulnerability which the aim is to map.

There are hundreds of methods of performing image partition for area-based methods (Pal and Pal, 1993). They are generally split into boundary-based (Canny, 1986) and similarity-based (Hussain et al, 2013, Freixenet et al, 2002). In boundary-based methods the image partition into polygons begins by detecting edges based on the places of greatest contrast and forming polygons from the extracted edges. In similarity-based methods the image partition begins with the detection of pixels with a common spectral identity which are spatially adjacent (Hussain et al, 2013). Widely used examples of area-based methods methods include fuzzy techniques (Lakshmi and Sankaranarayanan, 2010), saturation resolution merging, optimized high pass filter addition (Shahzad et al, 2017) and hulling (Laurentini, 1994, Carriera et al, 2016). Prominent boundary-based methods include the frequently used Grey level co-occurrence matrix (GLCM), which attempts to detect edges by measuring the amount of textural contrast (Kohli, 2013, Kohli et al, 2016, Kemper et al, 2015, Kuffer et al, 2018, Verma et al, 2019, Sun and Meng, 2019), random forests (Leonita et al, 2018, Vatsavai, 2013), canonical correlation forests (Gram-Hansen et al, 2019), snakes and radial casting (Mayunga et al, 2007), local binary patterns (Leonita et al, 2018), line based lacunarity (Kit et al, 2012), and differential attribute profiling (Kemper et al, 2015). Similarity-based methods include visual interpretation and polygon generation (Tarmizi et al, 2014), gaussian multiple instance learning (Vatsavai, 2013), PCA (principle components analysis) based lacunarity (Kit et al, 2012), graph theory

using Euler's characteristic to define the topology of neighbourhoods (Brelsford et al, 2018), the extraction of objects through common spectral profile (Kuffer and Barros, 2011), speckle divergence (Taubenbock, 2011), cluster analysis of buildings (Taubenbock and Kraff, 2014), clumpiness defined by an adjacency matrix (Baud et al, 2010), support vector machines (SVMs) (Leonita et al, 2018, Veljanovski et al, 2012), the region growing algorithm i.segment (Mboga et al, 2019) and many hierarchical methods (Taubenbock, 2011, Niebergall et al, 2007).

A number of these area-based methods however demonstrate shortfalls in their application to informal settlements. The use of visual interpretation such as that performed by Tarmizi et al (2014) is not automatic and is therefore unsuited to any large-scale image mapping. The additional lack of any quantitative basis means any results lack a consistent empirical foundation. Other methods such as the use of lacunarity encounter difficulty in distinguishing informal settlements from other environments such as vegetation and water bodies (Kit et al, 2012).

The methodological benefits of deep learning with the conceptual benefits of area-based methods can be combined. Section 2.2 discussed how CNNs can perform three main basic tasks with still images (Sharma, 2019, Qualcomm, 2020). These are image classification, object detection and segmentation (Sharma, 2019, Qualcomm, 2020).

Most deep learning methods which incorporate an area-based approach fall into the object detection category. Mask-RCNN is an example of a CNN which performs object detection, also commonly referred to as feature selection. Instead of pixel-wise segmentation, object detection produces areas using a 'propose and verify' method (Novotny et al, 2018). It involves regions of interest based training with bounding boxes pre-drawn (Bao and Chung, 2018, Chen and Jahanshahi, 2017, Jung et al, 2019). Mask-RCNN draws bounding boxes and performs segmentation simultaneously (Jung et al, 2019). It operates through the prediction of proposed areas, the refining of bounding boxes and the output of confidence scores for bounding boxes and the generation of a mask for each object from the originally proposed areas (Jung et al, 2019, Malhotra et al, 2018). Object detection and segmentation are closely linked in object detection CNNs such as Mask-RCNN (Gidaris and Komodakis, 2015). Such a method has been applied to informal settlement detection (Saindane et al, 2019, Quinn et al, 2018, Maiya and Babu, 2018, Li et al, 2017). A similar object detection approach is taken by Ibrahim et al (2019) but based on Google Street View imagery. Whilst object detection type CNNs have some success in area-based informal settlement detection (Maiya and Babu, 2018), systems such as

these still do not constitute a fully automated method (Quinn et al, 2018) and the proposing of regions by the network to perform the object detection amounts to an unnecessary computational cost and complexity (Saindane et al, 2019).

Although the 'propose and verify' type CNN methods are mainstream (Novotny et al, 2018), there are disadvantages of this approach. Basic segmentation tasks are more efficient through avoiding approximations to rectangular bounding box proposals, especially when the shape of the objects and final segmentations are of particular interest (Novotny et al, 2018). Segmentation methods, as opposed to region-based networks such as Mask-RCNN networks, can produce higher accuracies (Varatharasan et al, 2019). Vuola et al (2019) compared U-Net and Mask-RCNN and found Mask-RCNN lacked the ability to delineate boundaries of segments as well.

Because of the deficiencies of object detection based CNNs for informal settlement mapping, the use of post-processing of pixel-based CNN segmentation outputs presents an opportunity to create a more appropriate integrated methodology. The raw output of a CNN can be treated as a single band gray scale image with which to apply a similarity-based or boundary-based post-processing partition method. A variety of approaches have been taken to add post-processing methods to segmentation CNNs to turn raw outputs into area-based rather than pixelated outputs. Examples of post-processing methods include, denoising autoencoders (Larrazabel et al, 2019), conditional random fields (Knobelreiter et al, 2017, Larrazabel et al, 2019, Alam et al, 2017), SVMs (Niu and Suen, 2012), multiple inference (Jung et al, 2019), selecting the largest connecting component and hole filling (Jafari et al, 2016), spatial regularization (Scapra et al, 2018) and seed nuclei pixel growth (Kumar et al, 2017). Some of these methods are fully integrated with the training of the CNN, such as the conditional random field (Knobelreiter et al, 2017, Larrazabel et al, 2019, Alam et al, 2017).

To summarise, area-based methods are preferable because they have greater real-world correspondence to the phenomenon under study. This is particularly the case with informal settlements due to their nature as heterogenous entites with many different amenities. Additionally, where the attempt is ultimately to map social vulnerability, an area-based approach helps communities to be mapped, where the community level is where many contributors to social vulnerability manifest.

3.2. Evaluation Metrics of Area-Based Methods

In conjunction with the preference for area-based methods over pixel-based ones, some studies have recognised the need for accuracy measures to conceptually align with the method of analysis employed by using an area-based accuracy measure (Hussain et al, 2013, Hernando et al, 2012). A pixel "does not suitably represent the phenomenon under study" (Clinton et al, 2010: 290) and any assessment of uncertainty will be confined to a particular spatial unit disconnected to the spatial unit for which the uncertainty is being assessed, such as the spatial extent of the object in question (Zhan et al, 2005, Cai et al, 2018).

As a result, a category of area-based evaluation metrics has emerged (Awrangjeb and Fraser, 2014, Cai et al, 2018, Bonnet et al, 2015). These aim to measure the ability of ground truth reference polygons and predicted polygons to align geometrically and topologically (Montaghi et al, 2013). They have an emphasis on per-object rather than per-pixel evaluation and evaluate the shape, size and position similarity of the predicted and reference polygons in question instead of the numbers of pixels which overlap (Zhan et al, 2005). Such methods are also capable of quantitatively reflecting a qualitative assessment of a classification scheme (Shazhad et al, 2017). This is important because the spatial characteristics of the reference polygon and prediction polygon are of interest (Bonnet et al, 2015). They may be more interpretable and applicable to real world applications, with many usages being "directly associated with different properties of an object" (Zhan et al, 2005:2959) which pixel-based evaluation metrics may be incapable of assessing. Area-based evaluation metrics also have the advantage of being less susceptible to extensional uncertainty, where ground truth masks may be poorly drawn (Kuffer et al, 2018, Awrangjeb and Fraser, 2014, Leonita et al, 2018, Bonnet et al, 2015) and similarly where the definitions of informal settlements may vary in different places. The temporal dynamic nature of these environments may contribute to any uncertainty (Kuffer et al, 2018). Such uncertainty is especially part of the motivation for area-based evaluation metrics, with for example area-based methods having been demonstrated to be less susceptible to geo-referencing error or extensional uncertainty (Hussain et al, 2013).

Examples of area-based evaluation metrics include object matching, which is based on the average area of intersection between the reference and predicted polygons (Cai et al, 2018). Further examples include correctness and completeness, which are area-based equivalents of the pixel-based consumer's accuracy and producer's accuracy respectively (Cai et al, 2018, Zhan et al, 2005). A similar metric is Relative Area, which compares the area of intersection

of the polygons relative to the size of the reference polygon (Clinton et al, 2010), as well as Index D, which is based on the root sum of squares of the area of oversegmentation and undersegmentation (Clinton et al, 2010) and the relative overlapping area of the predicted and reference polygons (Montaghi et al, 2013). Further metrics are simsize and area fit index, which account for the relative area of the reference and predicted polygons independent of the area of intersection (Montaghi et al, 2013, Clinton et al, 2010). Relative position is another and measures the distance between the centroids of the reference and predicted polygons (Montaghi et al, 2013, Clinton et al, 2010). Tverskey's feature contrast model aims to account for shape complexity and common features contained in reference and predicted polygons as an evaluation metric (Zhan et al, 2005). The area-perimeter ratio measures how the ratio of the perimeter and area compares for both the predicted and reference polygons (Kuffer et al, 2016). Shape similarity aims to account for the relative radii of the reference and predicted polygons. A large literature exists in the field of computer vision to analyse shape similarity (Clinton et al, 2010) and there are also composite measures which combine metrics (Clinton et al, 2010).

In evaluating informal settlement detection, attempts largely use pixel-based evaluation method similar to that performed in Chapter 2. Metrics used include overall accuracy (Persello and Stein, 2017, Helber et al, 2018, Gram-Hansen et al, 2019, Li et al, 2017, Mboga et al, 2019, Wurm et al, 2019), average class accuracy (Persello and Stein, 2017, Wurm et al, 2019), producer's accuracy (Persello and Stein, 2017, Mboga et al, 2019), precision (Gadiaju et al, 2018, Mboga et al, 2019), recall (Gadiaju et al, 2018, Mboga et al, 2019) and the F1-score, which measures the amount of heterogeneity within each class (Gadiaju et al, 2018, Mboga et al, 2019) and the Kappa coefficient, which accounts for expected accuracy by controlling for class imbalances (Li et al, 2017). There is little attempt to incorporate area-based evaluation metrics into the detection of informal settlements using deep learning (Kuffer et al 2018). Kuffer et al (2016) do use area-based measures such as area fit index, simsize, relative position and area-perimeter ratio to evaluate informal settlement detection but using GLCM instead of deep learning, and the area-based evaluation metrics were only to fine tune the method rather than to produce headline results.

There are additionally semi area-based evaluation metrics, which account for place but neglecting their shape and geometry. The F1-score is an example (Wang et al, 2019, Quinn et al, 2018). This is a global accuracy measure and works by calculating the Jaccard Index of each ground truth in the test set and considering each a true positive or false negative based on a pre-defined pass mark. The F1-score is a summary statistic of these hits and misses defined.

The F1-score is described in Equation 3-6, and the Jaccard Index in Equation 3-5. A semi area-based such as the F1-Score has the benefit of viewing individual informal settlements conceptually as distinct entities instead of merely pixels without spatial context, of which the F1-Score is a global summary. However, a semi-area-based approach such as the F1-Score is incapable of comparing the similarity of the shapes or the relative complexity of the reference and predicted polygons and they are consequently limited in their analytical scope. Some studies have integrated semi area-based evaluation metrics after post-processing from CNNs and compared this to a pixel-based accuracy measure (Kumar et al, 2017, Jung et al, 2019, Quinn et al, 2018, Maiya and Babu, 2018).

There is however no prior work on the detection of informal settlements that employs area-based evaluation metrics to test the ability of a deep learning algorithm to make detections and which are in conceptual alignment with the phenomenon being studied - a need identified by Kuffer et al (2018).

The research will start by converting the pixelated output from a FCN into polygons as a form of post-processing; image partition into objects commonly takes this form in image analysis (Freixburg et al, 2012). I carry out optimisations with both pixel-based and area-based evaluation metrics and compare the results to examine how the optimisation of the two kinds of metric produce contrasting combinations of optimal hyperparameters. The production of area-based outputs and use of area-based evaluation metrics will additionally allow for an examination of the consistency of any areas identified by different network configurations; this is in order to examine the robustness of any findings and their consequent suitability to be added to flood risk maps.

3.3 Methodology

3.3.1 Data Source

I use as my data source the collection of test sets from the fully optimised set of 50 model runs presented in Chapter 2. Each contains 22 outputs and masks. This amounts to there being 1100 test set pixelated outputs in total. The total number of unique pixelated outputs however is just 66, with the consequence of there being many duplicates across the test sets. The benefit of this duplication for Chapter 2 was that it aimed to fine tune a method rather than produce a final classification. The refining benefitted from this duplication because the diverse number of network trainings enabled robust outcomes. I however aim to produce a final classification

for each area. Therefore, a decision must be made regarding these duplicates of how one might produce a final classification from them.

In producing a final classification from the original test set pixelated outputs, there are two options: either all 1100 test pixelated outputs are classified, and a voting procedure used to decide final outputs when there are duplicates; or to aggregate the duplicated pixel-based outputs to form 66 ensembles which are subsequently classified into areas.

I opt for the latter option of aggregating the 1100 total test outputs into 66 unique ensembles, henceforth referred to as aggregated pixelated outputs. The method used is called unweighted aggregation (Ju et al, 2018). Unweighted aggregation is a commonly used ensemble method in machine learning (Ju et al, 2018) involving the aggregation of different model outputs from different datasets sampled from a wider training dataset but using the same function. It involves aggregating the outputs of many models to produce multiple outputs from a single image.

The utilisation of many sub-models allows a diverse set of classifiers to combine their individual predictive skill information (Latinne et al, 2000). This amounts to a final classifier that contains more information than any individual one.

This is the case assuming that the errors in each sub-model are less correlated than the true predictions (Dietrich, 2000) so that specific weak classifiers can be combined to produce a resultant stronger classifier (Pekalska, 2000). The utilisation of the predictive skill of many different models as a result makes outcomes more robust (Kim and Lim, 2017, Li et al, 2016).

An analysis of the Brier scores from the 66 aggregated outputs as opposed to the 1100 non-aggregated pixelated outputs demonstrates this. The average Brier score from the aggregated pixelated outputs is 0.156. This is in contrast to the equivalent statistic for the average of the 1100 unaggregated pixelated outputs weighted according to the ground truth mask which each outputs predicts. This average is much greater, at 0.179.

As discussed in Section 2.4.2, the Brier Score shows the difference between the predicted probabilities from the true categories, instead of the number of correct or incorrect classifications (Rufibach, 2010). It is described in Equation 2-10.

In particular with the refined set of results being used as inputs in this chapter, the training set varies dramatically in characteristics in each of the 50 models due to the small training set size employed. Even small changes in the dataset can produce significant changes in outcomes (Li

et al, 2016). As a result, the benefits of utilising many models and aggregating them to an ensemble is stronger in this particular research.

In addition, pixel-level standard deviation across these aggregated pixelated outputs is 0.126, with a mean of 0.332. The high standard deviation means that the aggregated pixelated outputs account for a high level of information from the set of classifiers meaning the outcomes should be more skilful as a result.

There are additional benefits to this unweighted aggregation method. It will require significantly less computing power to convert only 66 aggregated pixelated outputs to areas rather than 1100, especially when attempting to optimise the process. Additionally, the aggregation of many pixelated outputs into a single ensemble will enable some background noise to be cancelled out, producing less noisy outputs (Li et al, 2016, Dietricht, 2000). This will potentially improve the results when a small Gaussian standard deviation is used, because smaller blur sizes are the main mechanism for cancelling out salt and pepper noise in outputs.

3.3.2 Canny Edge Detection Method

Methods of converting a pixelated greyscale output into segmented objects can be divided into similarity-based and boundary-based (Hussain et al, 2013, Freixenet et al, 2002, Savant, 2014, Raj et al, 2014). The former aims to detect sections of the image with similar adjacent pixel characteristics in order to define areas; the latter, the boundaries defining the desired areas are detected and the areas created from these. For the task of converting pixel-based informal settlement predictions from a CNN to area-based partitioned objects, an informed, reasoned judgement needs to be made of the optimal method for informal settlement partition. The optimal method of performing area-based methods are indeed frequently problem specific (Pal, and Pal, 1993). I conclude that a boundary-based method is optimal for a number of reasons.

First, an informal settlement, is a heterogeneous place consisting of many different amenities, such as roads, trees and shadows, which in and of themselves will be undescriptive of an informal settlement (Kohli et al 2012, Owen and Wong, 2013, Openshaw, 1992). For these reasons, Chapter 2 outputs required blurring. For such noisy areas boundary-based methods are usually preferable. This is because such heterogeneous entities making up a place may lack similarity and only in comparison to outside places do they make an area definable (Savant, 2014).

Second, defining areas using a boundary-based method is consistent with the data source being used in this chapter. The SDI data consist of polygons where local people have specifically defined their communities by their edges rather than using the similarity of specific places within their individual informal settlement as their starting point in mapping. SDI can therefore be considered a more boundary-based dataset than a similarity-based one.

Another advantage of focussing on the informal settlement boundary lies in the importance of the community's boundary conceptually to how that community's social vulnerability is defined. This is instead of directly comparing the area of overlap, because this brings with it the possibility that a classifier could show a strong overlap between reference and predicted polygon but where the boundaries of each bear little resemblance to each other.

The ability to accurately represent the boundary is significant in measuring the community aspect of social vulnerability. The boundary which a community uses to define themselves may be intrinsic to how they defend themselves during a flood. For example, the community may place flood trenches along the edge of the informal settlement which they have themselves defined. The edge of the informal settlement is likely to be of crucial importance in social vulnerability terms. This adds to the applicability of the SDI dataset described in Section 3.2.3 because in it, the boundaries of informal settlements are self-defined by the community rather than being based on an external interpretation of what that community's boundary is.

Third, this chapter will use as its starting point the output of a segmentation CNN. Boundary-based methods are especially useful when greyscale imagery is used since these edges are particularly identifiable in comparison to 3-band colour images (Savant, 2014). A segmentation CNN output is similar in nature to a greyscale image because it contains a single band.

Such a theoretical foundation is consistent with the conclusion of Kit et al (2012), who achieved better results comparing a boundary-based method to a similarity-based method when identifying informal settlements in Hyderabad, India.

Whereas a huge number of boundary-based methods exist, the Canny edge method is most appropriate. Canny edge is a multi-stage edge detector first proposed by Canny (1986) and it is chosen since it is a well-established method and is often used as a standard by which others are compared (Heath et al, 1998, Bhatnagar, 2017). The Canny edge algorithm has been applied to the extraction of buildings from a CNN output, in a similar way in which I aim to (Wu et al,

2018b). The Canny method was developed with three main intentions in mind as summarized in Canny, (1986), Bhatnagar (2017) and Jie and Ning (2012):

- Good Detection

  It is designed to have a low false negative rate and false positive rate or in other words, a high signal to noise ratio.

- Good Localization

  The Canny edge method is designed to approximate edges as closely as possible to the true centre of the edge.

- Low Spurious Response

  The method is designed to be interpreted by any edge as single edges rather than multiple, duplicated ones.

Additional reasons for the preferability of Canny edge lie in the various involved in its methodology. It has demonstrated success with noisy outputs (Canny, 1986, Mohmoud and Marshall, 2008, Gonzalez and Woods, 2002), which the output of my FCN is, due to the heterogeneous nature of informal settlements as they appear in visible light satellite imagery.

The Canny method corrects for noise through its initial stage of employing a Gaussian blur, in a similar way to the post-processing successfully used in Chapter 2. Noisier images generally require larger Gaussian standard deviations.

After the Gaussian blur is performed, the gradient vectors in the positive (G_x) and negative (G_y) direction are computed using the Sobel operator. The gradients for each direction are calculated for each pixel using a sliding 3x3 pixel kernel across the image, with the value in the pixel calculated from the sum of each value in the kernel multiplied by the corresponding pixel in the image. The resultant gradient G is calculated from G_x and G_y for each pixel in the image, as described in OpenCV (2019):

$$G_x = \begin{bmatrix} +1 & 0 & -1 \\ +2 & 0 & -2 \\ +1 & 0 & -1 \end{bmatrix}$$

(3-1)

$$G_y = \begin{bmatrix} +1 & +2 & +1 \\ 0 & 0 & 0 \\ -1 & -2 & -1 \end{bmatrix}$$

(3-2)

$$G = \sqrt{{G_x}^2 + {G_y}^2}$$

(3-3)

$$\theta = arctan\left(\frac{G_x}{G_y}\right)$$

(3-4)

Where:

$G_x =$ The Sobel gradient in the x direction.

$G_y =$ The Sobel gradient in the y direction.

$G =$ The resultant Sobel gradient.

$\theta =$ The angle of the resultant Sobel gradient.

The derived angle θ is rounded to one of eight possible values. These are: horizontal in either direction, vertical in either direction, and the four related diagonals.

The subsequent step in the Canny edge methodology thins potential edges to 1 pixel wide, known as non-maximum suppression. This is performed by examining each pixel classified as an edge. It is removed if the pixel is not the maximum for its direction connected to it.

The Canny edge method is also particularly suited to the defining of high entropy edges, or those which are disordered (Archariya et al, 2012). This is due to the final stage of the Canny edge methodology, which is called hysteresis thresholding. The user sets a high threshold and low threshold as tuneable parameters. All edge pixels below the low threshold are discarded, and all pixels above the high threshold are retained, with pixels in between the two thresholds

retained if they are connected to pixels above the high threshold via a chain of pixels. As a result, Canny edge has the ability to construct macro edges from micro edges and an ability to detect high entropy or disordered edges.

I believe this means that Canny edge may be particularly appropriate for finding the edges of informal settlements because an informal settlement outline is made up of the macro-edge dividing the main settlement from the surrounding area. This macro edge however will be made up of micro-edges with separations between the roofs of shacks. With its hysteresis thresholding method, Canny edge is therefore well suited to the detection of the edges of informal settlements.

3.3.3 Canny Edge Implementation

I use the Python Scikit Image (skimage) package (Van der Walt et al, 2014) because it allows adjustment of the size the Gaussian filter in comparison to other packages.

There are three tuneable parameters with implications for the outcome of the Canny edge process. The first is the standard deviation associated with the Gaussian blur. This Gaussian filtering processing is identical to that used in Section 2.3.2 as post-processing, and shown in Equation 2-9. In this first step, the use of a larger filter enables a greater number of edges to be removed but with the risk of removing true edges (Bhatnagar, 2017), although generally larger filters are preferable with noisier images.

The other two parameters are the values of the high and low thresholds for the hysteresis thresholding step. If they are too high, true edges will be removed in this step. If they are too low, false positives will be included (Bhatnagar, 2017). Fang et al (2009) suggest that the most important parameter value to optimize to achieve good results is the low threshold because it is the key determining factor behind the preservation of edge information.

The high threshold is usually chosen to be double the low threshold (Fang et al, 2009, Cao et al, 2018, Jie and Ning, 2014). For example, the default threshold parameters provided as part of the skimage Canny edge function are 10% and 20% of the maximum greyscale value in the image, which I adopt. Other values are however acceptable, with for example Setayesh et al (2010) using 7.8% and 39.2% as respective low and high hysteresis thresholds.

3.3.4 Turning Canny Edges into Polygons

Although there are good conceptual reasons for the use of the Canny edge detection algorithm, it itself cannot be relied upon to automatically produce polygons due to presence of gaps. A common solution to this is to use image contours which, by definition, are closed curves (Batsan et al, 2017). Using Canny edge detection with image contours combines the conceptual benefits of the former with a closed polygon output that is reliably guaranteed by the latter. Image contours are an edge-based method similar to the Canny edge, but contours are definitionally polygons with local continuity (Batsan et al, 2017). This means they are a reliable way of turning the Canny edges into polygons and removing gaps. The use of contours to fill gaps in Canny edge detection is common because of the ensured locally continuity of contours combined with the conceptual benefits of Canny edge detection. Examples include the use of the active contour model to recover the edges in the Canny edges (Batsan et al, 2017), subject tracking in videos using minimum cost routing to select optimal contours (Roh et al, 2007).

I develop a similar method to combine the benefits of the Canny edge method with the ability of contours to consistently produce usable polygons. The process of this conversion is summarised in Figure 3-1. Each Canny edge is matched with a contour in order to turn them into polygons.

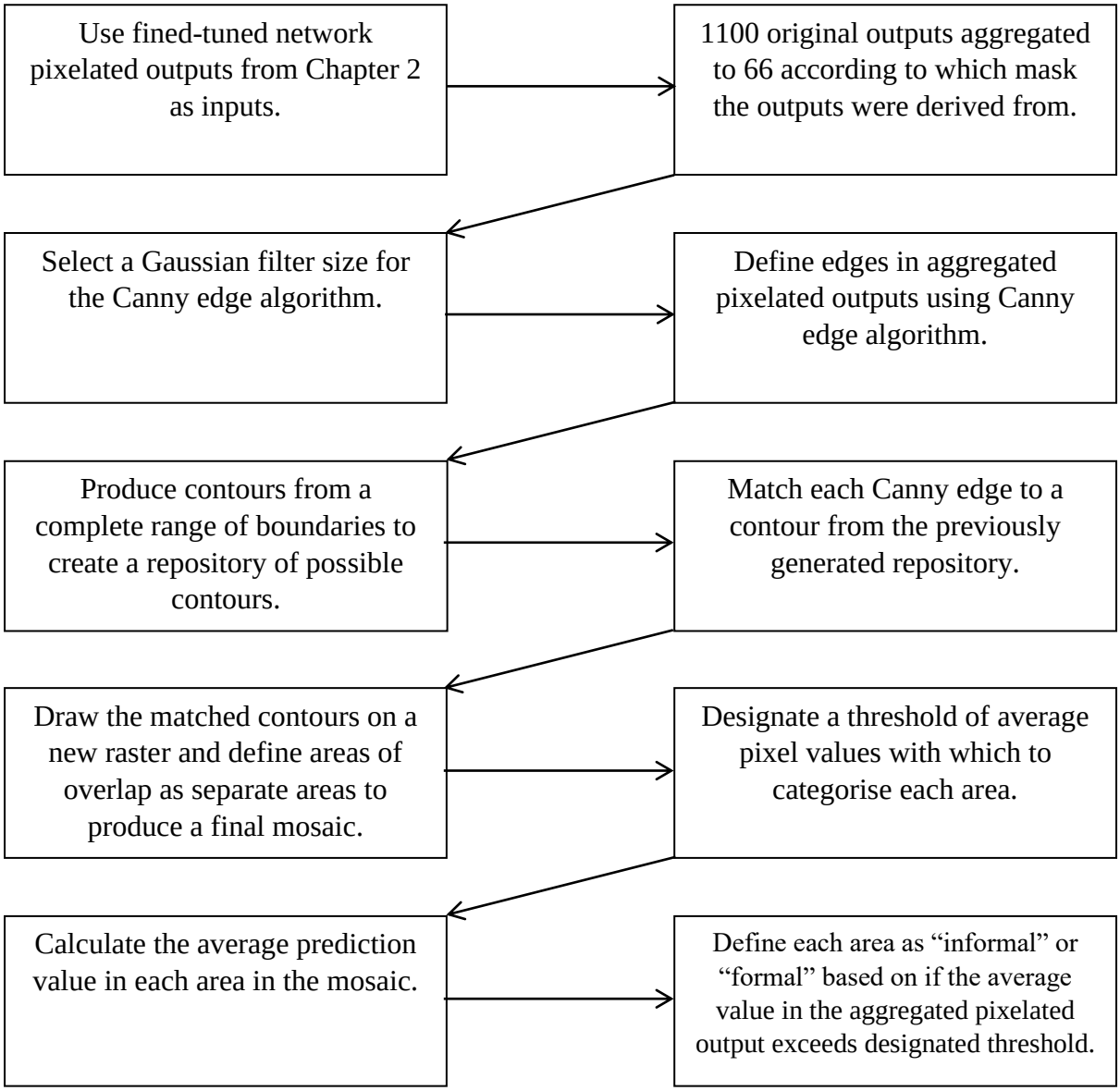

Figure 3-1: Flow diagram illustrating the process of turning aggregated pixelated outputs into areas.

After the initial production of edges by the Canny edge algorithm, the raster object containing these edges is aggregated by two times to increase the computational efficiency of subsequent steps. The Canny edges in this aggregated raster are separated into specific connected clumps according to queen's case, whereby Canny edge pixels are considered to constitute a single edge if they are connected diagonally. After this, any edges containing fewer than 10 pixels are removed in order to restrict the results to the main edges constituting the true objects in each image.

3.3.4.1 Generating Contours

I subsequently perform a search procedure which discovers the contours in the aggregated pixelated output which most closely correspond to the edges found using the Canny edge algorithm in order to produce complete areas. To do this, a repository of contours must be produced with which to find the contour which most closely matches each contour.

The 66 aggregated pixelated outputs of the FCN from Chapter 2 are blurred using a Gaussian filter with the same size as that used in the Canny edge method itself. These blurred outputs are subsequently converting to image format of values between 0 and 255 instead of predicted probabilities to ease of processing. Next, they are binarised by thresholding them at intervals of 2 between 0 and 255 in order to maximise the range of contours in the repository. Contours for the repository are produced along the boundaries for each of these binarised pixelated outputs. From the repository of all possible contours from all aggregated pixelated outputs the contour nearest to each individual Canny edge is identified using a search procedure described in Section 3.3.4.2.

The use of the combined methodology using both Canny edge detection and contouring as opposed to using contouring alone is for two reasons. First, the selection of contours to create areas is a more arbitrary process without the starting point of the detected edges using the Canny method.

Second, the detection of informal settlements using the Canny edge method has a strong conceptual foundation as laid out in Section 3.3.2. This is not the same for contours which are a similarity-based method instead of a boundary-based one. They do not have the same hysteresis to convert micro-edges into macro-edges.

3.3.4.2 Matching Canny Edges with Contours

I perform a search procedure in order to match each identified Canny edge with a corresponding contour which skirts its boundary and thereby convert that Canny edge into a polygon to be usable for analysis. This is visually demonstrated in Figure 3-2.

A matrix computing the distance between each Canny edge pixel and each contour pixel is then computed. The minimum distance between each Canny edge pixel and each pixel in a specific contour is computed. The contour with the lowest pixel distance to each Canny edge is selected as the optimal contour for that particular edge to transform that edge into a polygon.

The contours amounting to the optimal representation of each Canny edge are plotted. Where an identical contour is found to be optimal for more than one Canny edge, the duplicate contour is removed. Where two contours are nested in another, this inside area is treated as a separate area for analysis, whereby the intersections are treated as discrete polygons. The purpose of this is to enable more precise results to be produced by maximising the range of areas which make up the resultant mosaic. The background of this mosaic, which is not covered by any contours, is also treated as an area in same way.

Once the aggregated pixelated outputs have been divided into areas, each area is classified as either “informal” or “formal”, the same as those used in Chapter 2. This classification is made by going back to the original aggregated pixelated output and taking the mean of the pixel value within each area in the mosaic in order to classify it.

The mean is a suitable measure of central tendency to summarize the pixel prediction value within each area. A more robust measure of central tendency such as the median is unnecessary due to the contour-based method used to produce the areas. A contour naturally follows edges representing common pixel values and as a result, areas derived from the contours are likely to follow a uniform distribution without outliers. The mean of all the predictions within each area is calculated and used to classify each area into the “informal” and “formal” categories.

The threshold of average pixel predictions through which an area is classified into each category is varied between 0 and 1 and evaluated accordingly so that an optimal threshold can be identified. The outcome of the procedure is a raster with dimensions identical to both the pixel-based FCN outputs from which they were derived and the original masks used to train the FCN. This allows evaluation to take place.

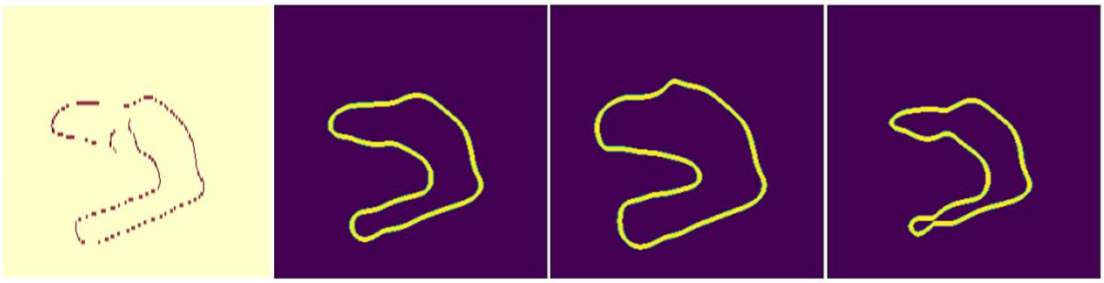

Original Canny Edge	Contour A	Contour B	Contour C
	MD = 3.25	MD = 5.23	MD = 8.83

Figure 3-2 Demonstration of how Contours are Selected for each Canny Edge: Demonstration of matching an incomplete Canny edge to contours. Contours A, B and C are sampled from the broader repository of contours derived from the original aggregated pixelated outputs as described in Section 3.3.4.1. Here Contour A is the one matched to the Canny edge as its minimum pixel distance (MD) to that contour is the lowest of the contours tested, whilst B and C are discarded.

3.3.5 Evaluation Metrics

Given that this research aims to explore the benefits of area-based outputs and evaluation metrics as opposed to pixel-based ones, it is important that the evaluation metrics employed reflect both approaches in order to make comparisons. Chapter 2 used overall accuracy, Brier score and AUC as evaluation metrics. These are pixel-based methods which did not account for connected area and the subjectivities of the phenomenon they claim to represent.

The Jaccard Index, sometimes referred to as Intersection over Union, is used as an evaluation metric in this chapter. It compares the extent of overlap or intersection between the predicted and reference polygon versus the union or total combined area of both reference and predicted objects. It can exist at either the pixel level or the area level (Jung et al, 2019) and so is ideally suited to optimisation and making direct comparisons. It additionally allows focus on a particular class and is purposed for categorical outputs which the areas produced by the proposed methodology will be. In conjunction with this benefit, it is additionally not subject to class imbalances unlike many other metrics such as overall accuracy (Wurm et al, 2019). This is in comparison to Chapter 2 where the outputs were probabilities instead of categories. The Jaccard Index is consequently a commonly used metric for evaluating the performance of deep learning in detecting informal settlements (Wang et al, 2019, Wurm et al, Helber et al, 2018,

Maiya and Babu, 2018) and in wider machine learning circles (Jung et al, 2019, Kumar et al, 2017).

The ground truths used in this evaluation are the same ground truth masks from which the FCN in Chapter 2 was originally trained. The Jaccard Index is calculated as follows:

$$J(A,B) = \frac{|A \cap B|}{|A \cup B|} = \frac{|A \cap B|}{|A| + |B| - |A \cap B|} \quad (3\text{-}5)$$

(Wang et al, 2019, Jung et al, 2019)

Where:

A = Area of polygons in the true dataset.

B = Area of polygons in predicted image.

$A \cap B$ = The intersection of areas A and B.

$A \cup B$ = The union of area A and B.

A Jaccard Index is computed on three levels. The first represents how the derived areas perform summarised across all 66 aggregated pixelated outputs, here known as the global Jaccard Index. The second computes a Jaccard Index value for each of the 66 aggregated pixelated outputs, known as the image level Jaccard Index. Finally, the Jaccard Index is calculated for each specific informal settlement in order to evaluate the method's ability to map specific areas.

The F1-score is also used as an evaluation metric. The F1-score is a global statistic summarising the informal settlement level Jaccard Indices and it is a common metric for evaluating informal settlement detection in this way (Leonita et al, 2018, Gadiraju et al, 2018, Liu, 2018, Wu et al, 2018a). Section 3.2.2 described how the F1-score is a semi area-based metric because although it uses areas rather than pixels without spatial context, it still does not account for the shape of the informal settlement or any other spatial characteristic of the predicted polygon relative to the reference polygon.

The F1-score uses a "pass mark" whereby a specific area is considered to be correctly identified by the method if the Jaccard Index value is greater than that pass mark. It is subsequently considered to be a true positive in Equation 3-6. The F1-score is calculated as follows:

$$F1 = \frac{2TP}{2TP + FN + FP}$$

(3-6)

(Jung et al, 2019, Mboga et al, 2019)

Where:

$TP =$ Number of Areas Classified as True Positives

$FP =$ Number of Areas Classified as False Positives

$FN =$ Number of Areas Classified as False Negatives

Area-Based Evaluation Metrics

I use two area-based evaluation metrics to evaluate the derived areas in conceptual alignment with the area-based outputs produced. The metrics chosen are conceptually aligned to social vulnerability which is the ultimate goal of identifying areas to map social vulnerability using deep learning.

A sensible area-based evaluation metric to decide upon, which is conceptually derived, would be to compare the relative distances of the centroid of the predicted polygon and the reference polygon. The metric is called relative position (Clinton et al 2010, Montaghi et al, 2013). Its emphasis on centroid location has the potential to evaluate the ability for information to be spread amongst a community in a flooding event, given that individual locations have the ability to act as focal points for information transfer across communities and for mitigation strategies to be coordinated.

Relative position is the "average ratio of the Euclidean distance to the distance between the centre of the reference object to the most distant segmented object" (Montaghi et al, 2013: 950). The optimal value of relative position is 0.

$$Relative\ Position = \frac{1}{n}\sum_{i=1}^{n}\frac{\sqrt{(X_p - X_r)^2 + (Y_p - Y_r)^2}}{d_{max}}$$

(3-7)

(Montaghi et al, 2013, Clinton et al, 2010)

Where:

$n =$ The number of samples being evaluated.

$d_{max} =$ The maximum distance between centroids across the sample.

$X_p =$ x-coordinate of the centroid of a particular predicted polygon.

$X_r =$ x-coordinate of the centroid of a particular reference polygon.

$Y_p =$ y-coordinate of the centroid of a particular predicted polygon.

$Y_p =$ y-coordinate of the centroid of a particular reference polygon.

A second area-based evaluation metric employed is the area-perimeter ratio. It is a geometry-based index designed to evaluate the similarity in shape between the reference polygon and predicted polygon. The optimal value of this is 1 (Kuffer et al, 2016). The use of the area-perimeter index is in alignment with the benefits of using the SDI dataset and the broader importance of community level factors. The SDI data is where the community have defined the edge of their community. The area-perimeter ratio represents the resemblance of the edges of the predicted and reference polygons by measuring how similar the shape of the two are.

It is important from a perspective of social vulnerability mapping that correspondence to informal settlement outlines is therefore sought, and an evaluation metric which accounts for the geometry and shape of an informal settlement is used as well as measuring the correspondence of the perimeter of the reference and predicted polygons.

$$Area - Perimeter\ Ratio = \frac{1}{n}\sum_{i=1}^{n}\frac{P_r/A_r}{P_p/A_p}$$

(3-8)

(Kuffer et al, 2016)

Where:

n =Number of samples.

P_r =Perimeter of the reference polygon.

P_p =Perimeter of the predicted polygon.

A_r = Area of the reference polygon

A_p = Area of the predicted polygon

3.4 Results

3.4.1 Global Jaccard Index Results

Of the total of 1100 original test set images from Chapter 2, 66 distinct images appear in the sample. Of these 66, the most common appears 27 times and the least common appears 11 times, with the median frequency being 16.5. A sufficient quantity of each image therefore appears in the original 1100 test set images, and so for each of the final 66 aggregated pixelated outputs there is strong level of aggregation. As a result, there can be a high level of confidence that a sufficient level of aggregation has been achieved in order to reduce noise and for a diverse set of classifiers to be used in detecting areas.

The two most important parameters impacting the results are the Gaussian standard deviation used to produce the Canny edges, and the threshold determining whether an area is informal or not; these two parameters will therefore be the focus of optimisation performed here. Jaccard Index values are obtained for Gaussian standard deviations between 6 and 16, at intervals of 2. For each of these standard deviations, the Jaccard Index is obtained for thresholds of between 0 and 1, with intervals of 0.05. This procedure allows for an optimal threshold and standard deviation to be obtained for final classification to take place.

An analysis of the Global Jaccard Index values shows a headline figure of 0.54 as the best result, as shown in Figure 3-3. Although very dependent on the object being detected and the

data used, in machine learning a Jaccard Index value of more than 0.5 is considered to be an acceptable result (Verma et al, 2019). This is achieved when using a standard deviation of 6 with a threshold of 0.3. This is virtually identical a similar attempt by Wang et al (2019) who also produced a statistic of 0.54 for a Global Jaccard Index value. It also falls well within the range of Jaccard Index values produced by similar studies detecting informal settlements such as 0.32-0.64 from Helber et al (2018) and 0.41-0.58 from Verma et al (2019). All standard deviations have their best scores achieved when the threshold is 0.3.

As a general rule, smaller standard deviations give higher values of the Jaccard Index. This is however not ubiquitous. A standard deviation of 14 for example has a higher maximum Jaccard Index (0.54) than for a standard deviation of both 12 (0.53) and 10 (0.53), although the difference the larger standard deviation makes here is minimal. Of the two parameters optimised, Figure 3-3 demonstrates that the threshold is far more influential on the Jaccard Index than the filter size. For example, the standard deviation achieving the highest Jaccard Index at the optimal threshold of 0.3 is less than 0.03 better than the worst standard deviation for the same threshold.

It is also possible to gain an insight into the skilfulness of a result by comparing it to that which would be expected through random chance. The values for random chance are calculated by taking the number of pixels in the reference polygon in each image and distributing this quantity of pixels randomly across that image as if they were predictions. For the global Jaccard Index random chance would produce a value of 0.20. This suggests that 0.54 is a highly skilful result relative to randomly locating informal settlements.

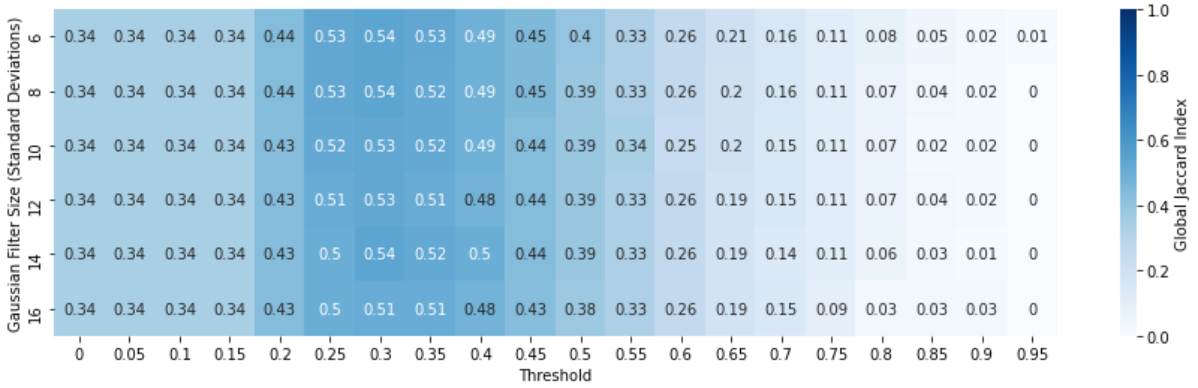

Figure 3-3 Fixed Threshold Global Jaccard Index Heatmap: Heatmap Global Jaccard Index values for each threshold and blur filter size, correct to 2 decimal places. A value of 1 is optimal.

3.4.2 Image Level Jaccard Index Values

The advantage of examining the Jaccard Index at the level of each image rather than at the global level is that the latter is ignorant of the nature of the pixels it is identifying. It shows the total pixel overlap but is ignorant of any spatial context of where that overlap is or which of the 66 images this overlap is. Examining each of the 66 images individually and deriving a Jaccard Index value for each goes somewhere to solving this problem because the overlap location is confined to a particular image.

Figure 3-4 summarises these image level statistics. The optimal set of parameters, according to an analysis of image level results, are similar to that when a global statistic was used. The optimal threshold is still 0.3 and the ideal standard deviation is also still 6 and this gives a median image level Jaccard Index of 0.53. This compares favourably when compared with the random median value of 0.16. Evaluating at a level of each image additionally allows for an examination of whether different parts of the distribution of Jaccard Index values benefit from different parameter values. The combination of parameters which optimises the Jaccard Index at the 75^{th} percentile is similar to previously, with an optimal threshold slightly lower at 0.25, and a standard deviation of 6. The respective optimal values for the 25^{th} and 75^{th} percentiles are 0.32 and 0.75. These values compare favourably to the equivalent random values of 0.05 and 0.35 for the same percentiles. The optimal threshold for the 25^{th} percentile is identical to that for the global Jaccard Index value and the median image level Jaccard Index value, at 0.3. As with the median and the 75^{th} percentile, the optimal 25^{th} percentile value is achieved with a standard deviation of 6.

a. 25th percentile.

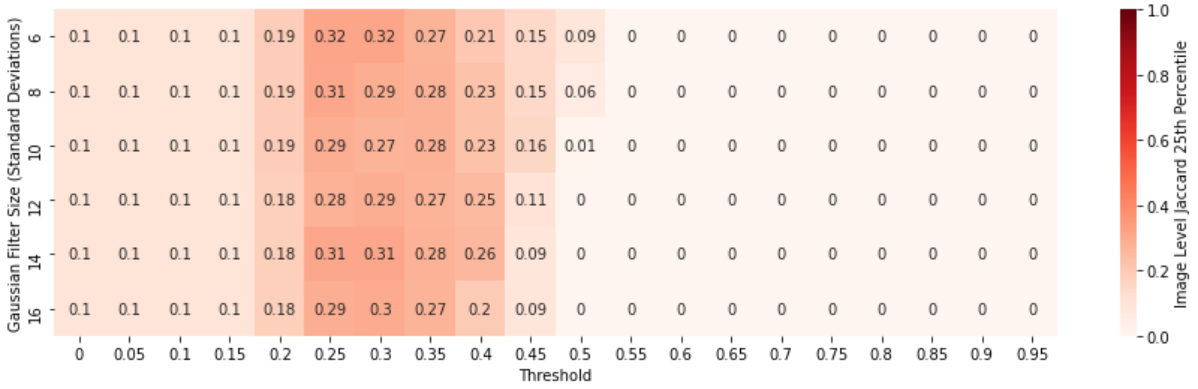

b. Median

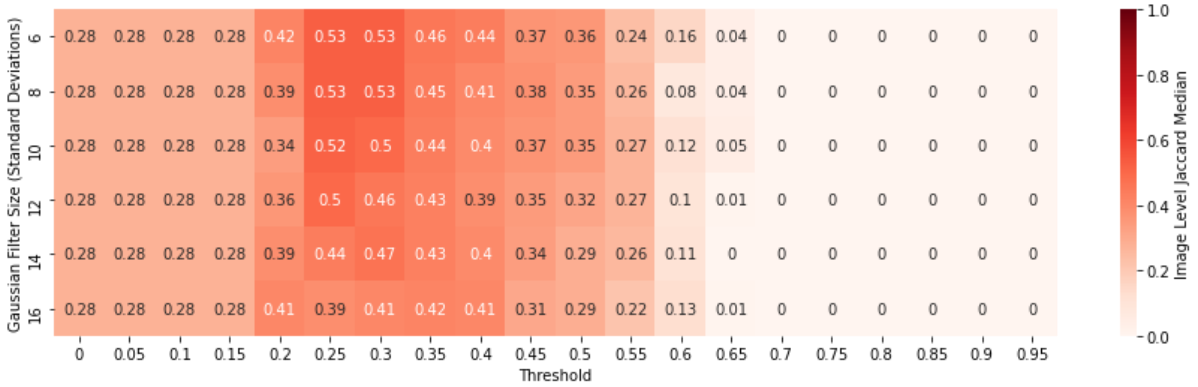

c. 75th percentile.

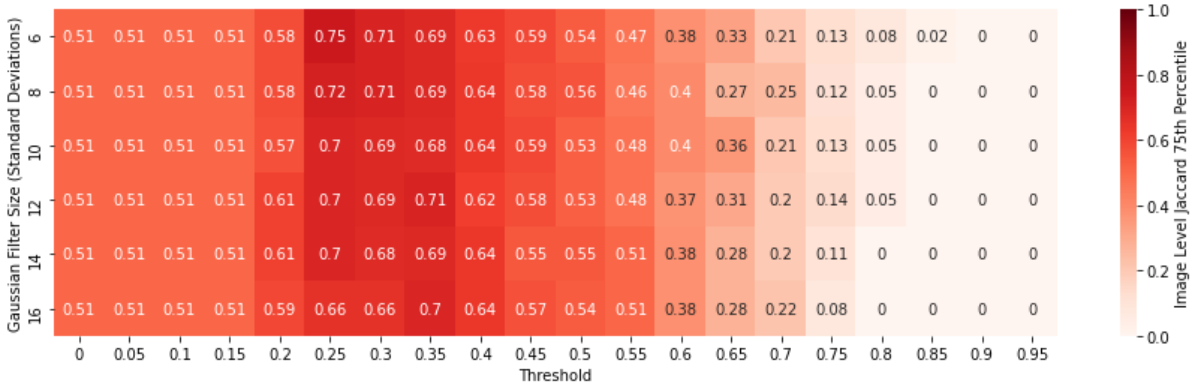

Figure 3-4 Fixed Threshold Image Level Jaccard Index: Heatmaps summarising (a.) 25th percentile, (b.) median, (c.) 75th percentile, correct to two decimal places of the Image Level Jaccard Indices from the 66 aggregated pixelated outputs. A value of 1 is optimal.

The broad similarity of optimal parameters across the distribution of image level Jaccard Index values demonstrates the threshold to be robust in optimally identifying areas. The minimal variation in optimal standard deviations across the distribution between the 25th and 75th percentiles may be a reflection of how the standard deviation seems to be relatively less important in determining the results as opposed to the threshold.

An analysis of the Jaccard Index at the image level additionally allows for an exploration of the relationship between the quality of the pixel predictions and the Jaccard Index for each image.

Because much of the relationship between Brier Score and image level Jaccard Index may be explained by the number of pixels in the ground truth mask for each, the partial correlation between the two is calculated. This is identical to the what is normally called the correlation, here called the full correlation, but here controls for an additional covariate in the form of the number of pixels in the ground truth mask. This is shown in Equation 3-9:

$$p_{BJ|N} = \frac{r_{BJ} - r_{BN}r_{JN}}{\sqrt{1 - r_{BN}}\sqrt{1 - r_{JN}}}$$

(3-9)

(Kim, 2015)

Where:

$p_{BJ|N}$ = The partial correlation between the Brier score and the Jaccard Index conditional upon the number of pixels in the ground truth mask.

r = Full correlation

B = Brier Score for each image

J = Jaccard Index for each image

N = Number of pixels in the ground truth mask

There is a correlation of just -0.615 between the Brier score obtained for each of the 66 pixel-based aggregated test outputs from Chapter 2 and masks and the Jaccard Index obtained for each of these aggregated pixelated outputs. Being far away from the value of -1 which would imply perfect conformity between the pixel and area-based methods. It implies that there is a large amount of variation in the image level Jaccard Level values which cannot be accounted

for by changes in the Brier score at the same scale. This represents a vindication of the use of an area-based method because the unexplained variation shows certain information may be discerned by it which a pixel-based method cannot.

A possible explanation for this lack of correlation may lie in the production of areas cancelling out the effects of salt and pepper noise. Salt and pepper noise has previously been defined in Section 2.4.1 as the presence of wrongly classified pixels within the broad area of another". The use an area-based method is therefore likely to create good results even when the Brier score of the pixel level results is poor due to this salt and pepper noise within informal settlements.

The use of area-based methods is able to say something fundamentally different to what can only be revealed at a pixel scale. Such a finding is consistent with Quinn et al (2018) and Verma et al (2019) who suggest the analysing informal settlements at the area level as opposed to the pixel level due to the high level of complexity of informal settlements, containing many different visible features such as trees, roads and buildings. As a result, informal settlements are difficult to represent at the pixel level.

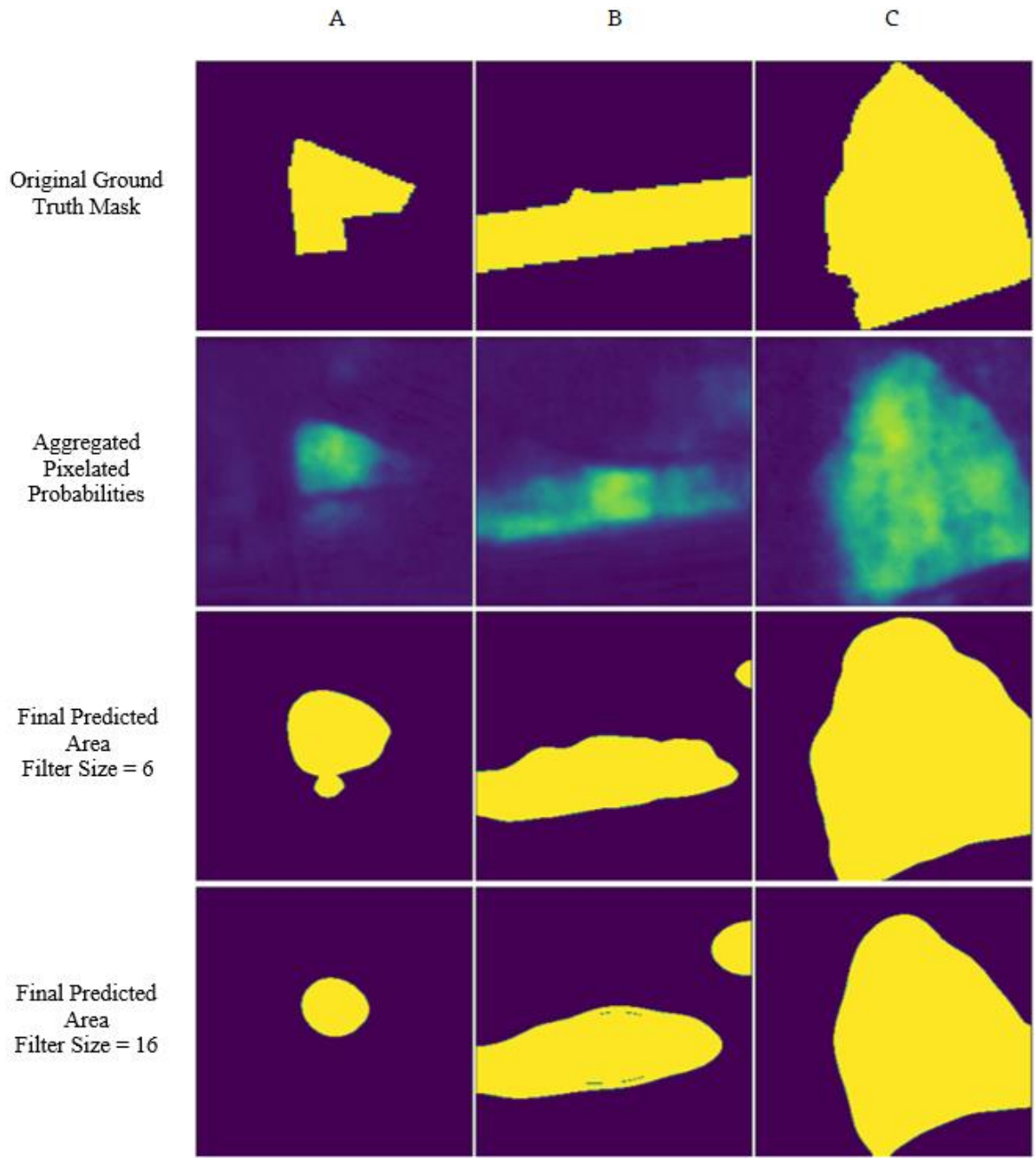

Figure 3-5 Visualisation of Outputs: Visualisation of outputs with a threshold of 0.3. Standard deviations of 6 and 16 are compared.

A visual analysis of images in Figure 3-5 using the optimal threshold of 0.3 appears to demonstrate why the Jaccard Index values are slightly higher for smaller standard deviations. It appears that the smaller blur sizes result in shapes with sharper edges in the masks being made more round with larger sizes. As a result, the more-blurred images show a lower level of agreement with the reference polygon itself.

Whereas the median of these image level Jaccard Indices shows a strong result, a closer examination of the images reveals that of the 66 images, four have a Jaccard Index of 0. This means that the predicted area fails to accurately identify any of the areas of informal settlement within a particular image. These are from the optimal threshold of 0.3 and the blur size of 6 which was established to be preferable from the visualised comparisons. A visual examination of these four in Figure 3-6 is revealing of the context of this. For two of the images, it appears that the issue lies in the original pixelated probabilities having no skill in recognising the ground truth mask. Additionally, of the two informal settlements which the original network output failed to identify, the settlements are long and thin. It may therefore be considered that informal settlements of this sort are inherently difficult to identify, possibly because the vast majority of informal settlements in the original dataset do not have this characteristic. There may be a lack of an ability of the network to detect these shapes. A glance at the original visible light satellite image from these two would seem to confirm this, the informal settlement is visually difficult to identify. The distinctive features of informal settlements, tightly packed, irregular small roofs are not clearly apparent in the images. The network appears incapable of transferring its skill of recognising most of the informal settlements in the sample to informal settlements where this pattern is not as clear. So arguably no blame can be attached to the original network for failing to identify these images, and likewise with the area creating methodology. Such a finding hints at the limitations of using satellite imagery to detect informal settlements. If some settlements are difficult to detect visually even the most sophisticated methods of computer vision are unlikely to identify these. Alternatively, it may be a limitation of the specific satellite imagery used in this study. These informal settlements may be possible to detect using higher resolution, commercial satellite imagery were to be used.

With the other two images however (D and F), there is evidence that the original network is skilful at identifying the particular areas relative to the formal area of the image. The network however is failing to convert this apparent skill into the necessary predicted probabilities for the area detection methodology to classify the derived areas as belonging to the informal category. The maximum pixel level predicted probability in image D is just 0.33, and for image F it is just 0.31. It is therefore unsurprising that the methodology is failing to classify these as informal settlements given that the global optimal threshold is 0.3.

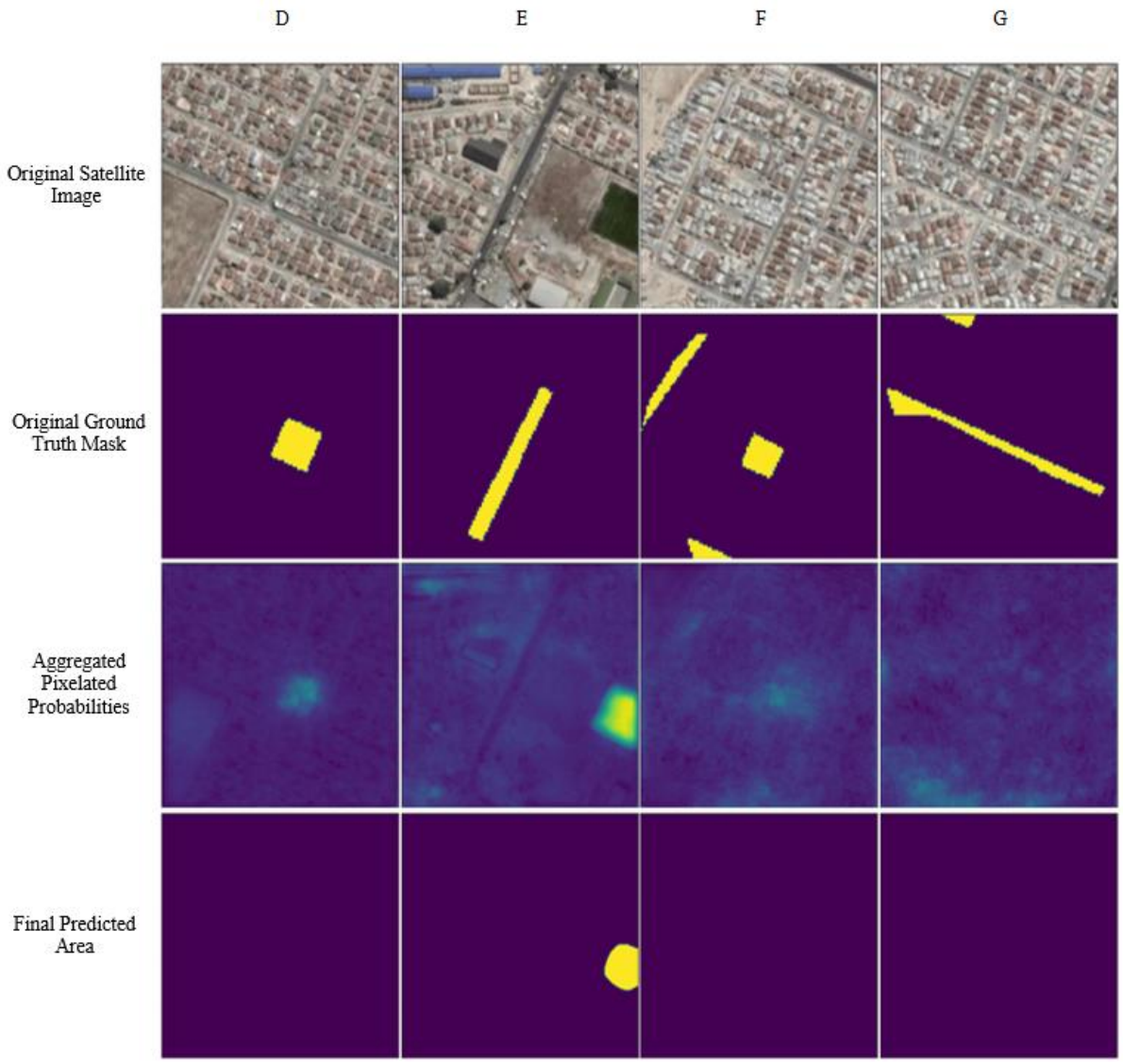

Figure 3-6 Visualisation of Outputs with an Image level Jaccard Index of 0: when a standard deviation of 6 is used and a threshold of 0.3.

This problem could potentially be solved by using a locally varying threshold. A method of adaptively determining an optimal threshold, known as the Otsu method, has been used by some (Jie and Ning, 2012, Hao et al, 2013, Cao et al, 2018, Fang et al, 2009). It is unsupervised and non-parametric (Hao et al, 2013). It is based upon the assumption that an image contains a foreground and a background; the Otsu method aims to find a threshold which minimizes the intra-class variance between these two (Jie and Ning, 2012). The threshold derived from minimized intra-class variance is likely to be the threshold which separates the foreground and background. Such a technique is therefore likely to have good application for partitioning informal settlements because each image contains in its ground truth masks regions in both the "informal" and "formal" categories. So the a priori assumption underpinning the Otsu method

that each image has a foreground and a background is valid for the aggregated pixelated outputs used in this research chapter. The foreground is the “informal” section of the aggregated pixelated output and background the “formal” category. The use of the Otsu thresholding method is also frequently used for remote sensing applications, demonstrating an ability to improve image classification in fields such as water image partition (Zhang et al, 2017b, Setiawan et al, 2017), change detection (Huang et al, 2015) and building extraction (Huang et al, 2016).

The image level Jaccard Indices are recalculated and optimised using the Otsu method. Seven new thresholds are calculated from -0.15 to 0.15 from the calculated Otsu threshold, at intervals of 0.05 as was the case for the fixed thresholds.

An examination of the Jaccard Index values using the Otsu method reveals the optimal median value has risen to 0.63 from a previous best of 0.53 without the use of this locally varying threshold method. For the optimal threshold and standard deviation the 75^{th} percentile value has improved from 0.75 without the Otsu method to 0.77 when using this new Otsu method. The pattern is similar for the 25^{th} percentile which has increased from 0.32 without the Otsu method to 0.37 when using it. The number of images with a Jaccard Index of 0 has however reduced from 4 with fixed thresholds to 0 using Otsu, when using the set of parameters which produce the optimal median of -0.1 and a blur standard deviation of 6.

a. 25th percentile

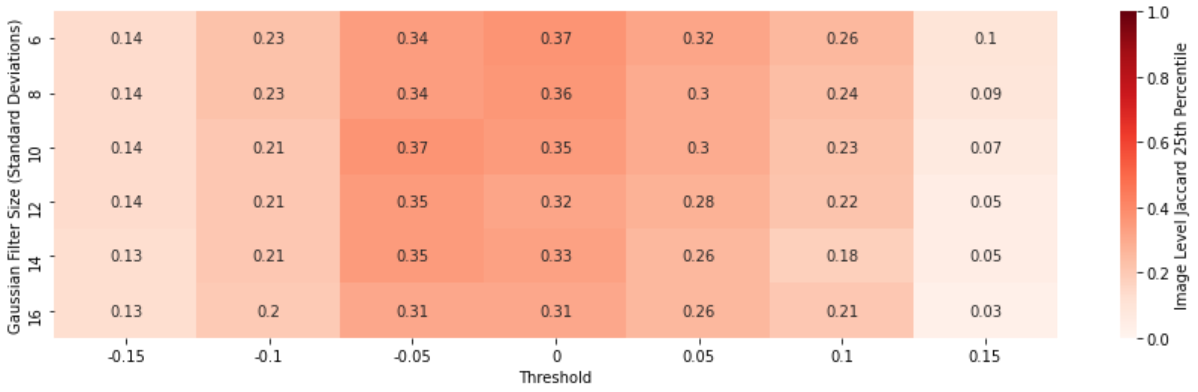

b. Median

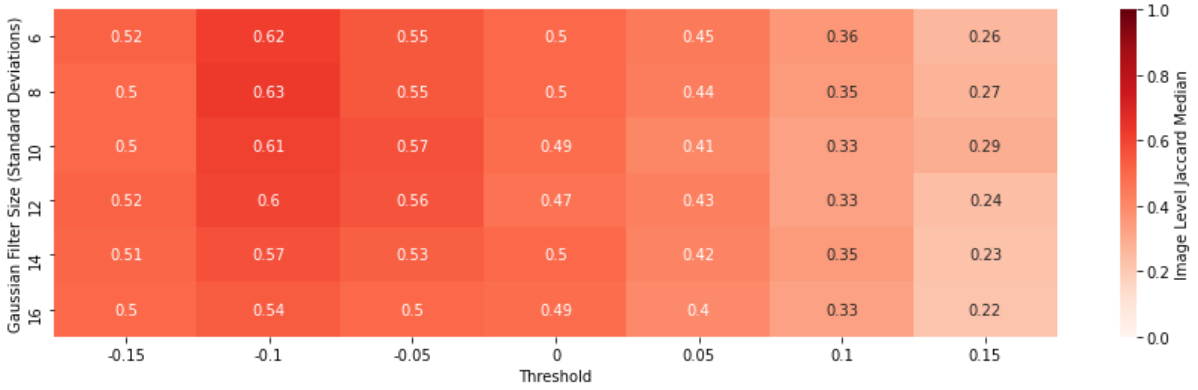

c. 75th percentile.

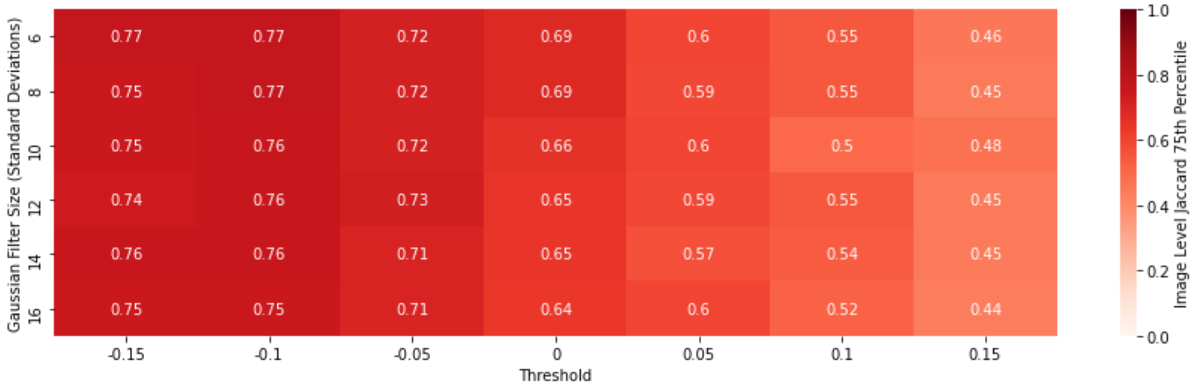

Figure 3-7 Otsu Threshold Image Level Jaccard Index: Heatmaps summarising (a.) 25th percentile, (b.) median, (c.) 75th percentile, correct to two decimal places of the Image Level Jaccard Indices from the 66 aggregated pixelated outputs. These results are where the locally varying threshold, or Otsu method is applied. A value of 1 is optimal.

3.4.3 Specific Settlement Level Assessment

A further step in the analysis lies in analysing Jaccard Index values at the level of specific informal settlements. This analysis is distinct from the calculation of image level Jaccard Indices because many images contain within them multiple informal settlements. This analysis is at the level of specific communities instead of analysing the amount of pixel overlap in an image with no regard for where those pixels are.

As mentioned previously, the F1-score is a metric summarising these local values. In producing an F1-score, Quinn et al (2018) use a Jaccard Index pass mark of 0.25 of each informal settlement, using this value of the Jaccard Index to denote a successful classification. A Jaccard Index value of 0.25 may seem like a relatively low pass mark, but there are good conceptual reasons for using a value similar for this chapter since the ultimate aim is to map social vulnerability rather than merely informal settlements. Social vulnerability is a strongly place-based concept which impacts communities beyond the direct effects of flooding. For example, only a small part of the community's spatial area being flooded can have consequences for the wellbeing of people at the spatial scale of the entire community. As a result, even the detection of a small portion of an informal settlement or socially vulnerable environment has value in producing social vulnerability layers of flood risk maps.

A pass mark of 0.25 is therefore similarly used in this research chapter to arbitrate a true positive from a false negative classification. Some predicted polygons overlap two reference polygons in the same image. In these circumstances, the Jaccard Index for each of the reference polygons needs to be calculated. The area of overpartition (where the method makes false positive classification) shared between the two reference polygons is, in the calculation of the Jaccard Index for each, allocated proportionally to the size of each reference polygon.

		Threshold																		
Blur Size	**Measure**	**0.05**	**0.1**	**0.15**	**0.2**	**0.25**	**0.3**	**0.35**	**0.4**	**0.45**	**0.5**	**0.55**	**0.6**	**0.65**	**0.7**	**0.75**	**0.8**	**0.85**	**0.9**	**0.95**
6	**TP**	66	66	66	74	89	90	79	73	65	61	48	42	31	24	16	11	9	5	1
	FP	30	30	30	61	24	12	10	11	1	1	6	7	1	0	1	1	0	0	0
	FN	64	64	64	56	41	40	51	57	65	69	82	88	99	106	114	119	121	125	129
	F1-Score	0.58	0.58	0.58	0.56	0.73	0.78	0.72	0.68	0.66	0.64	0.52	0.47	0.38	0.31	0.22	0.15	0.13	0.07	0.02
8	**TP**	66	66	66	73	89	86	78	74	64	61	51	41	30	25	15	10	8	6	1
	FP	30	30	30	60	16	11	7	7	4	11	5	0	0	0	1	1	0	0	0
	FN	64	64	64	57	41	44	52	56	66	69	79	89	100	105	115	120	122	124	129
	F1-Score	0.58	0.58	0.58	0.56	0.76	0.76	0.73	0.70	0.65	0.60	0.55	0.48	0.38	0.32	0.21	0.14	0.12	0.09	0.02
10	**TP**	66	66	66	70	88	84	78	72	65	58	50	37	31	19	17	11	7	3	0
	FP	30	30	30	60	13	8	4	5	1	4	2	0	0	0	0	0	0	0	0
	FN	64	64	64	60	42	46	52	58	65	72	80	93	99	111	113	119	123	127	130
	F1-Score	0.58	0.58	0.58	0.54	0.76	0.76	0.74	0.70	0.66	0.60	0.55	0.44	0.39	0.26	0.23	0.16	0.10	0.05	0.00
12	**TP**	66	66	66	70	88	82	77	70	63	55	48	37	28	19	16	13	7	3	0
	FP	30	30	30	48	13	13	7	4	3	7	4	7	0	0	1	1	0	0	0
	FN	64	64	64	60	42	48	53	60	67	75	82	93	102	111	114	117	123	127	130
	F1-Score	0.58	0.58	0.58	0.56	0.76	0.73	0.72	0.69	0.64	0.57	0.53	0.43	0.35	0.26	0.22	0.18	0.10	0.05	0.00
14	**TP**	66	66	66	69	86	84	78	71	59	52	45	35	23	17	16	9	5	2	0
	FP	30	30	30	40	12	11	6	2	2	4	5	5	7	1	2	2	0	0	0
	FN	64	64	64	61	44	46	52	59	71	78	85	95	107	113	114	121	125	128	130
	F1-Score	0.58	0.58	0.58	0.58	0.75	0.75	0.73	0.70	0.62	0.56	0.50	0.41	0.29	0.23	0.22	0.13	0.07	0.03	0.00
16	**TP**	66	66	66	71	87	84	74	69	56	51	43	35	24	19	13	8	6	2	0
	FP	30	30	30	43	12	7	7	5	2	3	5	3	3	3	1	0	0	0	0
	FN	64	64	64	59	43	46	56	61	74	79	87	95	106	111	117	122	124	128	130
	F1-Score	0.58	0.58	0.58	0.58	0.76	0.76	0.70	0.68	0.60	0.55	0.48	0.42	0.31	0.25	0.18	0.12	0.09	0.03	0.00

Table 3-1 Fixed Threshold F1-Score results: F1-scores as well as components of the F1-score. These components are TP (True Positives), FP (False Positives), FN (False Negatives), according to Equation 3-6. An F1-Score value of 1 is optimal.

A similar effect is seen in the F1-score in comparison to the global and image level Jaccard Indices. Table 3-1 breaks down scores for the true positives, false positives and false negatives which produce the F1-scores according to Equation 3-6. As with the image level and global Jaccard, larger gaussian blur standard deviations have the effect of worsening the value of the F1-score rather than improving it. With for example, the best F1-score value for a standard deviation of 6 being 0.78, for a threshold of 0.3, and the optimal F1-score for a blur size of 16 of 0.76. An examination of the results for a standard deviation of 6 and 16 for the 0.3 threshold reveals the reason for this. A standard deviation of 16 produces 84 true positives and 7 false positives from its optimal threshold. Whilst changing the blur size from 16 to 6 does increase the number of true positives from 84 to 90, this comes at the cost of increasing the number of false positives from 7 to 12. This is likely to be due to there being small pockets of false prediction which the greater blur of the larger standard deviation is able to successfully remove from being a false positive prediction, but which the smaller standard deviation is not. It as a result it not possible to declare the smaller blur size to be superior in all circumstances, since the smaller filter size produces more false positive areas.

A similar pattern of the superiority of smaller blur sizes is also seen with locally varying thresholds, with the optimal F1-score for a standard deviation of 6 being 0.73, whereas for a standard deviation of 16 it is 0.72.

		Threshold						
Blur Size	**Measure**	**-0.15**	**-0.1**	**-0.05**	**0**	**0.05**	**0.1**	**0.15**
6	**TP**	77	77	86	85	78	68	54
	FP	38	42	24	19	10	5	2
	FN	53	53	44	45	52	62	76
	F1-Score	0.63	0.62	0.72	0.73	0.72	0.67	0.58
8	**TP**	76	75	84	86	77	65	51
	FP	29	34	23	13	6	3	1
	FN	54	55	46	44	53	65	79
	F1-Score	0.65	0.63	0.71	0.75	0.72	0.66	0.56
10	**TP**	78	77	86	83	74	64	53
	FP	29	35	22	18	7	1	1
	FN	52	53	44	47	56	66	77
	F1-Score	0.66	0.64	0.72	0.72	0.70	0.66	0.58
12	**TP**	77	75	85	79	72	63	46
	FP	25	31	20	18	12	3	1
	FN	53	55	45	51	58	67	84
	F1-Score	0.66	0.64	0.72	0.70	0.67	0.64	0.52
14	**TP**	73	74	82	82	72	58	43
	FP	27	30	20	10	2	4	5
	FN	57	56	48	48	58	72	87
	F1-Score	0.63	0.63	0.71	0.74	0.71	0.60	0.48
16	**TP**	72	74	80	78	71	57	42
	FP	26	31	19	9	3	3	2
	FN	58	56	50	52	59	73	88
	F1-Score	0.63	0.63	0.70	0.72	0.70	0.60	0.48

Table 3-2 Fixed Threshold F1-Score results: F1-scores as well as components of the F1-score. These components are TP (True Positives), FP (False Positives), FN (False Negatives), according to Equation 3-6. These results are for when the Otsu locally varying threshold method is used. F1-Score values are correct to two decimal places. An F1-score values of 1 is optimal.

This optimal F1-score achieved using Otsu thresholding of 0.75 is lower than that achieved for the fixed threshold of 0.78. An examination of the specific true positives, false negatives and false positives reveals the reason for this. Changing from the fixed threshold optimal combination to the Otsu threshold optimal combination reduces the number of true positives from 90 to 86 and raises the number of false negatives from 40 to 44, and it increases the false positives from 12 to 13. From these data, the reason why the Otsu method fails to improve the

F1-score is not confned to any of the particular components of the F1-scor, but it is rather a combination of the number of true positives, false negatives and false positives for each.

The optimal F1-score of 0.78, achieved with a fixed threshold, is marginally lower than the value achieved by one similar study detecting informal settlements of 0.86 (Gadiraju et al, 2018). A possible explanation for this deficiency lies in the fact that most of the other studies using the F1-score use VHR satellite imagery, compared with the freely available satellite imagery I use in this research chapter. It is however greater than other values achieved by other studies, such as 0.54 (Liu, 2018) and 0.59 (Leonita et al, 2018, albeit not using deep learning). Although making direct comparisons with other studies' F1-scores has limitations due to them using different data in different locations, but they can nonetheless help contextualise the results obtained.

3.4.4 Area-Based Evaluation Metric Results

The successful Jaccard Index values achieved by the method lay a foundation for an assessment of the polygons produced using area-based evaluation metrics.

Many reference polygons are close in location to others in the original ground truth masks. Therefore, reference polygons which are close to others are removed for the examination of specific polygons due to the likelihood of one predicted polygon overlapping both. Where a predicted polygon covers two distinct reference polygons, what constitutes the perimeter and the true centre becomes confused. Forty polygons remain after removing those unsuitable for analysing the perimeter and centroids, from 130 in the original masks.

In addition to many reference polygons being unsuitable as a result of being too close spatially to one another, some informal settlements require adjustment due to having edges outside the borders of the image. Where an informal settlement's predicted and reference polygon both follow the edge of the image, without an appropriate weighting, results will interpret this circumstance as perfect alignment between a section of the perimeter of both the predicted and reference polygon. In reality however predicted and reference polygons both touching the edge of an image is not indicative of skill on behalf of the method. The polygons are only aligning because they happen to coincide with the edge of the image. As a result, for relative position and the area-perimeter ratio, results are weighted according to the proportion of the reference polygon which intersects with the edge of the image.

Similar to the Jaccard Indices and F1-score, both area-based evaluation metrics are compared and contrasted for all standard deviations and thresholds for both the fixed thresholds and Otsu thresholds.

For relative position, optimal results are achieved from the fixed threshold outputs from larger blur sizes and lower thresholds. There is a very strong trend of smaller thresholds producing lower relative position values. The optimal relative position value is 0. The optimal combination of standard deviation and threshold is 14 and 0.2 respectively, producing a relative position value of 0.41. For the similarly small thresholds of 0.25 and 0.3, the best results are also achieved with large standard deviation of 16, with relative position values of 0.45 and 0.55. For low threshold values there is a consistent benefit to using larger standard deviations. For threshold values of 0.2, 0.25 and 0.3, the relative position values are 0.43, 0.45 and 0.55 respectively for a standard deviation of 16. By comparison, the corresponding relative position values for a standard deviation of 6 are 0.60, 0.55 and 0.65.

Figure 3-8 Fixed Threshold Relative Position Heatmap: Fixed threshold relative position values, for different blur standard deviations and thresholds. Values correct to two decimal places. A value of 0 is optimal.

The use of Otsu thresholding presents dramatically improved results compared to where fixed thresholds were used, with an optimal value of 0.33 achieved for a threshold of -0.15 relative to the Otsu threshold, as shown in Figure 3-9. This is in comparison to the optimal value of 0.41 achieved for the fixed threshold results. The trend observed for fixed thresholds, whereby increased standard deviations produced better results, is not as apparent when the Otsu thresholding is applied.

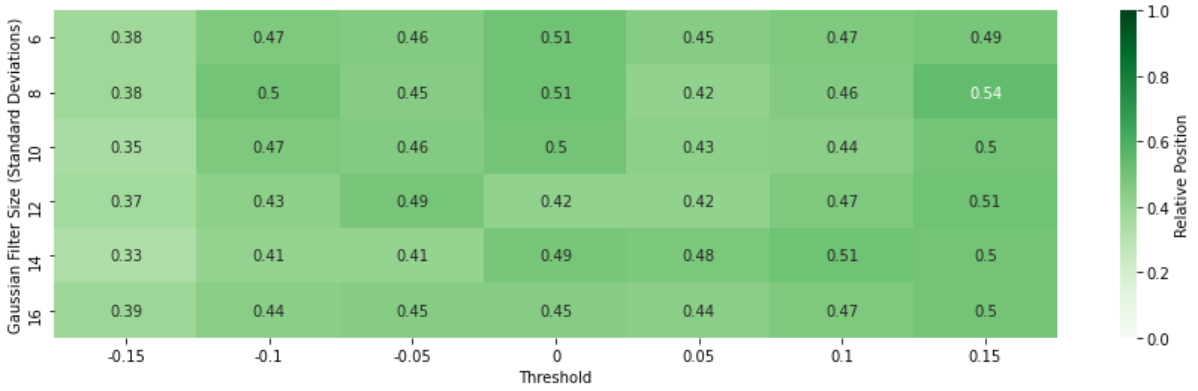

Figure 3-9 Otsu Threshold Relative Position Heatmap: Otsu threshold relative position values, for different blur standard deviations and thresholds. Values correct to two decimal places. A value of 0 is optimal.

An examination of the results for the area-perimeter ratio shows an optimal value of 1.98 when a fixed threshold of 0.9 is used, where a value of 1 is the best possible, as shown in Figure 3-10. Similar results are achieved when very high thresholds of 0.8, 0.85 and 0.9 are used. However, these values are likely to be unrepresentative because the image level Jaccard Index values were so small for the associated thresholds. The median Jaccard Index value from the standard deviation and threshold from which the value of 1.98 was obtained was 0.00. The apparently strong values for high thresholds are therefore likely to be a chance alignment of the areas and perimeters of the predicted and reference polygons.

Amongst the thresholds which gave better Jaccard Index values, 0.25 and 0.3, there is a clear pattern of smaller standard deviations producing better values of the area-perimeter ratio. For the 0.25 threshold, the value is 3.43 for a standard deviation of 6 and 3.88 for a standard deviation of 16. For the 0.3 threshold, a standard deviation of 6 gives an area-perimeter ratio of 3.53, with a value of 4.06 for a standard deviation of 16.

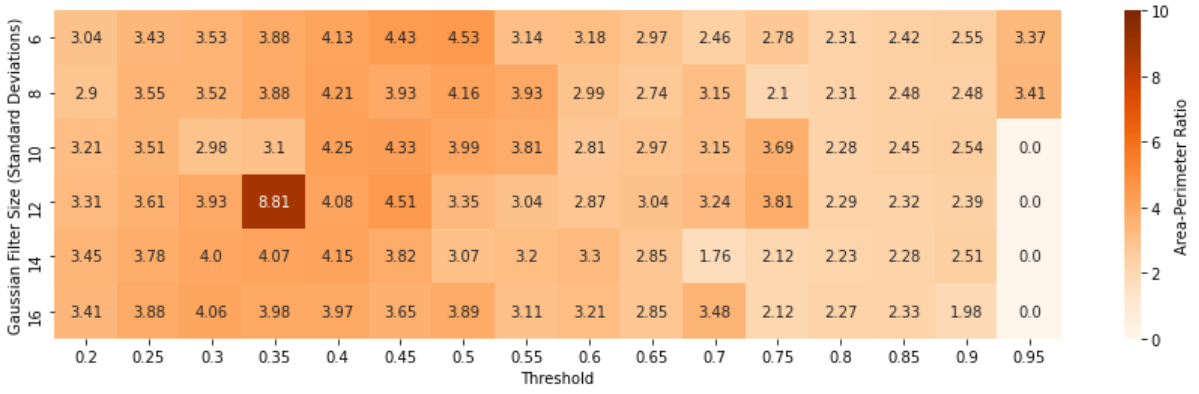

Figure 3-10 Fixed Threshold Area-Perimeter Ratio Heatmap: Fixed threshold area-perimeter ratio values, for different blur standard deviations and thresholds. Values correct to two decimal places. A value of 1 is optimal.

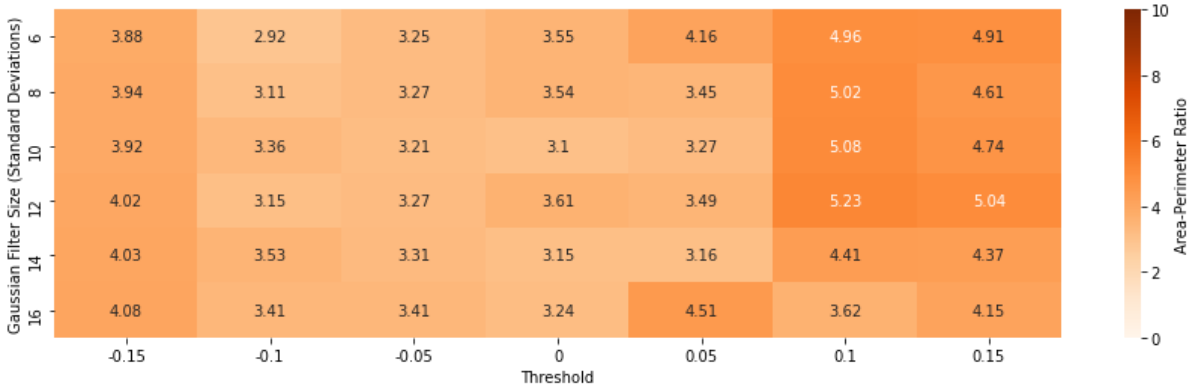

Figure 3-11 Otsu Threshold Area-Perimeter Ratio Heatmap: Otsu threshold area-perimeter ratio values, for different blur standard deviations and thresholds. Values correct to two decimal places. A value of 1 is optimal.

When Otsu thresholding is used the best image level Jaccard values were achieved for a relative threshold of -0.10 from the Otsu threshold, as shown in Figure 3-7. For this threshold, the best area-perimeter ratio value is 2.92, achieved with a standard deviation of 6, as shown in Figure 3-11. This is virtually identical to the optimal achieved with fixed thresholds of 2.90.

When using the Otsu method, it is encouraging that the best values for the image level Jaccard index closely correspond to the optimal values for the area-perimeter ratio. This suggests a strong utility of using the area-perimeter ratio given its optimal values are obtained from similar parameters to other metrics.

These optimal results however do not appear to be as strong as those achieved by the similar study performed by Kuffer et al (2016). Kuffer et al (2016) also tested using a variety of

parameters and achieved an optimal value of approximately 0.2 for the relative position and 1.3 for the area-perimeter ratio. The optimal value of 2.92 achieved for the area-perimeter ratio in this research is notably worse by comparison.

A value of the area-perimeter ratio being too high is either due to the predicted area being too large or the predicted perimeter being too short. Of these two the perimeter being too short is likely to be the cause of the poor results because, for the threshold and blur size from which the optimal value was obtained (0.2 and 8 respectively), the median Image level Jaccard Index value is good, at 0.50.

A further clue to the problem being with the perimeter of the predicted polygon lies in a comparison of the methods used by this research chapter and the comparative Kuffer et al (2016) paper. One crucial difference between the Canny edge methodology used here and the GLCM method performed by Kuffer et al (2016) is there is no gaussian blur component in Kuffer et al's (2016) method. It may therefore be the case that the use of a similarity-based image partition method may produce outputs with more representative edges because the blurring distorts the edges and produces ones which are too round and consequently a perimeter much shorter in the predicted polygon as opposed to the reference polygon, which as a result leads to the final area-perimeter ratio being too large.

Such a theory is consistent with the previous findings when looking at Jaccard Index values that smaller standard deviations have a greater ability to produce predicted polygons which more closely aligned with the exact spatial intricacies of the reference polygons. This was shown in the visualisation of the effect of changing the filter size from 6 to 16 in Figure 3-5.

It would be a valid inference from this, along with the superior results achieved by Kuffer et al (2016) using a non-blur based method, that the results of this study could be improved using an alternative boundary-based method not involving blurring or similarity-based image partition method. An example would be GLCM which focusses on detecting texture by measuring the frequency with which pixels with similar intensity values occur within a window (Sebastian et al, 2012). It is as a result not dependent on blurring.

3.4.5 Mapping All of Cape Town Using an Area-Based Method

The area-based method can be scaled up to make predictions of informal settlement locations across Cape Town. The study area for this mapping exercise is the same as that used in Chapter 2, ranging from a latitude of 34.01°S, to 33.80°S, and a longitude of 18.40°E to 18.70°E.

Using the same 9855 images from the methodology described in Section 3.3, the 9855 pixelated prediction arrays are converted into areas. From these areas a binary map differentiating informal settlement from non-informal settlement areas takes place at the final resolution of analysis of 1 arcsecond.

An additional benefit of an area-based approach is that it allows for a sub-pixel representation of informal settlements. When the areas in each of the 9855 images are converted into a single raster covering the whole of the city the value can be "0" representing formal settlement or "1", representing informal settlement. In addition to this, decimal values between 0 and 1 can be used for sub-pixel representation by showing the proportion within a pixel which is classed as informal settlement.

Results throughout have consistently pointed to 0.3 being the optimal threshold. Relative benefits however have been found of using both large and small filter sizes. Whilst smaller filter sizes have shown superior results for both the Global Jaccard Index and Image level Jaccard Indices, fewer false positives were created in the F1-score when using larger filter sizes. As a result, for this analysis two maps are made, using a blur standard deviation of 6 and 16, both with a threshold of 0.3.

In a similar way to Section 2.4.7, the OpenUp informal settlement map may be used to evaluate this map, to observe how many of the informal settlements the area-based maps identify. According to the OpenUp dataset, 123 areas can be found within the study which are informal settlements. The area-based method developed in this chapter may as a result be evaluated to see how many of these informal settlements the method identifies. These area-based maps are evaluated by taking the proportion of each of the 123 settlements which are overlapping by each area-based map and taking the median of these proportions as a summary statistic.

Taking the median of the overlap of all 123 informal settlements, the area-based method developed in this research chapter successfully manages to identify these with reasonable accuracy. For a filter size of 6, the median proportion of overlap is 0.56, and for the size 16 map this value is 0.58. The greater amount of overlap seen for the map with the larger filter

size seems counterintuitive upon consideration of results seen, given that for both the global level and image level Jaccard Indices the smaller filter size showed more optimal values. An explanation however may lie in the breakdown of the F1-scores in Table 3-1, where more false positives were created by the size 16 as opposed to the size 6 results. Section 3.4.3 speculated that this was because the larger blur filter size was more able to remove salt and pepper noise, which may be the case for the scaled-up map too.

The spatial resolution of the scaled-up map makes an evaluation for the whole of Cape Town using relative position impossible.

Percentage of OpenUp Settlement Detected	**Number of OpenUp Settlements Detected**	
	Filter Size 6	Filter Size 16
>0%	93	94
>25%	78	77
>50%	66	68
>75%	37	47

Table 3-3 Area-Based Scaled-Up Map Evaluation: Number of the 123 OpenUp informal settlements which are successfully predicted by both the size 6 and size 16 scaled up maps.

A breakdown of these overlaps reveals more about how this overlap is distributed across the 123 settlements. Table 3-3 shows the number of the OpenUp informal settlements which have a certain percentage of their area detected by each of the scaled-up area-based maps. Out of the 123 informal settlements, the filter size 6 map detects more than 0%, or at least some of 93 and the size 16 detects 94.

A breakdown of Table 3-3 is intriguing though. For the filter size 6 map just 37 have more than 75% of them detected. The filter size 16 map however detects significantly more, at 47. This may be mirroring a pattern seen in the results of the specific settlement analysis in Section 3.4.3, which suggested that the larger filter size was able to more effectively remove salt and pepper nosie, as with the median for these scaled-up maps.

This analysis however is not able to detect the number of false positives. A comparison of each of the scaled-up maps with the OpenUp map reveals large numbers of settlements which the method falsely predicts, as shown in Figure 3-12. In seeking to explain this, a reexamination of the similar analysis in Chapter 2 reveals clues of why this is. Section 2.4.7 speculated that

the pixel-based map experienced an inability to assign low predicted probabilities as a result of a lack of training due to the use of early stopping, for which L2 regularization as a means of preventing overfitted was recommended. Section 4.3.3 integrates population estimates to this analysis and elaborates in more detail the reason for this overestimate.

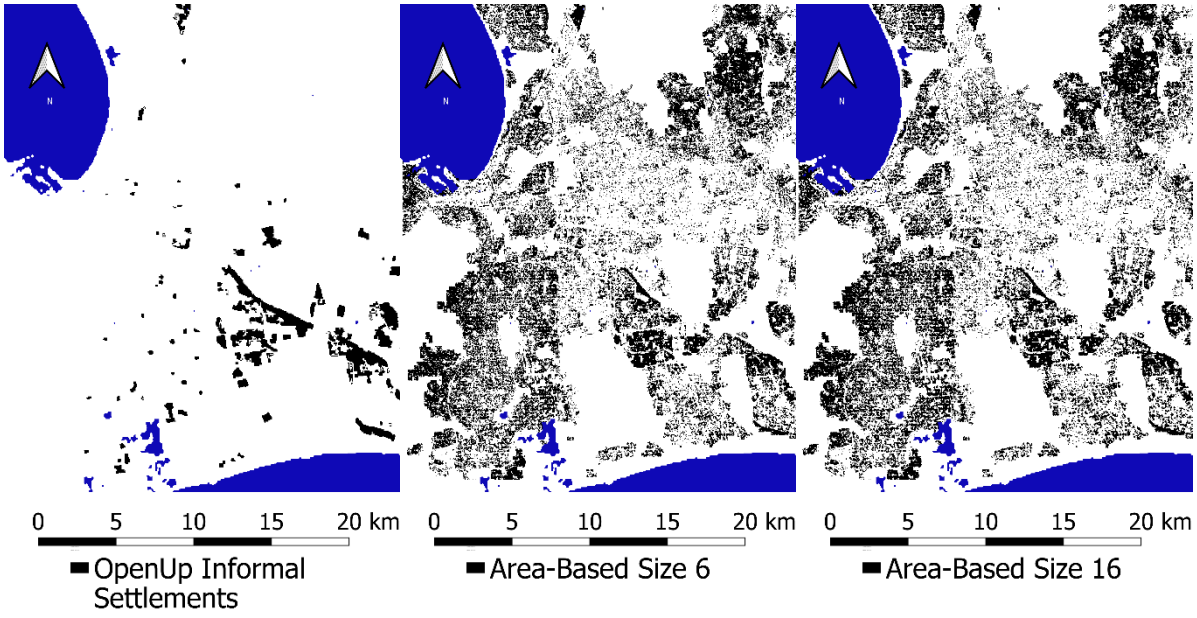

Figure 3-12 Scaled-Up Area-Based Informal Settlement Maps Compared to OpenUp dataset: Comparison of OpenUp informal settlement map with scaled-up area-based maps.

3.5 Discussion, Conclusions and Limitations

In this chapter I seek to extend Chapter 2 and its strengths and unique aspects to produce area-based outputs. It has conceptually grounded the benefits of area-based outputs because pixels are incapable of quantifying complex real-world phenomena which make up social vulnerability. In seeking consistency with this approach to classifying using an area-based rather than a pixel-based approach, the research has also attempted to evaluate the success of these using the area-based evaluation metrics relative position and area-perimeter ratio in addition to more traditional pixel-based and semi-area-based evaluation metrics the Jaccard Index and F1-score.

I have demonstrated the value of this additional methodology. This study optimised the outcome of the previously refined outputs of a FCN and converted them from constituting pixel-based probability to area-based binary outputs. The methodology of performing this conversion was additionally fine-tuned, with an optimal Global Jaccard Index value being achieved with a Gaussian blur size for the Canny edge of 6 and an average pixel probability

threshold of 0.3 to achieve an optimal Global Jaccard Index of 0.54. This represents a comparable figure to many other studies seeking to detect informal settlements using deep learning, such as 0.54 by Wang et al (2019) and 0.41-0.58 by Verma et al (2019). The optimal F1-score value obtained of 0.78 using fixed thresholds is also promising compared with comparable studies, such as 0.54 (Liu, 2018) and 0.59 (Leonita et al, 2018). The method struggles however when scaled up to the whole of Cape Town. Although the predicted areas of overlap show strong coverage compared with OpenUp informal settlements, there are a large number of false positives across the city, as demonstrated in Figure 3-12. This mismatch between the accuracy of the method within the original sample and across the city may be explained in a similar way to the scaling up in Section 2.4.7, where a lack of training was considered to be the problem. The recommendation in Chapter 2 was that a more bespoke method of avoiding overfitting, such as L2 regularization as opposed to early stopping.

Chapter 2 identified that the network struggled to assign low predicted probabilities to areas which are the most unlikely to be informal settlements, as shown in Figure 2-16. This was said in Section 2.5 to be due to a lack of training as a result of the use of early stopping as opposed to L2 regularization. L2 regularization is likely to be a method which increases the divergence of the predicted probabilities of informal and non-informal areas because its method of avoiding overfitting does not involve adding an additional term to the loss function rather than stopping training altogether.

A greater amount of training from the network is likely to create assign more divergent predicted probabilities between areas which are formal and informal. This will help the subsequent area-based method to distinguish informal settlements more accurately. As a result, these two recommendations to improve pixel-based techniques additionally have the ability to improve area-based estimations.

As a general rule, smaller blur standard deviations produce superior Jaccard Index and F1-score values. When analysing the image level Jaccard Index values, the pattern is similar. For example, the optimal median value achieved of 0.53 for a threshold of 0.3 and a standard deviation of 6, when a fixed threshold is used. A visual analysis of blur sizes suggests that in the Image level Jaccard Index values, smaller standard deviations tend to produce results with a greater conformity to the intricacies of the shapes of the original ground truth masks.

The fact that the correlation between the image level Jaccard Index and the Brier score for the same aggregated pixelated output is just -0.615 represents a key finding and strong justification

for the use of an area-based approach. It is indicative of how the strong results achieved are not necessarily reflective of there simply being very strong pixel probability performance and that something fundamental is added by using an area-based approach. Such an outcome shows that, as was speculated in the literature review, informal settlements and social vulnerability are difficult concepts to quantify at the pixel level. This strongly hints at the importance of an area-based approach to producing social vulnerability layers to flood risk maps. Studies seeking to detect informal settlements using deep learning may as a result seek to produce area-based outputs.

As the first piece of research measuring the ability of deep learning using area-based evaluation metrics, this study makes a clear contribution to present research in how deep learning can be optimised to produce prediction polygons which conform to the shape and position of reference polygons.

This research selected relative position and area-perimeter ratio as area-based metrics based theoretically on the importance of accurately defining the perimeter and conformity of the edge of the predicted and reference polygons for accurately measuring level of social vulnerability in that area.

The results of the relative position and area-perimeter ratio are worse than those performed by a comparable study using the GLCM method (Kuffer et al, 2016). It is likely that the use of the Canny edge method featuring blurring led to these worse results. A possible research path therefore may be to perform a study similar to this, which takes optimised outputs from deep learning and converting these to area-based outputs using a method not involving blurring, such as GLCM. This is despite the fact that the Canny edge method for edge detection was selected on conceptual grounds because the mechanism by which it detected edges is of particular application for informal settlements, whereby it constructs macro edges from micro edges. Empirical results obtained however suggest that the use of an edge-detection method involving blurring is sub-optimal for a task of this kind. The use of a GLCM method as opposed to Canny edge also has the potential to reduce the extent at which the network overestimates the number of informal settlements, as shown in Figure 3-12. This is because the edges of informal settlements being more precisely defined may mean that when fine-tuning the method more optimised parameters result which avoids the false positives in Figure 3-12.

Strong results achieved from the Jaccard Index and F1-score do not necessarily correspond to strong results in the area-based results. From this standpoint this research has demonstrated the

importance of using area-based evaluation metrics in addition to using pixel-based evaluation metrics. It additionally demonstrates the need for further research in fine tuning deep learning methods for detecting informal settlements using area-based evaluation metrics.

The benefits of deep learning for social vulnerability mapping are grounded technically rather than conceptually. Deep learning algorithms have the ability to automatically recognise patterns with a high level of abstraction, but without any conceptual grounding, leading to them being commonly described as "black box" methods (Openshaw, 1992). This research has demonstrated the ability to combine these technical advantages with a method for producing area-based outputs which have greater correspondence to real world processes. The use of area-based methods in this research has allowed the benefits of deep learning to be applied to such a holistic concept as social vulnerability through identification of informal settlements.

The results obtained have particular application to flood risk mapping. Many of the factors encompassing social vulnerability to flood risk mapping manifest at the community level. As a result, the development of an all-encompassing method, which produces area-based outputs in this chapter, has led to a conceptually-grounded framework suitable for producing the social vulnerability layer of a flood risk map.

With a view to applying the method to flood risk maps, across all results, a threshold of 0.3 is consistently the best value for scaling up to a final flood risk map to be created in Chapter 4. For the image level Jaccard Indices and F1-scores the optimal results are obtained using this threshold value. Therefore, it is recommended that social vulnerability layers to flood risk maps constructed using this methodology should use the 0.3 threshold. By contrast, no single standard deviation gives consistent benefits because whilst generally smaller standard deviations produce more optimal results, it has a tendency to produce more false positives in the F1-Score results. It is as a result recommended that in Chapter 4 social vulnerability layers to flood risk maps should be produced by comparing the exposure using both a standard deviation of 6 and 16. Small standard deviations have been established as being able to partition settlements with greater shape conformity, but also having far more false positive settlements being identified than with larger standard deviations. Both of the two approaches to flood risk mapping may therefore have applicability, depending on whether policymakers are most concerned with identifying all informal settlements or avoiding falsely classifying areas. Informal settlement maps of Cape Town and exposure values for each standard deviation should therefore each be made in Chapter 4.

The use of the Otsu method is promising in its ability to improve the median image level Jaccard Index values, with optimal values of 0.63 vs. 0.53 compared to when a fixed threshold is used. At times it performs worse though, in optimal values achieved by the F1-score as opposed to the fixed threshold (0.75 vs. 0.78). The optimal values with and without Otsu thresholding also perform no better for the area-perimeter ratio (2.92 vs. 2.90). It is therefore unclear whether the Otsu method provides any useful improvement compared to when a fixed threshold is used. The ambiguity in results combined with the a priori assumption inherent in the Otsu method that there is an amount of informal settlement in every image, means that more research is needed before locally varying thresholds may be applied to city-wide, scaled up flood risk maps.

4. Mapping Flood Risk: A Comparison of Income-based and Social Vulnerability-Based Risk Maps in Cape Town

4.1 Introduction

Section 1.1 described the problems with how global models account for human vulnerability through disaggregating income according to population density (Trigg et al 2016, van Vuuren et al, 2007, Jongman et al, 2012, Ward et al, 2017, Smith et al, 2019).

This is flawed for two main reasons. First, the assumption that income will be distributed equally among the population is problematic. Second, it means that higher income areas will be shown to be at greater risk when the consensus is that more impoverished environments are more socially vulnerable to flooding (Chatterje, 2010, Cutter et al, 2000, 2003, Porio, 2011, Romero-Lankao et al, 2016). There is consequently a need for a method of coupling social vulnerability to GFMs.

Chapters 2 and 3 in this thesis laid a foundation for developing this new method of flood risk mapping by detecting informal settlements. This chapter compares the standard population/income-based approaches to mapping risk with an alternative poverty-based approach and compares how the two methods relatively spatially allocate flood risk. This approach to estimating flood risk places human welfare rather than income or assets at the heart of the risk calculation.

Cape Town is used as a location for this due its many informal settlements (Drivdal, 2011) which flood frequently due to heavy winter rains and steep mountain slopes (Ziervogel et al, 2016, Goncalo et al, 2007, Holloway et al, 2008).

Arising from these facts, this final research chapter has the following aims. It aims to produce risk maps for Cape Town using different methods, based on both a pixel-based and area-based method of mapping informal settlements, building upon the informal settlement maps produced in Chapters 2 and 3. It will also compare the Expected Annual Exposure (the population expected to be exposed to flooding in a given year) using each map. Finally, it will compare how the maps spatially distribute risk differently.

4.2 Methodology

Study Area

The study area for this mapping exercise is the same as that used in Chapters 2 and 3, ranging from a latitude of 34.01°S, to 33.80°S, and a longitude of 18.40°E to 18.70°E.

4.2.1 Flood Inundation Data

Whilst traditionally physical flood modelling has been applied at a catchment level (Trigg et al, 2016), improvements in computing power (Bernhofer et al, 2018, Trigg et al, 2016) and more efficient representations of river flow (Trigg et al, 2016) and better remotely sensed datasets (Trigg et al, 2016, Bernhofen et al, 2018) have however allowed for GFMs to be developed which map flood inundation probabilities at a similar resolution but on a local scale.

The rise of GFMs have allowed for flood risk management in data poor environments (Bernohern et al, 2018), more informed flood defence decision making (Bernhofen et al, 2018), disaster risk management (Sampson et al, 2015) and commercial applications such as insurance (Sampson et al, 2015, Trigg et al 2016).

As a result, the use of a GFM is the correct approach for this thesis as opposed to a local or regional flood model approach. This is despite the fact that this study is carried out on a purely regional scale, in Cape Town alone. Some social vulnerability mapping approaches for example have taken a wholly regional or local approach (e.g. Jayaler et al, 2015). The benefits of testing the social vulnerability layer in this research chapter by the use of a GFM are that it could applied similarly in any part of the world, with the methodology employed remaining consistent. Peduzzi et al (2009) for example use a global Disaster Risk Index to compare disaster risk across different countries. The use of GFM is also consistent with the aims of the research which is for future researchers eventually to be able to produce a social vulnerability map globally. This research chapter utilising a GFM therefore allows it to provide a more representational insight into what a global flood risk map accounting for social vulnerability and flood inundation would look like. A local authority may prefer a regional flood model considering this to be more bespoke to their area, but usage by local authorities is not the primary focus of this thesis.

Examples of organisations which have produced GFMs include the European Centre for Medium Range Weather Forecasting (ECMRWF, Pappenberger et al, 2012), the Joint Research

Centre (JRC) of the European Commission (Dottori et al, 2016), the flood risk intelligence consultancy Fathom (Sampson et al, 2015), the Centro Internazionale in Monitoraggio Ambientale (CIMA) Research Foundation (Rudari et al, 2015), the University of Tokyo Institute of Industrial Science (CaMa-UT) (Yamazaki et al, 2011), and the Dutch applied research institute Deltares (GLOFRIS, Winsemius et al, 2013).

When selected a GFM the three main considerations are their process representation of flood inundation, their treatment of extreme flow generation and what their spatial resolution is (Sampson et al, 2015).

The representation of flood extent may be one-dimensional (CIMA-UNEP) or two-dimensional (GLOFRIS) coupled one and two-dimensional (ECMRWF, CaMa-UT) and hydrodynamic two-dimensional (JRC, Fathom, Bernhofen et al, 2018).

The various process representations of flood inundation are summarised by Neal et al (2012). One-dimensional approaches focus on fully representing the physical processes associated with individual channels without associated floodplains. Two-dimensional approaches represent floodplains without the channels. Coupled one and two-dimensional modelling combines a one-dimensional treatment of main channels and two-dimensional for floodplains. Two-dimensional hydrodynamic process representation combines the two approaches with sub-grid representation of channels and floodplains.

Extreme flow generation is difficult to represent in GFMs because heavy precipitation events are spatially highly localised and infrequent. Some GFMs use time series precipitation for the area in question and convert this to river discharge (CaMa-UT, GLOFRIS, JRC), albeit often with an extreme value distribution correction to attempt to accurately represent extreme values. Other models however, working on the assumption that many parts of the world lack detailed precipitation data, attempt to extrapolate the frequency distribution of various river flow intensities from data rich areas to data poor areas (CIMA-UNEP, ECMRWF, Fathom). This method is called regionalized flood frequency analysis (Sampson et al, 2015).

The spatial resolution of GFMs includes values such as 540m (CaMa-UT, ECMWF, Bernhofen et al, 2018), and 900m (GLOFRIS, JRC, Bernhofen et al, 2018) to 90m (Fathom, Bernhofen et al, 2018).

I use the Fathom Global Flood Model Version 2 from Sampson et al (2015). The specific flood maps used are from Emerton et al (2020) as part of a study assessing responses and flood risk

management in Cyclones Idai and Kenneth in 2019. The outputs used are obtained for ten inundation return periods between 5 and 1000 years.

The Fathom model is ideally suited to the task of combining physical flood hazard mapping and social vulnerability mapping because it was explicitly designed for flood inundation mapping in data-poor locations where local flood mapping has not taken place (Sampson et al, 2015). It as a result has high spatial resolution outputs of approximately 90m or 3 arcseconds. The use of the Fathom model is therefore consistent with the reason for mapping informal settlements in this thesis, which often are data-poor environments, as Section 1.4.2 outlined. An intercomparison of the Fathom model with five other GFMs in Nigeria and Mozambique is performed by Bernhofen et al (2018), who found particular benefits of the Fathom model for the simulation of floodplains; of particular relevance since this is where informal settlements are commonly found in Cape Town. The Fathom model's approximately 90m spatial resolution means it additionally has the advantage of being more spatially resolute in comparison to many other GFMs such as (CaMa-UT, ECMWF), which have 540m resolution, and (GLOFRIS, JRC) which have 900m resolution (Bernhofen et al, 2018). This enables superior modelling of smaller channels (Bernhofen et al, 2018).

A common hazard for the informal settlement communities in Cape Town is its heavy rainfall events (Ziervogel et al, 2016, Goncalo et al, 2007, Desportes et al, 2016) which are notoriously difficult for GFMs to accurately simulate (Apel et al, 2016) so for this study a regionalized density duration analysis method, which may better account for extreme rainfall, is preferred. The Fathom model utilises a statistical technique called IDF (Intensity Duration Frequency) relationships, as a form of regionalized flood frequency analysis. This method takes a number of data points for different Koppen climate classifications and the relationship between average annual rainfall, intensity and frequency of extreme rainfall events is extrapolated (Sampson et al, 2015).

A key benefit of the Fathom Global Flood Model Version 2 is its 2D hydrodynamic process to distribute flood inundation (Bernhofen et al, 2018, Sampson et al, 2015). In the Bernhofen et al (2018) intercomparison, the Fathom model performed strongly in its representation of the inundation on floodplains due to its 2D inundation process representation relative to models which use 1D or simpler 2D methods. Neal et al (2012) tested different models for the River Niger and found the use of 2D hydrodynamic treatment improved results. In conjunction with

this, the Fathom model additionally integrates an efficiency improvement for implementing 2D shallow water equations from Bates et al (2010).

The raw flood data rasters were in the form of flood depth but at the beginning of the analysis they were converted to a binary form with "1" meaning flooded and "0" meaning not flooded, in a similar way to the that carried out by Bernhofen et al (2018) for their intercomparison. The advantage of this simplification comes down to an avoidance of the overinterpretation of flood depth in two ways. First, the values of the flood depth are likely to be uncertain as GFMs are much less accurate than their local variants (Yamazaki et al, 2017). Second, from a perspective of thinking about how flooding affects human populations, the nature of the relationship between flood depth and human impact is also highly uncertain.

The research adopts and combines both the fluvial and pluvial elements of the Fathom flood model. Fluvial flooding refers to inundation due to river levels overcoming their banks following intense or prolonged rainfall (Houston et al, 2011). Pluvial flooding on the other hand is in reference to "surface water flooding resulting from intense rainfall" (Houston et al, 2011: 2). Studies combining the effects of fluvial and pluvial flooding are however rare due to the uncertainty related to pluvial flooding (Apel et al, 2016). This uncertainty derives from the difficulty of modelling high intensity rainfall events in spatially specific locations, rather than for whole catchments as is required for fluvial floods, as well as the difficulties of simulating small channels as opposed to larger channels which control fluvial processes. (Apel et al, 2016). The complexities of climate in Cape Town make this necessary however, with flooding taking place in informal settlements as a result of winter storms and heavy rainfall (Ziervogel et al, 2016, Goncalo et al, 2007, Holloway et al, 2008, Desportes et al, 2016).

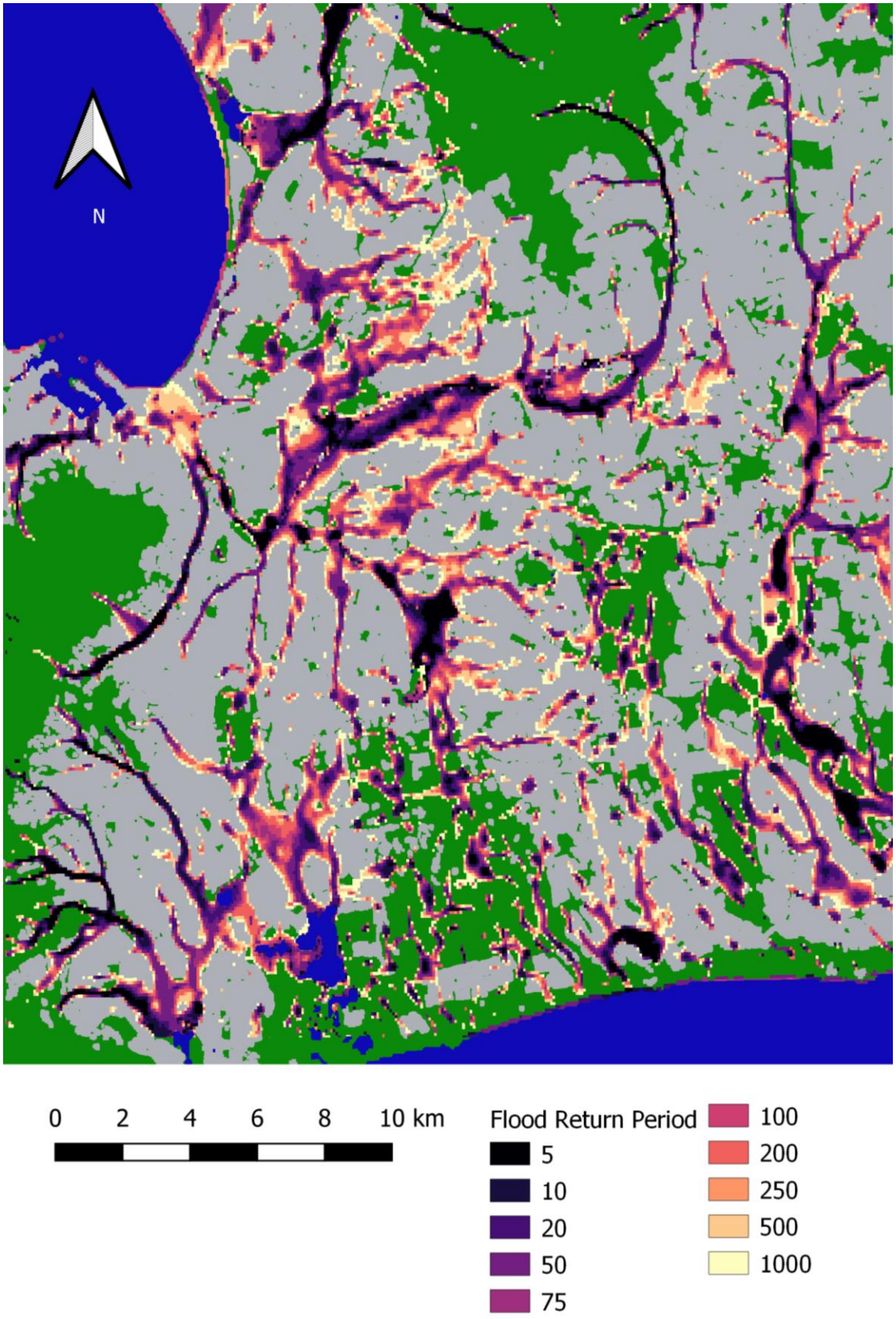

Figure 4-1: Map of Flood Hazard from the Fathom model, including return periods between 5 and 1000 years.

4.2.2 Integration of Flood Protection Standards

An integration of the effects of flood protection standards is generally considered necessary to make the results more representative because the Fathom model does not integrate it into its methodology. This study uses the FLOPROS (FLOod PROtection Standards) database (Scussolini et al, 2015). The FLOPROS dataset has been applied to simulating the effects of climate change (Alfieri et al, 2017) mapping locations where future flooding adaptation and defences are needed due to increased rainfall (Willner et al, 2018) and measuring the compound effects of riverine and coastal flooding (Ward et al, 2018).

It is a crowdsourced facility and features three "layers" in order to produce a regional level estimate of flood risk in the study are. The most reliable and valid measure is known as the design layer. This includes data of known flood defence instalments in the places in question. The second is called the policy layer, which is produced in a similar way to the design layer but includes standards which are objectives of governments or legal requirements rather than actual defences. The final and most speculative layer is known as the model layer. This simply interpolates regional economic output to estimate the standard of flood protection on the basis that more prosperous places are likely to be better defended.

Out of these three there is a merged layer formed. The merged layer is formed by prioritising the design layer over the other two. If no design layer data point exists the policy layer is used and the model layer only being used if no data for either the policy layer or the model layer.

For Cape Town, there is a single value in the FLOPROS database and this is constructed from the "policy" layer. This data is henceforth converted from a vector form to a raster form and reprojected to the same spatial resolution as the population data and flood output from the Fathom model with a bilinear interpolation using the projectRaster function from the R raster library (Hijmans, 2017). If a grid cell is registered as flooding for a given return period, and the defence standard estimate for that cell is above that return period, the cell is converted to register as being a non-flooded cell.

Due to the large uncertainty related to the FLOPROS dataset (Ward et al, 2018), this chapter compares exposures both with and without the inclusion of flood protection standards.

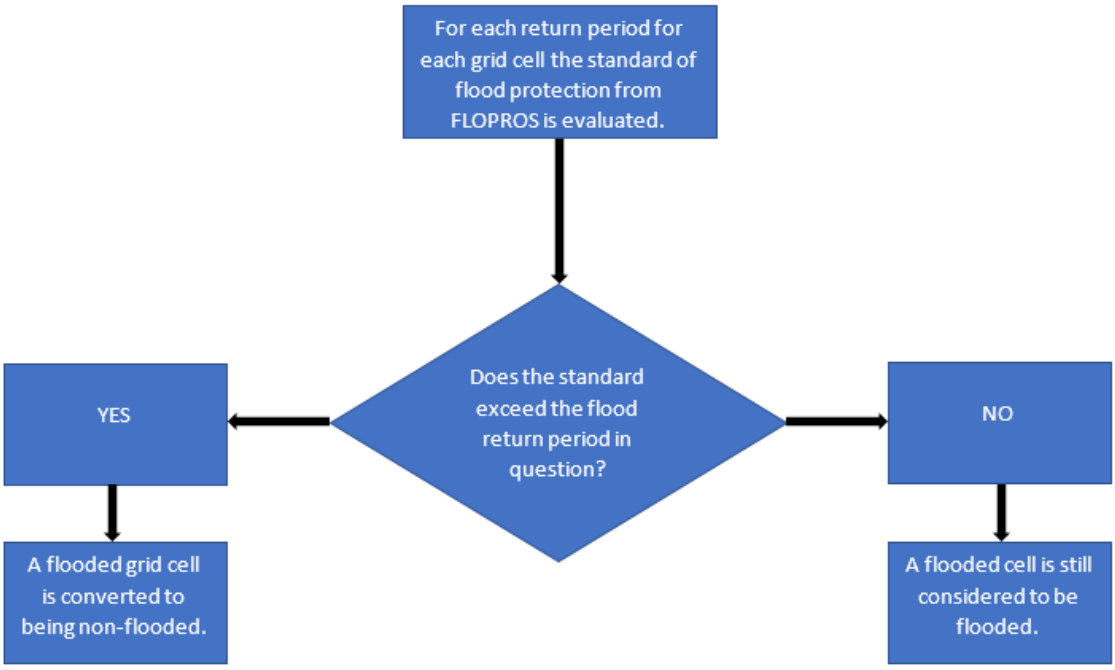

Figure 4-2 Flow diagram of how the FLOPROS data used to adjust the inundated population figures based on standards of flood protection.

4.2.3 Gridded Population Layer

Three gridded population datasets are compared and contrasted in order to ensure the version used to produce exposure values is one which is ideally suited to the task of optimally mapping flood risk in Cape Town and in particular in informal settlements.

The first gridded population dataset my research employs is the Worldpop dataset for the year 2020, with a resolution of 3 arcseconds, or approximately 90m at the equator. The Worldpop data is produced by using a random forest to disaggregate country level population data using remotely sensed data mostly associated with land use type (Stevens et al, 2015). This dataset has a finer spatial resolution than other, older alternatives such as GRUMP and GPW. An assessment of the accuracy of this method in Cambodia, Kenya and Vietnam revealed the random forest method to be superior to others used previously (Stevens et al, 2015). There may be a tendency of population data however to concentrate people around rivers since many of the variables used to disaggregate the census data are correlated with the probability of flood inundation (Tatem et al, 2014) and therefore there is a risk of confounding. Examples include variables describing the proximity to water bodies, aridity and elevation (Stevens et al, 2015).

The second gridded population dataset used is the High Resolution Settlement Layer (HRSL). For South Africa this map was produced for the year 2015 as a partnership between Facebook Connectivity Lab and the Center for International Earth Science Information Network (CIESIN, 2019) at Columbia University. The dataset was specifically designed to detect undermapped populations of the world (Stevens et al, 2019, CIESIN, 2019). It is a method which disaggregates census data in a similar way to the Worldpop dataset, but uses computer vision methods, including CNNs, to detect buildings to distribute populations in DigitalGlobal imagery (CIESIN, 2019).

A comparison of this gridded dataset by Stevens et al (2019) with several others pointed to its suitability for a task such as this. Relative to the other gridded population datasets the HRSL showed greater correlation with built up area values.

The final population dataset to be experimented with is the High Resolution Population Density Map (HRPDM). This was similarly made by Facebook Connectivity Lab in partnership with CIESIN (Bonafilia et al, 2019) and uses a similar methodology to HRSL but used binary classification as opposed to segmentation in order to improve its computational efficiency. In addition to the disaggregation method employed by HRSL, Open Street Map labels were also used as ground truths to assist the training of the detection of buildings (Bonafilia et al, 2019).

Both the HRSL and HRPDM datasets have a spatial resolution of 1 arcsecond, representing approximately 30m at the latitude of Cape Town. These represent the most spatially resolute of any of the population datasets or the flood model outputs. As a result, the Worldpop population dataset, FLOPROS data and the flood model outputs are reprojected to this resolution so analysis can take place at the highest spatial resolution available.

Smith et al (2019) find that datasets such as HRSL and HRPDM reduce estimates of global exposure to flooding in comparisons to datasets such as Worldpop because the more resolute maps place people more precisely and as a result people are less distributed across floodplains.

The population within the study area is according to each of the Worldpop, HRSL, HRPDM gridded datasets, 3480000, 3080000 and 4380000, correct to three significant figures.

4.2.4 Exposure Calculations

For Cape Town the Expected Annual Exposure (EAE) is calculated. The total number of people flooded by each return period is divided by the return period and then the area under this curve calculated using the trapezium rule, in a similar way to Ward et al (2011) as shown in Equation 4-1.

$$EAE = \sum_{I=1}^{9} \frac{(P_R + P_{R+1})(R_I - R_{I+1})}{2}$$

(4-1)

(Ward et al, 2011)

Where:

EAE = Expected Annual Exposure

P_R = Population Flooded for the Return Period in Question.

R_I = Return Period in Question.

I = Index of return periods, 1-9, corresponding to return periods of 5-1000.

EAE = Expected Annual Exposure, the number of people who will be flooded in an average year. Calculated by summing multiple 9 trapezia.

4.2.5 Producing Risk Maps

It is possible to combine flood risk data from all 10 return periods to produce risk maps for Cape Town. Here for each grid cell the minimum return period that causes inundation is taken and a hazard profile map is obtained with the inverse of this determining the level of hazard probability for that cell, as shown in Equations 4-2 - 4-5. This creates a hazard profile map which is then used to create risk maps using both a traditional population disaggregation method with approaches focussing on social vulnerability using the FCN derived informal settlement predictions. Maps are also produced comparing these maps to demonstrate where one method disproportionately distributes flood risk compared with another. This enables the assessment the benefits of vulnerability-based risk mapping as opposed to more traditional population disaggregated income-based methods. These will be called “comparison maps”.

4.3 Results

4.3.1 Population Layer Evaluation

The three gridded population datasets can be assessed for their accuracy in order to reach a critical, reasoned judgement as to which of the three is most appropriate for producing representative flood risk maps. The accuracy can be assessed both in an informal settlement context by comparing the population estimates for each of the gridded population datasets and the population values for informal settlements in the SDI dataset. In addition, the accuracy of each gridded population dataset can be assessed more generally by comparing them to the population figures in the Main Places (the smallest spatial unit in the South African 2011 Census).

For the 66 informal settlements used to train the original FCN, 55 come with estimates of their populations. These are compared with the population estimates from the three gridded population datasets used in this study, Worldpop, HRSL and HRPDM, as shown in Figure 4-3.

For each of the three gridded datasets the populations in these 55 informal settlements are largely consistent with one another. There are however, large differences between these estimates and those of the SDI dataset. For the Worldpop dataset for example, expressed as a percentage these range from as low as 0.3% to as high as 2003.4% on a settlement-by-settlement basis, with a median of 33% and lower and upper quartiles of 11.7% and 101.9%, where 100% represents perfect agreement, as shown in Figure 4-3. Similarly, for the HRSL dataset the largest underestimate is 0.3% of the SDI population value, with a maximum of 1907.3%, a median of 31.9% and lower and upper quartiles of 11.75% and 82.9%.

This demonstrates that although there is great underestimation and overestimation depending on the informal settlement in question, there is an overall tendency for the datasets to underestimate the population of these informal settlements, with the median for the HRPDM giving a similar value of 30%.

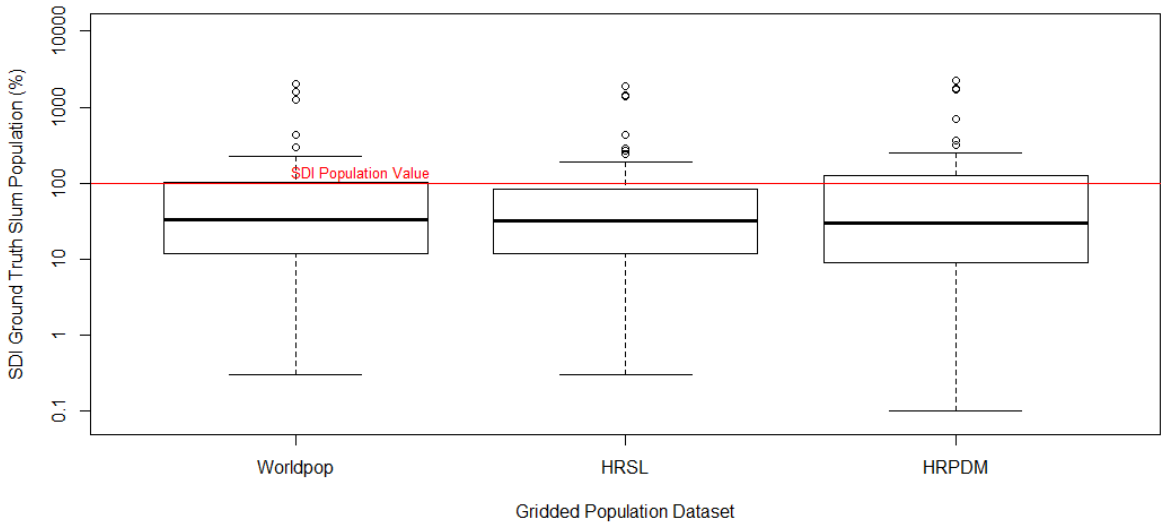

Figure 4-3 Boxplot comparing the gridded population dataset value and estimate in the SDI population dataset in the SDI informal settlements: A value of 100% shows perfect agreement.

Because the area of each of these informal settlements is known, the population densities can be calculated to examine how realistic the population estimates are in the SDI dataset. These range from being as high as $7.7m^{-2}$ to as low as $0.002m^{-2}$. These each represent unrealistic population densities, with typical population densities in informal settlements being $0.06m^{-2}$ (Engstrom et al, 2015), $0.3m^{-2}$ (Desgroppes and Taupin, 2011) and $0.053\text{-}0.125m^{-2}$ (Kit et al, 2013). On this basis it appears most likely that the error lies with the SDI population estimate instead of those of the gridded datasets. The reason why the values in the SDI dataset have a tendency to overestimate population relative to the gridded datasets may lie in their fundamental purpose. The raison d'etre of these enumeration data lies not in producing accurate information about conditions in the informal settlements but in pressurizing for municipal authorities to make informal settlement improvements and to avoid evictions (SDI, 2018, Byrne et al, 2018, Tomlinson, 2017, SDI, 2018, Byrne et al, 2018, d'Cruz et al, 2009). The community mappers may therefore have vested interests in overestimating the populations in these informal settlements to improve the likelihood of informal settlement upgrades or to reduce probabilities of evictions (Makau et al, 2012). On the other hand, there is evidence both in South Africa and globally that household surveys, undercount populations for similar reasons to censuses. In particular, the counting the population in all dwellings due to their disorganised nature, which makes certain dwelling hard for surveyors to access or identify

(Carr-Hill, 2013, Maluleke and van Eeden, 2013). The true number of informal settlement dwellers is consequently hard to ascertain. The comparisons between the SDI population values and the gridded population datasets must as a result be viewed with caution.

In coming to a reasoned judgement regarding the optimal gridded population dataset to use, more emphasis should as a result be on comparing the population estimates from these to the 2011 South African Census, due to it being a better established, more comprehensive dataset.

All three datasets use disaggregation of the census data, but Worldpop disaggregates national level census data (Stevens et al, 2015) and with HRSL the disaggregation at the second-level administrative level (Fries et al, 2020), a level above the Main Places being evaluation here. The comparison involving census data is as a result valid despite these data being used in the first place to produce them.

Part of the motivation for producing the social vulnerability maps in this thesis is the unreliability of census data in informal settlements (Wardop et al, 2018, Carr-Hill, 2013, Maluleke and van Eeden, 2013). It may therefore seem counterintuitive to produce these social vulnerability maps using population datasets obtained from census data. But the census tracts from which the gridded population dataset contain both formal and informal areas, where the formal areas are likely to have less undercount relative to the informal settlements in the census (Carr-Hill, 2013, Maluleke and van Eeden, 2013). This will have the effect of moderating the effect of any informal settlement undercount in the final disaggregated dataset. The use of deep learning on satellite imagery to detect specific buildings in the HRSL and HRPDM (CIESIN, 2019) to derive these means that the method is well placed to capture the high population densities in informal settlements and is unlikely to be subject to undercounts in the same way as censuses.

With the census data, there is a far greater level of agreement with the three gridded datasets than with the SDI data. The median percentage of the census value which each of the three gridded datasets represent are 120.9% for Worldpop, 107.0% for HRSL and 154.1% for HRPDM, where 100% represents perfect agreement.

The gridded dataset with the greatest conformity is the HRSL, as shown in Figure 4-4, with its largest overestimate being 109.5% of the 2011 Census value, with there being no underestimates. This contrasts to the maximum overestimates of the Worldpop and HRPDM datasets which have the largest overestimates of 123.8% and 162.5% respectively. All three

datasets however represent population values consistently higher than those seen from the 2011 Census data. This is likely to be due to population growth in the period between the production of the gridded maps and the 2011 Census.

On the basis of primarily the comparisons with the 2011 Census data and secondarily comparisons with the SDI population data, maps comparing methods of distributing flood risk should use the HRSL dataset. Its population estimates for the 17 Main Places which lie entirely within the study area have a median estimate closest to the 2011 Census values of 107.0% as opposed to 120.9% for Worldpop and 154.1% for HRPDM.

The HRSL dataset's estimates of the population within informal settlements have less extreme values and the median is closer to the SDI population, with the underestimate less than that suggested by Worldpop and HRPDM.

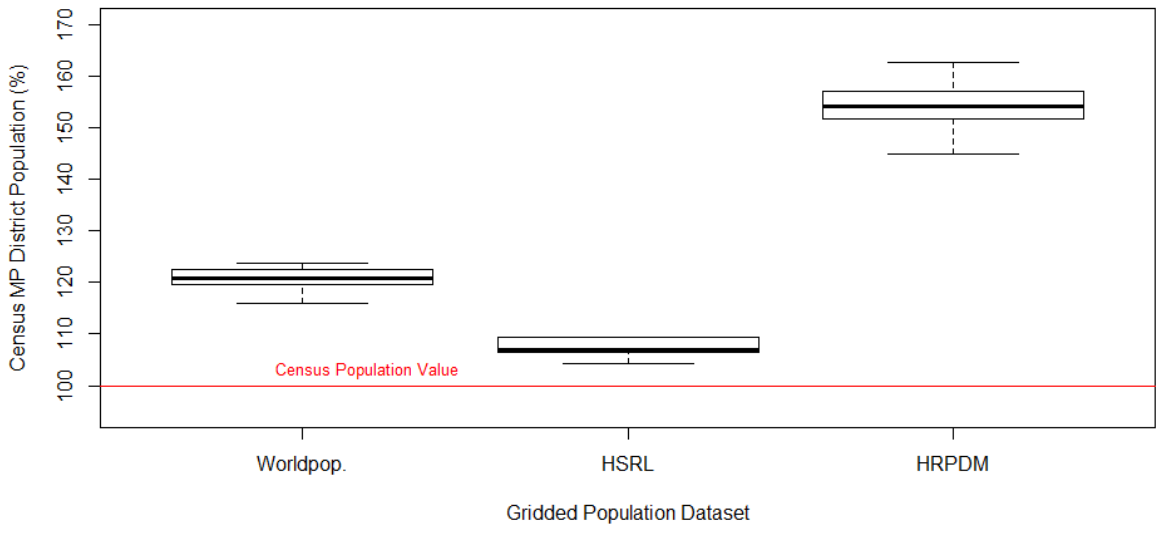

Figure 4-4 Boxplot comparing the gridded population dataset value and estimate in 2011 South African Census in each Main Place (MP): A value of 100% shows perfect agreement.

4.3.2 Expected Annual Exposure Values

The EAE in Cape Town is 25600 people according to the HRSL dataset[2], this corresponds to 0.83% of the population as presented in Table 4-1. All EAE values are correct to three

[2] EAE values were also calculated for the Worldpop and HRPDM datasets, with little difference made to the findings.

significant figures. The EAE values are shown as raw values and percentages of the total population for the HRSL dataset in each MP lying completely within the study area to show where in Cape Town people are most exposed to flooding.

According to the HRSL gridded population dataset, the MP with the highest percentage of the population at risk from flooding is the Goodwood MP, with 2.22% of the population expected to be flooded in a given year, with a similarly high percentage exposed of 1.95% in the Athlone MP. The values are visually represented in Figure 4-5.

	HRSL	
	EAE	**%**
Total Population	25600	0.83
MP Name		
Milnerton	635	0.62
Parow	1700	1.35
Bellville	521	0.43
Belhar	440	0.73
Delft	597	0.36
Matroosfontein	290	0.35
Elsies Rivier	392	0.84
Goodwood	1210	2.22
Epping Industria	0	0.00
Langa	662	1.16
Athlone	5060	1.95
Gugulethu	209	0.19
Nyanga	28	0.04
Crossroads	209	0.55
Philippi	881	0.42
Mfuleni	304	0.56
Mitchells Plain	3970	1.20
Grassy Park	834	0.95

Table 4-1 Main Place EAE values: Values of EAE for each Main Place (MP) in Cape Town lying completely in the study area according to all three gridded population datasets used. Values expressed as totals and percentages of the total population in that MP.

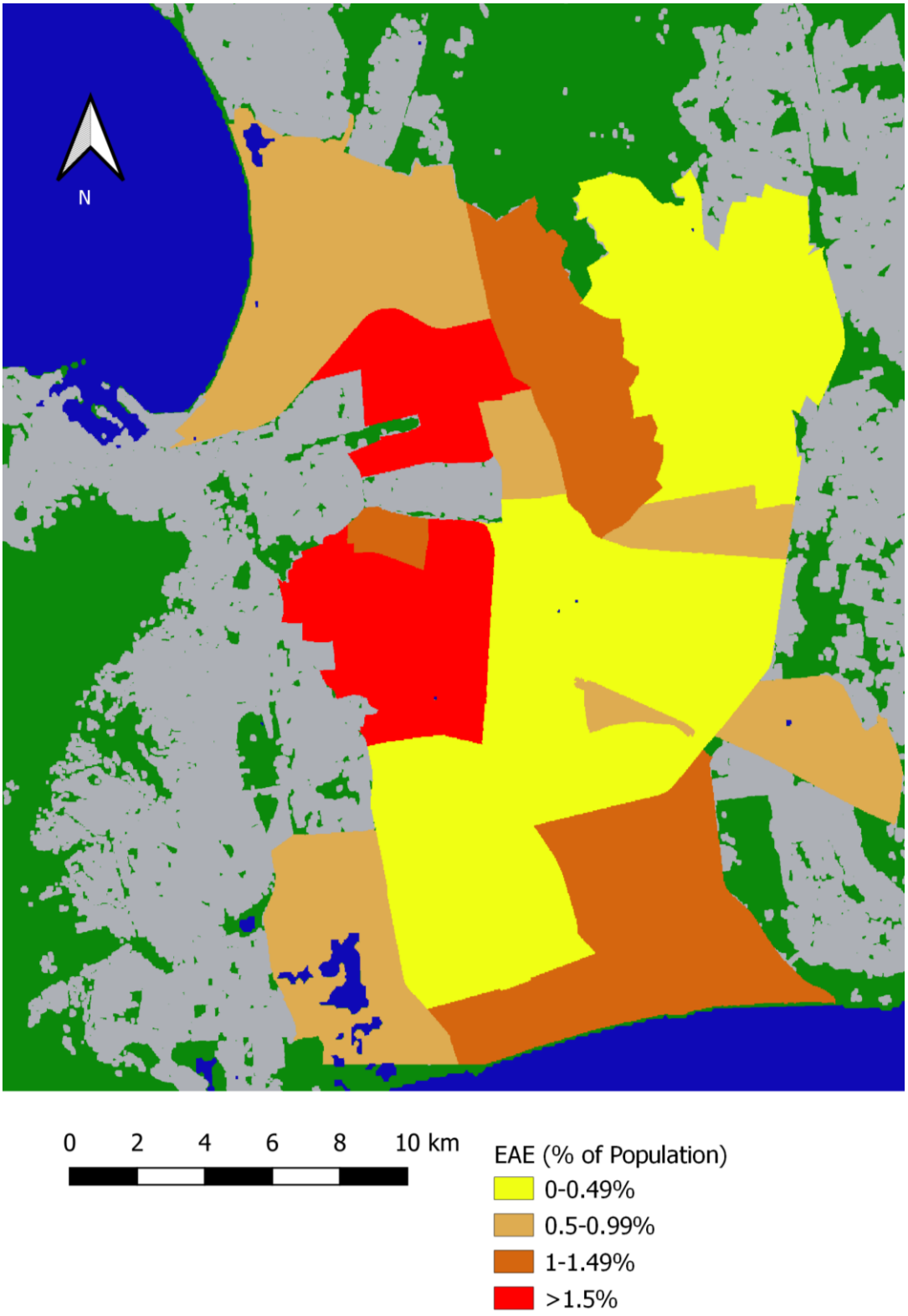

Figure 4-5 Choropleth map showing the EAE for each Main Place (MP) in Cape Town, expressed as a percentage of the whole population in that MP.

The FLOPROS dataset estimates that the whole of Cape Town is protected against a 1 in 100 year flooding event. This is on the basis of what is termed by the FLOPROS dataset as the "policy" layer, meaning that the 1 in 100 year value is based on authorities aspirations of the flood intensity they intend to protect against. This will not necessarily be reflected in reality however. First, it derives from a value of extremely coarse spatial resolution. It is a value derived from a single data point covering the whole of the Western Cape Province of South Africa. It is virtually impossible for the standard of flood protection to be uniform across a region this large. Second, empirical evidence would seem to undermine the claim that all places in Cape Town are protected against a 1 in 100 year flooding event. There are for example many informal settlements in Cape Town which flood almost annually (Divdal, 2011).

It is as a result necessary to assess how the EAE changes if the true standard of flood protection were lower than FLOPROS by various amounts. Figure 4-6 demonstrates how the EAE reduces dramatically from 25600 to 4440 if the standard of flood protection of 1 in 100 is assumed. This is a reduction of 82.7%. More limited amounts of flood protection on the other hand appear to have very little mitigating effect. A small standard of protection against a 1 in 5 year event has the effect of reducing the EAE from 25600 to 23900, just a 6.6% reduction. And with 1 in 10 year flood protection the EAE value becomes 18900, a 26.2% reduction relative to when there is no flood protection.

The frequent occurrence of flooding in many informal settlements suggests very poor standards of flood protection in many of these areas. As a result, exposure values and risk maps aimed at measuring flooding in informal settlements should compare exposure values for a variety of levels of flood protection. This is especially since other studies have found similar findings regarding the poor standard of flood protection in informal settlements (Kundzewicz, 1999, Douglas, 2017).

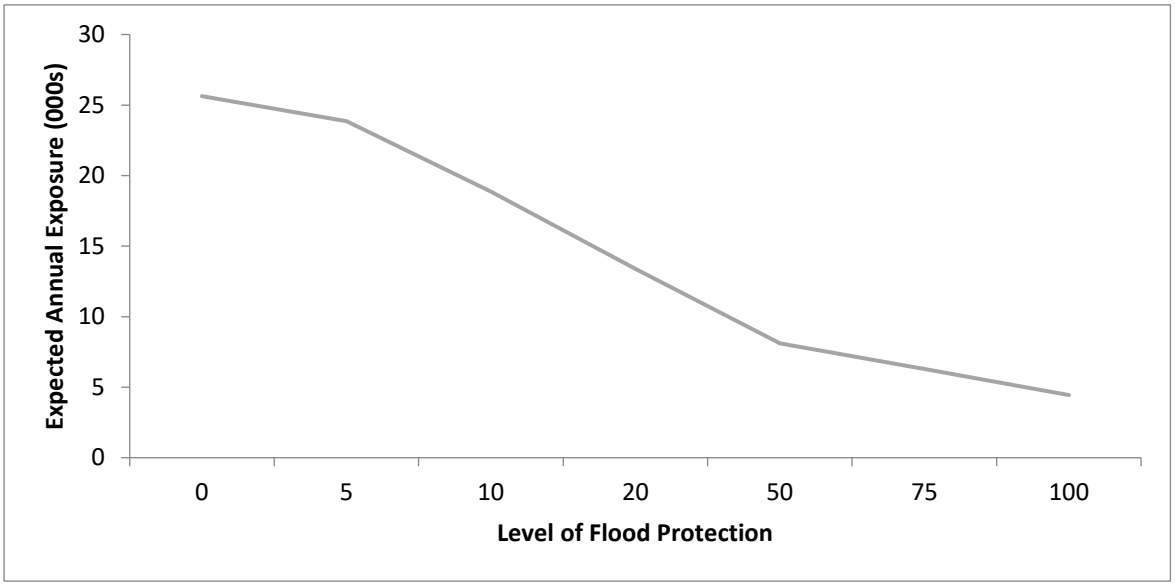

Figure 4-6: The effect on the EAE of different standards of flood protection using the HRSL gridded population map.

4.3.3 Informal Settlement Layer Evaluation

Due to aforementioned issues with the population statistics included in the SDI dataset, I measure the informal settlement dweller populations in this dataset according to the HRSL dataset. This will be used to calculate the proportion of the population of Cape Town who are informal settlement dwellers and give a corresponding EAE value.

Section 2.4.6 produced an informal settlement layer and this was evaluated against the OpenUp informal settlement map of Cape Town in Section 2.4.7. This research chapter expands upon this by integrating the HRSL population layer into this evaluation. The Municipal Authority (City of Cape Town) estimates that the proportion of the population living in informal settlements in Cape Town is 20.5% (City of Cape Town, 2021)This figure the municipal authority derived from the 2011 South African Census (City of Cape Town, 2021). This figure can be used to evaluate the accuracy of the various methods of mapping informal settlements which have been developed.

Here the method developed in Chapter 2 is tested both with and without post-processing in order to independently examine the effectiveness of the post-processing on a larger scale than that which was carried out in Chapter 2. The final product has a spatial resolution of 1 arcsecond to match that of the HRSL gridded population dataset and consists of 9855 original Google Maps images, as described in Section 2.4.6. The pixel-based map with post-processing is identical to the one presented in Section 2.4.6.

The use of the predicted probabilities has use in portraying more information than a mere binary map because the full distribution of values may be shown instead of merely 0s and 1s. This is the case assuming that parts of Cape Town may display some visual features of informal settlements but not others and the predicted probabilities will account for this and rank each pixel along a continuous scale instead of a discrete one. Conceptually however, the predicted probabilities from the FCN represent the probability of a pixel belonging to either of the two categories based on the maximum likelihood principle. The network used was also fine-tuned using overall accuracy and AUC. Both of these metrics conceptually assume the predicted probabilities are in fact rounded to either a 0 or 1, depending on how each category is labelled. This is in contrast to the Brier score, which emphasises the distance between the predicted probability and the ground truth.

As a result, as well as a layer showing the full probabilities, this section produces an informal settlement layer where the predicted probabilities are binarised to "0" for "formal" and "1" for "informal" using a threshold of 0.5 because the binarised results represent the most literal interpretation of the predicted probabilities from the FCN.

This results section will subsequently compare and contrast these various methods of performing this in order to come to a reasoned and critical judgement of the optimal informal settlement layer to use to produce the final set of risk maps.

The pixel-based map with post-processing is the map originally presented in Section 2.4.6 and it dramatically overestimates the proportion of the population in Cape Town living in informal settlements, at 59.4%, as opposed to the municipal authority's estimate of 20.5%. Part of this may be due to a lack of training caused by using early stopping, as states in Section 2.4.7.

The reason for the apparent bias created by the post-processing may lie in the relative imbalance between the proportion of informal settlements in the training images and the proportion in Cape Town as a whole. The post-processing parameters may only be successful assuming a certain balance of classes. There are consequently good reasons why the fine-tuned post-processing may have a counterproductive effect on the accuracy of the scaled-up map.

Informal Settlement Mapping Method	People Living in informal settlements	Population living in informal settlements (%)	EAE of informal settlement dwellers
Official Estimate	632000*	20.5	
Pixel Based	1830000	59.4	14336
Pixel Based Binary	1950000	63.3	13728
Pixel Based No Post-Processing	1170000	37.8	8781
Pixel Based No Post-Processing Binary	639000	20.7	4421
Area Based Size 6	1580000	51.2	10893
Area Based Size 16	1630000	52.9	11248
Area Based Size 6 No Post-processing equivalent	647000	21.0	3860
Area Based Size 16 No Post-processing equivalent	607000	19.7	3532

Table 4-2 Comparison of Methods of Informal Settlement Mapping: Summary of population figures are accurate to three significant figures, with percentages accurate to one decimal place. * denotes the assumed number of informal settlement dwellers using the HRSL dataset extrapolated from the City of Cape Town percentage estimate of informal settlement dwellers of 20.5%.

As a result, an additional informal settlement map is produced without the post-processing in order to compare the results. With the effect of post-processing taken out, the proportion of informal settlement dwellers in Cape Town drops from 59.4% to 37.8%, much closer to the estimated value of 20.5%.

These results however are based on multiplying the predicted probability by the HRSL population estimate in each grid cell. The use of predicted probabilities produced by the FCN pertain to the probabilities of the respective pixel belonging to either the “informal” or “formal” category. This is as a result of the use of the binary crossentropy loss function which is based on the probability using the maximum likelihood principle. The use of the binary crossentropy

loss function therefore results in the most literal interpretation of the FCN outputs being to convert them to binaries.

The informal settlement predictions without post-processing and also binarised suggest that 20.7% of Cape Town's population live in informal settlements. This is virtually identical to the official estimate of 20.5%. The reason why the binarised estimate aligns so closely with the official estimate may be because, as has already been discussed, the binarised map represents the most literal interpretation of the predicted probabilities.

For the area-based approach, Chapter 3 recommended producing maps using a Gaussian blur filter size of both 6 and 16 due to relative advantages and disadvantages of each. Chapter 3 found that a filter size of 6 produced superior Jaccard Index values due to having edges with greater conformity to the ground truth masks. But a filter size of fewer false positives when calculating the F1-score. As a result, this analysis produces informal settlement prediction maps of all of Cape Town using both a filter size of 6 and 16.

The maps using an area-based approach also seem to overestimate the number of informal settlement dwellers. According to the size 6 map, 51.2% of Cape Town's population live in informal settlements, with this figure being slightly higher for the size 16 map at 52.9%, both higher than the municipal authority's 20.5% estimate. Intriguingly however, the map produced with the larger Gaussian filter size estimates more informal settlement dwellers. Section 3.4.3 suggested the opposite should be the case, that the larger filter size results in fewer false positive results. Although this is counterintuitive based on the results in Section 3.4.3, it may be explained by the larger Gaussian filter size having a greater ability to remove salt and pepper noise. Section 2.4.1 showed that the strength of blurring is to remove this salt and pepper noise so as to correctly classify ground truth areas. With the scaled-up map it is likely that this effect cancels out the effect seen in Section 3.4.3, where the larger filter size removes false positives relative to the smaller filter size.

The likely reasons for the failure of the post-processing with the pixel-based maps is likely to apply equally to the area-based maps too. As a result, an equivalent correction is applied to the threshold of the production of the area-based maps. A threshold of 0.52 instead of the 0.3 threshold is applied to the area-based method to produce an equivalent area-based map. This aligns with the 0.22 difference between the post-processing and non-post-processing pixel-based maps which was found to be preferable in the fine tuning process in Chapter 2.

These “area-based no-processing equivalent” results show outcomes similar to the effect of removing post-processing for the pixel-based maps. For a blur size of 6 for example, applying a post-processing equivalent correction turns the estimated proportion living in informal settlements in Cape Town from 51.2% to 21.0%.

In coming to a reasoned, critical judgement regarding the best informal settlement map to proceed with, the close estimate of 20.7% in comparison to the 20.5% is the closest estimate to the official estimate from Table 4-2. This was obtained from the binarised pixel-based map without post-processing. This demonstrates the fundamental accuracy of the pixel-based map prior to when the binarisation occurred. However, using a binarised map conveys less information than when the full-pixelated probabilities are included, because it places probabilities of informal settlements on a continuous scale, which may infer the difference between various levels of settlement formality to be shown by the predicted probabilities. The pixel-based map without post-processing but not binarized, is therefore the map which should be used as the informal settlement component.

The binarised map gives a near perfect proportion of informal settlement dwellers, at 20.7%, but the equivalent map with predicted probabilities substantially overestimates the proportion of informal settlement dwellers, at 37.8% due to an inability to assign low probabilities (see Section 2.4.7).

The analysis of the percentile distribution of informal settlement predicted probabilities in Figure 2-16 explains why the unbinarised informal settlement map struggles to produce population estimates which align with official estimates, yet the binarized version does. The network struggles to assign low probabilities even to the places least likely to be informal settlements. Section 2.5 speculated that a lack of training of the network was the cause of this, possibly a result of the use of early stopping as a means of correcting for overfitting. The proposed solution to this in Section 2.5 was the use of L2 regularization as a more suitable method of avoiding overfitting.

When full predicted probabilities are shown, the conformity to the official estimate of the proportion of informal settlement dwellers is not as close as the binarized equivalent. The use of the version with full predicted probabilities however is still favoured. This is because of fact that the full predicted probabilities show more information than when the probabilities are dichotomised, it is worth using the full predicted probabilities. This is whilst the equivalent

binarized map shows the fundamental accuracy of this set of predictions because they represent the most literal interpretation of those probabilities.

The decision to use the pixel-based map is based on it more closely conforming to the official estimate of the number of informal settlement dwellers in Cape Town and the ability of the full pixelated probabilities to show more information. However, Section 3.2 described the importance conceptually of an area-based approach for social vulnerability mapping. Although the flood risk maps developed in this thesis will as a result not incorporate this advantage, the methods developed for area-based mapping in Chapter 3 still make a valuable contribution and give lessons for how such maps can be improved in future, ultimately to be used in the intended way, despite not being used to make the final maps in this research chapter.

4.3.4 Does Flooding Disproportionately Affect Informal Settlement Dwellers?

The mapping of informal settlement dweller populations enables an assessment of whether flooding in Cape Town disproportionately affects informal settlement dwellers. It is popularly assumed that this will regularly be the case in reference to informal settlements because areas exposed to flooding are more likely to be avoided by planners constructing more formal environments, leaving only marginal land on flood plains available to rural-urban migrants who go on to inhabit informal settlements (Porio, 2011, Cutter et al, 2000, Cutter 2003).

This is not defined as an element of social vulnerability, as described in Section 1.2. This is because of the focus in this thesis on the empirical measurement of socioeconomic circumstances and how these influence people's hazard outcomes, so integrating external factors such as these add unnecessary complexity to this concept. The phenomenon is different from social vulnerability since something being exposed implies a direct interaction with the hazard itself, whereas for a factor to be classified as a component of social vulnerability it usually implies independence from the hazard (Brooks, 2003). Whether informal settlement dwellers are disproportionately exposed to flooding is still important to study because it can provide additional information on the overall socioeconomic factors influencing flood risk.

Figure 4-7 graphs each of the return periods and the proportion flooded who live in informal settlements, against the city-wide average proportion. Population figures use the preferred HRSL gridded population map. The ratio of the Cape Town population who are informal settlement dwellers used is 0.378, from the pixelated informal settlement map with no post-processing.

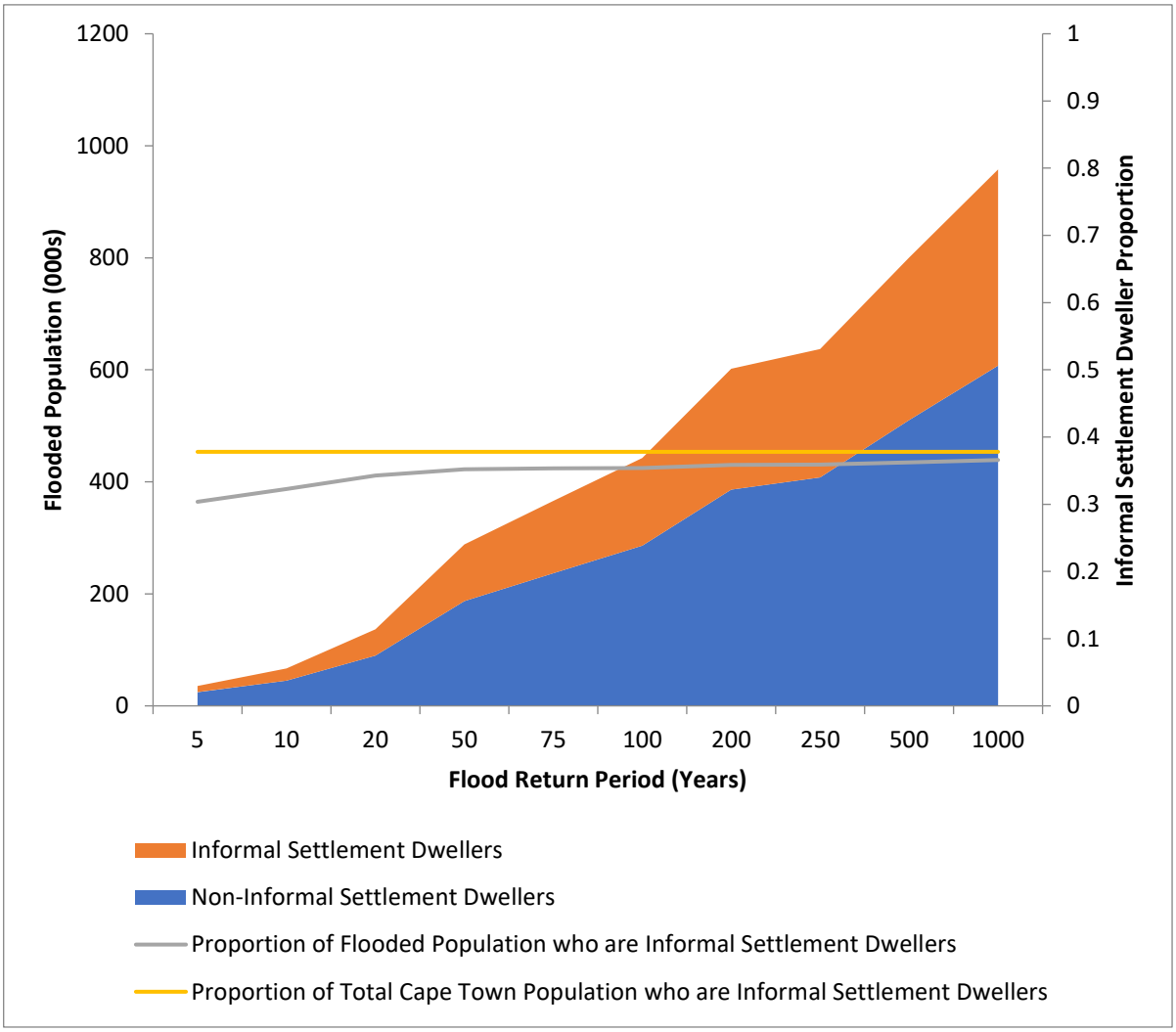

Figure 4-7 Graphing the proportion of informal settlement dwellers exposed to flooding against the population of Cape Town in general.

Figure 4-7 shows that informal settlement dwellers are not disproportionately more likely to be exposed to flooding. For a 1 in 5 year flood event, as a proportion, 0.304 of those flooded are informal settlement dwellers, as opposed to the city wide average proportion of 0.378. This rises to 0.366 for a much rarer but larger 1 in 1000 year flooding event. For no flood return periods are informal settlement dwellers disproportionately more likely to be affected.

A possible explanation for this lies in the slopes where both formal and informal areas of the city lie. Pluvial flooding is generally more common in flatter land where there is no easy drainage. A possible reason why informal settlement dwellers are not disproportionately exposed to flooding is that informal settlements lie on steeper ground than more formal parts of the city. The MERIT Digital Elevation Model (DEM) is the same as that used in the Fathom

model and it is used to calculate the slope for percentiles of informal settlement prediction (Yamazaki et al, 2017).

Percentile Value of Informal Settlement Predicted Probability	Slope (°)
1 - 10	0.56
11 - 20	0.56
21 - 30	0.57
31 - 40	0.60
41 - 50	0.64
51 - 60	0.67
61 - 70	0.71
71 - 80	0.77
81 - 90	0.86
91 - 100	1.02

Table 4-3 DEM Derived Informal Settlement Slope Values: The slope values in informal settlements in Cape Town for the percentiles of the informal settlement predicted probabilities from the "Pixel Based No Post-Processing equivalent" informal settlement map.

Table 4-3 shows that there may be some truth to this. When the city is split into groups of ten by percentile of the informal settlement predicted probability, the 10% of areas of the city most likely to be informal settlements are on the steepest slopes, at 1.02° in comparison to 0.56° in the 10% of areas least likely to be informal settlements. However, the difference in these slopes is very slight and as a result, this explanation is insufficient to explain why informal settlement dwellers appear to be disproportionately less exposed to flooding, despite the fact that in the MERIT DEM smoothing and a coarse spatial resolution may underestimate the extent of these slopes (Yamazaki et al, 2017).

Whilst the slopes of informal settlements may be a factor specifically in Cape Town, such a conclusion may not apply to informal settlements around the world in general. It is common globally for informal settlements to predominantly exist on low-lying flood plains (Abunyewah et al, 2018, Morin et al, 2016). Examples of cities where this is the case are Manila (Porio, 2011, Morin et al, 2016), Kigali City (Bizimana and Schilling, 2009) and Kolkata (Rumbach and Shirgaokar, 2017). It must be stated therefore that the conclusion about slopes in Cape Town and informal settlements is not necessarily applicable on a global scale.

4.3.5 Producing Risk Maps

I produce four different flood risk maps each with a different treatment of human vulnerability. Two additional maps are produced showing the difference between these flood risk maps. These will allow a direct comparison with how each risk map distributes flood risk across space. In this chapter these are referred to as "comparison maps". The four risk maps and two comparison maps are mathematically described in Equations 4-2 – 4-7.

Map A shows total population exposure by replicating a traditional flood risk mapping method. The hazard component is multiplied by the population headcount in each grid cell in a similar way to risk equation type conceptual models such as Equations 1-2 and 1-3. Alternative maps that incorporate social vulnerability (as proxied by informal settlement status) are presented in Figures 4-10 and 4-11. One uses the pixelated informal settlement probabilities and the other uses total vulnerable population which combines population and informal settlement predicted probability. These maps aim to measure something fundamentally different from Map A. It attempts not to measure the total economic output at risk from flooding, but to map the total vulnerable population. However, a direct comparison with Map A is inappropriate because of the difference in skew of the pixel values of the gridded population values and the pixelated informal settlement values. The raw pixel values for the HRSL gridded population dataset have a skew of 2.72, whereas the informal settlement predicted probabilities have a skew of 1.53, each correct to two decimal places. The reason why the skew is much greater for the population values instead of the values for informal settlement predicted probabilities is because populations are naturally clustered in certain areas in cities, whereas the informal settlement predicted probabilities derived from the FCN are naturally distributed more uniformly between 0 and 1.

This research chapter is aiming to produce comparison maps between informal settlement based and population-based maps. The great difference however in skew between the population figures and the informal settlement predicted probabilities means that the differential between the two maps will be disproportionately shown by the more skewed map due to its more diverse range of values. In relative terms, the more skewed map will naturally be responsible for a greater relative difference when comparison maps are produced.

As a result, to measure the difference between the sets of maps requires each pixel in each map to be expressed as a percentile. Such a method is applicable to the investigation since I am

interested in this research chapter in exploring how different methods relatively distribute risk instead of examining absolute risk.

As a result, Map B shows population in a similar way to Map A but expressed as percentiles. Likewise, Map C applies the similar correction but to the informal settlement predicted probabilities.

Map D subsequently shows the product of the population and the informal settlement predicted probability, with this value then being converted into a percentile in a similar way to Maps B and C. This results in a map depicting total exposed informal settlement dwellers in order to measure overall flood risk.

Map A.

$$Total\ Population\ Exposure = H \times P \tag{4-2}$$

Map B.

$$Total\ Population\ Exposure_i = H \times P_i \tag{4-3}$$

Map C.

$$Social\ Vulnerability = H \times I_i \tag{4-4}$$

Map D.

$$Total\ Vulnerable\ Population\ Exposure = H\ \times (P_i \times I_i)_i \tag{4-5}$$

Where:

H = Hazard Profile, or the most frequent flood return period which causes flood inundation in a given grid cell.

I = Informal Settlement Predicted Probability.

P = Gridded Population from the HRSL gridded population map.

i = The ith percentile of the given variable

These maps are shown in Figures 4-8 - 4-11.

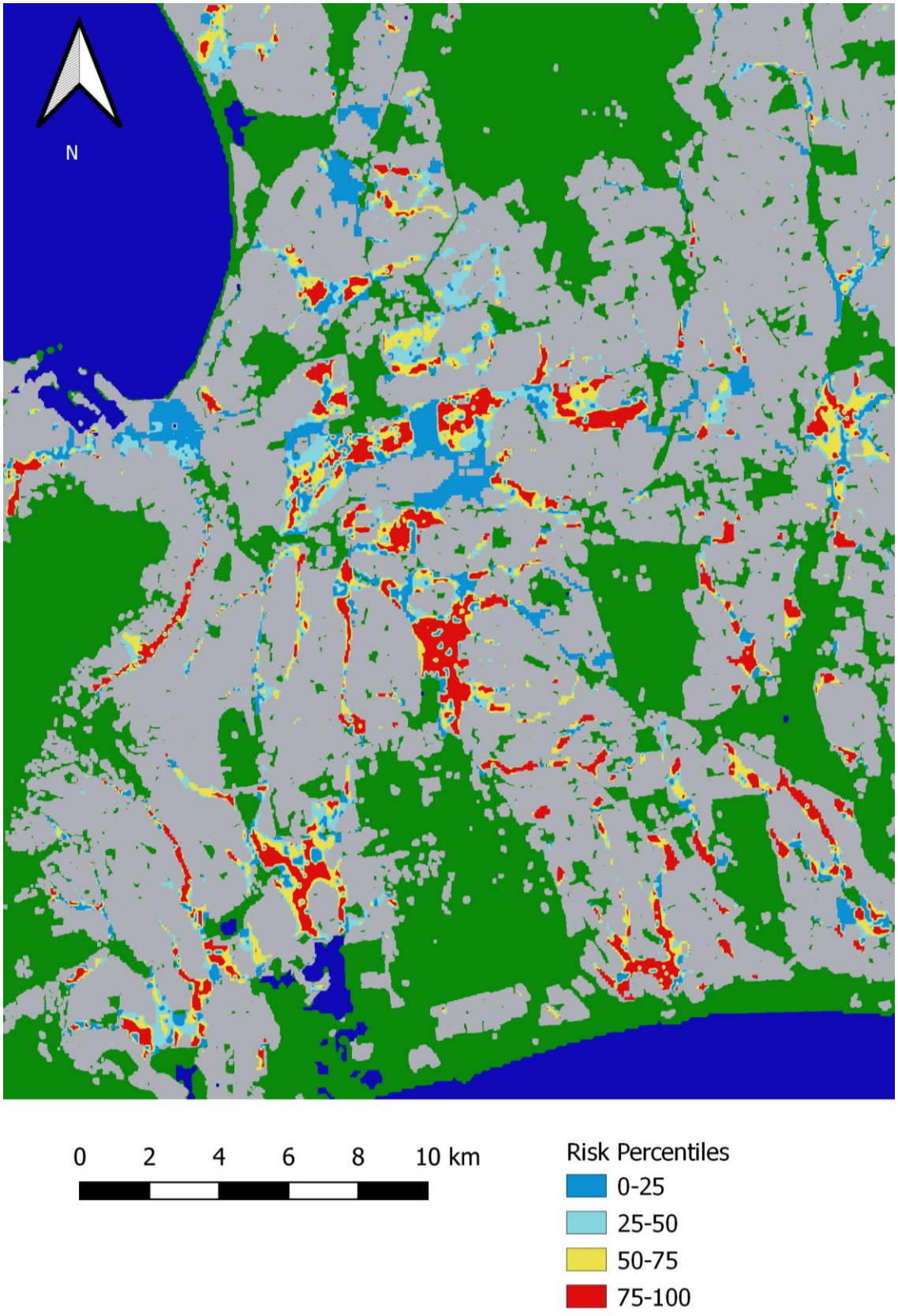

Figure 4-8 Risk Map A, showing the traditional method of population dissagrgeation, according to Equation 4-2.

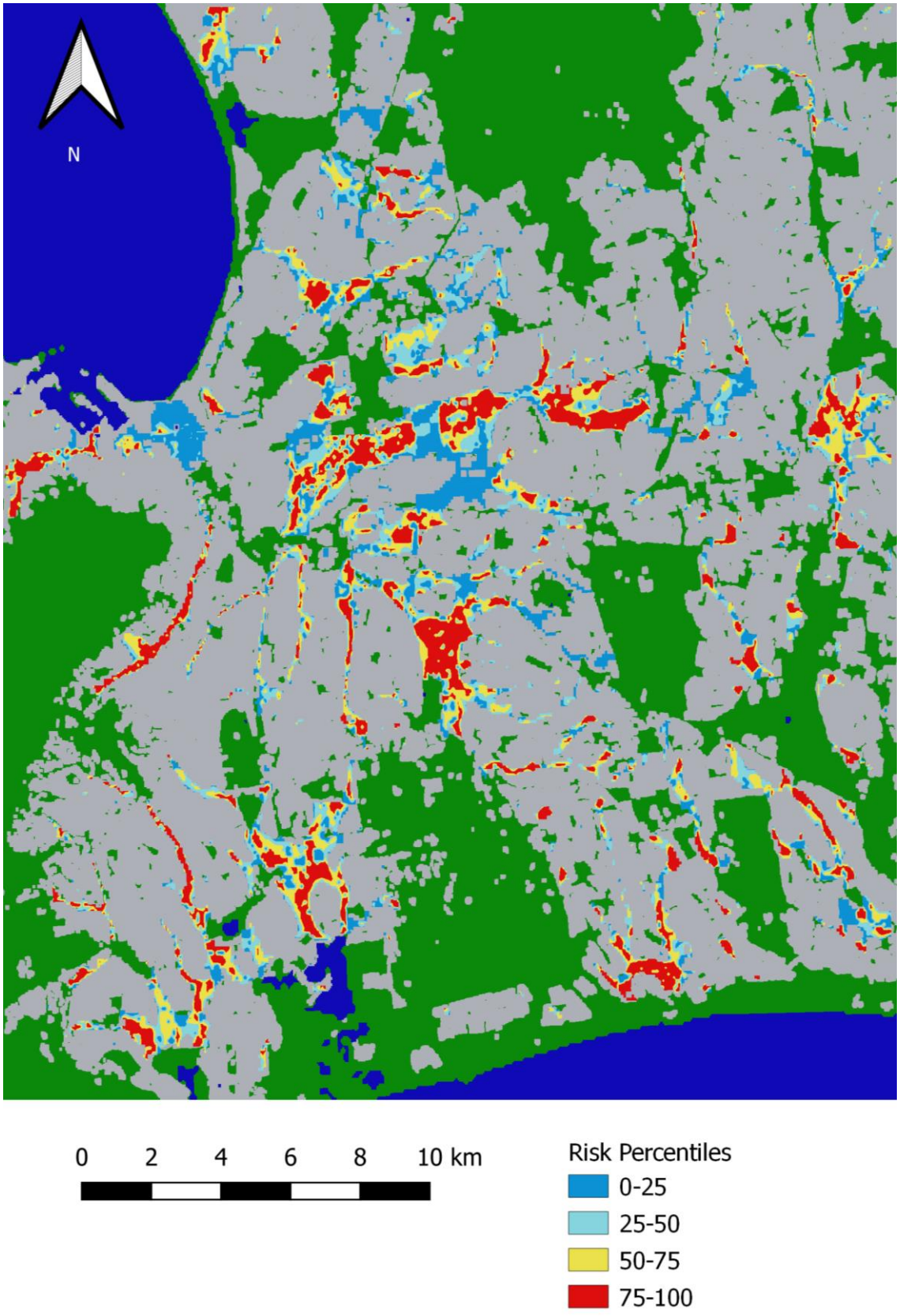

Figure 4-9 Risk Map B, showing the traditional method of population dissagrgeation, according to Equation 4-3.

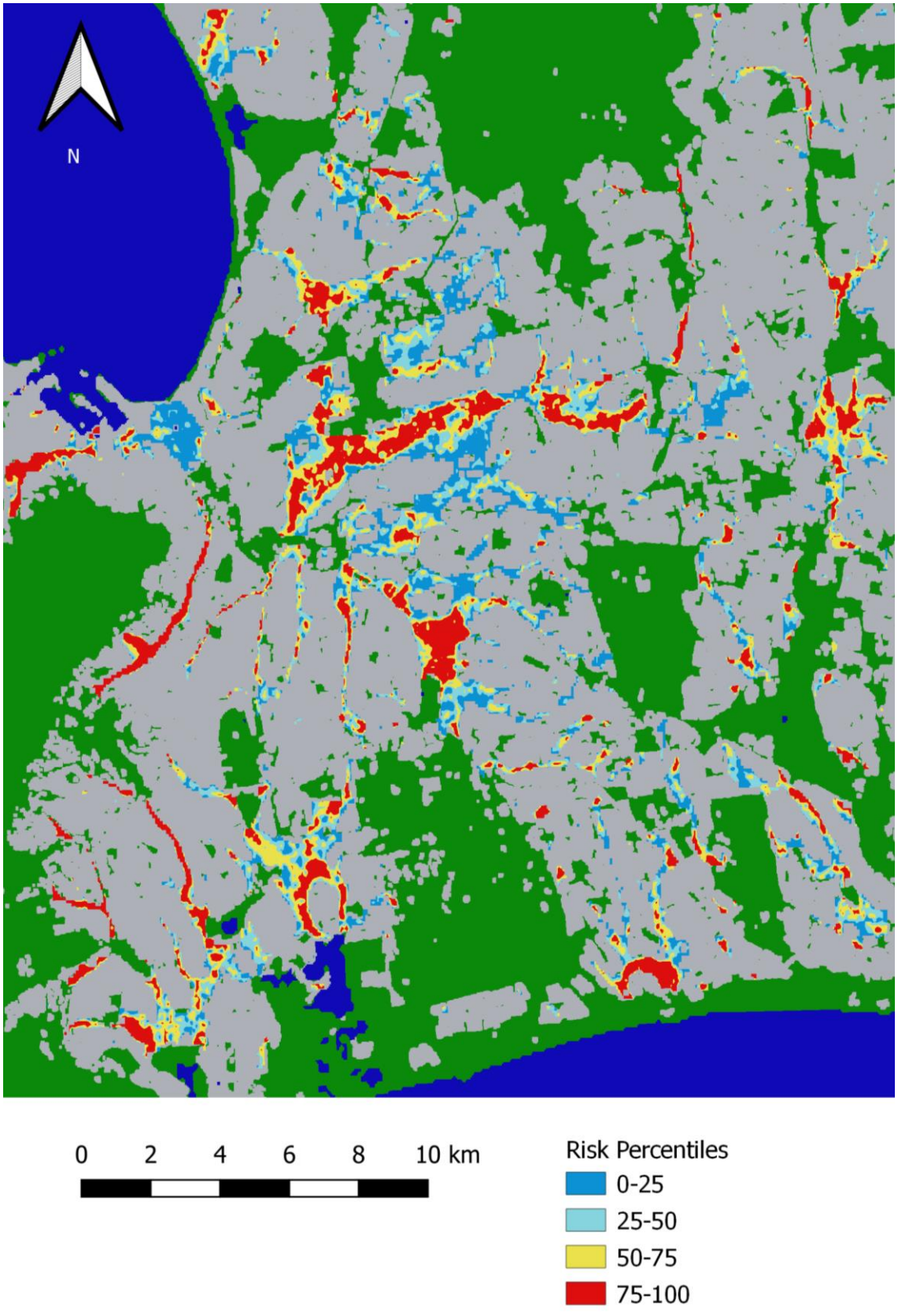

Figure 4-10 Risk Map C, showing social vulnerability, according to Equation 4-4.

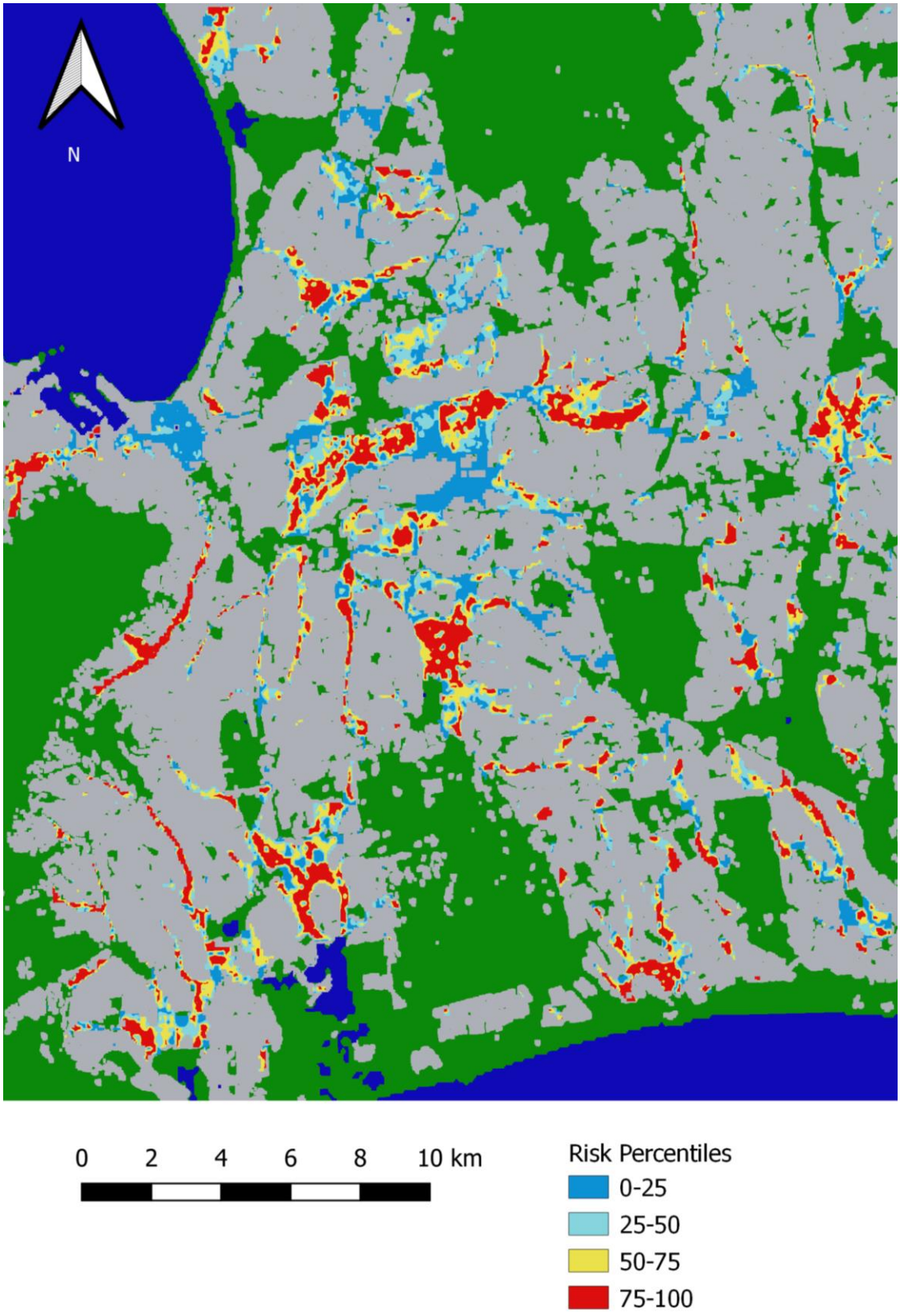

Figure 4-11 Risk Map D, showing total vulnerable population, according to Equation 4-5.

4.3.6 Producing Spatial Comparison Maps

In order to directly contrast and evaluate the relative benefits of the risk maps which have been produced, it is important to produce separate maps comparing how each of the risk maps spatially distributes flood risk. In particular, this comparison shows how investment in flood protection would be differentially allocated when using one method of distributing flood risk as opposed to another.

The focus of these comparison maps lies in the relative distribution based on the various methods of representing the human component of flood risk, rather than what the absolute flood risk is. As a result, for the comparison maps just the 1000 year return is used in order to maximise the flooded area available to make reasonable comparisons. A cell is represented as being flooded if any return period shows flooding in that cell. This enables the comparison maps to more clearly show the difference made by the different treatments of human vulnerability.

The two maps which account for informal settlement probability are Maps C and D, with the control representing the traditional form of mapping being Map B. Map B is chosen as the control as opposed to Map A because it is in the form of percentiles like Maps C and D so a more direct comparison can be made. Two comparison maps are as a result produced to compare Map C and Map B and Map D and Map B. These maps are subsequently referred to as Maps E and F and are described in Equations 4-6 and 4-7.

Map E.

$$Spatial\ Comparison = H_{1000} \times (I_i - P_i)_i \quad (4\text{-}6)$$

Map F.

$$Spatial\ Comparison = H_{1000} \times ((P_i \times I_i) - P_i)_i \quad (4\text{-}7)$$

Where:

H_{1000} = The 1 in 1000 year flood return period map.

I = Informal Settlement Predicted Probability.

P = Gridded Population from the HRSL gridded population map.

i = The ith percentile of the given variable

The risk maps (Maps B, C and D) are expressed as percentiles in order to make the relative contributions of both population and informal settlement predicted probability equal and to remove the effect of skew. The percentiles presented in Table 4-4 for Maps B and C are therefore the percentiles of the pixelated values of population and informal settlement predicted probability.

Similarly, the two comparison maps, Maps E and F are also expressed as percentiles such as to make the differences between the risk maps comparable in order to come to a judgement regarding whether Map C or D are more successful at highlighting informal settlements as vulnerable to flood risk. In Maps E and F, a percentile of 50 for a particular pixel represents no difference in the relative level of risk allocated by the two risk maps the comparison map is analysing. A value above 50 indicates that the vulnerability-based risk map derived from informal settlement predicted probabilities disproportionately allocates risk in that pixel, and vice versa. Because the focus of this research chapter is not on absolute flood risk but the relative flood risk of informal settlements and other areas of the city, it makes sense to use percentiles in this way.

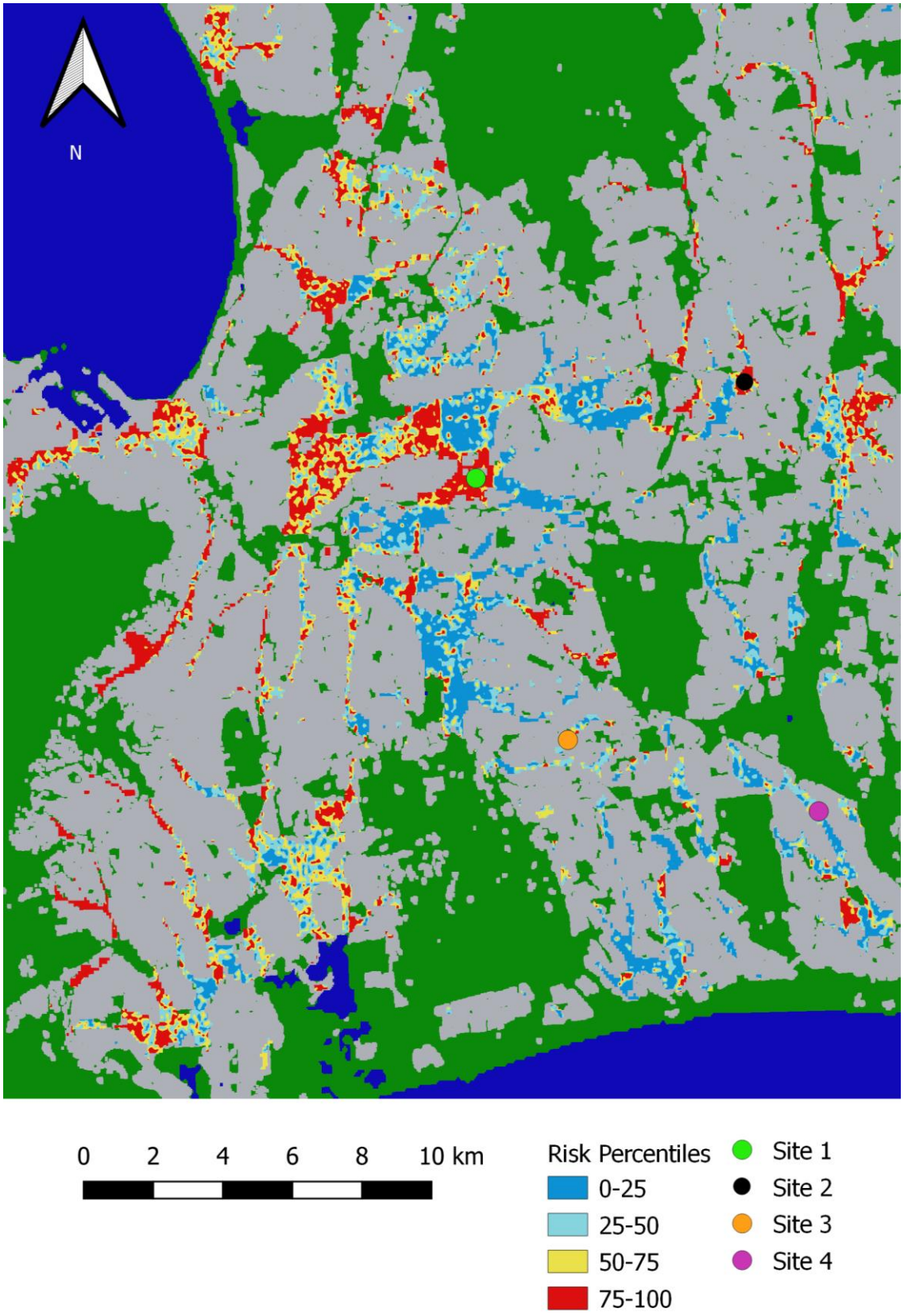

Figure 4-12 Map E comparing how Maps B and D differentially allocate flood risk across space. This amounts to a comparison of the traditional population approach and a social vulnerability approach.

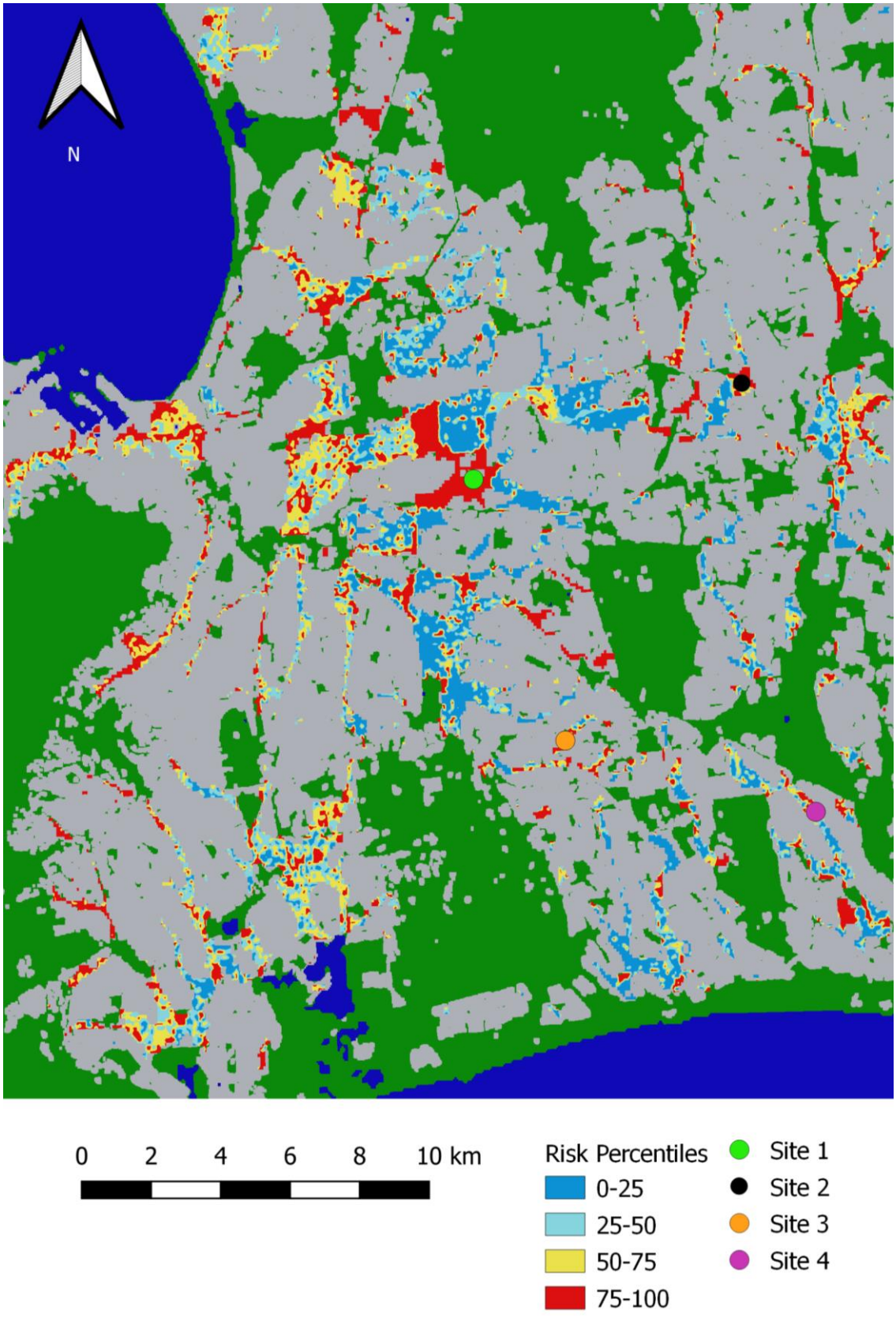

Figure 4-13 Map F comparing how Maps C and D differentially allocate flood risk across space. This amounts to a comparison of the traditional population approach and a total vulnerable population approach.

Figures 4-12 and 4-13 show the two comparison maps. Map E compares a social vulnerability map to a traditional population method of distributing risk. Map F compares the total vulnerable population with the same traditional approach compared in Map E.

The two comparison maps allow for an evaluation of the relative differences of the various methods of distributing flood risk. Four sites which are suggested by the comparison maps as having flood risk disproportionately allocated to them by vulnerability-based map are chosen for this to illustrate whether these maps are effective and how they may potentially be improved.

Site 1 is Epping Industria near the centre of the study area, Site 2 is Triangle Farm in the East of the city. Sites 3 and 4 are in the Cape Flats, a prominent area of informal settlements in the city (Drivdal, 2011, Despotes et al, 2016). Site 3 is in Schoolside Informal Settlement and Site 4 is Nonqubela near Matthew Goniwe Memorial High School. These sites and their locations are described in Table 4-4 and these are plotted on the comparisons in Figures 4-12 and 4-13.

Comparing the percentiles of Map E and F for each site gives an insight into which of the two vulnerability-based risk maps (C and D) which integrate informal settlement prediction is better at highlighting the levels of vulnerability seen in informal settlements.

An area which both Maps E and F disproportionately allocate risk to is Epping Industria in the centre of the map, with both comparison maps having high percentiles. In Map E this site is on the 62^{nd} percentile, as shown in Table 4-4. Whereas in Map F this value is 84^{th}.

		Site 1	Site 2	Site 3	Site 4
Site Name		Epping Industria	Triangle Farm	Schoolside Informal Settlement	Nonqubela
Latitude		33.93417°S	33.91083°S	34.00250°S	34.02250°S
Longitude		18.56083° E	18.64500°E	18.58750°E	18.66500°E
Visual Appearance		Industrial	Industrial	Informal Settlement	Informal Settlement
Risk Maps	Map B Percentile	1	17	98	99
	Map C Percentile	13	36	95	98
	Map D Percentile	0	6	93	97
Comparison Maps	Map E Percentile	62	60	43	44
	Map F Percentile	84	64	78	82

Table 4-4 Comparison of Sites in Risk Maps and Comparison Maps: The percentile values of three of the flood risk maps (Maps B, C and D) at each of the four chosen sites (1,2,3,4), where a value greater than 50 indicates the vulnerability based map overestimates flood risk relative to the traditional, population disaggregation method.

A visual examination in Figure 4-14 reveals that there are no informal settlements here, but instead industrial areas. The reason why the comparison maps show that vulnerability-based methods disproportionately allocate risk lies in an examination of the original percentiles of the risk maps. The site has comparatively few people living in it relative to others, having a population percentile shown by Map B of 1 derived from the HRSL map. Its informal settlement prediction percentile is 13.

Site 1 Site 2

Site 3 Site 4

Figure 4-14 Satellite Imagery of Sites: Visual examination of the four selected sites where the comparison maps suggest that vulnerability-based risk maps integrating informal settlement probabilities disproportionately allocate risk to as opposed to the more traditional method of allocating. Top Left: Site 1, Top Right: Site 2, Bottom Left: Site 3, Bottom Right: Site 4.

Whilst the FCN has been successful at allocating a low predicted probability to this area, it is in percentile terms not as low as the prediction for population, and as a result the vulnerability-

based map which integrates these FCN predictions appears to disproportionately allocate risk to this area.

Site 2 contains a similar pattern, with a percentile of 60 in Map E and 64 in Map F. It similarly has low percentile estimates for the population and informal settlement predicted probability in Maps B and C of 17 and 36 respectively, with the percentile for the population-based Map B being lower than the Map C with its FCN derived informal settlement predicted probability, in a similar way to Site 1. It also appears to be an industrial area upon visual examination.

This shows that Sites 1 and 2 have a comparatively low population due to being industrial areas rather than residential areas, but the network struggles to assign low informal settlement predicted probabilities to them. This is what is subsequently causing Maps E and F to reveal the vulnerability-based maps to disproportionately allocate risk in these areas.

These visual examinations of the comparison maps reveal a deficiency in the method when it comes to industrial areas because of the difficulty the FCN has in identifying industrial areas as belonging to the "formal" category in its original training as shown in Figure 2-16. In future studies this calls for a greater variety of imagery in the training set, on top of the argument already made for greater training set variety in respect to class imbalance and failure of the FCN to assign low predicted probabilities to areas visibly not informal settlement.

Sites 3 lies in the Cape Flats, a prominent area of informal settlements in the South East of the City (Drivdal, 2011, Despotes et al, 2016), more specifically the Schoolside Informal Settlement. Map E fails to show a disproportionate allocation using the informal settlement predicted probabilities, with a percentile of 43, whereas for Map F the percentile value is 78. This suggests that Map D which integrates both informal settlement predicted probability and population is far better at showing informal settlements to be high risk environments.

Satellite imagery shows this area demonstrates clear signs of informal settlements. The FCN appears to be correctly identifying this, with this area being in the 95th percentile according to the FCN. But the similar percentile for the population-based map, Map B, is also high at 98. Given the very small difference in percentile between Maps B and C, the value comparing these in Map E is shows little difference, at just 43. This means that using the vulnerability method of Map C does not preferentially allocate risk relative to the traditional method. Map F reveals a greater difference between the two maps than Map E did, with a percentile of 78 as

opposed to 43. This suggests that Map D is a far superior map in showing informal settlements to be high flood risk environments than Map C.

Site 4 also exists in the Cape Flats, at Nonqubela near the Matthew Goniwe Memorial High School. Visual analysis also shows that this is an informal settlement. The percentile value for Map E is 44 and for Map F it is 82. These values show that as with Site 3, Site 4 shows that Map C is disproportionately more successful than Map B in allocating flood risk in informal settlements. This similarity with Site 3 is the same when the percentiles for Maps B and C are examined. Map B for Site 4 has a percentile of 99 for Map B and 98 for Map C.

A visual analysis of Sites 3 and 4 shows that both contain informal settlements. For each of these sites it should be expected that both comparison maps would show that the vulnerability based methods of mapping would disproportionately allocate risk to areas such as Sites 3 and 4.

For Map C compared with Map B in the form of Map E, the percentile are respectively 43 and 44 for Sites 3 and 4. From a perspective of seeking to develop methods of mapping flood risk which account for socially vulnerable populations as opposed to the traditional population disaggregated method, this would seem to be troublesome. It means that the Map C vulnerability-based map actually places a slightly risk than the traditional method in an area with informal settlements, as shown by Map E. Map C is no better at spatially allocating flood risk to informal settlements than the traditional, population-based Map B.

The opposite seems to be the case however for Map D. The associate comparison map, Map F, gives percentiles of 84 and 91 for Sites 3 and 4, showing that Map F is much more successful at disproportionately allocating flood risk to these informal settlement sites. As a result, it appears that Map D, the map which accounts for the total vulnerable population is superior to Map C in highlighting the social vulnerability of populations.

The lack of success of Map C may be due to the success of the HRSL gridded population map being effective at identifying the high population densities of informal settlements. This is demonstrated by the percentiles of Map B, the population-based map, which are 98 and 99 for the informal settlement sites. This may be due to the use of computer vision with the HRSL dataset to detect individual buildings in order to disaggregate census level population data (CIESIN, 2019). This method is ideally suited to assigning high population densities to

informal settlements with which these environments are regularly associated. So because of this, even the population based risk map allocates high levels of risk to informal settlements.

Map D, which accounts for both population and informal settlement predicted probability, would as a result appear to be a more appropriate map if one is seeking to emphasise informal settlements as being at risk of flooding. Traditional methods of flood risk mapping which disaggregate population are likely to allocate large amounts of flood risk to informal settlements due to the high population densities in these environments. The reason why Map D as a result is more effective is because it accounts for the high population density of informal settlements.

As a result, using Map D, which has been found to be the most effective risk map in terms of allocating high flood risk to informal settlements, I now calculate the EAE of these areas highlighted as being of disproportionate risk as shown by the Map F comparison map, with only sites which appear above various different percentiles in this comparison map included. These sites are the ones where Map D disproportionately allocates risk to a much greater extent than the map representing the traditional method, Map B.

I use an adjustment to correct for the problem seen in industrial areas, whereby only sites with an above 50^{th} percentile population value are included in the calculation. It can be asserted with confidence, in light of Sites 3 and 4, which were visually found to be informal settlements and had population densities, according to Map B in the 98th and 99th percentile respectively, that a 50^{th} percentile will not exclude any informal settlements from this analysis.

The population exposed to flooding is calculated based on the population living in areas appearing a percentile above a certain threshold of Map F. Percentiles of 50, 60, 70, 80 and 90 are chosen to highlight the number people demonstrated to more vulnerable according to the vulnerability-based method as opposed to the population-based method. Table 4-5 presents these EAE values.

Map F Percentile	EAE of Disproportionately Vulnerable Areas	% of Cape Town EAE
>50	5220	20.4%
>60	3500	13.7%
>70	1690	6.6%
>80	595	2.3%
>90	557	2.2%

Table 4-5 EAE of Disproportionately Vulnerable Areas According to Map F: EAE of areas which appear above a certain percentile of Map F. These are areas which appear vulnerable according to the vulnerability map in comparison to the population-based risk map. The percentage of the total EAE of Cape Town is also shown for context are shown. EAE figures correct to three significant figures.

The total number of people shown to be disproportionately at risk, according to the 50th percentile is 5220 correct to three significant figures. For context, the EAE for the whole of Cape Town using the HRSL gridded population dataset in Section 4.4.2 was 25600. This demonstrates that the number of people whose flood risk is disproportionately shown using a vulnerability-based map is high, it amounts to 20.4% of the total EAE across the whole city.

4.4 Discussion, Conclusions and Limitations

Headline figures from this research are an Expected Annual Exposure (EAE) of 25600 for Cape Town within the study area. Based on the 2011 South African Census Main Places, the two areas of the city with most exposed population to flooding are Goodwood and Athlone, with 2.21% and 1.95% of the population expected to be flooded in a given year in each of these Main Places.

I use the HRSL dataset in order to produce the final set of exposure values for informal settlement dwellers and producing risk maps. The decision to use the HRSL as opposed to the Worldpop dataset or the HRPDM was based primarily on greater conformity to population values seen in the 2011 South African Census and secondarily on a lesser tendency to underestimate population in the SDI dataset and the other two having more extreme values of overestimation.

The preference however is a minor one and it is unlikely any different conclusions would have been reached when the informal component of the map was integrated into the analysis and the

risk maps were made. Other researchers performing subsequent studies may use either of the other two datasets if there are any similar minor preferences towards either of the two alternative gridded population datasets used in this study.

The population values in the SDI dataset may lack reliability. This is revealed partly by the large divergence from values estimated in the same settlements from the three gridded population datasets and additionally unrealistic values for the population density. For flood risk mapping focussing on informal settlements, the use of gridded population datasets rather than small scale community mapping may therefore be advantageous, particularly given the way the HRSL and HRPDM datasets can identify the high population densities in informal settlements through their method of directly detecting dwellings.

The integration of flood protection has a great effect when the standard of flood protection is very high. For the HRSL dataset, a 1 in 100 standard of flood protection reduces the EAE of flooding by 82.7%, correct to three significant figures. A smaller standard of flood protection is relatively ineffective however, with a 1 in 5 protection standard reducing the EAE by just 6.6%. Given that many informal settlements in Cape Town flood almost annually (Divdal, 2011), this indicates that attempts to protect informal settlements from flooding will require extensive protection to make any meaningful difference to the people living in informal settlements at risk of flooding. Whilst this study demonstrates the sensitivity of the EAE to the standard of flood protection in informal settlements in Cape Town, the research is not able to identify specific locations of possible protection because of the granular nature of the flood defence layer used. Future studies may seek to repeat the study with more detailed accounting of flood defence infrastructure in the city.

The fact that informal settlement dwellers in Cape Town are not disproportionately more likely to experience flooding is a surprising one. It runs contrary to the literature which suggests some informal settlements in Cape Town flood almost annually (Divdal, 2011) whilst more affluent areas of the City are generally unaffected by flooding (Ziervogel et al, 2016). Such a finding may be partially explained by informal settlements lying on steeper slopes, since this makes pluvial flooding, the type of flooding which most affects informal settlements in the city (Ziervogel et al, 2016, Goncalo et al, 2007, Desportes et al, 2016), less likely to occur. However the top 10% of areas of the city most likely to be informal settlements according to the informal settlement predicted probability map, have a median slope of just 1.02°. This is too little to

fully account for informal settlements being disproportionately less likely to experience flooding.

One possible additional reason for this discrepancy is in inaccuracies in the flood model. Previous studies suggest that pluvial or surface flooding is the form of flooding most likely to affect informal settlements in Cape Town (Ziervogel et al, 2016, Goncalo et al, 2007, Desportes et al, 2016). This is however the component of flood modelling with the greatest uncertainty associated with it (Apel et al, 2016, Sampson et al, 2015). If the flood model is failing to capture pluvial, surface flooding in informal settlement areas this could explain the discrepancy. This may especially be the case given the DEM used may have too greater smoothing to adequately model pluvial flooding.

Alternatively, it may be due to differences in flood protection which the Fathom model is not accounting for. This model assumes there will be no surface drainage. However, the more formal areas of Cape Town will have in place drainage systems which the model is not accounting for, since the integration of stormwater drainage is part of the planning process for the building of formal areas (Goncalo et al, 2007, Holloway et al, 2008). As a result, the exposure in formal areas of the city may be exaggerated.

Despite the difficulties in the flood model, in particular in reference to surface or pluvial flooding, a modelling approach is nonetheless a preferred method of flood risk mapping regardless of whether one uses a traditional population disaggregated income approach or a social vulnerability one. This is because deductive physical modelling represents an inclusion conceptually of the actual physical processes which cause the flooding. This is as opposed to statistical methods used in many present comparable studies which use a purely inductive method (Sahoo and Bhaskaran, 2018, Danumah et al, 2019, Hategekimana et al, 2018). As a result, there needs to be greater research collaboration between the urban resilience and hydrological modelling research communities so that social vulnerability mapping and flood modelling can be integrated.

Future studies replicating this exercise should take notice of the skewness of the pixel values from the gridded population maps and informal settlement predicted probabilities. Naturally, population values will be more heavily skewed than informal settlement predicted probabilities, which are distributed between 0 and 1. The nature of the skew of the gridded population values and informal settlement predicted probabilities necessitates the use of transformations to the pixel values of both layers in making comparisons between how these maps spatially distribute

risk. The dataset with a relatively more diverse range of values will inevitably be responsible differences when the two risk maps are compared and therefore distort the comparisons.

Comparisons between population-based risk mapping and vulnerability-based mapping using informal settlement predicted probabilities must account for areas of low population density which may not be easy for the FCN to allocate a low predicted probability to in comparison to the low population. Section 4.4.6 showed industrial areas to be a particular example of this. As a result, comparisons between these sites and other areas will always show up on the comparison maps as environments being disproportionately socially vulnerable to flooding, when there are no informal settlements here. Vulnerability based flood risk maps should as a result correct for these occurrences.

The HRSL employed in the analysis uses a computer vision-based technique designed to detect buildings in order to disaggregate census level population data and it should therefore be ideal for detecting the high population densities in informal settlements. This study has shown as a result of this that in informal settlements, a direct comparison between a traditional population disaggregation-based method and an informal settlement-based approach will not spatially allocate any greater flood risk to informal settlements. Therefore, to properly integrate informal settlements it is necessary to adopt an approach to mapping which measures total vulnerable population by accounting for both informal settlement predicted probability as well as population density.

In this study I took the areas which the Map F comparison map demonstrated to be disproportionately at risk and calculated the EAE of these areas across the city. The result was that around 20.4% of the EAE across all of Cape Town, or 5220 people are found in areas whose risk would be disproportionately shown using the method of risk mapping shown in Map D, or the map which accounts for both population density and informal settlement predicted probability.

Finally, in this chapter, I compared a number of differing methods of integrating a layer representing social vulnerability into the exposure estimates and risk maps. The pixel-based mapping developed in this chapter with full post-processing gave an estimate for the percentage informal settlements dwellers which was too high, whereas much more realistic estimates were achieved when the post-processing included in the fine tuning in chapter was not applied. Post-processing appears to be detrimental to the ability for the FCN to accurately predict informal settlements. Other studies which detect informal settlements using deep learning use a diverse

variety of imagery, not just patches featuring ground truth informal settlements (Verma et al, 2019, Mboga et al, 2019, Quinn et al, 2018). The fine tuning of the methodologies in this chapter used only patches with known informal settlements in them, rather than including patches with informal settlements in proportion to the number of informal settlement dwellers in the city. Future studies repeating this exercise should as a result fine tune their methods based on a more diverse set of imagery, with many images not containing informal settlements, to make the proportion of informal settlements in the training images more representative of the proportion of area constituting informal settlements in Cape Town as a whole.

5. Conclusions and Recommendation for Further Research

In this thesis I have reviewed literature and identified gaps in the research community's ability to effectively map flood risk. The original aim of the thesis was to develop a scalable technique for mapping social vulnerability in urban areas with freely available software and data.

Chapter 1 reviewed present issues with flood risk mapping and why informal settlements are particularly at risk of flooding due to social vulnerability. Social vulnerability was defined in Chapter 1 as the propensity for socioeconomic factors to cause certain places to be at a greater likelihood of being more negatively affected by a given hazard than other places.

The chapter discussed how global flood models (GFMs) however typically treat the human component of risk in a way which is designed to measure risk to economic output rather than human vulnerability and that there are presently a lack of methods of social vulnerability mapping able to be coupled to GFMs.

Previous social vulnerability mapping studies are not designed for this task because they are produced by applying dimensional reduction to census data and are as a result insufficient for data poor environments. They also have a spatial resolution constrained to the size of census tracts and are as a result not of a resolution compatible with GFMs and a further spatial mismatch is created when attempting to couple data derived from census tracts to GFMs which operate at grid cell levels.

Participatory methods, as described in Section 1.4.2, are too labour intensive to be scaled up consistently to be applied on the large spatial scales needed for a global flood risk map. Remote sensing is recognised as a solution because of its ability to be applied consistently and cost effectively over large spatial scales. Informal settlements provide the chance to map social vulnerability in this way because they are known to be a particularly socially vulnerable environment and identifiable from satellite imagery.

Upon consideration of these research gaps, this thesis used a deep learning approach to map informal settlements as a proxy for social vulnerability and for these maps to be combined with the physical risk map from a GFM. The end product of this is a more complete method of mapping flood risk which incorporates social vulnerability.

5.1 Contributions from Each Research Chapter

Chapter 2 sought to address the problem of detecting informal settlements by using a Fully Convolutional Network (FCN). It used freely available satellite imagery in order for the final method developed across all three research chapters to be cost efficient and therefore suited to the ultimate aim of producing flood risk maps aimed at measuring threat to human wellbeing rather than risk to economic output. The results demonstrate the basic utility of this method including fine-tuning the network's hyperparameters to optimise the network's performance. The final trained network was extrapolated to produce predictions of informal settlements across the whole of Cape Town to produce an informal settlement layer to be attached to a GFM in Chapter 4.

A success using such a small training set size of 44 images demonstrated the ability for informal settlements to be mapped in smaller towns and cities in low and middle income countries where only small amounts of data on informal settlements exist. This will allow an expansion of the number of possible places where informal settlement maps, such as the one produced in Chapter 2, may be produced.

Chapter 2 additionally applied post-processing to the final outputs in the form of applying a gaussian filter and changes in the discriminant threshold. These were partly to do with further fine tuning the results but also to integrate the technical benefits of deep learning with a post-processing method to make it conceptually consistent with the nature of informal settlements as places. This research chapter is the first study of its kind to take this approach. The results show the potential of the applied post-processing methods to improve the overall accuracy, albeit more so for the blurring.

Chapter 3 discussed the pixel-based approach to detecting informal settlements and its strengths being its high resolution and spatial consistency as a unit of analysis. But also commented on the weaknesses of a pixel-based approach and in particular the lack of correspondence between pixels and real-world phenomena, in particular social vulnerability because of the importance of the community level for social vulnerability.

The 1100 pixelated outputs produced in Chapter 2 were converted into area-based outputs using the Canny edge algorithm. Examining the correlation between the pixel-based Brier score and Jaccard Index represents a strong confirmation of the value of an area-based approach because there is a large amount of unexplained variation between the two. The research has therefore

demonstrated that the technical benefits of deep learning - its ability to automatically detect patterns with a high-level of abstraction, can be combined with the conceptual benefits of area-based methods, to be combined to produce an all-encompassing method of detecting informal settlements.

The results from this were comparable to similar studies using the Jaccard Index to evaluate informal settlement detections, given good validation of the overall method. A key contribution of Chapter 3 is that it is the first to use area-based evaluation metrics to gauge the success of a deep learning study detecting informal settlements. The advantage of area-based evaluation metrics is their consistency with the conceptual benefits of producing area-based outputs. The results for these were disappointing, however an analysis of the reasons for the failure of these to inform the methods future studies should employ. The likely reason for the failure of the method to produce good results is the use of a method of producing areas involving blurring. This is due to the blurring removing the fine intricacies of many of the edges of the predicted polygons to create more rounded edges, distorting the ratio between the area and perimeter. This insight is an important one for future studies since this study is the first of its kind to use area-based evaluation metrics to evaluate the detection of informal settlements using deep learning.

Chapter 4 uses a physical flood model rather than a statistical one, which many similar mapping studies use. This gives a stronger foundation to the findings since the results are derived deductively from physics rather than inductively from mere statistics.

Chapter 4 found that informal settlement in Cape Town are not disproportionately more likely to be exposed to flooding relative to non-informal settlement dwellers. A possible reason for this was found to be that informal settlements in Cape Town lie on steeper slopes, a better quality of drainage in formal areas not accounted for by the model, and a lack of an ability of the model to map pluvial flooding and solve small scale flood processes on steep slopes, which is the sort which mostly affects informal settlements in Cape Town.

Chapter 4 is the first research of its kind to integrate the predicted probabilities from deep learning to the mapping of flood risk. With this method it compared the vulnerability-based approach to the more traditional method of population disaggregation. With these results produced, this thesis was able to give a headline figure for the additional number of people shown to be at risk of flooding by calculating the EAE for area shown to be disproportionately at risk according to the vulnerability-based map compared to the traditional method. Chapter 4

found that the new method predicts 20.4% of the total EAE across Cape Town, are predicted to be flooded in the areas shown to be disproportionately at risk. This sizeable figure demonstrates the value of the new method of flood risk mapping and calls for there to be more research of this sort. It represents a meaningful divergence in which places are deemed to be at risk of flooding. The two methods of flood risk mapping would result in significant differences in flood mitigation strategies and how spending on flood defence would be allocated. The results as a result may be of interest to aid agencies and governments.

The HRSL dataset was speculated to have strength because it involves the detection of buildings directly and the use of these to disaggregate census tract population data (CIESIN, 2019). Datasets such as these are as a result well placed to accurately assign high population densities to informal settlements and these datasets are consequently well suited to studies of this kind. However, Chapter 4 found that the success of the HRSL in doing this means it actually assigns high risk using the traditional population-based mapping approach. As a result, the thesis found that for vulnerability-based maps there is an importance associated with factoring in population density in as well as informal settlement predicted probability.

5.2 Main Thesis Contributions

Of the contributions made in each chapter, those in Chapter 4 represent the key contributions of the thesis as a whole because this represents the culmination of the thesis as a whole and ties together the conceptual work in Chapter 1 and the empirical work in Chapters 2 and 3. Chapter 4 makes a key contribution in that it demonstrates the possibility of mapping social vulnerability using deep learning and to couple this with a GFM. The difference this makes to the EAE in informal settlements demonstrates that mapping vulnerability in this way is also a key contribution which shows the importance of mapping in this way and calls for more research in this area.

In light of approaches future research along these lines should take, this research has made a key contribution in demonstrating two important considerations when producing social vulnerability maps using predicted probabilities from informal settlements. First, it is important that maps depicting total vulnerable population are used rather than merely social vulnerability are used. Second, the precise method used will show industrial areas to have high levels of social vulnerability and this requires correction.

As a case study, Cape Town demonstrated to be ideal for a number of reasons. The 75 informal settlements in the city in the SDI dataset proved to be sufficient for producing good results using the deep learning methodology. Section 1.6 additionally stated that Cape Town was suitable as a case study because of the frequent flooding which occurs in its informal settlements so there are large numbers of flooded areas where the traditional method and new method can be compared. The GFM outputs contained large areas of inundation where this was the case to allow for a meaningful comparison.

The well documented informal settlements in Cape Town also helped to make it an ideal case study. The OpenUp dataset allowed for an alternate dataset with which to provide additional evaluation of the scaled-up maps. Moreover, the official estimate from the City of Cape Town municipal authority of the number of informal settlement dwellers in the city allowed for a similar evaluation.

The results in this thesis were obtained without any visit to Cape Town and the research was based entirely on secondary data. Because of its use of only secondary data, ostensibly a visit to Cape Town would not have affected the results of this thesis. There may have been benefits to the research of visiting Cape Town. For example, it may have been useful to personally confirm the accuracy of the informal settlement delineations, given that informal settlements are such fast changing environments and may have changed since they were originally mapped. However, not visiting Cape Town was also part of the overriding parameters of the methodology of the thesis, which aimed to develop a method of flood risk mapping in a way which is cost-efficient. If the method required personal visitation to have validity, if would no longer be viable in a cost efficient way on large spatial scales. The demonstration of the utility of the method independent of any in-situ visit is therefore in fact a key strength of the thesis.

I believe that the thesis throughout was faithful to the emphasis placed on social vulnerability in Section 1.2. Here, social vulnerability was described as being a holistic entity which is difficult to quantify or measure objectively. This thesis has remained consistent with this through its mapping of social vulnerability through the detection of informal settlements which are areas or places where a variety of social mechanisms and interactions are occurring. Their detection as a result allows social vulnerability's complex, multidimensional nature to be accounted for in the final map. In the thesis this was particularly the case given the use of post-processing methods and use of area-based methods to conceptually ground the deep learning methodology and make it consistent with the phenomenon under study, that of social

vulnerability. Finally, the use of the community derived SDI dataset allowed the ground truth informal settlements to be congruent with the social processes of that community.

It must also be noted how the final social vulnerability map produced succeeds in addressing the main problems identified with other social vulnerability mapping attempts. The final social vulnerability map is gridded and so solves the problem of congruence with GFMs as opposed to social vulnerability maps which come from census tracts. When scaled up the method's ability to map informal settlements is limited only by the ability of remote sensing and subsequent deep learning. It is unlimitedly political considerations or human error in its undercount of population as censuses often are. The final social vulnerability map is as a result not constrained by the mechanisms of mapping social vulnerability which those dependent on censuses are often subject to – mainly informal settlement undercounts.

In comparison to participatory methods, the final method is intrinsically less labour intensive. Although the geolocation of the images was a labour intensive process as this had to be done manually, once one has a sufficient training dataset, deep learning can be used to scale-up for predicted probabilities to a large scale in an automated way without any further manual work. This is not the case for participatory methods where the manual component encompasses the entirety of the method instead of merely the formation of a training set.

5.3 Suggestions for Further Research

As results have been evaluated throughout chapters 2, 3 and 4, a number of potential improvements have been made apparent which could be carried out by future research.

Some technical developments on the deep learning aspect of this research have been made apparent after considering the results and findings of the three chapters. The strengths of the SDI dataset are discussed in Section 1.7. These include its collection by the local community and consequent relevance to social vulnerability because many of the factors contributing to social vulnerability and responses manifest at the community level. Using the SDI dataset therefore remains a good pathway for future research to proceed with. The problem of small sample sizes however is a problem naturally occurring with the SDI dataset, because there are a limited number of samples in each city. Although there are far more informal settlements across the SDI dataset globally, deep learning methods at present struggle to generalise across environments.

However, a small sample size opens up the possibility for certain technical improvements which for larger sample sizes would be too computationally intensive to be practical. As Section 2.5 discussed, second order optimizers are a method which enable improved training due to their incorporation of the rate of change of the loss function, not just its gradient (Li et al, 2019).

The issue of the class imbalance associated with each set of training, as discussed in Section 4.3.3, was suggested as a key reason why the network, when scaled up to the whole of Cape Town, overestimated the proportion of informal settlement dwellers in the city. A key technical improvement future studies include should take official estimates of the proportion of informal settlement dwellers in the respective city where the training is taking place. If no good estimates of the kind from Cape Town exist in a particular city, taking estimates from cities of similar economic situation and in similar areas geographically and extrapolating and coming to a reasoned, expert judgement from these may be an option to estimate the correct proportion. Separate satellite imagery should subsequently be included from more formal areas of the city to ensure that the proportion of informal settlement in the dataset aligns with the class imbalance in the city's official estimate.

As Section 2.5 also outlined, another technical improvement which could be made is L2 regularization. It is a more nuanced method of preventing overfitting than the early stopping used in Chapter 2 because it allows more training and the avoidance of overfitting simultaneously. This should remove the problem identified and place more confidence on the predictions of formal areas and allow the social vulnerability-based maps to concentrate flood risk in informal settlements.

Another set of improvements future research could apply lie in taking a further step fowards the ultimate aims of the mapping exercise. The ultimate objective of this line of research is to produce a social vulnerability layer to be attached to a GFM.

This thesis only mapped social vulnerability on a small spatial scale. But if it is to be applied on larger spatial scales, the network must be able to detect informal settlements across a variety of different environments. The appearance of informal settlements is varied across environments, in different cities and different countrie, making it difficult for one network to identify informal settlements in a way that is spatially consistent.

Currently, research attempting to develop methods of identifying informal settlements in a manner which is generalizable across different cities has been limited in its success. The approach presented in this thesis is as a result not ready to be replicated to produce larger spatial scale maps because this would require the ability of the network to recognise informal settlements across a range of environments.

A study which specifically attempts to make the deep learning detection of informal settlements generalizable across different environments would as a result be a valuable contribution towards the overall goal of producing large scale maps showing social vulnerability to flooding. Dataset augmentation is a key method of making networks more generalizable and GANs represent an up and coming method of dataset augmentation used in deep learning. However, so far however they have not been used for dataset augmentation in deep learning studies detecting informal settlements. As a result, using a GAN to aid the generalizability of the detection of informal settlements has the ability to aid the research community's ability to produce a large-scale social vulnerability layer for a flood risk map.

Outside of the 66 Cape Town informal settlement images used in this thesis, there are 1000s more in over 100 cities globally which could be utilised for a study such as this in order to maximise the range of patterns which a network could be skilled a recognising as beloinging to the informal settlement category on a global scale.

This thesis produces a social vulnerability map containing just one variable. The research as a result lacks the complexity to fully represent a holistic entity such as social vulnerability which encompasses many different interlocking factors. As with the lack of generalizability of deep learning detecting informal settlements mentioned previously, there are at present a lack of deep learning studies which manage to recognise more vulnerable from less vulnerable informal settlements. A study similar to this but which not only identifies informal settlements, but more vulnerable from less vulnerable informal settlements would as a result represent an important step forward in methods of mapping social vulnerability to flooding. Part of the basis for using the SDI data was so future studies could attempt this task, because on top of the boundaries of the informal settlements having well defined spatial coordinates, it contains attribute data for each informal settlement describing the socioeconomic conditions in each informal settlement. In this thesis, I have demonstrated the ability of the SDI dataset to be used for deep learning to detect informal settlements and this lays a strong foundation for such a study.

Integrating data from ancillary sources such as OpenStreetMap (Bakillah et al, 2014) may aid this. The dataset contains community mapped variables and amenities and as a result has the ability to similarly map the socioeconomic conditions within informal settlements in a similar way to the socioeconomic variables within the SDI dataset. Examples of these variables are health facilities, waste management and transport infrastrcutre (Bakillah et al, 2014).

OpenStreetMap is similarly a global dataset from which selected variables could be combined or corroborated with the socioeconomic variables from within each of the SDI informal settlements to make these data used to train the network to recognise more from less vulnerable informal settlements (Bakillah et al, 2014).

A study classifying areas as formal or informal as well as identifying more from less socially informal settlements requires a network architecture able to perform more than one task simultaneously.

Identifying formal from informal areas is a classification task, whereas the assignment of vulnerability values to informal settlements is a regression task. Multi-task CNNs performing joint classification and regression are designed for the accomplishment of such separate but conditional tasks simultaneously under a single loss function (Liu et al, 2018, El-Sappagh et al, 2020, Gao et al, 2020).

As with the suggested generalizability improvement using the GAN, a study of this kind should utilise data globally from the 1000s of SDI informal settlements in order to give the network sufficient training and to maximise the information available to it to enable such differentiation to take place.

6. References

Abunyewah, M., Gajendran, T. and Maund, K., 2018. Profiling informal settlements for disaster risks. *Procedia engineering*, *212*, pp.238-245.

Adams, T., 2017. AI-powered social bots. *arXiv preprint arXiv:1706.05143*.

Adelekan, I., Johnson, C., Manda, M., Matyas, D., Mberu, B., Parnell, S., Pelling, M., Satterthwaite, D. and Vivekananda, J., 2015. Disaster risk and its reduction: An agenda for urban Africa. *International Development Planning Review*, *37*(1), pp.33-43.

Adeola, F.O., 2009. Katrina cataclysm: Does duration of residency and prior experience affect impacts, evacuation, and adaptation behavior among survivors?.*Environment and Behavior*, *41*(4), pp.459-489.

Adger, W.N., 1999. Social vulnerability to climate change and extremes in coastal Vietnam. *World development*, *27*(2), pp.249-269.

Adger, W.N., 2006. Vulnerability. *Global environmental change*, *16*(3), pp.268-281.

Agarap, A.F., 2018. Deep learning using rectified linear units (relu). *arXiv preprint arXiv:1803.08375*.

Ahsan, M.N. and Warner, J., 2014. The socioeconomic vulnerability index: a pragmatic approach for assessing climate change led risks–a case study in the south-western coastal Bangladesh. *International Journal of Disaster Risk Reduction*, *8*, pp.32-49.

Ajami, A., Kuffer, M., Persello, C. and Pfeffer, K., 2019. Identifying a Slums' Degree of Deprivation from VHR Images Using Convolutional Neural Networks. *Remote sensing*, *11*(11), p.1282.

Albawi, S., Mohammed, T.A. and Al-Zawi, S., 2017, August. Understanding of a convolutional neural network. In *2017 International Conference on Engineering and Technology (ICET)* (pp. 1-6). IEEE.

Alfieri, L., Bisselink, B., Dottori, F., Naumann, G., de Roo, A., Salamon, P., Wyser, K. and Feyen, L., 2017. Global projections of river flood risk in a warmer world. *Earth's Future*, *5*(2), pp.171-182.

Alizadeh, M., Alizadeh, E., Asadollahpour Kotenaee, S., Shahabi, H., Beiranvand Pour, A., Panahi, M., Bin Ahmad, B. and Saro, L., 2018. Social vulnerability assessment using artificial neural network (ANN) model for earthquake hazard in Tabriz city, Iran. *Sustainability*, *10*, p.3376.

Alwang, J., Siegel, P.B. and Jorgensen, S.L., 2001. *Vulnerability: a view from different disciplines* (Vol. 115). Social protection discussion paper series.

Amadio, M., Mysiak, J. and Marzi, S., 2019. Mapping Socioeconomic Exposure for Flood Risk Assessment in Italy. *Risk Analysis*, *39*(4), pp.829-845.

Ammour, N., Alhichri, H., Bazi, Y., Benjdira, B., Alajlan, N. and Zuair, M., 2017. Deep learning approach for car detection in UAV imagery. *Remote Sensing*, *9*(4), p.312.

Apel, H., Martínez Trepat, O., Hung, N.N., Do, T.C., Merz, B. and Nguyen, D., 2016. Combined fluvial and pluvial urban flood hazard analysis: concept development and application to Can Tho city, Mekong Delta, Vietnam. *Natural Hazards and Earth System Sciences (NHESS)*, *16*, pp.941-961.

Armstrong, C.M. and Larkin, L.L., 2019. Using the social vulnerability index to forecast disaster migration.

Ashley, S.T. and Ashley, W.S., 2008. Flood fatalities in the United States. *Journal of Applied Meteorology and Climatology*, *47*(3), pp.805-818.

Bai, X., Dawson, R.J., Ürge-Vorsatz, D., Delgado, G.C., Barau, A.S., Dhakal, S., Dodman, D., Leonardsen, L., Masson-Delmotte, V., Roberts, D.C. and Schultz, S., 2018. Six research priorities for cities and climate change.

Bakillah, M., Liang, S., Mobasheri, A., Jokar Arsanjani, J. and Zipf, A., 2014. Fine-resolution population mapping using OpenStreetMap points-of-interest. *International Journal of Geographical Information Science*, *28*(9), pp.1940-1963.

Bao, S. and Chung, A.C., 2018. Multi-scale structured CNN with label consistency for brain MR image segmentation. *Computer Methods in Biomechanics and Biomedical Engineering: Imaging & Visualization*, *6*(1), pp.113-117.

Bates, P.D., Horritt, M.S. and Fewtrell, T.J., 2010. A simple inertial formulation of the shallow water equations for efficient two-dimensional flood inundation modelling. *Journal of Hydrology*, *387*(1-2), pp.33-45.

Baud, I., Kuffer, M., Pfeffer, K., Sliuzas, R. and Karuppannan, S., 2010. Understanding heterogeneity in metropolitan India: The added value of remote sensing data for analyzing sub-standard residential areas. *International Journal of Applied Earth Observation and Geoinformation*, *12*(5), pp.359-374.

Bengio, Y., 2012. Practical recommendations for gradient-based training of deep architectures. In *Neural networks: Tricks of the trade* (pp. 437-478). Springer, Berlin, Heidelberg.

Bernhofen, M.V., Whyman, C., Trigg, M.A., Sleigh, P.A., Smith, A.M., Sampson, C.C., Yamazaki, D., Ward, P.J., Rudari, R., Pappenberger, F. and Dottori, F., 2018. A first collective validation of global fluvial flood models for major floods in Nigeria and Mozambique. *Environmental Research Letters*, *13*(10), p.104007.

Birkmann, J., 2005a. Danger need not spell disaster But how vulnerable are we? United Nations University Institute for Environment and Human Security (UNU-EHS): Bonn.

Birkmann, J., 2005b. Measuring Vulnerability. Report on the 1st meeting of the expert working group "Measuring Vulnerability" of the United Nations University Institute for Environment and Human Security (UNU-EHS). Bonn.

Birkmann, J., 2007. Risk and vulnerability indicators at different scales: applicability, usefulness and policy implications. *Environmental Hazards*, *7*(1), pp.20-31.

Bischke, B., Bhardwaj, P., Gautam, A., Helber, P., Borth, D. and Dengel, A., 2017, September. Detection of Flooding Events in Social Multimedia and Satellite Imagery using Deep Neural Networks. In *MediaEval*.

Bivand, R (2020) rgdal: Bindings for the 'Geospatial' Data Abstraction Library [*Online*]. Available from: < https://cran.r-project.org/web/packages/rgdal/index.html> Accessed: [22/10/2020].

Bizimana, J.P. and Schilling, M., 2009. Geo-Information Technology for Infrastructural Flood Risk Analysis in Unplanned Settlements: a case study of informal settlement flood risk in the Nyabugogo flood plain, Kigali City, Rwanda. In *Geospatial techniques in urban hazard and disaster analysis* (pp. 99-124). Springer, Dordrecht.

Blaschke, T., 2010. Object based image analysis for remote sensing. *ISPRS journal of photogrammetry and remote sensing*, *65*(1), pp.2-16.

Block, J., Yazdani, M., Nguyen, M., Crawl, D., Jankowska, M., Graham, J., DeFanti, T. and Altintas, I., 2017, October. An unsupervised deep learning approach for satellite image analysis with applications in demographic analysis. In 2017 IEEE 13th International Conference on e-Science (eScience)(pp. 9-18). IEEE.

Bogardi, J. and Birkmann, J., 2004. Vulnerability assessment: the first step towards sustainable risk reduction. *Disaster and Society—From Hazard Assessment to Risk Reduction, Logos Verlag Berlin, Berlin*, pp.75-82.

Bohle, H.G., 2001. Vulnerability and criticality: perspectives from social geography. *IHDP update*, *2*(1), pp.3-5.

Bollin, C., Cárdenas, C., Hahn, H. and Vatsa, K.S., 2003. *Disaster risk management by communities and local governments*. Inter-American Development Bank.

Bonafilia, D., Gill, J., Kirsanov, D., Sundram, J. (2019) Mapping the world to help aid workers, with weakly, semi-supervised learning. [*Online*]. Available from < https://ai.facebook.com/blog/mapping-the-world-to-help-aid-workers-with-weakly-semi-supervised-learning>, [Accessed: 01/08/20].

Bonnet, S., Gaulton, R., Lehaire, F. and Lejeune, P., 2015. Canopy gap mapping from airborne laser scanning: an assessment of the positional and geometrical accuracy. *Remote Sensing*, *7*(9), pp.11267-11294.

Borie, M., Pelling, M., Ziervogel, G. and Hyams, K., 2019b. Mapping narratives of urban resilience in the global south. *Global Environmental Change*, *54*, pp.203-213.

Borie, M., Ziervogel, G., Taylor, F.E., Millington, J.D., Sitas, R. and Pelling, M., 2019a. Mapping (for) resilience across city scales: An opportunity to open-up conversations for more inclusive resilience policy?. *Environmental Science & Policy*, *99*, pp.1-9.

Boureau, Y.L., Ponce, J. and LeCun, Y., 2010. A theoretical analysis of feature pooling in visual recognition. In *Proceedings of the 27th international conference on machine learning (ICML-10)* (pp. 111-118).

Bowles, C., Chen, L., Guerrero, R., Bentley, P., Gunn, R., Hammers, A., Dickie, D.A., Hernández, M.V., Wardlaw, J. and Rueckert, D., 2018. Gan augmentation: Augmenting training data using generative adversarial networks. *arXiv preprint arXiv:1810.10863*.

Brecht, H., Deichmann, U. and Wang, H.G., 2013. *A global urban risk index*. Policy Research Working Paper 6506. The World Bank East Asia Pacific Region Development Research Group.

Brelsford, C., Martin, T., Hand, J. and Bettencourt, L.M., 2018. Toward cities without slums: Topology and the spatial evolution of neighborhoods. *Science advances*, *4*(8), p.eaar4644.

Brooks, N., 2003. Vulnerability, risk and adaptation: A conceptual framework. *Tyndall Centre for Climate Change Research Working Paper*, *38*, pp.1-16.

Brouwer, R., Akter, S., Brander, L. and Haque, E., 2007. Socioeconomic vulnerability and adaptation to environmental risk: a case study of climate change and flooding in Bangladesh. *Risk Analysis*, *27*(2), pp.313-326.

Busgeeth, K., Brits, A. and Whisken, J.B., 2008. Potential application of remote sensing in monitoring informal settlements in developing countries where complimentary data does not exist.

Byrne, J., Bolnick, J., Dobson, S., Patel, S., Kallergis, A., and MacPherson., N. 2018. *Know Your City: Slum Dwellers Count*. Cape Town: SDI.

Cai, L., Shi, W., Miao, Z. and Hao, M., 2018. Accuracy assessment measures for object extraction from remote sensing images. *Remote Sensing*, *10*(2), p.303.

Canny, J., 1986. A computational approach to edge detection. *IEEE Transactions on pattern analysis and machine intelligence*, *6*, pp.679-698.

Cao, J., Chen, L., Wang, M. and Tian, Y., 2018. Implementing a parallel image edge detection algorithm based on the Otsu-canny operator on the Hadoop platform. *Computational intelligence and neuroscience*, *2018*.

Carr-Hill, R., 2013. Missing millions and measuring development progress. *World Development*, *46*, pp.30-44.

Castillejo-González, I.L., López-Granados, F., García-Ferrer, A., Peña-Barragán, J.M., Jurado-Expósito, M., de la Orden, M.S. and González-Audicana, M., 2009.Object-and pixel-based analysis for mapping crops and their agro-environmental associated measures using QuickBird imagery.*Computers and Electronics in Agriculture*, *68*(2), pp.207-215.

Center for International Earth Science Information Network (2019) *High Resolution Settlement Layer. [Online]. Available from:* < https://ciesin.columbia.edu/data/hrsl/>. [Accessed: 01/08/2020].

Centre for Research on the Epidemiology of Disasters, 2017. Criteria [*Online*]. Available from*:* < http://www.emdat.be/explanatory-notes>. [Accessed: 29/03/2017].

Chakraborty, J., Tobin, G.A. and Montz, B.E., 2005. Population evacuation: assessing spatial variability in geophysical risk and social vulnerability to natural hazards. *Natural Hazards Review*, *6*(1), pp.23-33.

Chakraborty, S. and Mukhopadhyay, S., 2019. Assessing flood risk using analytical hierarchy process (AHP) and geographical information system (GIS): application in Coochbehar district of West Bengal, India. *Natural Hazards*, *99*(1), pp.247-274.

Chatterjee, M., 2010.Slum dwellers response to flooding events in the megacities of India. *Mitigation and Adaptation Strategies for Global Change*, *15*(4), pp.337-353.

Chen, F.C. and Jahanshahi, M.R., 2017. NB-CNN: Deep learning-based crack detection using convolutional neural network and Naïve Bayes data fusion. *IEEE Transactions on Industrial Electronics*, *65*(5), pp.4392-4400.

Chomsri, J. and Sherer, P., 2013. Social vulnerability and suffering of flood-affected people: case study of 2011 mega flood in Thailand. *Kasetsart Journal of Social Sciences*, *34*(3), pp.491-499.

City of Cape Town, (2021) About informal housing. [*Online*] Available from: <https://www.capetown.gov.za/Family and home/Residential-property-and-houses/Informal-housing/About-informal-housing>. [Accessed: 28/03/2021].

Clark, G.E., Moser, S.C., Ratick, S.J., Dow, K., Meyer, W.B., Emani, S., Jin, W., Kasperson, J.X., Kasperson, R.E. and Schwarz, H.E., 1998. Assessing the vulnerability of coastal communities to extreme storms: the case of Revere, MA., USA. *Mitigation and adaptation strategies for global change*, *3*(1), pp.59-82.

Clinton, N., Holt, A., Scarborough, J., Yan, L.I. and Gong, P., 2010. Accuracy assessment measures for object-based image segmentation goodness. *Photogramm.Eng. Remote Sens*, *76*(3), pp.289-299.

Colten, C.E., 2006. Vulnerability and place: flat land and uneven risk in New Orleans. *American Anthropologist*, *108*(4), pp.731-734.

Cross, S.S., Harrison, R.F. and Kennedy, R.L., 1995. Introduction to neural networks. *The Lancet*, *346*, pp.1075-1079.

Cutter, S.L. and Finch, C., 2008. Temporal and spatial changes in social vulnerability to natural hazards. *Proceedings of the National Academy of Sciences*, *105*(7), pp.2301-2306.

Cutter, S.L., 1996. Vulnerability to environmental hazards. *Progress in human geography*, *20*(4), pp.529-539.

Cutter, S.L., 2003. The vulnerability of science and the science of vulnerability. *Annals of the Association of American Geographers*, *93*(1), pp.1-12.

Cutter, S.L., Boruff, B.J. and Shirley, W.L., 2003. Social vulnerability to environmental hazards. *Social science quarterly*, *84*(2), pp.242-261.

Cutter, S.L., Emrich, C.T., Webb, J.J. and Morath, D., 2009. *Social vulnerability to climate variability hazards: a review of the literature.* University of South Carolina: Columbia.

Cutter, S.L., Mitchell, J.T. and Scott, M.S., 2000. Revealing the vulnerability of people and places: a case study of Georgetown County, South Carolina. *Annals of the association of American Geographers*, *90*(4), pp.713-737.

Danumah, J.H., Odai, S.N., Saley, B.M., Szarzynski, J., Thiel, M., Kwaku, A., Kouame, F.K. and Akpa, L.Y., 2016. Flood risk assessment and mapping in Abidjan district using multi-criteria analysis (AHP) model and geoinformation techniques,(cote d'ivoire). *Geoenvironmental Disasters*, *3*(1), pp.10-22.

Datalya, 2017, Convolutional Neural Networks (CNN) [*Online*]. Available from: < https://datalya.com/blog/machine-learning/convolutional-neural-networks-cnn>. [Accessed: 20/10/2020].

Davidson, R.A. and Shah, H.C., 1997. *An urban earthquake disaster risk index*. John A. Blume Earthquake Engineering Center: Standford.

D'Cruz, C., McGranahan, G. and Sumithre, U., 2009. The efforts of a federation of slum and shanty dwellers to secure land and improve housing in Moratuwa: from savings groups to citywide strategies. *Environment and Urbanization*, *21*(2), pp.367-388.

De Bono, A., Chatenoux, B., Herold, C. and Peduzzi, P., 2013. Global Assessment Report on Disaster Risk Reduction 2013: From shared risk to shared value-The business case for disaster risk reduction.

de Brito, M.M., Evers, M. and Almoradie, A.D.S., 2018. Participatory flood vulnerability assessment: a multi-criteria approach. *Hydrology & Earth System Sciences*, *22*(1).

der Heide, E.A., 2006. The importance of evidence-based disaster planning. *Annals of emergency medicine*, *47*(1), pp.34-49.

Desgroppes, A. and Taupin, S., 2011. Kibera: The biggest slum in Africa?. *Les Cahiers d'Afrique de l'Est/The East African Review*, *44*, pp.23-33.

Desportes, I., Waddell, J. and Hordijk, M., 2016. Improving flood risk governance through multi-stakeholder collaboration: a case study of Sweet Home informal settlement, Cape Town. *South African Geographical Journal*, *98*(1), pp.61-83.

Di, X., Sindagi, V.A. and Patel, V.M., 2018, August. Gp-gan: Gender preserving gan for synthesizing faces from landmarks. In *2018 24th International Conference on Pattern Recognition (ICPR)* (pp. 1079-1084). IEEE.

DLR-DFD. 2016. *GUF Product Specifications (GUF_DLR_v01).* Oberpfaffenhofen: DLR-DFD. Engstrom, R., 2018. Linking Pixels and Poverty: Using Satellite Imagery to Map Poverty.

Dobson, S., 2017. Community-driven pathways for implementation of global urban resilience goals in Africa. *International journal of disaster risk reduction*, *26*, pp.78-84.

Dottori, F., Salamon, P., Bianchi, A., Alfieri, L., Hirpa, F.A. and Feyen, L., 2016. Development and evaluation of a framework for global flood hazard mapping. *Advances in water resources*, *94*, pp.87-102.

Douglas, I., 2017. Flooding in African cities, scales of causes, teleconnections, risks, vulnerability and impacts. *International journal of disaster risk reduction*, *26*, pp.34-42.

Dumoulin, V. and Visin, F., 2018. A guide to convolution arithmetic for deep learning. *arXiv preprint arXiv:1603.07285*.

Dwyer, A., Zoppou, C., Nielsen, O., Day, S. and Roberts, S., 2004. *Quantifying Social Vulnerability: A methodology for identifying those at risk to natural hazards*. Geoscience Australia: Canberra.

Ebert, A., Kerle, N. and Stein, A., 2007, September. Remote sensing based assessment of social vulnerability. In *5th International Workshop on Remote Sensing and Disaster Response* (pp. 10-12).

El-Din, Y.S., Moustafa, M.N. and Mahdi, H., 2020. Deep convolutional neural networks for face and iris presentation attack detection: Survey and case study. *arXiv preprint arXiv:2004.12040*.

El-Sappagh, S., Abuhmed, T., Islam, S.R. and Kwak, K.S., 2020. Multimodal multitask deep learning model for Alzheimer's disease progression detection based on time series data. *Neurocomputing*, *412*, pp.197-215.

Emerton, R., Cloke, H., Ficchi, A., Hawker, L., de Wit, S., Speight, L., Prudhomme, C., Rundell, P., West, R., Neal, J. and Cuna, J., 2020. Emergency flood bulletins for Cyclones Idai and Kenneth: A critical evaluation of the use of global flood forecasts for international humanitarian preparedness and response. *International Journal of Disaster Risk Reduction*, *50*, p.101811.

Engstrom, R., Hersh, J. and Newhouse, D., 2016. Poverty from space: using high resolution satellite imagery for estimating economic well-being and geographic targeting. *Unpublished paper*.

Engstrom, R., Sandborn, A., Yu, Q., Burgdorfer, J., Stow, D., Weeks, J. and Graesser, J., 2015, March. Mapping slums using spatial features in Accra, Ghana. In *2015 Joint Urban Remote Sensing Event (JURSE)* (pp. 1-4). IEEE.

Ergunay, O., 2011. The project of flood risk mitigation in areas subject to flooding in GAP (Southeastern Anatolia Development Project) region [*Online*]. Available from: < at http://www.gapsel.org/condocs/kapasite_gelistirme_egitim/eptisa_gap_kitap.pdf>

Esch, T., Marconcini, M., Felbier, A., Roth, A., Heldens, W., Huber, M., Schwinger, M., Taubenböck, H., Müller, A. and Dech, S., 2013. Urban footprint processor—Fully automated processing chain generating settlement masks from global data of the TanDEM-X mission. *IEEE Geoscience and Remote Sensing Letters*, *10*(6), pp.1617-1621.

Etwire, P.M., Al-Hassan, R.M., Kuwornu, J.K. and Osei-Owusu, Y., 2013. Application of livelihood vulnerability index in assessing vulnerability to climate change and variability in Northern Ghana. *Journal of Environment and Earth Science*, *3*(2), pp.157-170.

Fang, M., Yue, G. and Yu, Q., 2009. The study on an application of otsu method in canny operator. In *Proceedings.The 2009 International Symposium on Information Processing (ISIP 2009)* (p. 109).Academy Publisher.

Fayjie, A.R., Hossain, S., Oualid, D. and Lee, D.J., 2018, June. Driverless car: Autonomous driving using deep reinforcement learning in urban environment. In *2018 15th International Conference on Ubiquitous Robots (UR)* (pp. 896-901). IEEE.

Fekete, A., 2009. Validation of a social vulnerability index in context to river-floods in Germany. *Natural Hazards and Earth System Sciences*, *9*(2), pp.393-403.

Fekete, A., 2011. Assessment of social vulnerability for river-floods in Germany. United Nations University. *Institute for Environmental and Home Security, Bonn*.

Fekete, A., 2012. Spatial disaster vulnerability and risk assessments: challenges in their quality and acceptance. *Natural hazards*, *61*(3), pp.1161-1178.

Fekete, A., 2019. Social vulnerability (re-) assessment in context to natural hazards: Review of the usefulness of the spatial indicator approach and investigations of validation demands. *International Journal of Disaster Risk Science*, *10*(2), pp.220-232.

Fewtrell, T.J., Bates, P.D., Horritt, M. and Hunter, N.M., 2008. Evaluating the effect of scale in flood inundation modelling in urban environments. *Hydrological Processes: An International Journal*, *22*(26), pp.5107-5118.

Field, C.B., Barros, V.R., Mach, K.J., Mastrandrea, M.D., van Aalst, M., Adger, W.N., Arent, D.J., Barnett, J., Betts, R., Bilir, T.E. and Birkmann, J., 2014. Technical summary. In *Climate change 2014: Impacts, adaptation, and vulnerability. Part A: Global and sectoral aspects. Contribution of working group II to the fifth assessment report of the intergovernmental panel on climate change* (pp. 35-94). Cambridge University Press.

Fotheringham, A.S. and Wong, D.W., 1991. The modifiable areal unit problem in multivariate statistical analysis. *Environment and planning A*, *23*(7), pp.1025-1044.

Freixenet, J., Muñoz, X., Raba, D., Martí, J. and Cufí, X., 2002, May. Yet another survey on image segmentation: Region and boundary information integration. In *European conference on computer vision* (pp. 408-422).Springer, Berlin, Heidelberg.

Frid-Adar, M., Diamant, I., Klang, E., Amitai, M., Goldberger, J. and Greenspan, H., 2018. GAN-based synthetic medical image augmentation for increased CNN performance in liver lesion classification. *Neurocomputing*, *321*, pp.321-331.

Fries, B., Smith, D.L., Wu, S., Dolgert, A.J., Guerra, C.A., Hay, S.I., García, G.A., Smith, J.M., Oyono, J.N.M., Donfack, O.T. and Nfumu, J.O.O., 2020. Measuring the accuracy of gridded human population density surfaces: a case study in Bioko Island, Equatorial Guinea. *BioRxiv*.

Gadiraju, K.K., Vatsavai, R.R., Kaza, N., Wibbels, E. and Krishna, A., 2018, November. Machine Learning Approaches for Slum Detection Using Very High Resolution Satellite Images. In 2018 IEEE International Conference on Data Mining Workshops (ICDMW) (pp. 1397-1404).IEEE.

Gandhi, R. 2018 *Improving the Performance of a Neural Network*. [*Online*] Available from : <https://towardsdatascience.com/how-to-increase-the-accuracy-of-a-neural-network-9f5d1c6f407d>. [Accessed: 29/12/2019].

Gao, F., Yoon, H., Wu, T. and Chu, X., 2020. A feature transfer enabled multi-task deep learning model on medical imaging. *Expert Systems with Applications*, *143*, p.112957.

Gao, H., Yuan, H., Wang, Z. and Ji, S., 2019. Pixel transposed convolutional networks. *IEEE transactions on pattern analysis and machine intelligence*, *42*(5), pp.1218-1227.

Gebrehiwot, A., Hashemi-Beni, L., Thompson, G., Kordjamshidi, P. and Langan, T.E., 2019. Deep convolutional neural network for flood extent mapping using unmanned aerial vehicles data. *Sensors*, *19*(7), p.1486.

Geiss, C. and Taubenböck, H., 2013. Remote sensing contributing to assess earthquake risk: from a literature review towards a roadmap. *Natural Hazards*, *68*(1), pp.7-48.

GFDRR (Global Facility for Disaster Reduction and Recovery). 2013. *Stories of Impact: Big Disaster Planning Pays Off in Odisha, India.* The World Bank, Washington, D.C.

Gidaris, S. and Komodakis, N., 2015. Object detection via a multi-region and semantic segmentation-aware cnn model. In *Proceedings of the IEEE international conference on computer vision* (pp. 1134-1142).

Global Urban Footprint (GUF); DLR 2016.

Goncalo, A.A., Bouchard, B.C., Wilson, K.M. and Susienka, M.J., 2007. Improving flood risk management in informal settlements of Cape Town.

Goodfellow, I., Pouget-Abadie, J., Mirza, M., Xu, B., Warde-Farley, D., Ozair, S., Courville, A. and Bengio, Y., 2014. Generative adversarial nets. In *Advances in neural information processing systems* (pp. 2672-2680).

Google Cloud, 2019. *Google Maps Platform* [Online]. Available from: https://cloud.google.com/maps-platform/, [Accessed, 26/01/2020].

Google, 2019. *Google Colabatory*. [computer program]. Available at: < https://colab.research.google.com/notebooks/welcome.ipynb> [Accessed 23/12/2019].

Google, 2020 Colabatory [*Online*]. Available from: <https://research.google.com/colaboratory/faq.html#resource-limits>. [Accessed: 16/09/2020].

Gram-Hansen, B.J., Helber, P., Varatharajan, I., Azam, F., Coca-Castro, A., Kopackova, V. and Bilinski, P., 2019, January. Mapping informal settlements in developing countries using machine learning and low resolution multi-spectral data. In *Proceedings of the 2019 AAAI/ACM Conference on AI, Ethics, and Society* (pp. 361-368).

Gumbel, E.J., 1941. The return period of flood flows. *The annals of mathematical statistics*, *12*(2), pp.163-190.

Guo, T., Dong, J., Li, H. and Gao, Y., 2017, March. Simple convolutional neural network on image classification. In *2017 IEEE 2nd International Conference on Big Data Analysis (ICBDA)* (pp. 721-724). IEEE.

Hallegatte, S., Green, C., Nicholls, R.J. and Corfee-Morlot, J., 2013. Future flood losses in major coastal cities. *Nature climate change*, *3*(9), pp.802-806.

Hao, G., Min, L. and Feng, H., 2013, August. Improved self-adaptive edge detection method based on Canny. In *2013 5th International Conference on Intelligent Human-Machine Systems and Cybernetics* (Vol. 2, pp. 527-530).IEEE.

Heath, M., Sarkar, S., Sanocki, T. and Bowyer, K., 1998. Comparison of edge detectors: a methodology and initial study. *Computer vision and image understanding*, *69*(1), pp.38-54.

Helber, P., Gram-Hansen, B., Varatharajan, I., Azam, F., Coca-Castro, A., Kopackova, V. and Bilinski, P., 2018.Mapping Informal Settlements in Developing Countries with Multi-resolution, Multi-spectral Data.*arXiv preprint arXiv:1812.00812*.

Hernando, A., Tiede, D., Albrecht, F. and Lang, S., 2012. Spatial and thematic assessment of object-based forest stand delineation using an OFA-matrix. *International Journal of Applied Earth Observation and Geoinformation*, *19*, pp.214-225.

Herrmann, J., 2007. Disaster Response Planning & Preparedness. *Spiritual Care and Mental Health for Disaster Response and Recovery*, p.11.

Hewitt, K., 1983. Interpretations of calamity from the viewpoint of human ecology.

Hijmans, R (2020) Geographic Data Analysis and Modeling [*Online*]. Available from: <https://www.rdocumentation.org/packages/raster/versions/3.3-13#:~:text=%20%20%20Name%20%20%20Description%20,%20%20Direction%20%2054%20more%20rows%20> Accessed: [22/10/2020].

Hijmans, R. J., 2017. Package "raster" 2.6.7. [computer program]. Available at: < https://cran.r-project.org/web/packages/raster/raster.pdf [Accessed 27 April 2018].

Hinz, T., Navarro-Guerrero, N., Magg, S. and Wermter, S., 2018. Speeding up the hyperparameter optimization of deep convolutional neural networks. *International Journal of Computational Intelligence and Applications*, *17*(02), p.1850008.

Hogan, D.J. and Marandola, E., 2005. Towards an interdisciplinary conceptualisation of vulnerability.Population, Space and Place, *11*(6), pp.455-471.

Holand, I.S. and Lujala, P., 2013. Replicating and adapting an index of social vulnerability to a new context: a comparison study for Norway. *The Professional Geographer*, *65*(2), pp.312-328.

Holloway, A.J., Roomaney, R., Pharoah, R., Solomon, F.J. and Cousins, D., 2008. *Weathering the storm: Participatory risk assessment for informal settlements*. Disaster Mitigation for Sustainable Livelihoods Programme (DiMP).

Houston, D., Werrity, A., Bassett, D., Geddes, A., Hoolachan, A. and McMillan, M., 2011. Pluvial (rain-related) flooding in urban areas: the invisible hazard.

Howe, J., Pula, K. and Reite, A.A., 2019, September. Conditional generative adversarial networks for data augmentation and adaptation in remotely sensed imagery. In *Applications of Machine Learning* (Vol. 11139, p. 111390G). International Society for Optics and Photonics.

Hsiang, S.M. and Jina, A.S., 2014. *The causal effect of environmental catastrophe on long-run economic growth: Evidence from 6,700 cyclones* (No. w20352). National Bureau of Economic Research.

Huang, F., Yu, Y. and Feng, T., 2019. Automatic extraction of impervious surfaces from high resolution remote sensing images based on deep learning. *Journal of Visual Communication and Image Representation*, *58*, pp.453-461.

Huang, L., Fang, Y., Zuo, X. and Yu, X., 2015.Automatic change detection method of multitemporal remote sensing images based on 2D-otsu algorithm improved by firefly algorithm. *Journal of Sensors*, *2015*.

Huang, Z., Cheng, G., Wang, H., Li, H., Shi, L. and Pan, C., 2016, July.Building extraction from multi-source remote sensing images via deep deconvolution neural networks. In *2016 IEEE International Geoscience and Remote Sensing Symposium (IGARSS)* (pp. 1835-1838). Ieee.

Hussain, M., Chen, D., Cheng, A., Wei, H. and Stanley, D., 2013. Change detection from remotely sensed images: From pixel-based to object-based approaches. *ISPRS Journal of photogrammetry and remote sensing*, *80*, pp.91-106.

Ibrahim, M.R., Haworth, J. and Cheng, T., 2018. URBAN-i: From urban scenes to mapping slums, transport modes, and pedestrians in cities using deep learning and computer vision. *arXiv preprint arXiv:1809.03609*.

Ibrahim, M.R., Titheridge, H., Cheng, T. and Haworth, J., 2019. predictSLUMS: A new model for identifying and predicting informal settlements and slums in cities from street intersections using machine learning. *Computers, Environment and Urban Systems*, *76*, pp.31-56.

Ingirige, B., Amaratunga D., Kumaraswamy, M., Liyanage C., Aslam P., Towashiraporn, P. and Wedawatta, G. 2014. *Private investment in Disaster Risk Management.* Background Paper prepared for the 2015 Global Assessment Report on Disaster Risk Reduction. Geneva, Switzerland: UNDRR.

Jafari, M.H., Karimi, N., Nasr-Esfahani, E., Samavi, S., Soroushmehr, S.M.R., Ward, K. and Najarian, K., 2016, December. Skin lesion segmentation in clinical images using deep learning.In *2016 23rd International conference on pattern recognition (ICPR)* (pp. 337-342).IEEE.

Jalayer, F., De Risi, R., Kyessi, A., Mbuya, E. and Yonas, N., 2015. Vulnerability of built environment to flooding in African cities. In *Urban Vulnerability and Climate Change in Africa* (pp. 77-106). Springer, Cham.

Jang, H. and Cho, S., 2016. Automatic tagging for social images using convolution neural networks. *Journal of KIISE, 43*(1), pp.47-53.

Jean, N., Burke, M., Xie, M., Davis, W.M., Lobell, D.B. and Ermon, S., 2016. Combining satellite imagery and machine learning to predict poverty. *Science*, *353*(6301), pp.790-794.

Jie, G. and Ning, L., 2012, March. An improved adaptive threshold canny edge detection algorithm.In *2012 International Conference on Computer Science and Electronics Engineering* (Vol. 1, pp. 164-168).IEEE.

Jongman, B., Ward, P.J. and Aerts, J.C., 2012. Global exposure to river and coastal flooding: Long term trends and changes. *Global Environmental Change*, *22*(4), pp.823-835.

Ju, C., Bibaut, A. and van der Laan, M., 2018. The relative performance of ensemble methods with deep convolutional neural networks for image classification. *Journal of Applied Statistics*, *45*(15), pp.2800-2818.

Jung, H., Lodhi, B. and Kang, J., 2019. An automatic nuclei segmentation method based on deep convolutional neural networks for histopathology images. *BMC Biomedical Engineering*, *1*(1), pp.24-35.

Kaur, D. and Kaur, Y., 2014. Various image segmentation techniques: a review. *International Journal of Computer Science and Mobile Computing*, *3*(5), pp.809-814.

Kemper, T., Mudau, N., Mangara, P. and Pesaresi, M., 2015.Towards an automated monitoring of human settlements in South Africa using high resolution SPOT satellite imagery.*The International Archives of Photogrammetry, Remote Sensing and Spatial Information Sciences*, *40*(7), pp.1389-1394.

Keskar, N.S., Mudigere, D., Nocedal, J., Smelyanskiy, M. and Tang, P.T.P., 2016. On large-batch training for deep learning: Generalization gap and sharp minima. *arXiv preprint arXiv:1609.04836*.

Kienberger, S., 2012. Spatial modelling of social and economic vulnerability to floods at the district level in Búzi, Mozambique. *Natural Hazards*, *64*(3), pp.2001-2019.

Kim, P.K. and Lim, K.T., 2017. Vehicle type classification using bagging and convolutional neural network on multi view surveillance image. In *Proceedings of the IEEE Conference on Computer Vision and Pattern Recognition Workshops* (pp. 41-46).

Kim, S., 2015. ppcor: an R package for a fast calculation to semi-partial correlation coefficients. Communications for statistical applications and methods, *22*(6), p.665-674.

King, D., 2001. Uses and limitations of socioeconomic indicators of community vulnerability to natural hazards: data and disasters in Northern Australia. *Natural Hazards*, *24*(2), pp.147-156.

Kingma, D.P. and Ba, J., 2014. Adam: A method for stochastic optimization. *arXiv preprint arXiv:1412.6980*.

Kirti, R. and Bhatnagar, A., 2017. Image Segmentation Using Canny Edge Detection Technique.*porc. of international journal of techno-management research*, pp.8-14.

Kit, O., Lüdeke, M. and Reckien, D., 2012.Texture-based identification of urban slums in Hyderabad, India using remote sensing data.*Applied Geography*, *32*(2), pp.660-667.

Kit, O., Lüdeke, M. and Reckien, D., 2013. Defining the bull's eye: satellite imagery-assisted slum population assessment in Hyderabad, India. *Urban geography*, *34*(3), pp.413-424.

Knobelreiter, P., Reinbacher, C., Shekhovtsov, A. and Pock, T., 2017. End-to-end training of hybrid CNN-CRF models for stereo. In *Proceedings of the IEEE Conference on Computer Vision and Pattern Recognition* (pp. 2339-2348).

Kohli, D., 2013, September. Spatial metrics and image texture for slum detection. In *Proceedings of the 14th N-AERUS/GISDECO Conference, N-AERUS XIV, Enschede, The Netherlands* (pp. 12-14).

Kohli, D., Sliuzas, R., Kerle, N. and Stein, A., 2012. An ontology of slums for image-based classification. *Computers, Environment and Urban Systems*, *36*(2), pp.154-163.

Kuffer, M. and Barros, J., 2011. Urban morphology of unplanned settlements: the use of spatial metrics in VHR remotely sensed images. *Procedia Environmental Sciences*, *7*, pp.152-157.

Kuffer, M., Pfeffer, K., Sliuzas, R. and Baud, I., 2016.Extraction of slum areas from VHR imagery using GLCM variance.*IEEE Journal of selected topics in applied earth observations and remote sensing*, *9*(5), pp.1830-1840.

Kuffer, M., Wang, J., Nagenborg, M., Pfeffer, K., Kohli, D., Sliuzas, R. and Persello, C., 2018.The scope of earth-observation to improve the consistency of the SDG slum indicator.*ISPRS international journal of geo-information*, *7*(11), pp.428-447.

Kuhlicke, C., Scolobig, A., Tapsell, S., Steinführer, A. and De Marchi, B., 2011. Contextualizing social vulnerability: findings from case studies across Europe. *Natural Hazards*, *58*(2), pp.789-810.

Kumar, N., Verma, R., Sharma, S., Bhargava, S., Vahadane, A. and Sethi, A., 2017. A dataset and a technique for generalized nuclear segmentation for computational pathology. *IEEE transactions on medical imaging*, *36*(7), pp.1550-1560.

Kundzewicz, Z.W., 1999. Flood protection—sustainability issues. *Hydrological Sciences Journal*, *44*(4), pp.559-571.

Kussul, N., Lavreniuk, M., Skakun, S. and Shelestov, A., 2017. Deep learning classification of land cover and crop types using remote sensing data. *IEEE Geoscience and Remote Sensing Letters*, *14*(5), pp.778-782.

Kusumastuti, R.D., Husodo, Z.A., Suardi, L. and Danarsari, D.N., 2014. Developing a resilience index towards natural disasters in Indonesia. *International journal of disaster risk reduction*, *10*, pp.327-340.

Lakshmi, S. and Sankaranarayanan, D.V., 2010.A study of edge detection techniques for segmentation computing approaches.*IJCA Special Issue on "Computer Aided Soft Computing Techniques for Imaging and Biomedical Applications" CASCT*, pp.35-40.

Larrazabal, A.J., Martinez, C. and Ferrante, E., 2019, October. Anatomical Priors for Image Segmentation via Post-Processing with Denoising Autoencoders. *In*: *International Conference on Medical Image Computing and Computer-Assisted Intervention* (pp. 585-593). Springer, Cham.

Latinne, P., Debeir, O. and Decaestecker, C., 2000, June.Different ways of weakening decision trees and their impact on classification accuracy of DT combination.In *International Workshop on Multiple Classifier Systems* (pp. 200-209).Springer, Berlin, Heidelberg.

LatLong.net., 2020. *Get Latitude and Longitude.* [*Online*]. Available from: <https://www.latlong.net/>. [Accessed: 23/01/2020].

Laurentini, A., 1994. The visual hull concept for silhouette-based image understanding.*IEEE Transactions on pattern analysis and machine intelligence*, *16*(2), pp.150-162.

LeCun, Y., Bengio, Y. and Hinton, G., 2015. Deep learning. N*ature*, *521*(7553), pp.436–444.

Lein, H., 2009. The poorest and most vulnerable?On hazards, livelihoods and labelling of riverine communities in Bangladesh. *Singapore Journal of Tropical Geography*, *30*(1), pp.98-113.

Leonita, G., Kuffer, M., Sliuzas, R. and Persello, C., 2018. Machine Learning-Based Slum Mapping in Support of Slum Upgrading Programs: The Case of Bandung City, Indonesia. *Remote sensing*, *10*(10), pp.1522-1547.

Lewis, D. and Purcell, P. H. (2014) *From Disaster Risk Reduction To Resilience: A New Urban Agenda for the 21st Century*. Background Paper: UNDRR Sendai Framework.

Ley, A., 2019.Community Resilience and Placemaking through Translocal Networking. *The Journal of Public Space*, *4*(2), pp.165-178.

Li, F. F., Johnson, J., Yeung, S. 2019. Convolutional Neural Networks for Visual Recognition. CS231n. Stanford University [*Online*]. Available from: <https://compsci682-fa19.github.io/>. [Accessed: 20/01/2020].

Li, H., Li, Y. and Porikli, F., 2016.Convolutional neural net bagging for online visual tracking. *Computer Vision and Image Understanding*, (*153)*, pp.120-129.

Li, X. and Yeh, A.G.O., 2002. Neural-network-based cellular automata for simulating multiple land use changes using GIS. *International Journal of Geographical Information Science*, *16*(4), pp.323-343.

Li, Y., Huang, X. and Liu, H., 2017. Unsupervised deep feature learning for urban village detection from high-resolution remote sensing images. *Photogrammetric Engineering & Remote Sensing*, *83*(8), pp.567-579.

Lin, W.Y. and Hung, C.T., 2015. Applying spatial clustering analysis to a township-level social vulnerability assessment in Taiwan. *Geomatics, Natural Hazards and Risk*, *7*(5), pp.1659-1676.

Lipson, H. and Kurman, M., 2016. *Driverless: intelligent cars and the road ahead*. Mit Press: Cambridge Massachusetts.

Liu, M., Zhang, J., Adeli, E. and Shen, D., 2018. Joint classification and regression via deep multi-task multi-channel learning for Alzheimer's disease diagnosis. *IEEE Transactions on Biomedical Engineering*, *66*(5), pp.1195-1206.

Liu, Q., Chen, W., Zhao, L. and Ma, C., 2019, October. Research On Cone Bucket Target Detection Based On Improved Faster R-CNN Deep Network. In *IOP Conference Series: Materials Science and Engineering* (Vol. 631, No. 5, p. 052021). IOP Publishing.

Liu, R., 2018 Mapping the temporal dynamics of slums from vhr imagery.

Liu, W., Wang, Z., Liu, X., Zeng, N., Liu, Y. and Alsaadi, F.E., 2017. A survey of deep neural network architectures and their applications. *Neurocomputing*, *234*, pp.11-26.

Loggia, C. and Govender, V., 2019, November. A hybrid methodology to map informal settlements in Durban, South Africa. In *Proceedings of the Institution of Civil Engineers-Engineering Sustainability* (pp. 1-12). Thomas Telford Ltd.

Lummen, N.S. and Yamada, F., 2014. Implementation of an integrated vulnerability and risk assessment model. *Natural hazards*, *73*(2), pp.1085-1117.

Maiya, S.R. and Babu, S.C., 2018. Slum Segmentation and Change Detection: A Deep Learning Approach. *arXiv preprint arXiv:1811.07896.*

Makau, J., Dobson, S. and Samia, E., 2012. The five-city enumeration: the role of participatory enumerations in developing community capacity and partnerships with government in Uganda. *Environment and Urbanization*, *24*(1), pp.31-46.

Malhotra, K., Davoudi, A., Siegel, S., Bihorac, A. and Rashidi, P., 2018.Autonomous detection of disruptions in the intensive care unit using deep mask R-CNN.In *Proceedings of the IEEE Conference on Computer Vision and Pattern Recognition Workshops* (pp. 1863-1865).

Maluleke, R. and Van Eeden, A., 2013. The relationship between settlement type and undercount in the South African census of 2011. *Town and Regional Planning*, *62*, pp.1-11.

Mayunga, S.D., Coleman, D.J. and Zhang, Y., 2007. A semi-automated approach for extracting buildings from QuickBird imagery applied to informal settlement mapping. *International Journal of Remote Sensing*, *28*(10), pp.2343-2357.

Mboga, N., Georganos, S., Grippa, T., Lennert, M., Vanhuysse, S. and Wolff, E., 2019. Fully Convolutional Networks and Geographic Object-Based Image Analysis for the Classification of VHR Imagery.Remote Sensing, *11*(5), p.597.

Mboga, N., Persello, C., Bergado, J. and Stein, A., 2017. Detection of informal settlements from VHR images using convolutional neural networks. *Remote sensing*, *9*(11), p.1106.

Meer, P., 2004. Robust techniques for computer vision. *Emerging topics in computer vision*, pp.107-190.

Mitlin, D. and Satterthwaite, D., 2013. *Urban poverty in the global south: scale and nature*. Routledge: New York.

Mitlin, D., 2008. With and beyond the state—co-production as a route to political influence, power and transformation for grassroots organizations. *Environment and Urbanization*, *20*(2), pp.339-360.

Montaghi, A., Larsen, R. and Greve, M.H., 2013. Accuracy assessment measures for image segmentation goodness of the Land Parcel Identification System (LPIS) in Denmark. *Remote sensing letters*, *4*(10), pp.946-955.

Morimoto, T., 2019. Spatial analysis of social vulnerability to floods based on the MOVE framework and information entropy method: Case study of Katsushika Ward, Tokyo. *Sustainability*, *11*(2), p.529.Simon, D., McGregor, D. and Nsiah-Gyabaah, K., 2004. The changing urban-rural interface of African cities: definitional issues and an application to Kumasi, Ghana. *Environment and urbanization*, *16*(2), pp.235-248.

Morin, V.M., Ahmad, M.M. and Warnitchai, P., 2016. Vulnerability to typhoon hazards in the coastal informal settlements of Metro Manila, the Philippines. *Disasters*, *40*(4), pp.693-719.

Mossoux, S., Kervyn, M., Soulé, H. and Canters, F., 2018. Mapping population distribution from high resolution remotely sensed imagery in a data poor setting. *Remote Sensing*, *10*(9), p.1409.

Müller, I., Taubenböck, H., Kuffer, M. and Wurm, M., 2020. Misperceptions of Predominant Slum Locations? Spatial Analysis of Slum Locations in Terms of Topography Based on Earth Observation Data. *Remote Sensing*, *12*(15), p.2474.

Musungu, K., Motala, S. and Smit, J., 2012. Using multi-criteria evaluation and GIS for flood risk analysis in informal settlements of Cape Town: the case of Graveyard Pond. *South African Journal of Geomatics*, *1*(1), pp.92-108.

Nakagawa, Y. and Shaw, R., 2004. Social capital: A missing link to disaster recovery. *International Journal of Mass Emergencies and Disasters*, *22*(1), pp.5-34.

Nanni, L., Ghidoni, S. and Brahnam, S., 2017. Handcrafted vs. non-handcrafted features for computer vision classification. *Pattern Recognition*, *71*, pp.158-172.

Nardo, M., Saisana, M., Saltelli, A., Tarantola, S., Hoffman, A. and Giovannini, E., 2005. Handbook on constructing composite indicators.

Neal, J., Schumann, G. and Bates, P., 2012. A subgrid channel model for simulating river hydraulics and floodplain inundation over large and data sparse areas. *Water Resources Research*, *48*, W11506, doi:10.1029/2012WR012514.

Nicolas Morizet. Introduction to Generative Adversarial Networks. [Technical Report] Advestis. 2020. ffhal-02899937f

Niebergall, S., Loew, A. and Mauser, W., 2007, April. Object-oriented analysis of very high-resolution QuickBird data for mega city research in Delhi/India. In *2007 Urban Remote Sensing Joint Event* (pp. 1-8). IEEE.

Nielsen, M. 2017. *Neural Networks and Deep Learning*. [*Online*] Available from: < http://neuralnetworksanddeeplearning.com/index.html>. [Accessed: 27/04/2018].

Nijhawan, R., Sharma, H., Sahni, H. and Batra, A., 2017, December. A deep learning hybrid CNN framework approach for vegetation cover mapping using deep features. In *2017 13th International Conference on Signal-Image Technology & Internet-Based Systems (SITIS)* (pp. 192-196). IEEE.

Niu, X.X. and Suen, C.Y., 2012. A novel hybrid CNN–SVM classifier for recognizing handwritten digits. *Pattern Recognition*, *45*(4), pp.1318-1325.

Nogueira, K., Fadel, S.G., Dourado, Í.C., Werneck, R.D.O., Muñoz, J.A., Penatti, O.A., Calumby, R.T., Li, L.T., dos Santos, J.A. and Torres, R.D.S., 2018. Exploiting ConvNet diversity for flooding identification. *IEEE Geoscience and Remote Sensing Letters*, *15*(9), pp.1446-1450.

Novotny, D., Albanie, S., Larlus, D. and Vedaldi, A., 2018. Semi-convolutional operators for instance segmentation. In *Proceedings of the European Conference on Computer Vision (ECCV)* (pp. 86-102).

Noy, I., 2015. A non-monetary global measure of the direct impact of natural disasters.

O'Keefe, P., Westgate, K. and Wisner, B., 1976. Taking the naturalness out of natural disasters. *Nature*, *260*, pp.566-567.

OpenCV, 2019.Canny Edge Detector [*Online*]. Available from: < https://docs.opencv.org/2.4/doc/tutorials/imgproc/imgtrans/canny_detector/canny_detector.html>. Accessed: [31/03/2020].

Openshaw, S., 1992. Some suggestions concerning the development of artificial intelligence tools for spatial modelling and analysis in GIS. *The annals of regional science*, *26*(1), pp.35-51.

OpenUp, 2017, Informal Settlements Matrix [*Online*] Available from: <http://code4sa.org/projects/ismatrix.html>. [Accessed: 07/09/2020].

Our World in Data, 2019 **Global numbers affected by natural disastersaffected. [Onlinbe]. Available from :** <https://ourworldindata.org/grapher/number-affected-by-natural-disasters?tab=table&time=earliest..2015.>. [Accessed: 18/12/2020].

Owen, K.K. and Wong, D.W., 2013. An approach to differentiate informal settlements using spectral, texture, geomorphology and road accessibility metrics. *Applied Geography*, *38*, pp.107-118.

Pappenberger, F., Dutra, E., Wetterhall, F. and Cloke, H.L., 2012. Deriving global flood hazard maps of fluvial floods through a physical model cascade. *Hydrology and Earth System Sciences*, *16*(11), pp.4143-4156.

Parker, D.J., Priest, S.J. and Tapsell, S.M., 2009. Understanding and enhancing the public's behavioural response to flood warning information. *Meteorological applications*, *16*(1), pp.103-114.

Patterson, O., Weil, F. and Patel, K., 2010. The role of community in disaster response: conceptual models. *Population Research and Policy Review*, *29*(2), pp.127-141.

Paul, S.K. and Routray, J.K., 2011. Household response to cyclone and induced surge in coastal Bangladesh: coping strategies and explanatory variables. *Natural Hazards*, *57*(2), pp.477-499.

Peduzzi, P., Dao, H., Herold, C. and Mouton, F., 2009. Assessing global exposure and vulnerability towards natural hazards: the Disaster Risk Index. *Natural hazards and earth system sciences*, *9*(4), pp.1149-1159.

Pękalska, E., Skurichina, M. and Duin, R.P., 2000, June. Combining fisher linear discriminants for dissimilarity representations .In *International Workshop on Multiple Classifier Systems* (pp. 117-126).Springer, Berlin, Heidelberg.

Pelling, M., 1998. Participation, social capital and vulnerability to urban flooding in Guyana. *Journal of International Development*, *10*(4), pp.469-486.

Pelling, M., 1999. The political ecology of flood hazard in urban Guyana. *Geoforum*, *30*(3), pp.249-261.

Pelling, M., 2018. Breaking the cycle of risk accumulation in Sub-Saharan Africa. *Field Actions Science Reports. The journal of field actions,* (Special Issue 18), pp.12-15.

Perry, M., 2007. Natural disaster management planning. *International Journal of Physical Distribution & Logistics Management*. 37(5), pp.409-433.

Persello, C. and Stein, A., 2017. Deep fully convolutional networks for the detection of informal settlements in VHR images. *IEEE geoscience and remote sensing letters*, *14*(12), pp.2325-2329.

Porio, E., 2011. Vulnerability, adaptation, and resilience to floods and climate change-related risks among marginal, riverine communities in Metro Manila.*Asian Journal of Social Science*, *39*(4), pp.425-445.

Pouyanfar, S., Tao, Y., Sadiq, S., Tian, H., Tu, Y., Wang, T., Chen, S.C. and Shyu, M.L., 2019, September. Unconstrained Flood Event Detection Using Adversarial Data Augmentation. In *2019 IEEE International Conference on Image Processing (ICIP)* (pp. 155-159). IEEE.

Prechelt, L., 1998. Early stopping-but when?. In *Neural Networks: Tricks of the trade* (pp. 55-69). Springer, Berlin, Heidelberg.

Preston, B.L., Yuen, E.J. and Westaway, R.M., 2011. Putting vulnerability to climate change on the map: a review of approaches, benefits, and risks. *Sustainability Science*, *6*(2), pp.177-202.

Qualcomm, 2020, *Classification, Object Detection and Image Segmentation* [Online]. Available from : <https://developer.qualcomm.com/software/qualcomm-neural-processing-sdk/learning-resources/image-segmentation-deeplab-neural-processing-sdk/classification-object-detection-segmentation>. [Accessed:11/10/2020].

Quinn, J.A., Nyhan, M.M., Navarro, C., Coluccia, D., Bromley, L. and Luengo-Oroz, M., 2018. Humanitarian applications of machine learning with remote-sensing data: review and case study in refugee settlement mapping. *Philosophical Transactions of the Royal Society A: Mathematical, Physical and Engineering Sciences*, *376*(2128), p.20170363.

Rahman, N., Ansary, M.A. and Islam, I., 2015. GIS based mapping of vulnerability to earthquake and fire hazard in Dhaka city, Bangladesh. *International journal of disaster risk reduction*, *13*, pp.291-300.

Raj, D. S. Harisha, D. S., Deepak, M., Kumar, K. R. P. 2014 Edge Detection in Angiogram Images Using Modified Classical Image Processing Technique. *International Journal of Engineering Research & Technology. 3(7),* pp. 718-721.

Robinson, D., Dhu, T. and Schneider, J., 2006. Practical probabilistic seismic risk analysis: A demonstration of capability. *Seismological Research Letters*, *77*(4), pp.453-459.

Roh, M.C., Kim, T.Y., Park, J. and Lee, S.W., 2007. Accurate object contour tracking based on boundary edge selection. *Pattern Recognition*, *40*(3), pp.931-943.

Romero-Lankao, P., Gnatz, D.M. and Sperling, J.B., 2016. Examining urban inequality and vulnerability to enhance resilience: insights from Mumbai, India. *Climatic Change*, *139*(3-4), pp.351-365.

Ronneberger, O., Fischer, P. and Brox, T., 2015, October. U-net: Convolutional networks for biomedical image segmentation. In *International Conference on Medical image computing and computer-assisted intervention* (pp. 234-241). Springer, Cham.

Rudari, R., Silvestro, F., Campo, L., Rebora, N., Boni, G. and Herold, C., 2015. Improvement of the global flood model for the GAR 2015. *United Nations Office for Disaster Risk Reduction (UNISDR), Centro Internazionale in Monitoraggio Ambientale (CIMA), UNEP GRID-Arendal (GRID-Arendal): Geneva, Switzerland*, *69*.

Rufat, S., Tate, E., Burton, C.G. and Maroof, A.S., 2015. Social vulnerability to floods: Review of case studies and implications for measurement. *International Journal of Disaster Risk Reduction*, *14*, pp.470-486.

Rufibach, K., 2010. Use of Brier score to assess binary predictions. *Journal of clinical epidemiology*, *63*(8), pp.938-939.

Rumbach, A. and Shirgaokar, M., 2017. Predictors of household exposure to monsoon rain hazards in informal settlements. *Natural Hazards*, *85*(2), pp.709-728.

Sahoo, B. and Bhaskaran, P.K., 2018. Multi-hazard risk assessment of coastal vulnerability from tropical cyclones–A GIS based approach for the Odisha coast. *Journal of environmental management*, *206*, pp.1166-1178.

Saindane, P., Ganapathy, G., Prabhavalkar, N., Bhatia, N. and Vaidya, A., 2019. Comparison and Analysis of Algorithms Used for Detecting Slums in Satellite Images. *Available at SSRN 3346363*.

Salami, R.O., Von Meding, J.K. and Giggins, H., 2017. Urban settlements' vulnerability to flood risks in African cities: A conceptual framework. *Jàmbá: Journal of Disaster Risk Studies*, *9*(1), pp.1-9.

Sample, I. 2020. What are deepfakes – and how can you spot them? [*Online*]. Available from : <https://www.theguardian.com/technology/2020/jan/13/what-are-deepfakes-and-how-can-you-spot-them>. [Accessed; 25/10/20].

Sampson, C.C., Smith, A.M., Bates, P.D., Neal, J.C., Alfieri, L. and Freer, J.E., 2015. A high-resolution global flood hazard model. *Water resources research*, *51*(9), pp.7358-7381.

Satterthwaite, D. 2020. Alternative data sources for cities and communities. [*Online*]. Available from: <https://www.iied.org/alternative-data-sources-for-cities-communities>. [Accessed: 16/03/2020].

Savant, S., 2014. A review on edge detection techniques for image segmentation. *International Journal of Computer Science and Information Technologies*, *5*(4), pp.5898-5900.

Scarpa, G., Gargiulo, M., Mazza, A. and Gaetano, R., 2018.A cnn-based fusion method for feature extraction from sentinel data. *Remote Sensing*, *10*(2), p.236.

Scherer, D., Müller, A. and Behnke, S., 2010, September. Evaluation of pooling operations in convolutional architectures for object recognition. In *International conference on artificial neural networks* (pp. 92-101). Springer, Berlin, Heidelberg.

Schmidtlein, M.C., Deutsch, R.C., Piegorsch, W.W. and Cutter, S.L., 2008. A sensitivity analysis of the social vulnerability index. *Risk Analysis*, *28*(4), pp.1099-1114.

Schneiderbauer, S. and Ehrlich, D., 2004. *Risk, hazard and people's vulnerability to natural hazards: A review of definitions, concepts and data*. Office for Official Publication of the European Communities: Italy.

Schumann, G.P., Vernieuwe, H., De Baets, B. and Verhoest, N.E.C., 2014. ROC-based calibration of flood inundation models. *Hydrological processes*, *28*(22), pp.5495-5502.

Scussolini, P., Aerts, J.C.J.H., Jongman, B., Bouwer, L.M., Winsemius, H.C., De Moel, H. and Ward, P.J., 2015. FLOPROS: An evolving global database of flood protection standards. *Nat. Hazards Earth Syst. Sci. Discuss*, *3*, pp.7275-7309.

SDI, 2020. Know Your City [*Online*]. Available from: <http://knowyourcity.info/explore-our-data/country/?country=south-africa>. [Accessed: 10/02/2019].

SDI. 2017. *SDI Annual Report 2017*. Cape Town: SDI.

SDI. 2018. *Strategic Plan 2018 – 2022*. Cape Town: SDI.

Sebastian, V., Unnikrishnan, A. and Balakrishnan, K., 2012. Gray level co-occurrence matrices: generalisation and some new features. *arXiv preprint arXiv:1205.4831*.

Setayesh, M., Zhang, M. and Johnston, M., 2010, November.Improving edge detection using particle swarm optimisation.In *2010 25th International Conference of Image and Vision Computing New Zealand* (pp. 1-8).IEEE.

Setiawan, B.D., Rusydi, A.N. and Pradityo, K., 2017, November. Lake edge detection using Canny algorithm and Otsu thresholding. In *2017 International Symposium on Geoinformatics (ISyG)* (pp. 72-76).IEEE.

Shahzad, N., Ahmad, S.R. and Ashraf, S., 2017. An assessment of pan-sharpening algorithms for mapping mangrove ecosystems: a hybrid approach. *International Journal of Remote Sensing*, *38*(6), pp.1579-1599.

Sharifzadeh, F., Akbarizadeh, G. and Kavian, Y.S., 2019. Ship classification in SAR images using a new hybrid CNN–MLP classifier. *Journal of the Indian Society of Remote Sensing*, *47*(4), pp.551-562.

Sharma, P. 2019 Image Classification vs. Object Detection vs. Image Segmentation [Online]. Available from: <https://medium.com/analytics-vidhya/image-classification-vs-object-detection-vs-image-segmentation-f36db85fe81>. [Accessed, 26/01/2020].

Siagian, T.H., Purhadi, P., Suhartono, S. and Ritonga, H., 2014. Social vulnerability to natural hazards in Indonesia: driving factors and policy implications. *Natural hazards*, *70*(2), pp.1603-1617.

Siegrist, M. and Gutscher, H., 2008. Natural hazards and motivation for mitigation behavior: People cannot predict the affect evoked by a severe flood. *Risk Analysis*, *28*(3), pp.771-778.

Simon, D. and Leck, H., 2015. Understanding climate adaptation and transformation challenges in African cities. *Current Opinion in Environmental Sustainability*, *13*, pp.109-116.

Simon, D., 2003. Dilemmas of development and the environment in a globalizing world: theory, policy and praxis. *Progress in Development Studies*, *3*(1), pp.5-41.

Simon, D., 2008. Urban environments: issues on the peri-urban fringe. *Annual review of environment and resources*, *33*, pp.167-185.

Smith, A., Bates, P.D., Wing, O., Sampson, C., Quinn, N. and Neal, J., 2019. New estimates of flood exposure in developing countries using high-resolution population data. *Nature communications*, *10*(1), pp.1-7.

Stark, T., 2018. Using Deep Convolutional Neural Networks for the Identification of Informal Settlements to Improve a Sustainable Development in Urban Environments. *Technische Universität München*.

Stark, T., Wurm, M., Taubenböck, H. and Zhu, X.X., 2019, May. Slum Mapping in Imbalanced Remote Sensing Datasets Using Transfer Learned Deep Features.In *2019 Joint Urban Remote Sensing Event (JURSE)* (pp. 1-4).IEEE.

Stevens, F.R., Gaughan, A.E., Linard, C. and Tatem, A.J., 2015. Disaggregating census data for population mapping using random forests with remotely-sensed and ancillary data. *PloS one*, *10*(2), p.e0107042.

Stevens, F.R., Reed, F., Gaughan, A.E., Sinha, P., Sorichetta, A., Yetman, G. and Tatem, A.J., 2019, July. How Remotely Sensed Built Areas And Their Realizations Inform And Constrain Gridded Population Models. In *IGARSS 2019-2019 IEEE International Geoscience and Remote Sensing Symposium* (pp. 6364-6367). IEEE.

Sun, Z. and Meng, Q., 2019. Object-based automatic multi-index built-up areas extraction method for WorldView-2 satellite imagery. *Geocarto International*, *35(8)*, pp.801-817.

Susman, P., O'Keefe, P. and Wisner, B., 1983. Global disasters, a radical interpretation. *Interpretations of calamity*, pp.263-283.

Tarmizi, N.M., Shahriman, N., Maarof, I. and Samad, A.M., 2014. A concept of urban poverty area identification using spatial correlation studies on high resolution satellite imagery. In *Proceedings of the FIG Congress*.

Taş, M., Taş, N., Durak, S. and Atanur, G., 2013. Flood disaster vulnerability in informal settlements in Bursa, Turkey. *Environment and Urbanization*, *25*(2), pp.443-463.

Tatem, A., Gething, P., Pezzulo, C., Weiss, D. and Bhatt, S., 2014. Final Report: Development of High-Resolution Gridded Poverty Surfaces. *United Kingdom: University of Southampton University of Oxford*, *10*.

Taubenböck, H. and Kraff, N.J., 2014. The physical face of slums: a structural comparison of slums in Mumbai, India, based on remotely sensed data. *Journal of Housing and the Built Environment*, *29*(1), pp.15-38.

Taubenböck, H., 2011. The vulnerability of a city—diagnosis from a bird's eye view. *The tsunami threat—research and technology*, pp.107-128.

Taubenböck, H., Post, J., Roth, A., Zosseder, K., Strunz, G. and Dech, S., 2008. A conceptual vulnerability and risk framework as outline to identify capabilities of remote sensing. *Natural Hazards and Earth System Sciences*, *8*(3), pp.409-420.

Taylor, F.E., Millington, J.D., Jacob, E., Malamud, B.D. and Pelling, M., 2020. Messy maps: Qualitative GIS representations of resilience. *Landscape and Urban Planning*, *198*, p.103771.

Tolentino Jr, A.S., 2007. The challenges of tsunami disaster response planning and management. *technology*, *7*(1), pp147-154.

Tomlinson, R., 2017. The Scalability of the Shack/Slum Dwellers International Methodology: Context and Constraint in Cape Town. *Development Policy Review*, *35*(1), pp.115-133.

Trigg, M.A., Birch, C.E., Neal, J.C., Bates, P.D., Smith, A., Sampson, C.C., Yamazaki, D., Hirabayashi, Y., Pappenberger, F., Dutra, E. and Ward, P.J., 2016. The credibility challenge for global fluvial flood risk analysis. *Environmental Research Letters*, *11*(9), p.094014.

UNDRR, 2004. *Living with risk: A global review of disaster reduction initiatives* (Vol. 1). United Nations Publications: Geneva, Switzerland.

UNDRR, 2009. *UNDRR terminology on disaster risk reduction*. United Nations International Strategy for Disaster Risk Reduction: Geneva, Switzerland

UNDRR, 2013. United Nations Plan of Action on Disaster Risk Reduction for Resilience. *Geneva, Switzerland*.

UNDRR, 2015a. *Making Development Sustainable: The Future of Disaster Risk Management. Global Assessment Report on Disaster Risk Reduction*. Geneva, Switzerland: United Nations Office for Disaster Risk Reduction (UNDRR).

UNDRR, 2015c. *Sendai Framework for Disaster Risk Reduction* [Online]. Available from: < http://www.UNDRR.org/we/coordinate/sendai-framework>. [Accessed: 21/03/17].

UNDRR. 2015b. Accelerating and Mainstreaming Disaster Risk Reduction Efforts. *Geneva, Switzerland.*

UNEP. 2013. *Cyclone Phailin in India: Early Warning and Timely Actions Save Lives.* UNEP, Global Environmental Alert Service. November 2013.

United Nations Development Programme. Bureau for Crisis Prevention, 2004. *Reducing Disaster Risk: A Challenge for Development-a Global Report*. United Nations.

United Nations Human Settlements Programme, 2003. *The challenge of slums: global report on human settlements, 2003*. Earthscan/James & James.

Usamah, M., Handmer, J., Mitchell, D. and Ahmed, I., 2014. Can the vulnerable be resilient? Co-existence of vulnerability and disaster resilience: Informal settlements in the Philippines. *International journal of disaster risk reduction*, *10*, pp.178-189.

Van der Walt, S., Schönberger, J.L., Nunez-Iglesias, J., Boulogne, F., Warner, J.D., Yager, N., Gouillart, E. and Yu, T., 2014. scikit-image: image processing in Python. *PeerJ*, *2*, p.e453.

van Vuuren, D.P., Lucas, P.L. and Hilderink, H., 2007. Downscaling drivers of global environmental change: Enabling use of global SRES scenarios at the national and grid levels. *Global Environmental Change*, *17*(1), pp.114-130.

Varatharasan, V., Shin, H.S., Tsourdos, A. and Colosimo, N., 2019, November. Improving Learning Effectiveness For Object Detection and Classification in Cluttered Backgrounds. In *2019 Workshop on Research, Education and Development of Unmanned Aerial Systems (RED UAS)* (pp. 78-85). IEEE.

Vatsavai, R.R., 2013, August. Gaussian multiple instance learning approach for mapping the slums of the world using very high resolution imagery. In *Proceedings of the 19th ACM SIGKDD international conference on Knowledge discovery and data mining* (pp. 1419-1426).

Veljanovski, T., Kanjir, U., Pehani, P., Oštir, K. and Kovačič, P., 2012. Object-based image analysis of VHR satellite imagery for population estimation in informal settlement Kibera-

Nairobi, Kenya. *In*: B. Escalante-Ramirez ed. 2012. *Remote Sensing-Applications*., pp.407-434.

Verma, D., Jana, A. and Ramamritham, K., 2019. Transfer learning approach to map urban slums using high and medium resolution satellite imagery. *Habitat International*, *88*, p.101981.

Villagrán De Léon, J.C., 2006. Vulnerability: a conceptual and methodological review. SOURCE—studies of the university: research, counsel, education. *UNU Institute for Environment and Human Security (4)*.

Vuola, A.O., Akram, S.U. and Kannala, J., 2019, April.Mask-RCNN and U-net ensembled for nuclei segmentation.In *2019 IEEE 16th International Symposium on Biomedical Imaging (ISBI 2019)* (pp. 208-212).IEEE.

Vyas, S. and Kumaranayake, L., 2006. Constructing socio-economic status indices: how to use principal components analysis. *Health policy and planning*, *21*(6), pp.459-468.

Walia, A.S., 2017. *Types of Optimization Algorithms used in Neural Networks and Ways to Optimize Gradient Descent*. [*Online*] Available from: <https://towardsdatascience.com/types-of-optimization-algorithms-used-in-neural-networks-and-ways-to-optimize-gradient-95ae5d39529f> [Accessed: 30/12/2019].

Wang, J., Kuffer, M., Roy, D. and Pfeffer, K., 2019. Deprivation pockets through the lens of convolutional neural networks. *Remote sensing of environment*, *234*, p.111448.

Ward, P.J., Couasnon, A., Eilander, D., Haigh, I.D., Hendry, A., Muis, S., Veldkamp, T.I., Winsemius, H.C. and Wahl, T., 2018. Dependence between high sea-level and high river discharge increases flood hazard in global deltas and estuaries. *Environmental Research Letters*, *13*(8), p.084012.

Ward, P.J., De Moel, H., Aerts, J.C.J.H. and Glade, T., 2011. How are flood risk estimates affected by the choice of return-periods?. *Natural Hazards & Earth System Sciences*, *11*(12), pp.3181–3195.

Ward, P.J., Jongman, B., Aerts, J.C., Bates, P.D., Botzen, W.J., Loaiza, A.D., Hallegatte, S., Kind, J.M., Kwadijk, J., Scussolini, P. and Winsemius, H.C., 2017. A global framework

for future costs and benefits of river-flood protection in urban areas. *Nature climate change*, *7*(9), pp. 642–646.

Wardrop, N.A., Jochem, W.C., Bird, T.J., Chamberlain, H.R., Clarke, D., Kerr, D., Bengtsson, L., Juran, S., Seaman, V. and Tatem, A.J., 2018. Spatially disaggregated population estimates in the absence of national population and housing census data. *Proceedings of the National Academy of Sciences*, *115*(14), pp.3529-3537.

WBEF, 2020. The future of informal settlements in the developing [Online]. Available from : <worldhttps://www.rics.org/en-hk/wbef/megatrends/urbanisation/the-future-of-informal-settlements-in-the-developing-world/>. [Accessed:18/12/2020].

Whiteside, T.G., Boggs, G.S. and Maier, S.W., 2011. Comparing object-based and pixel-based classifications for mapping savannas. *International Journal of Applied Earth Observation and Geoinformation*, *13*(6), pp.884-893.

Williams, D.S., Máñez Costa, M., Sutherland, C., Celliers, L. and Scheffran, J., 2019. Vulnerability of informal settlements in the context of rapid urbanization and climate change. *Environment and Urbanization*, *31*(1), pp.157-176.

Willner, S.N., Levermann, A., Zhao, F. and Frieler, K., 2018. Adaptation required to preserve future high-end river flood risk at present levels. *Science advances*, *4*(1), p.eaao1914.

Winsemius, H.C., Van Beek, L.P.H., Jongman, B., Ward, P.J. and Bouwman, A., 2013. A framework for global river flood risk assessments. *Hydrology and Earth System Sciences*, *17*(5), pp.1871-1892.

Wisner, B., Blaikie, P., Cannon, T., Davis I. (2004) At Risk—natural hazards, people's vulnerability and disasters. 2nd edn. Routledge, London.

Wisner, B., J.- G. Gaillard and I. Kelman (2012), 'Framing disaster: theories and stories seeking to understand hazards, vulnerability and risk', *In* B. Wisner, I. Kelman and J.- G. Gaillard (eds), *The Routledge Handbook of Hazards and Disaster Risk Reduction*, London and New York: Routledge

Wolf, S., 2012. Vulnerability and risk: comparing assessment approaches. *Natural Hazards*, *61*(3), pp.1099-1113.

Wu, G., Guo, Z., Shi, X., Chen, Q., Xu, Y., Shibasaki, R. and Shao, X., 2018b. A boundary regulated network for accurate roof segmentation and outline extraction. *Remote Sensing*, *10*(8), p.1195.

Wu, G., Shao, X., Guo, Z., Chen, Q., Yuan, W., Shi, X., Xu, Y. and Shibasaki, R., 2018a. Automatic building segmentation of aerial imagery using multi-constraint fully convolutional networks. *Remote Sensing*, *10*(3), p.407.

Wu, S.Y., Yarnal, B. and Fisher, A., 2002. Vulnerability of coastal communities to sea-level rise: a case study of Cape May County, New Jersey, USA. *Climate Research*, *22*(3), pp.255-270.

Wurm, M., Stark, T., Zhu, X.X., Weigand, M. and Taubenböck, H., 2019. Semantic segmentation of slums in satellite images using transfer learning on fully convolutional neural networks. *ISPRS journal of photogrammetry and remote sensing*, *150*, pp.59-69.

Yabin, H.U., Yi, M.A. and Jubai, A.N., 2018. Research on high accuracy detection of red tide hyperspecrral based on deep learning Cnn. *International Archives of the Photogrammetry, Remote Sensing and Spatial Information Sciences*, *42*, p.3.

Yamazaki, D., Ikeshima, D., Tawatari, R., Yamaguchi, T., O'Loughlin, F., Neal, J.C., Sampson, C.C., Kanae, S. and Bates, P.D., 2017. A high-accuracy map of global terrain elevations. *Geophysical Research Letters*, *44*(11), pp.5844-5853.

Yamazaki, D., Kanae, S., Kim, H. and Oki, T., 2011. A physically based description of floodplain inundation dynamics in a global river routing model. *Water Resources Research*, *47*(4), W04501, doi:10.1029/2010WR009726.

Yang, L. and Cervone, G., 2018. Analysis of remote sensing imagery for disaster assessment using deep learning: a case study of flooding event. *Soft Computing*, *23*(24), pp.13393-13408.

Yang, S., He, S., Du, J. and Sun, X., 2015. Screening of social vulnerability to natural hazards in China. *Natural Hazards*, *76*(1), pp.1-18.

Yaseen, K., Tariq, A. and Akram, M.U., 2013. A Comparison and Evaluation of Computerized Methods for OD Localization and Detection in Retinal Images. *International Journal of Future Computer and Communication*, *2*(6), p.613.

Yoon, D.K., 2012. Assessment of social vulnerability to natural disasters: a comparative study. *Natural hazards*, *63*(2), pp.823-843.

Young, I.T. and Van Vliet, L.J., 1995. Recursive implementation of the Gaussian filter. *Signal processing*, *44*(2), pp.139-151.

Zebardast, E., 2013. Constructing a social vulnerability index to earthquake hazards using a hybrid factor analysis and analytic network process (F'ANP) model. *Natural hazards*, *65*(3), pp.1331-1359.

Zeng, J., Zhu, Z.Y., Zhang, J.L., Ouyang, T.P., Qiu, S.F., Zou, Y. and Zeng, T., 2012. Social vulnerability assessment of natural hazards on county-scale using high spatial resolution satellite imagery: a case study in the Luogang district of Guangzhou, South China. *Environmental Earth Sciences*, *65*(1), pp.173-182.

Zhan, Q., Molenaar, M., Tempfli, K. and Shi, W., 2005. Quality assessment for geo-spatial objects derived from remotely sensed data. *International Journal of Remote Sensing*, *26*(14), pp.2953-2974.

Zhang, G., Zheng, G., Gao, Y., Xiang, Y., Lei, Y. and Li, J., 2017b. Automated water classification in the Tibetan plateau using Chinese GF-1 WFV data. *Photogrammetric Engineering & Remote Sensing*, *83*(7), pp.509-519.

Zhang, H., Zheng, Z., Xu, S., Dai, W., Ho, Q., Liang, X., Hu, Z., Wei, J., Xie, P. and Xing, E.P., 2017a. Poseidon: An efficient communication architecture for distributed deep learning on {GPU} clusters. In *2017 {USENIX} Annual Technical Conference ({USENIX}{ATC} 17)* (pp. 181-193).

Zhang, Z., 2016. A gentle introduction to artificial neural networks. *Annals of translational medicine*, *4*(19), pp370-375.

Zheng, K., Wei, M., Sun, G., Anas, B. and Li, Y., 2019. Using vehicle synthesis generative adversarial networks to improve vehicle detection in remote sensing images. *ISPRS International Journal of Geo-Information*, *8*(9), p.390.

Zhou, Q., Leng, G., Su, J. and Ren, Y., 2019. Comparison of urbanization and climate change impacts on urban flood volumes: Importance of urban planning and drainage adaptation. *Science of the Total Environment*, *658*, pp.24-33.

Zhu, X., Liu, Y., Li, J., Wan, T. and Qin, Z., 2018, June. Emotion classification with data augmentation using generative adversarial networks. In *Pacific-Asia conference on knowledge discovery and data mining* (pp. 349-360). Springer, Cham.

Zhu, X.X., Tuia, D., Mou, L., Xia, G.S., Zhang, L., Xu, F. and Fraundorfer, F., 2017. Deep learning in remote sensing: A comprehensive review and list of resources. *IEEE Geoscience and Remote Sensing Magazine*, *5*(4), pp.8-36.

Ziervogel, G., Waddell, J., Smit, W. and Taylor, A., 2016. Flooding in Cape Town's informal settlements: barriers to collaborative urban risk governance. *South African Geographical Journal*, *98*(1), pp.1-20.